Structured population models with internal cell cycle

Charlotte Sonck

Proefschrift voorgedragen tot het behalen van de graad van
Doctor in de Wetenschappen: Wiskunde
Academiejaar 2015-2016

Promotoren:
Prof. Dr. Willy Govaerts
Prof. Dr. Markus Kirkilionis (Warwick University, UK)

Vakgroep Toegepaste Wiskunde, Informatica en Statistiek
Faculteit Wetenschappen, Universiteit Gent
Krijgslaan 281, B-9000 Gent

"Essentially, all models are wrong, but some are useful."

– George Box

Contents

Dankwoord

Wow, na meer dan 6 jaar is het eindelijk zover. Het schrijven van dit dankwoord heb ik tot het laatste moment uitgesteld (je weet immers nooit of het ongeluk zou brengen), maar nu neem ik toch graag de tijd om iedereen te bedanken die me tijdens de afgelopen jaren gesteund of geholpen heeft.

Allereerst wil ik graag mijn promotor Willy Govaerts bedanken. We hebben de afgelopen jaren geregeld samen onze hersenen gepijnigd. Bedankt voor de vele feedback, inspiratie en steun. Mijn co-promotor Markus Kirkilionis is ook een onmisbare schakel geweest voor dit onderzoek. Markus, your enthusiasm worked really contagious and always gave me new energy to continue the research and explore new horizons. Dankjewel!

Ik wil ook graag de leden van mijn examencommisie bedanken. Bedankt Jan Baetens, Peter Dawyndt, Hans De Meyer, André de Roos, Marnix Van Daele en Wim Vanroose om de tijd vrij te maken om mijn doctoraatswerk door te nemen en naar Gent te komen voor de interne en publieke verdediging. Dankzij jullie feedback en kritische vragen is deze resulterende doctoraatsthesis veel duidelijker dan de initiële versie. Marnix, jij bent als examenvoorzitter in het bijzonder bedankt voor het regelen van tal van praktische zaken.

De werksfeer in S9 is al die jaren tip top geweest, waarvoor ik iedereen heel dankbaar ben. Ik heb geluk gehad dat ik tussen zulke leuke en joviale mensen heb mogen werken. In het bijzonder bedankt aan m'n bureaugenootjes! Virginie en Kim, bedankt om er zo'n gezellige bureau van te maken tijdens mijn eerste vier doctoraatsjaren!

Virginie, het was enorm leuk met jou als onderzoeksgroepgenootje. De conferenties samen in Dresden en Orlando waren de max, aan beide conferenties heb ik hele leuke herinneringen zoals samen lekkere tapas eten in Dresden en ons te pletter zweten in Sea World. Bedankt dat je er altijd was als ik eens nood had aan een babbel. Voor dat laatste kon ik ook altijd terecht bij jou, Kim. Het was genieten om je puppy-, honden- en reisverhalen te horen. Jammer dat het moeilijk is om geregeld in contact te blijven (waarvoor ik de verantwoordelijkheid neem), maar ik ben altijd blij met zo'n jaarlijkse update-mail (ook al duurt het dan weer enkele weken tegen dat ik antwoord ;)). Virginie en ik waren steeds bereid om je uit de nood te helpen als je last had van een "bakperiode", en dat is helaas iets waar ik minder bij kan helpen bij mijn twee nieuwe bureaugenoten. Ondanks dit grote gebrek, zijn Roy en Dieter tijdens de afgelopen jaren toch ook al superbureaugenoten gebleken. Het was aanpassen, zo plots enkel mannen in mijn bureau, maar gelukkig bleek al snel dat Dieter even nieuwgierig is als Virginie en dat ik bij jullie makkelijk mezelf kon zijn. Bedankt, Dieter en Roy, om zulke goedlachse en hulpvaardige collega's te zijn! Jullie hebben ondertussen zelfs de hormonen horende bij twee zwangerschappen overleefd, dus jullie zijn geslaagd voor de ultieme bureaugenotentest. Dieter, onze google-man, bedankt om me te helpen met zo vele praktische zaken (te veel om op te noemen - zo kom ik er makkelijk vanaf) en me zo'n stijlicoon te vinden. Roy, bedankt voor de latex- en andere hulp en om mijn liefde voor bepaalde kleuren (en Nele) te delen. En gelukkige verjaardag, Roy!

In een vakgroep zoals TWIST heb je allerlei soorten collega's, waaronder ook een heel pak informatici. Daardoor durven de gesprekken wel eens een bepaalde nerderige richting uit te gaan, maar gelukkig hebben deze collega's ook hun nut bewezen. Bedankt voor de D3-implementaties Bart, ze maken mijn thesis een pak mooier (en wie vindt deze cover niet fantastisch?). Herman, bedankt om me op een cruciaal moment te helpen met het doorploeteren van een stuk `C++`-code. Zo heb ik je nog eens kunnen herinneren aan de vele voordelen van `C++`. Benoit, bedankt voor je hulp om TortoiseSVN terug werkend te krijgen, dat heeft me veel tijd bespaard. Niels, bedankt voor de MatContM-ondersteuning en om zo'n fijne onderzoeksgroepgenoot te zijn. En niet te vergeten: enorm bedankt om ervoor te zorgen dat ik nog eens Age of Empires kon spelen! Bij de vele hulpvaardige collega's horen ook Glad en Nico. Glad, bedankt voor de vele latex-tips en -hulp en Nico, bedankt om de taak van latex-goeroe over te nemen van Glad. Uiteraard zijn jullie ook stuk

voor stuk bedankt om zo'n aangename collega's te zijn! Bij zo veel leuke collega's is het gevaarlijk om iemand te vergeten, dus bedankt aan iedereen voor de leuke koffiepauzes, lesmomenten en lunches!

Het nadeel van zo lang bij TWI/TWIST te vertoeven, is dat ik ondertussen ook al veel topcollega's heb zien afzwaaien. Catherine, bedankt om zo'n enthousiaste collega en organisatietalent te zijn! Machteld en Karel, de middagpauzes in de cafetaria zijn niet hetzelfde zonder jullie, al zijn ze nu wel minder gevaarlijk om lang te blijven plakken. Bedankt Machteld om samen met mij uitstapjes naar het stoffenspektakel te ondernemen en zo'n gezellig persoon te zijn. Karel, ik ben fan van je linkse kantje en de wereldverbeteraar in je. Nele, bij jou kon ik altijd terecht om bepaalde zorgen of nieuwtjes te delen, waarvoor bedankt! Stéphanie, het was heel leuk om jou als collega en zelfs even als bureaugenoot te hebben. Davy, "den flauwe plezanten", bedankt om zo'n hulpvaardige en leuke collega geweest te zijn! Bert, ik hoop dat je mij emotioneel rijk vindt. Bedankt voor het aansnijden van interessante gespreksonderwerpen tijdens de pauzes. Jan, mijn geboortedag-genoot, het was heel leuk om samen met jou te werken bij TWIST en samen te kunnen trakteren. Gelukkig kan ik ook buiten TWIST op je rekenen als enthousiaste vriend. Bashir, I would like to thank you for your friendship during your stay in Belgium. Een speciale dankjewel ook aan een heel actieve niet-TWISTer binnen de TWIST-activiteiten, Joyce. Bedankt om zo je best te doen om de groep samen te krijgen voor leuke activiteiten!

Naast collega's ben ik ook mijn familie en vrienden heel dankbaar voor de steun en ontspanning tijdens deze doctoraatsjaren. Moeke en vava, bedankt voor de vele hulp en me de kans te geven om dit te verwezenlijken. Jullie hebben er, elk op je eigen manier, voor gezorgd dat ik steeds het uiterste uit mezelf wil halen en ik denk dat dit doctoraat daar een mooi voorbeeld van is. Bedankt Fientje voor de vele doctoraat-tips. Handig om iemand in mijn nabije familie te hebben die de ergernissen die soms bij een doctoraat horen, helemaal begrijpt. Karel, jou moet ik in het bijzonder bedanken voor je technische hulp bij het werkzaam krijgen van `C++` op mijn laptop en het ontwerpen van mijn cover (hopelijk was 1 euro voldoende als betaling). Helaas heb ik tijdens mijn jaren aan de S9 ook afscheid moeten nemen van drie van mijn grootouders, maar ik weet dat ik mede dankzij hun vertrouwen in mijn kunnen, zo sterk in mijn schoenen sta. Bedankt dus oma, José en peter voor

alles. Bedankt oma Lucie voor de zondagse lekkernijen en de vele steun. Ik hoop binnenkort wat meer op bezoek te kunnen komen. Ook wil ik graag de rest van mijn familie, tantes en nonkels, neven en nichten, bedanken voor de ontspannende familiemomenten en -reizen en de vele steun op allerlei vlak (zoals het kippenpension bij Koen, gezellig bijpraten met Madelena, de Emilina-shuttle door Michaël,...). Het doet deugd om te weten dat ik op jullie kan rekenen als het nodig is. Ik wil ook heel graag mijn schoonfamilie bedanken. Bedankt Marc en Martine, voor de vele steun, zowel emotioneel als praktisch. Ook bedankt aan Jonas, Sabrine, Janne, Briek, Annechien en Jasper om me mijn zinnen te helpen verzetten. Ik heb het geluk gehad dat ik het doctoraatsleven (en de bijhorende vreugden en zorgen) ook met enkele vrienden heb kunnen delen. Bedankt voor de leuke lunches en de vriendschap Nelle, Joks en Katrien. Het pendelen was veel plezanter dankzij jou, Nelle! Lies, jou wil ik ook heel graag bedanken voor de vriendschap, het vele gebabbel tijdens de lessen vroeger en de leuke dates. Ook de 2 wiskunde-Sofie's, Ilse, Arne, Lien en de "nieuwe" vrienden via Nelle & Jens (Griet & Tomasz, Lien & Dimi), bedankt voor de welgekomen ontspanning zo nu en dan!

Last but not least, wil ik graag de man van mijn leven bedanken. Ruben, samen met jou maak ik zotte plannen en maken we het ons vooral heel druk. De afgelopen jaren waren bij momenten heel hectisch, maar ik zou er niets aan veranderen. Samen met jou kan ik alles aan. Bedankt om me zo graag te zien en zo'n "zalige zot" te zijn. Emilina, mijn lief en vrolijk meisje, jou wil ik bedanken om me al mijn zorgen op slag te doen vergeten als ik jouw schaterlach hoor. Ik zie jullie en Stormageddon heel graag.

Charlotte Sonck
Maart 2016

Acronyms & symbols

cell cycle

G1	first Gap phase of the cell cycle	8
S	Synthesis phase of the cell cycle	8
G2	second Gap phase of the cell cycle	8
M	Mitosis phase of the cell cycle	8
Cdk	cyclin-dependent protein kinase	10
CKI	Cyclin-dependent Kinase Inhibitor	10
APC	Anaphase-Promoting Complex	13
Cdc20	protein of APC	13
Cdh1	protein of APC	13
CycB	important cyclin in the S-G2-M phase for budding yeast	13
IE	Intermediary Enzyme	14
SK	Starter Kinase	15
TF	Transcription Factor for SK	15

cell cycle models

m	cell mass (dimensionless)	16
μ	growth rate parameter	51,76

budding yeast cell cycle model

$[\mathbf{CycB}]_\mathbf{T}$	total concentration of CycB	16
$[\mathbf{CycB}]$	concentration of CycB-Cdk dimer	16
$[\mathbf{Trimer}]$	concentration of CycB-Cdk-CKI trimer	16

$[\mathbf{Cdh1}]$	concentration of Cdh1-APC	16

Toy model

$\mathbf{X}$	concentration of cyclin-Cdk dimer	66
$\mathbf{Y}$	concentration of active Cdh1-APC	66
$\mathbf{A}$	concentration of a protein that activates Cdh1 at Finish	66
$\mathbf{m_{max}}$	maximal mass of a cell	66

equations

ODE	Ordinary Differential Equation	34
DDE	Delay Differential Equation	26
PDE	Partial Differential Equation	27

bifurcation theory ODEs

H	Hopf point	35
LP	Limit Point	35
LPC	Limit Point of Cycles	35
HHS	orbit Homoclinic-to-Hyperbolic-Saddle	35
HSN	orbit Homoclinic-to-Saddle-Node	35

bifurcation theory maps

PD	Period Doubling bifurcation	36
LP	Limit Point bifurcation	37
NS	Neimark-Sacker bifurcation	38

study of the budding yeast model

$\mathbf{m_{REP}}$	mass at transition from G1 to S-G2-M phase	51
$\mathbf{m_{DIV}}$	mass at division	51
$\mathbf{m_{NEW}}$	mass of a newborn cell	51
ν	ratio of m_{DIV} to m_{NEW}	51
$\mathbf{I}$	elapsed time between the birth of a cell and its division	51
$\mathbf{\Delta_1 t}$	time in G1 phase	59
$\mathbf{\Delta_2 t}$	time in S-G2-M phase	57

population model

i-state	individual state	21
p-state	population state	21
Ω	i-state space	21
$\mathbf{\Omega_i}$	i-state space	73
$\mathbf{\Omega_b}$	i-state space of newborn cells	73
$\mathbf{S}$	nutrient concentration in the bioreactor	71
$\mathbf{S^0}$	nutrient concentration in the feeding bottle of the chemostat	72
$\mathbf{D}$	dilution rate	72
$\mathbf{x}$	i-state of a cell	71
$\mathbf{x_0}$	i-state of a cell at birth	71
$\mathcal{F}(\ldots)$	survival probability	72
$\beta(\ldots)$	division rate	72
$\gamma(\ldots)$	food consumption rate	72
$\mathbf{f}(\mathbf{S})$	intrinsic rate of change of nutrient	72
$\mathbf{g}(\ldots)$	individual evolution rate	73
$\mu_\mathbf{d}(\ldots)$	mortality rate	73
$\mathbf{b}(\ldots)$	population birth rate	74
ϕ	splitting parameter (cell with mass m splits into cells with masses ϕm and $(1-\phi)m$)	73
NMM	No-Minimal-Mass model	77
MM1	Minimal-Mass model 1	77
MM2	Minimal-Mass model 2	77
$\mathbf{m_{min}}$	minimal mass a cell must have to divide in MM-models	77
$\mathbf{X_{DIV}}$	X-value at division	77
$\mathbf{\bar{S}}$	constant nutrient concentration in the bioreactor	78
$\mathbf{\bar{b}}(\mathbf{x})$	time-invariant distribution of the birth rate over x	78
$\mathbf{a}$	age of a cell (in minutes)	
$\mathbf{x_{0ijkl}}$	general discretisation point of Ω_b	81
$\mathbf{x_{0i}}$	adaptive discretisation point of Ω_b	84
$\mathbf{\bar{b}}(\mathbf{x_{0i}})$	number of cells born per unit of time and volume in the birth cohort with state x_{0i}	85
$\mathbf{\bar{b}_{tot}}$	total number of cells born per unit of time and volume	95
$\mathbf{N}$	number of birth cohorts	83

δ	minimal mass-distance between 2 discretisation points	83
ε	lower threshold for the fraction of cells born in a birth cohort	83
$\varepsilon_{\mathcal{F}}$	lower threshold for $\mathcal{F}$ to stop the age integration of the cells born in a birth cohort	85
$\theta(\ldots)$	total nutrient consumption by a cell up to a certain age	82
$\Theta(\ldots)$	total nutrient consumption by a cell over its entire life-time	82
$\mathbf{r_0}(\ldots)$	number of cells born per unit of time and volume with a certian birth state from mother cells up to a certain age	82
$\mathbf{R_0}(\ldots)$	number of cells born per unit of time and volume with a certian birth state from all possible mother cells	82
`reltol`	scalar relative tolerance used in the age integration	105

CHAPTER 1

Introduction

Mathematical models of "the real world" bridge the gap (or at least the gap that exists according to most people) between mathematics and real life. In the recent years, mathematical modelling has become so popular that in personal blogs and teachers' handbooks one argues that it should be integrated in the mathematics education from start on, because students would thus feel the "real use" of mathematics. In this thesis, the focus is on mathematical models in population biology. Population models can help to understand the involved dynamic processes and to make practical predictions. One of the great advantages of the use of mathematics in population biology, is that one is forced to be exact about the assumptions one makes and, of course, mathematics are a great framework for logical reasoning and analysis of problems. The study of populations dates back from the, by now well known, exercise in an arithmetic book of 1202 written by Leonardo of Pisa which involved the building of a mathematical model for a growing rabbit population (later resulting in the Fibonnaci sequence).

The individual organism is the basic unit in population models. It is often useful to make a distinction between different individuals on the basis of certain physiological characteristics that influence their life trajectory. This collection of physiological traits, is called the *individual state* or *i-state* and may include e.g. age, size or sex. Population models that make such a distinction between the individuals are called structured population models, as opposed to unstructured population models that

consider identical or "average" organisms. In this thesis, we consider structured population models of unicellular organisms. The novelty is that we use the chemical components of a mathematical submodel for the cell cycle as *i*-state. Existing structured population models that consider the cell cycle, use a continuous component to represent the progression through the cycle or e.g. a combination of the cell's mass and age. However, during the last fifteen years Tyson and Novák and collaborators have presented several mathematical models for the cell cycle of different organisms based on the concentrations of chemicals such as cyclins that play a role in the process. We incorporate two of these models to describe how the *i*-state of a cell changes during its life-time and, importantly, to describe when it divides. A population model reflects how a certain population will behave in the future, given its current state and environmental conditions that influence the time evolution of the population. The current state of the population is called the *p-state* and is represented by a frequency distribution over all *i*-states. We consider chemostat models, i.e. the cell population is inside a stirred bioreactor to which fresh nutrient is continuously added, while the culture liquid (containing both the cells and the nutrient) is continuously removed at the same rate to keep the culture volume constant. The only environmental factor in our models is the limiting nutrient concentration in the bioreactor. We incorporate a nutrient dependency in the equation for the mass increase of the cell cycle models. The equations for the population dynamics consist of a renewal equation coupled with a delay differential equation. We are particularly interested in the equilibria of the model. An equilibrium consists of a constant nutrient concentration and a time-invariant distribution of the births over the possible *i*-states. To be able to numerically solve the equilibrium equations, we have to discretise the birth space resulting in a finite number of birth cohorts with corresponding equations. To decrease the number of birth cohorts, we use the funnel effect of the considered cell cycle models, and further use an adaptive mesh. The equilibrium of the population model can be calculated as the fixed point of a map. The calculation of the fixed point is implemented using `C++`. We consider different options for the cell division criteria, initially following Tyson and Novák who let a cell divide when the concentration of the cyclin-Cdk dimer is decreasing and equal to 0.1, but also consider e.g. the impact on the fixed point of a minimal mass criterion for division, of a discrete mapping of the mass at birth to the value of the dimers at division and of a density probability function for the value of the dimers at division. We give an overview of the different chapters in the thesis.

In **Chapter 2** an introduction to the different topics needed to comprehend this thesis is given. Section 2.1 describes the key features of the cell cycle and how a mathematical model can reflect them. In Section 2.2 an overview of population models is given, with the main focus on structured population models. An overview of the main mathematical forms of structured population models is given, an example of a model for cells with nutrient dependency that uses the progression through the cell cycle as i-state is given and a numerical method to calculate the equilibrium of a structured cell population model is explained. In the last Section 2.3 of this chapter, we introduce mathematical methods that will be used later on in this thesis. We give some background on the bifurcation theory of ODEs and maps, and explain the method of pseudo-arclength continuation.

In **Chapter 3** we study the bifurcation structure of a cell cycle model for budding yeast of Tyson and Novák using the Matlab numerical bifurcation software MatCont. We find that not only the S-G2-M phase but also the G1 phase of the cell cycle contains both stable steady states and stable periodic orbits. A closer investigation of the periodic orbits in the model is done. We find and discuss a relation between the growth rate of the cell and the mass increase after DNA-replication. We relate this to a constant phase fraction of a periodic orbit traversed during S-G2-M phase and derive a relation between the growth rate and the time spent in S-G2-M space. We discuss the budding yeast model as a slow-fast system and show how the boundary value problem of the cell cycle can efficiently be computed as the fixed point of a map. The robustness of the model with respect to the parameter k'_{13} is investigated and leads to the result that the constitutive expression of the Starter kinase not only leads to a premature transition from G1 to S phase and smaller cells (as is experimentally known and confirmed by other models) but can also lead to nonviable cells in this model. In the last section of the chapter, we introduce a simplified model for the cell cycle by Tyson and Novák, the Toy model. This model will be used as internal cell cycle mechanism of the structured population models in the main part of Chapters 4 and 5.

Chapters 4 and 5 cover the major part of our study. In **Chapter 4** we focus on the modelling part of our study on structured population models with internal cell cycle. We introduce the chemostat model for a population of unicellular organisms

which live in a continuous culture and attach a physiological structure to these cells describing their internal cell cycle. The progression through the cell cycle depends on the concentration of the limiting nutrient in the bioreactor. In Section 4.1 we describe the structured population model in general terms. The i-state of the cell describes its progression through the cell cycle by using well-studied mathematical models. In Section 4.2 we present the cell cycle equations and explain the cell division conditions. We make the distinction between population models where cells can only divide when their mass satisfies a minimal mass criterion (Minal-Mass models MM1 and MM2) and a model without minimal mass criteron (No-Minimal-Mass model NMM). In Section 4.3 we give the equations for the equilibrium $(\bar{S}, \bar{b}(x))$. To enable the computation of the equilibrium, the birth space is discretised which results in a finite number of birth cohorts. In Section 4.4 we discuss a general discretisation of the birth space, using a uniform meshing, and give the equations for the discretised population model and the equilibrium. The internal state of each birth cohort, together with the nutrient consumption by the cells in the cohort, is integrated over age until the survival probability of the cells in the cohort becomes negligible. The discretisation of the birth space is simplified in Section 5.1 making use of the funnel effect which the Toy model and more elaborated cell cycle models display. This results in only discretising the mass component. We use an adaptive discretisation, which means that the birth cohorts are not fixed: the age integration is performed on an initial list of cohorts resulting in a new list of birth cohorts. This new list of birth cohorts depends on the i-states of the newborn cells, born from mother cells in the initial list of cohorts, and two parameters δ and ε. δ represents the "inhibition zone" of an existing cohort, which means that the masses in the new list of birth cohorts differ minimally δ from each other. ε is a lower threshold for the fraction of cells born in a cohort. We give the resulting equations for the population model and motivate how the equilibrium equations can be rewritten as the fixed point equation of a map.

In **Chapter 5** we discuss the computational results for the structured population models introduced in Chapter 4. In Section 5.1 we briefly discuss how we implement this map and discuss the convergence results for the models NMM, MM1 and MM2. In the NMM model, all cells divide immediately after birth, which is not very realistic. For the MM1 model, we find a non-trivial fixed point with 41 birth cohorts which we discuss in more detail. To represent a fixed point, we introduce a

cohort-to-cohort representation that indicates graphically for every birth cohort to which birth cohorts the daughter cells of dividing cells that were born in this certain birth cohort, contribute. This representation was implemented by Bart Mesuere using the D3 JavaScript library. For the MM2 model, we find a similar non-trivial fixed point. The focus in the rest of the chapter is on the MM1 model. In Section 5.2 we discuss the numerical effects that occur when calculating the fixed point by iterating the map and compare the impact of changing δ and `reltol` (the scalar relative tolerance in the age integration) on the speed and precision of the calculation of the fixed point. In Section 5.3 we investigate how the convergence behaviour changes under variation of the parameter S^0 (the nutrient concentration in the feeding bottle of the chemostat). For some values of S^0 non-trivial fixed points coexist with cycles, both stable in terms of the map. In Section 5.4 we investigate how sensitive the fixed point (for a parameter value for which there also exists a stable cycle) is to perturbations and in Section 5.5 we use the observed cyclic behaviour for several S^0 values to make an "educated" guess for the fixed point. In Section 5.6 three fixed point continuation methods for free S^0 are discussed: a very simple method that uses a previous fixed point as prediction (we call this the zero-order prediction method), a continuation method where the prediction of the new fixed point is based on the 2 previously computed fixed points (we call this the chord prediction) and a modified version of the pseudo-arclength continuation method. In Section 5.7 we discuss the results of these fixed point continuation methods for a free dilution rate D. In Section 5.8 we discuss which D value is optimal to maximize the yield and in Section 5.9 we study the non-trivial fixed points that have very few cohorts for small D values. As a generalisation of our population model, we consider two adaptations in the last sections. In Section 5.10 we adapt one of the cell division criteria proposed by Tyson and Novák and study the effect on the resulting fixed point. And finally, in Section 5.11, we incorporate a more extended model for the cell cycle as internal structure for the cells, namely the budding yeast model of Tyson and Novák.

In **Chapter 6** we document how the study of our structured population models was implemented. The code is written in `C++` using `Microsoft Visual C++ 2010 Express`. We summarize which external libraries we used and explain how to get the code operating with `Microsoft Visual C++ 2010 Express`. We give an overview of the data structures, functions and global constants and give examples of how these functions were used for some of the calculations in

Chapter 5.

Finally, in **Chapter 7** we discuss different possibilities for future work on this subject.

CHAPTER 2

Preliminaries

Overview

In this chapter we give an introduction to different topics needed to comprehend this thesis. Section 2.1 describes the key features of the cell cycle and how they can be translated in a mathematical model. In Section 2.2 an overview of population modeling techniques is given. Unstructured population models are briefly discussed, but the main focus of the section (and this thesis) are population models with an internal structure for the individual. An overview of the main mathematical forms for such models is given in Section 2.2.1, an example of a model for cells with nutrient dependency that uses the progression through the cell cycle as individual structure is given in Section 2.2.2 and a numerical method to calculate the equilibrium of a structured cell population model is discussed in Section 2.2.3. In the last Section 2.3 mathematical methods are introduced that will be used in this thesis. In Sections 2.3.1 and 2.3.2 some background on the bifurcation theory of respectively ODEs and maps is given. Finally, in Section 2.3.3 the method of pseudo-arclength continuation is discussed.

2.1 Mathematical modeling of the cell cycle

In the recent review articles [83] and [84] Tyson and Novák give examples of the lines of thought that, over the last 50 years, led to our current understanding of cellular information processing, respectively use the modeling of the eukaryotic cell cycle as illustration of the general principles of mathematical modeling in biology. This section is mostly based on the chapter "Cell cycle controls" of Tyson and Novák in [81].

2.1.1 The phases of the cell cycle

The cell cycle is the succession of events by which a growing cell duplicates its components, in particular its genetic material, and divides into two daughter cells. This process of cell growth and cell division for an eukaryotic cell is usually divided into four stages (see Figure 2.1), namely the first Gap phase (G1), Synthesis (S, where the DNA-replication takes place), the second Gap phase (G2) and Mitosis (M, where the cell divides). When Mitosis is finished, the daughter cells each have the same number and kind of chromosomes in their nuclei as the parent cell originally had, as well as the same "hardware" (proteins, RNA, phospholipid bilayers, carbohydrates). A daughter cell then enters the first Gap phase G1 during which it mainly grows and prepares for a possible division later on. At the critical point "Start" (the transition from G1 to S phase), a cell confirms that internal and external conditions are opportune to start a new round of DNA synthesis and division and the cell enters S phase. This transition is irreversible: once a cell commences with the DNA synthesis, it goes to completion. During the Synthesis phase, each chromosome copies itself. By the end of the S phase, each chromosome consists of a pair of sister chromatids held together by specific tethering proteins, called cohesins. This is followed by the second gap phase G2 during which the cell grows further and prepares for replication. The cell then enters Mitosis, which has a metaphase and an anaphase. During the metaphase, the so-called metaphase spindle or mitotic spindle is formed. The replicated chromosomes are then attached by microtubules to opposite poles of the spindle. At the second critical point "Finish", the cell enters anaphase. The cohesins are removed so that the sister chromatids can be segregated to opposite sides of the cell. Shortly thereafter, the cell itself divides and two daughter cells in G1 stage are born, after which the cycle can start again.

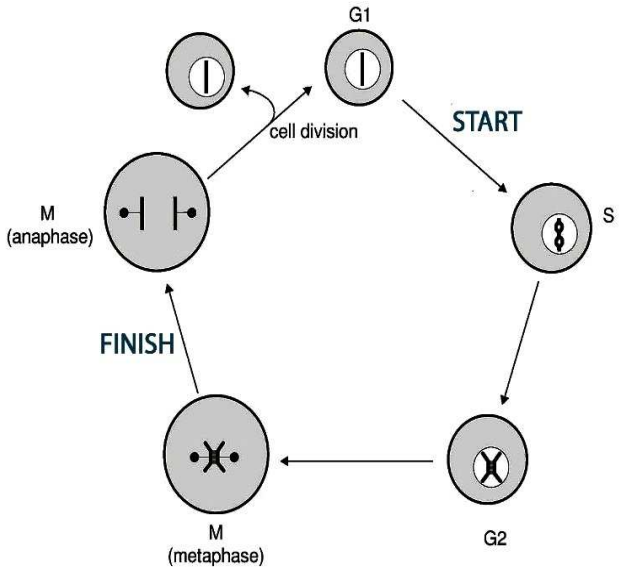

Figure 2.1: Schematic illustration of the different stages of the cell cycle (by Tyson and Novák in [81]). A newborn cell is initially in the first Gap phase G1. At Start, the cell enters into the Synthesis phase S where it replicates its chromosomes. After a second Gap phase G2, the cells enters into the Mitosis phase M. During the metaphase of Mitosis, the replicated chromosomes are aligned on the metaphase spindle. At the Finish transition, the cell is ready to divide and shortly thereafter it divides during the anaphase of Mitosis and produces two daughter cells which are initially in G1 phase.

The chromosome cycle of the cell (DNA synthesis and sister chromatid separation) runs in parallel with the growth cycle whereby the cell's hardware is duplicated and partitioned, more or less evenly, between the daughter cells. There are exceptions to this rule, such as oocytes (immature eggs in an ovary) which grow very large without dividing and embryos (fertilized eggs) which divide rapidly without growing. But in general, the long-term viability of a cell line depends on balanced growth and division. This is achieved in most cells by a size requirement for the Start transition. Before cells can commit to chromosome replication and division, cells must grow to a critical size. A second regulatory constraint is to hold off the Finish transition if the DNA replication or chromosome alignment have not been performed properly, in order to avoid daughter nuclei without a full set of chromosomes.

It may be more convenient to subdivide the process into the parts G1 and S-G2-M, seperated by the two transitions (Start and Finish) as proposed by K. Nasmyth [65]. This is supported in the work of Tyson & Novák (see [2, 4, 10, 11, 14, 66, 67, 81, 79, 80]).

2.1.2 Molecular mechanisms of the cell cycle

The modern history of the study of the cell cycle goes back to 1976 when Paul Nurse identified the gene cdc2 in fission yeast [70]. This gene controls the progression of the cell cycle from the G1 phase to the S phase and the transition from the G2 phase to Mitosis. In 2001 P. Nurse received the Nobel Prize for Physiology or Medicine "for the discovery of cyclin and cyclin-dependent kinase, central molecules in the regulation of the cell cycle" together with Leland Hartwell and Timothy Hunt for their work on the key regulators of the eukaryotic cell cycle [69].

A network of molecular signals control the cell cycle events, of which the central components are cyclin-dependent protein kinases (Cdks). When a Cdk is paired with a suitable cyclin partner, it becomes an active kinase and it can phosphorylate target proteins involved in cell cycle events (see Figure 2.2). By attaching phosphate groups to these target proteins, the latter's behaviour can be changed. Cdk targets include proteins involved in DNA replication, chromosome condensation, spindle formation, and other crucial events of the cell cycle. For example, a Cdk-cyclin dimer can phosphorylate histones (proteins involved in DNA packaging) and thereby initiate chromosome condensation at the G2-M transition.

The activity of Cdk can be regulated throughout the cell cycle in different ways. When the concentration of a cyclin in the cell is low, the cyclin detaches from the Cdk, inhibiting the activity of the kinase. It is generally assumed that the Cdks are always present in abundance throughout the cell cycle, which means that their activity is regulated by the availability of the cyclins. The availability of the cyclins depends on the rates of cyclin synthesis and degradation, which can be regulated during the cell cycle. Secondly, a CKI (cyclin-dependent kinase inhibitor) can bind to a Cdk-cyclin dimer and make it inactive. The synthesis and degradation rates of CKIs are also cell-cycle regulated. Finally, a specific tyrosin residue can phosphorylate Cdk and inhibit the activity of Cdk. The phosphorylation state of Cdk

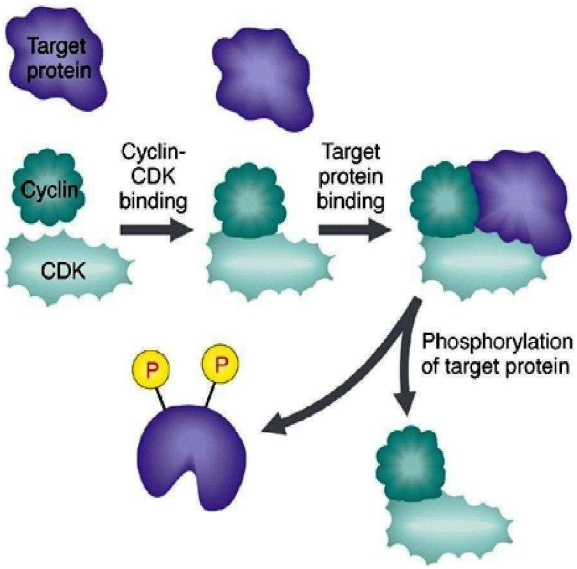

Figure 2.2: Cyclin-dependent kinase (Cdk) requires a cyclin partner in order to be activated and recognize proper targets. It phosphorylates a target protein using ATP as the phosphate donor. Source: `http://www.bio.miami.edu/dana/250/25008_13.html`.

fluctuates during the cell cycle as the activities of the tyrosine kinase Wee1 and the tyrosine phosphatase[1] Cdc25 fluctuate. The different regulatory mechanisms of Cdk are illustrated in Figure 2.3.

It was soon discovered that there exists a bewildering variety of cyclins and cyclin-dependent kinases. The information about proteins that control cell growth and cell division in eukaryotes is enormous and the process of growth and division is very complex. An additional problem is that the details of the process vary from organism to organism and that many parameters are hard to determine by experimental methods. Experimental results are therefore usually obtained in a few special cases, like budding yeast (*Saccharomyces cerevisiae*), fission yeast (*Schizosaccharomyces pombe*) and frog egg cells. However, in lower eukaryotes the number of components is much lower than in higher eukaryotes, namely one Cdk and 2 to 4 crucial cyclins. This indicates that one Cdk is sufficient and that Cdk-cylin dimers can

[1] A phosphatase can dephosphorylate other proteins by removing attached phosphate groups, as opposed to a kinase.

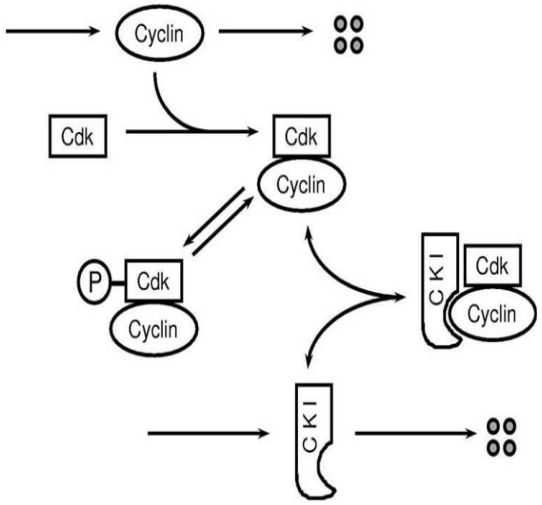

Figure 2.3: Possible regulation mechanisms of Cyclin-dependent kinase activity (by Tyson and Novák in [81]): by availability of the cyclin subunits, by phosphorylation of the Cdk subunit and by binding to the inhibitor CKI.

substitute one another to a large extent. Tyson and Novák describe the cell cycle as "a complex, nonlinear, dynamical system of interactions between Cdk-cyclin dimers and their regulatory agents: transcription factors, degradation machinery, CKIs, and tyrosine-modifying enzymes" [81]. The basic principles are by now reasonably well understood and present-day researchers work hard on building mathematical models, mainly in the form of nonlinear ODEs systems. We will discuss the quite extended model for the cell cycle of budding yeast of John Tyson and Béla Novák [81]. Tyson and Novák also propose a "Toy model" in [81] which already covers the basic modeling and bifurcation ideas. We will come back to this "Toy model" in Section 3.3.

The two cell-cycle phases G1 and S-G2-M (as proposed by Nasmyth [65], see Figure 2.1) are correlated with low and high Cdk activity respectively. During G1 phase, cyclin levels are low because cyclin mRNA synthesis is inhibited and cyclin protein is rapidly degraded. At Start (beginning of the S-G2-M phase), cyclin synthesis is induced and cyclin degradation is inhibited. The initial rise in Cdk activity initiates the replication of DNA (S phase) but a further increase is needed to drive the cell into the Mitosis anaphase. At Finish, a group of proteins, called the anaphase-

promoting complex APC is activated. The APC attaches a "destruction label" to specific target proteins, which then are degraded by the cell's specific proteolyticic (protein-killing) components. The APC consists of a core complex of polypeptids plus two proteins called Cdc20 and Cdh1. Activation of Cdc20 at Finish is needed for the degradation of the cohesins at anaphase and for the activation of Cdh1. Cdc20 and Cdh1 need to be both active to label cyclins for degradation, so that the control system can return to the low activity of cyclins in the G1 phase. The situation is complicated since cyclin-Cdk activates Cdc20 but inhibits Cdh1.

The transitions Start and Finish are usually irreversible ([80], see also [67] for a discussion of this ancient notion in terms of reaction networks) and related to the antagonistic relationship between the central components of the cell cycle machinery. The APC extinguishes Cdk activity by destroying cyclins, while cyclin-Cdk dimers inhibit APC by phosphorylating Cdh1. This leads, roughly speaking, to two stable steady states of the systems: a G1 state with high Cdh1-APC activity and low cyclin-Cdk activity, and a S-G2-M state with high cyclin-Cdk activity and low Cdh1-APC activity. For further information on the biochemical background and the history of the subject we refer to [11, 13, 81] and references therein.

2.1.3 Mathematical model of the cell cycle

During the last fifteen years, Tyson and Novák presented several mathematical models for the cell cycle, of which we will discuss the budding yeast model [81, 80]. This model is based on their understanding of the controls in budding yeast (see Figure 2.4), but it can be applied to other organisms such as fission yeast and mammalian cells by changing the regulatory proteins (see Table 10.2 in [81]). Budding yeast is the common yeast used in baking ("baker's yeast") and brewing ("brewer's yeast"). In Figure 2.5 the basic mechanisms are illustrated. Solid lines correspond to transitions between different states of the chemical components and indicate the creation and degeneration of the chemical components. Dashes lines show the influence of a chemical component on a certain pathway. Note that the cyclin is denoted by CycB.

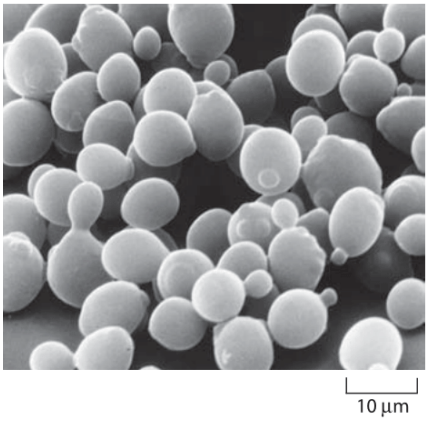

Figure 2.4: Electron micrograph of budding yeast *Saccharomyces cerevisiae* cells (Ira Herskowitz and E. Schabtach at `http://book.bionumbers.org/how-big-is-a-budding-yeast-cell/`).

The following interactions are visualized in Figure 2.5:

- The antagonistic relationship between cyclin-Cdk and Cdh1-APC is clear in (1) and (2).
- Cdc20 is synthesized during S-G2-M phase of the cell cycle since the concentration of CycB-Cdk is high during this phase (see (3)).
- At the Finish transition, Cdc20 is activated abruptly by signals from the mitotic process itself, represented by the Intermediary Enzyme (IE) (see (4) and (5)).
- When there are mitotic spindle abnormalities, a Cdc20-inhibitory signal is generated through the Mad pathway (see (6)).
- Interactions (5), (4), (7) and (2) form a negative feedback loop at exit from mitosis. This is re-enforced by the ability of activated Cdc20 ($Cdc20_A$) to directly degrade CycB-Cdk (see (8)).
- CKI (Cyclin-dependent Kinase Inhibitor) is prevalent in G1 phase and inhibits CycB-Cdk (see (9)).
- When CKI is phosphorylated, it is labelled for rapid proteolysis[2] (see (10)). CKI can be phosphorylated by its antagonist CycB-Cdk (see (11)), but since

[2] Proteolysis is the breakdown of proteins into smaller polypeptides or amino acids.

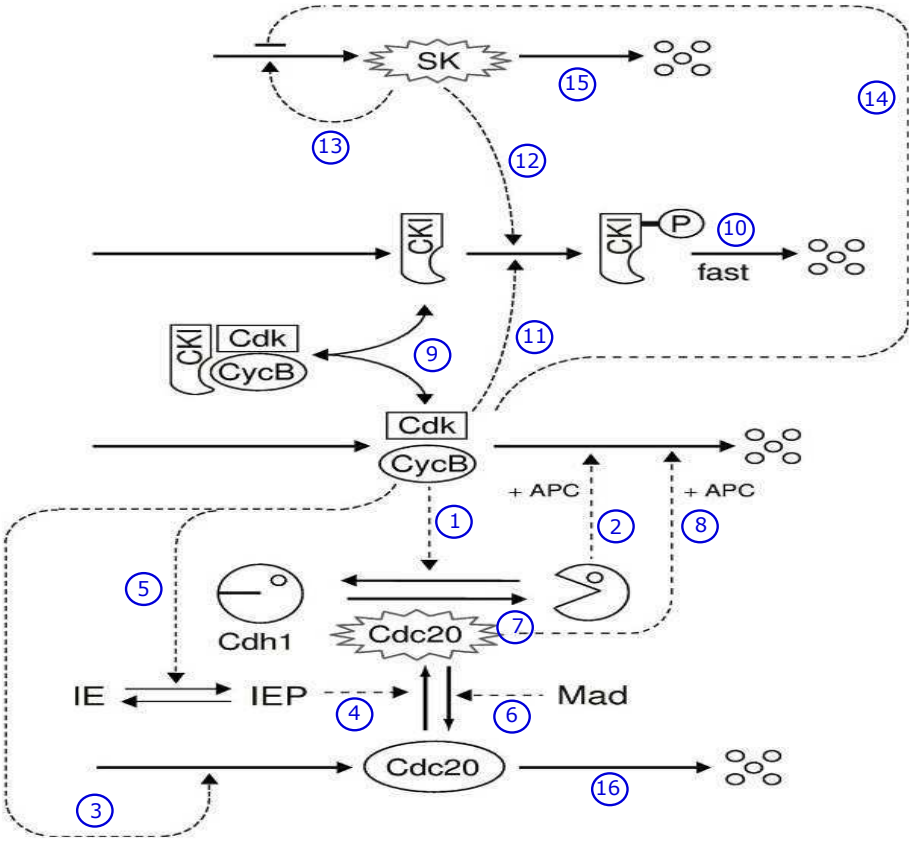

Figure 2.5: The basic cell cycle engine in budding yeast cells (by Tyson and Novák in [81]). Dynamical properties of this mechanism are expressed quantitatively by sets of kinetic equations in the form of differential equations such as (2.1).

the CycB-Cdk activity is low in G1 phase, this interaction is not sufficient to make the CKI level drop. In order to leave the G1 state, the cell produces a Starter Kinase (SK) whose task is to phosphorylate CKI (see (12)). SK is produced in late G1 phase and helps CycB-Cdk overcome its enemies.

- SK has a positive effect on its own production (see (13)). The positive feedback loop is made with the help of the Transcription Factor (TF) for SK: SK activates TF and the activated TF enforces the production of SK. CycB-Cdk has a negative effect on the production of SK (see (14)) by deactivating TF, which plays a role when the CycB-Cdk level is again high enough in S-G2-M phase.
- Both SK and Cdc20 have a constant degradation rate (see (15) and (16)).

Tyson and Novák translated the network in Figure 2.5 into the following model for the cell cycle of budding yeast for a fixed cell mass m:

$$\begin{aligned}
\frac{\mathrm{d}[CycB]_T}{\mathrm{d}t} &= k_1 - (k_2' + k_2''[Cdh1] + k_2'''[Cdc20]_A)[CycB]_T,\\
\frac{\mathrm{d}[Cdh1]}{\mathrm{d}t} &= \frac{(k_3' + k_3''[Cdc20]_A)(1-[Cdh1])}{J_3 + 1 - [Cdh1]} - \frac{(k_4 m[CycB] + k_4'[SK])[Cdh1]}{J_4 + [Cdh1]},\\
\frac{\mathrm{d}[Cdc20]_T}{\mathrm{d}t} &= k_5' + k_5'' \frac{(m[CycB])^n}{J_5^n + (m[CycB])^n} - k_6[Cdc20]_T,\\
\frac{\mathrm{d}[Cdc20]_A}{\mathrm{d}t} &= \frac{k_7[IEP]([Cdc20]_T - [Cdc20]_A)}{J_7 + [Cdc20]_T - [Cdc20]_A} - \frac{k_8[Mad][Cdc20]_A}{J_8 + [Cdc20]_A} - k_6[Cdc20]_A,\\
\frac{\mathrm{d}[IEP]}{\mathrm{d}t} &= k_9 m[CycB](1-[IEP]) - k_{10}[IEP],\\
\frac{\mathrm{d}[CKI]_T}{\mathrm{d}t} &= k_{11} - (k_{12}' + k_{12}''[SK] + k_{12}'''m[CycB])[CKI]_T,\\
\frac{\mathrm{d}[SK]}{\mathrm{d}t} &= k_{13}' + k_{13}''[TF] - k_{14}[SK],\\
\frac{\mathrm{d}[TF]}{\mathrm{d}t} &= \frac{(k_{15}'m + k_{15}''[SK])(1-[TF])}{J_{15} + 1 - [TF]} - \frac{(k_{16}' + k_{16}''m[CycB])[TF]}{J_{16} + [TF]},
\end{aligned} \tag{2.1}$$

where

$$\begin{aligned}
[CycB] &= [CycB]_T - [Trimer],\\
[Trimer] &= \frac{2[CycB]_T[CKI]_T}{\Sigma + \sqrt{\Sigma^2 - 4[CycB]_T[CKI]_T}},\\
\Sigma &= K_{eq}^{-1} + [CycB]_T + [CKI]_T.
\end{aligned}$$

The values of the fixed parameters in (2.1) are given in Table 2.1 (see [81]). The concentrations of the proteins in (2.1) are dimensionless quantities since Tyson and Novák define their values as grams of the protein per grams of total cell mass. The cell mass m is also introduced as a dimensionless quantity, although it is less obvious in their work why this is the case. $[CycB]_T$ is a measure for the total concentration of the S-G2-M cyclin. We denote the concentration of the CycB-Cdk dimer as $[CycB]$ and the concentration of the CycB-Cdk-CKI trimer as $[Trimer]$, hence $[CycB]_T = [CycB] + [Trimer]$. The total concentration of CKI is denoted by $[CKI]_T$. We have $[CKI]_T = [CKI] + [Trimer]$ since we assume that the phosphorylated CKI's degenerate fast. $[TF]$ represents the concentration of active Transcription Factor for SK. The concentration of Cdh1-APC is denoted by $[Cdh1]$. Typically, $[CycB]_T$ is low and $[Cdh1]$ is high during G1 phase and vice versa during S-G2-M phase.

Table 2.1: Fixed pameters in (2.1).

Parameter (value in min^{-1})		**Parameter** (value in min^{-1})		**Parameter** (value dimensionless)	
$\mathbf{k_1}$	0.04	$\mathbf{k_9}$	0.1	$\mathbf{J_3}$	0.04
$\mathbf{k_2'}$	0.04	$\mathbf{k_{10}}$	0.02	$\mathbf{J_4}$	0.04
$\mathbf{k_2''}$	1	$\mathbf{k_{11}}$	1	$\mathbf{J_5}$	0.3
$\mathbf{k_2'''}$	1	$\mathbf{k_{12}'}$	0.2	$\mathbf{J_7}$	0.001
$\mathbf{k_3'}$	1	$\mathbf{k_{12}''}$	50	$\mathbf{J_8}$	0.001
$\mathbf{k_3''}$	10	$\mathbf{k_{12}'''}$	100	$\mathbf{J_{15}}$	0.01
$\mathbf{k_4}$	35	$\mathbf{k_{13}'}$	0	$\mathbf{J_{16}}$	0.01
$\mathbf{k_4'}$	2	$\mathbf{k_{13}''}$	1	$\mathbf{n}$	4
$\mathbf{k_5'}$	0.005	$\mathbf{k_{14}}$	1	[**Mad**]	1
$\mathbf{k_5''}$	0.2	$\mathbf{k_{15}'}$	1.5	$\mathbf{K_{eq}}$	1000
$\mathbf{k_6}$	0.1	$\mathbf{k_{15}''}$	0.05		
$\mathbf{k_7}$	1	$\mathbf{k_{16}'}$	1		
$\mathbf{k_8}$	0.5	$\mathbf{k_{16}''}$	3		

In building this model it is assumed (this is called a quasi-equilibrium hypothesis) that CycB-Cdk-CKI trimers are always in equilibrium with CKI monomers and CycB-Cdk dimers. To be precise, the reactions

$$Trimer \underset{k^-}{\overset{k^+}{\rightleftharpoons}} CKI \; + \; CycB-Cdk \tag{2.2}$$

lead to the equation

$$\frac{d[Trimer]}{dt} = k^-[CKI][CycB] - k^+[Trimer],$$

using the law of mass action. We assume that the reactions in (2.2) are so fast that the equilibrium is attained instaneously, i.e.

$$[Trimer] = K_{eq}[CycB][CKI] = K_{eq}([CycB]_T - [Trimer])([CKI]_T - [Trimer]),$$

where $K_{eq} = \frac{k^-}{k^+}$. From this follows the expression for $[Trimer]$ in (2.1).

The equations in (2.1) can be related to the regulatory path. The equation for $[CycB]_T$ can be interpreted as follows:

- k_1 is the constant production rate of CycB which combine rapidly with the Cdk's (available in abundance),
- k_2' is the (constant) degradation rate of the CycB-Cdk dimers,
- k_2'' is the constant in the law of mass action that models the degradation of CycB-Cdk dimers by Cdh1-APC complexes (see (2)),
- k_2''' is the constant in the law of mass action that models the degradation of CycB-Cdk dimers by the direct influence of activated Cdc20 (see (8)).

The equation for the total concentration of Cdc20 $[Cdc20]_T$ consists of:

- A constant production rate k_5'.
- The term $k_5'' \frac{(m[CycB])^n}{J_5^n + (m[CycB])^n}$, which represents the increase in production rate due to $m[CycB]$ (see (3)) as a Hill equation with $n = 4$. See Figure 2.6 for a graphical interpretation of this term.
- The term $-k_6[Cdc20]_T$, which represents the constant degradation rate of Cdc20 (see (16)).

The equation for the concentration of active Cdc20 $[Cdc20]_A$ is more complex and consists of:

- No constant production rate since Cdc20 is only activated through IEP.
- The term $\frac{k_7[IEP]([Cdc20]_T - [Cdc20]_A)}{J_7 + [Cdc20]_T - [Cdc20]_A} = \frac{k_7[IEP][Cdc20]_{IA}}{J_7 + [Cdc20]_{IA}}$ (where Cdc20_{IA} is inactive Cdc20), which represents the activation of Cdc20_{IA} by IEP (see (4)) as Michaelis-Menten kinetics. The maximum production (or activation) rate is $k_7[IEP]$. The production rate is half the maximum rate if $[Cdc20]_{IA} = J_7$.
- The term $-\frac{k_8[Mad][Cdc20]_A}{J_8 + [Cdc20]_A}$, which represents the deactivation of Cdc20_A by Mad (see (6)) as Michaelis-Menten kinetics. The maximum deactivation rate is $k_8[Mad]$ and when $[Cdc20]_A = J_8$ the deactivation rate is half of this maximum rate.

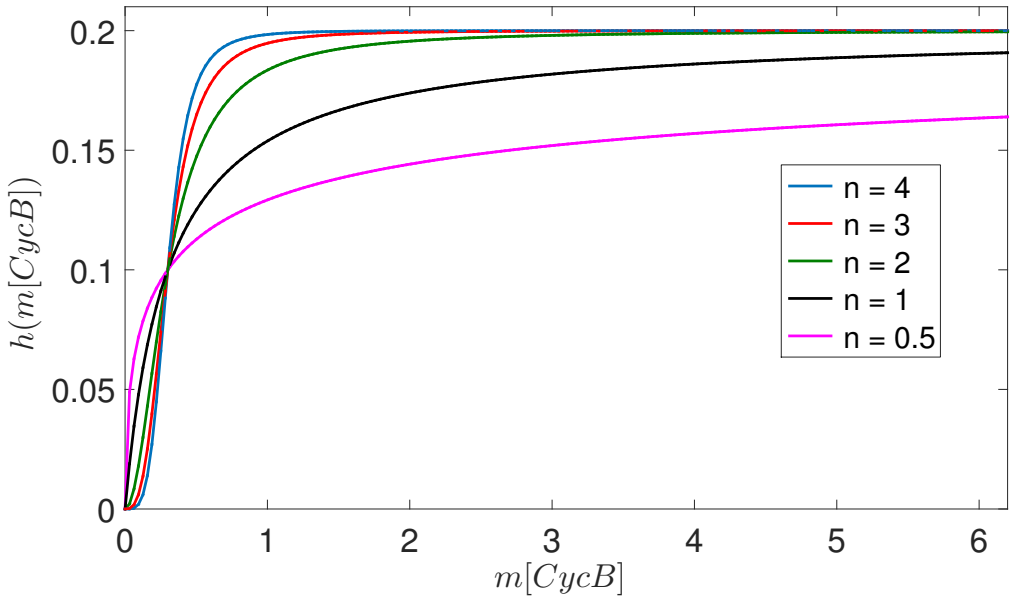

Figure 2.6: Hill equation $h(m[CycB]) = k_5'' \frac{(m[CycB])^n}{J_5^n + (m[CycB])^n}$ as a function of $m[CycB]$ for different n values ($k_5'' = 0.2, J_5 = 0.3$). With increasing n the function is initially steeper and the maximal value of k_5'' is faster approximated.

- The term $-k_6[Cdc20]_A$, which represents the constant degradation rate of Cdc20 (see (16)).

The equation for $[Cdh1]$ (meaning $[Cdh1\text{-}APC]$) can be interpreted as follows:

- The first term represents the production rate of Cdh1 by active Cdc20 (see (7)). This is a special type of Michaelis-Menten kinetics where the influence of $[Cdh1]$ on its production rate is more complex: if $[Cdh1]$ is very large, the production rate is maximal (equal to $k_3' + k_3''[Cdc20]_A$); when $[Cdh1] = 0$, the production rate is the maximal one divided by $J_3 + 1$; and when $[Cdh1] = 1 - J_3$ the production rate is half of the maximal one.

- The second term represents the degradation rate due to $m[CycB]$ (see (1)) and $[SK]$ (indirect in the diagram as SK acts as an ally of the CycB-Cdk dimers) as Michaelis-Menten kinetics. The maximum degradation rate is $k_4 m[CycB] + k_4'[SK]$ and when $[Cdh1] = J_4$ the deactivation rate is half of this maximum rate.

The other equations in (2.1) can be interpreted and linked to Figure 2.5 in a similar way. Note that the CycB-Cdk dimers always occur in (2.1) as the product $m[CycB]$.

As a rationale for this, Tyson and Novák argue that the CycB-Cdk dimers are assembled in the cytoplasma of the cell and then move into the nucleus of the cell. This means that for interactions with the other chemical components of the nucleus, the concentration of the dimers in the whole cell is important (instead of only the concentration in the nucleus $[CycB]$). Tyson and Novák assume that the concentration of CycB-Cdk dimers in the whole cell is proportional to the cell mass m and $[CycB]$. More general information about biochemical kinetics and the corresponding mathematical equations can be found in [8, 32, 34, 64].

For a growing cell, Tyson and Novák add one equation with logistic growth:

$$\frac{dm}{dt} = \mu m(1 - \frac{m}{m_{max}}). \tag{2.3}$$

The rationale of this assumption is that cells grow at a constant relative rate μ when they are small and there is some intrinsic threshold m_{max} above which they cannot grow.

2.2 Population models

Mathematical models in population biology have become increasingly popular to help understand the involved dynamic processes and to make practical predictions. In this section we cover the basic concepts in population models, explain the different subdivisions that exist and give some examples. This section is based on the book of J.A.J. Metz and O. Diekmann [62] and on the introduction of the lecture notes on "Modeling Population Dynamics" of A.M. de Roos (University of Amsterdam, 2011).

The basic unit in population models is the individual organism. Changes in the population are the result of events that occur within the individual organisms (such as ageing, birth, death and immigration). It is often useful to distinguish individual organisms from each other on the basis of a certain set of physiological characteristics (e.g. age, size, saturation level of a predator, sex) that influence its life history. The chance to die may, for example, change as an individual grows older. The collection of physiological traits used to characterize the individuals within a population, is called the *individual state* or *i-state*. Let Ω denote the set of possible *i*-states, called the *i-state space*.

A population model must reflect how a population, a certain group of individual organisms, will behave in the future, given the current state of the population and the environmental conditions that influence the time evolution of the population. The current state of the population is called the *population state* or *p-state* and can be represented by a frequency distribution $n : \Omega \to \mathcal{R}^+$. This frequency distribution evolves over time due to physiological processes within the individuals, births and deaths. Environmental conditions that have an impact on the dynamics of the populations can, for example, be temperature, food abundance, number of predators or competitors. Actually, one should consider all external factors to the individual itself since the nature of the other individuals could also play a role in, for example, a model with cannibalism. The *i*-state of an individual can determine its potential reproduction (or growth or chance of death or ...), while the environmental conditions can modulate this potential and adapt it to the realized reproduction.

Unstructured population models are models in which the individual organisms of the population are assumed to be identical or can be represented by an "average"

type. The p-state then simply is the total number of individuals within the population N. Unstructured population models can be classified into two large classes: the discrete-time models and the continuous-time models. Discrete-time models are used to model populations for a single species where the total number of individuals only changes in discrete steps, e.g. annual plants. The state of the population is only determined at specific points in time and must relate N at time $t+1$ with N at the previous time point t. In general, this is done by a difference equation of the form

$$N_{t+1} = f(N_t), \tag{2.4}$$

with $f(N_t)$ a nonlinear function of N_t, or the equivalent map

$$N \mapsto f(N). \tag{2.5}$$

When there is a continuous overlap of generations, continuous-time models for a single species are used. The general equation for such a model is in the form of an Ordinary Differential Equation (ODE):

$$\frac{\mathrm{d}N(t)}{\mathrm{d}t} = B(N) - D(N) + M(N), \tag{2.6}$$

with $B(N)$ the birth rate, $D(N)$ the death rate and $M(N)$ the migration rate. We give two of the first widely discussed continuous-time models as an example. One of the simplest models without migration was first proposed by Malthus in 1798 [60]:

$$\frac{\mathrm{d}N(t)}{\mathrm{d}t} = bN - dN = rN, \tag{2.7}$$

with b and d positive constants and $r = b - d$. This model is density independent, meaning that the death and birth rate at the individual level are not influenced by any aspect of the population. If $N(0) = N_0$, the solution of (2.7) is

$$N(t) = N_0 \exp{(b-d)t}. \tag{2.8}$$

When $b > d$ the population grows exponentially and when $b < d$ it dies out. A more realistic model with limitation is the famous logistic model, proposed by Verhulst in 1838 [85]:

$$\frac{\mathrm{d}N(t)}{\mathrm{d}t} = rN\left(1 - \frac{N}{K}\right), \tag{2.9}$$

with r and K positive constants, where K represents the carrying capacity of the environment. In this model the population cannot grow beyond some maximum density (which for example can depend on the available food resources).

There also exist unstructured population models for the interaction between different species, in both discrete-time and continuous-time. The main types of interaction are a predator-prey situation, competition and mutualism or symbiosis. Examples of unstructured population models can be found in many textbooks of mathematical biology, e.g. [55] and [64].

A relatively new approach to model complex systems composed of autonomous, interacting agents is called agent-based modelling or individual-based modelling. The agents have certain behavioral rules, often quite simple rules, and can interact with other agents which then influences their behaviour. Agent-based models put emphasis on modelling the heterogeneity of agents across a population and can also incorporate learning rules. It offers a way to model social systems that are composed of agents who interact with and influence each other, learn from their experiences, and adapt their behaviours in such a way that they are better suited to their environment. Applications exist in a wide range of areas, and also in biology applications exist, such as e.g. modelling of the adaptive immune system. More information about agent-based modelling and simulation can be found in the tutorial [59].

In the following Sections 2.2.1, 2.2.2 and 2.2.3 we will focus on structured population models. More information about population models (both unstructured and structured) can be found in [76].

2.2.1 Structured population models

One of the first books that extensively handles the subject of structured population models and gives an overview of the subject is “The Dynamics of Physiologically Structured Populations” by J.A.J. Metz and O. Diekmann, published in 1986 [62]. Some further elaborate examples can be found in [5, 21, 33, 55, 64, 78]. Structured population models can be classified using several criteria. In analogy with unstructured population models, they can either describe a discrete-time setting, which

leads to matrix population models, or a continuous-time setting, which leads to integral population models. Another criterion leads to the dichotomy of deterministic structured population models versus stochastic population models. But first, let us focus on the internal structures that are most commonly used in structured population models, as the choice of the internal structure is one of the most important choices in building such a model.

Choice of structure

The choice of the internal structure depends on which individual physiological characteristics one assumes to be important for the behaviour of the individual in terms of growing, dying, replicating and so on. Individuals that have the same initial *i*-state and experience the same environmental conditions, will follow the same life-track (except for a stochastic model with a low number of individuals of that *i*-state). So depending on which behaviour one wishes to distinguish, the *i*-state is chosen.

Commonly used one-dimensional internal structures are an age structure or a stage structure (examples can be found in [5, 33, 19]), a size structure (examples in [9, 19, 24, 25]) and a spatial structure (examples in [5]). Some structured population models include a higher-dimensional *i*-state, e.g. the model of Heijmans in [62] that uses both age and size to model a population of cells.

Main mathematical forms

We can make the distinction between the following main mathematical forms used to model the frequency distribution at population level: matrix population models in a discrete-time setting and integral population models in a continuous-time setting. The latter type can be subdivided in delay differential equation models for populations described by discrete stages and partial differential equation models for populations described in terms of a continuous variable or several continuous variables.

Matrix population models use discrete stages as possible *i*-states and only calculate the frequency distribution at discrete time points, say $t \in \mathcal{N} = \{0,1,2,\ldots\}$. The *p*-distribution at time *t* is given by the following vector (assuming there are *k* discrete

stages):

$$n(t) = \begin{pmatrix} n_1(t) & \dots & n_k(t) \end{pmatrix}^T, \tag{2.10}$$

with $n_l(t)$ the number of individuals with i-state l at time t. A matrix population model is then defined by

$$n(t+1) = A\,n(t), \tag{2.11}$$

with A a $k \times k$-matrix called the Population Projection Matrix (PPM) or transition matrix. $A = \left(a_{ij}\right)$ contains the life-history parameters, more precisely a_{ij} determines how the number of stage j individuals at time t influences the number of stage i individuals at time $t+1$:

$$n_i(t+1) = \sum_{j=1}^{k} A_{ij}\, n_j(t). \tag{2.12}$$

For the simplest form of A, one assumes that individuals cannot stay in a stage for more than one time period and A is time-independent. Typically age then is the stage class variable. In that case, the transition matrix has the general form

$$A = \begin{pmatrix} s_1 b_1 & s_1 b_2 & \dots & s_1 b_{k-1} & s_1 b_k \\ s_2 & 0 & \dots & 0 & 0 \\ 0 & s_3 & \dots & 0 & 0 \\ \vdots & \vdots & & \vdots & \vdots \\ 0 & 0 & \dots & s_k & 0 \end{pmatrix}. \tag{2.13}$$

s_i is the probability of surviving from stage $i-1$ to stage i and b_i is the average number of individuals produced by an individual of stage i. $s_1 b_i$ is then the average number of individuals produced by an individual of stage i that actually survive from birth until stage 1, which is also called the fecundity of stage i. A transition matrix of the form (2.13) is known as a Leslie matrix [57].

A more general stage class variable is the stage in the life cycle. This could emerge when there really are discrete life stages (e.g. caterpillar - cocoon - butterfly) or could be defined by some measurable feature (e.g. individual size or weight) that predicts the fate of the individual over the next time period. Stage-classified matrix models can be graphically represented by life cycle graphs (see [33]).

The long-run behaviour (meaning for $t \to \infty$) of the population defined by (2.11)

with a constant matrix A is

$$n(t) \approx c_1 \lambda_1^t w_1, \tag{2.14}$$

with λ_1 the eigenvalue of A with the greatest modulus (the dominant or principal eigenvalue), w_1 the corresponding (right) eigenvector and c_1 a constant. The Perron-Frobenius theorem (see e.g. [33]) can be used to check if the principal eigenvalue is real and positive and if all components of w_1 are positive. If this is the case, in the long-run the total population size grows exponentially at rate λ_1 and w_1 represents the stable stage distribution.
Matrix population models could be, besides linear and deterministic as we discussed, nonlinear (with $A(t)$ dependent on $n(t)$) or stochastic (with A not constant in time). More information about matrix population models can be found in [7, 8, 15, 33]. In [7] Integral Projection Models (IPMs) are discussed and compared to matrix population models for single-species stage structured populations. IPMs use continuous life history functions that are functions of a continuous range of stages and models time as a discrete variable.

Delay differential equation (DDE) models use discrete stages as possible *i*-state, and describe its dynamics in continuous time. The *p*-distribution at time t is given by the vector (2.10). An ordinary differential equation describes the change over time for each of the n_i's. These equations can contain a time-delay term to account for the time that the individuals need to move through a stage, so the models of this mathematical form consist of delay differential equations. E.g. if we consider a model with 2 stages (a juvenile stage and an adult stage), a possible model is

$$\frac{\mathrm{d}n_1(t)}{\mathrm{d}t} = -\mu_1 n_1(t) + b_2 n_2(t) - b_2 n_2(t-\tau_1) e^{-\mu_1 \tau_1}, \tag{2.15}$$

$$\frac{\mathrm{d}n_2(t)}{\mathrm{d}t} = b_2 n_2(t-\tau_1) e^{-\mu_1 \tau_1} - \mu_2 n_2(t), \tag{2.16}$$

with μ_i the death rate of stage i, τ_1 the duration of stage 1 (the juvenile stage) and b_2 the rate of production of offspring by an individual of stage 2 (the adult stage since only adults can produce offspring). The number of juveniles that become adults at time t is the number of juveniles born at time $t-\tau_1$ (so the number of juveniles that by time t have gone through the whole juvenile stage) times the probability that they survived the τ_1 time units.
DDE models seem particularly well suited for models of interacting species, see e.g.

[6]. More information can be found in [78].

Partial differential equation (PDE) models use a continuous variable (or continuous variables) to describe the *i*-state and describe the dynamics in continuous time. E.g. if the *i*-state is described by the age a of the individual, the *p*-state is the density distribution $n(a,t)$. The dynamics of $n(a,t)$ can be described by two equations:

$$\frac{\partial n(a,t)}{\partial t} + \frac{\partial n(a,t)}{\partial a} = -\mu(a)\, n(a,t) \tag{2.17}$$

$$n(0,t) = \int_0^\infty b(a)\, n(a,t)\, \mathrm{d}a. \tag{2.18}$$

$\mu(a)$ represents the mortality rate and $b(a)$ represents the reproductive rate, both as a function of the age of the individual. Equation (2.17) describes the changes in the density distribution as individuals age and die. (2.17) is known both as McKendrick's partial differential equation [61] and as the Von Foerster equation [86]. Equation (2.18) is the boundary condition, it describes how many newborns are produced at time t in total. A dependence on the environment can be included in the equations through direct density dependency of the parameters or through dynamic feedback from the resources.
As another example of a PDE model we consider a size-structured population with a dependency on the resources in the environment R [19]. The growth equation for an individual of size s with available resources R is

$$\frac{\mathrm{d}s}{\mathrm{d}t} = g(s,R), \tag{2.19}$$

$$s(0) = s_b. \tag{2.20}$$

All individuals are born with the same size s_b. The *p*-state is the density distribution $n(s,t)$. The model consists of the following equations:

$$\frac{\partial n(s,t)}{\partial t} + \frac{\partial g(s,R)\, n(s,t)}{\partial s} = -\mu(s,R)\, n(s,t) \tag{2.21}$$

$$g(s_b,R)\, n(s_b,t) = \int_{s_b}^\infty b(s,R)\, n(s,t)\, \mathrm{d}s, \tag{2.22}$$

with $\mu(s,R)$ the rate of mortality and $b(s,R)$ the reproduction rate. (2.22) is the boundary condition of the model. The initial condition of the density distribution is given as $d(s)$: $n(s,0) = d(s)$. The model is completed with an equation for the food

dynamics:

$$\frac{\mathrm{d}R}{\mathrm{d}t} = G(R) - \int_{s_b}^{\infty} I(s,R)\, n(s,t)\mathrm{d}s, \tag{2.23}$$

where $G(R)$ is the intrinsic nutrient change (independent of the individuals) and $I(s,R)$ is the feeding rate of an individual of size s at available resources R.
More information and other examples of PDE models can be found in [62, 64]. The PDE models include the most detailed information on the vital rates, but are also the most difficult to study numerically and analytically. The PDE may be reduced to a renewal equation by the method of characteristics (see e.g. [8, 33]). For numerical studies the "Escalator Boxcar Train" (EBT) method, developed by Goudriaan [37] and de Roos [16, 18], can be used. The basis of the EBT formulation as an approximation of a partial differential equation model, consists of the subdivision of the population into distinct cohorts of individuals, the description of the dynamics of the individuals in these cohorts by ODEs and the renumbering or shifting of these cohorts at equidistant time intervals (when a new cohort is formed). The discrete time element is introduced by the decision to stop to add newborns to a particular cohort and to start the formation of a new cohort. The resulting approximation may be rather high-dimensional (though finite-dimensional), depending on the size of the time interval and the resulting number of cohorts. Individuals in a cohort are originally not identical, but are represented by using mean values for the *i*-state variables. An advantage of the EBT method is that it allows a biological interpretation of the cohorts.

Deterministic or stochastic

In the study of structured population models most of the considered models are deterministic. A model is deterministic when, given an initial state of the population, the trajectory (dynamic path) of the system is unique. In stochastic models the initial state of the population determines a family of possible trajectories, each with a certain probability to occur. In [62], the authors restrict themselves to deterministic models. The reasoning behind this choice is not that one assumes that the behaviour of the individual organism is pre-determined (given the environmental conditions), stochastic effects at the individual level may still play a role, but one invokes the "law of large numbers". This law states that a deterministic model can be viewed as the limit of a particular stochastic model when there are sufficiently many individuals. A reason to prefer a deterministic model to a stochastic one is that they allow a more

detailed investigation than mere simulations of the dynamics. Stochastic effects also tend to blur structural features in the behaviour of deterministic models.

2.2.2 Nutrient dependency in structured cell population models

Structured cell population models need to incorporate a mechanism for the cell division. In the introductory chapter of [62] Metz and Diekmann explain a relatively simple model in which the only *i*-state variable is the cell size. To incorporate the observed variability in cell sizes at division, Metz and Diekmann include a stochastic element for the fission. Two different options are considered: either a function for the probability to undergo fission per unit of time is given as a function of the cell size, or the division size is stochastically determined at the birth of a cell (if the cell is still alive when it reaches this size). These two options correspond to two different possibilities to determine the size at division: during the progression of its life (or during specific stages) or at birth. We will come back to this in Section 5.10. In [62] the model is extended by incorporating nutrient limitations. A feedback-loop between population size and nutrient availability is modeled by introducing a nutrient level S and specifying how the individual growth rate depends on S, how nutrient consumption depends on both S and the cell size, and what the intrinsic changes (independent of the consumption by cells) of S are.

In [71] a structured cell population model for phytoplankton is considered in which the progression through the cell cycle is used as internal structure, instead of cell size or age. A simple chemostat model is presented with the distribution of cells along the cell cycle as p-state. The progression through the cell-cycle is represented by a continuous variable p. The transition point hypothesis is used, which says that an environmental factor has no effect on cell progression beyond a certain transition point p_c in the cycle. p is normalized so that cells are born with $p = 0$ and the average cell divides at $p = 1$. The nutrient concentration inside the chemostat S is used as the environmental factor influencing the cell cycle. The cell cycle is subdivided into a nutrient-dependent segment $[p_0, p_c]$ and a nutrient-independent segment (see Figure 2.7).

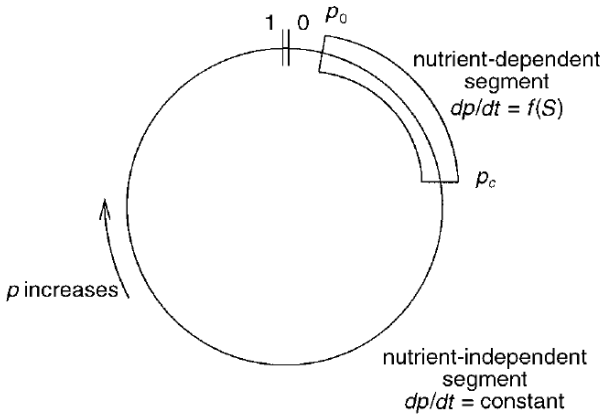

Figure 2.7: Schematic representation of the cell cycle subdivided in a nutrient-dependent segment and a nutrient-independent segment. [71]

The maturation velocity $v = \frac{dp}{dt}$ is a constant v_c in the nutrient-independent segment and is proportional to the nutrient uptake for $p \in [p_0, p_c]$:

$$\frac{dp}{dt} = v_0 \frac{S}{K+S}.$$

The population equations of the model are

$$\begin{aligned} \frac{\partial N(p,t)}{\partial t} + v_0 \frac{S}{K+S} \frac{\partial N(p,t)}{\partial p} &= -(D+B(p))\,N(p,t) \quad \text{for } p \in [p_0, p_c], \\ \frac{\partial N(p,t)}{\partial t} + v_c \frac{\partial N(p,t)}{\partial p} &= -(D+B(p))N(p,t) \quad \text{otherwise,} \end{aligned}$$

with D the dilution rate of the chemostat and $B(p)$ the division rate. The boundary condition for the flux of newborn cells (under the assumption that each cell divides into two daughter cells) at $p = 0$ is

$$N(0,t)\,v_c = 2\int_0^\infty B(p)N(p,t)\,dp,$$

and the dynamics for the nutrient are given by

$$\frac{dS}{dt} = D(S_{in} - S) - V_m \frac{S}{K+S} N_{tot},$$

with S_{in} the inflowing nutrient concentration and V_m the maximum uptake rate of nutrient by a cell. The authors assume that differences in nutrient uptake among

cells can be considered negligible, so the total uptake is computed by multiplying individual nutrient uptake by the total number of cells N_{tot}. Simulation results demonstrate oscillations in cell numbers and population structure. The authors derive similar results for a model that includes nutrient storage by the cells. The found dynamics were different from existing studies and resulted from the novelty in the considered studies in [71]: the interaction between nutrient and the progression through the cell cycle.

In Chapter 4 we will introduce a chemostat population model for unicellular organisms in which the internal structure of the cell is related to the cell cycle in a more complex manner than the one-dimensional representation by p in [71].

2.2.3 Equilibrium computations

Efficient numerical techniques for equilibrium computations of physiologically structured population models have only been developed since 1997. As an example, we will describe the method to calculate the equilibrium of size-structured models using the numerical approach in [23, 53, 54, 22], following the appendix in [19]. We consider a size-strucured model described by (2.19)-(2.23). The resource density at equilibrium is denoted by $\tilde{R}$. The size of an individual at age a that has experienced a constant resource density $\tilde{R}$ during its lifetime is denoted as $s(\tilde{R},a)$. $H(\tilde{R},a)$ represents the probability that an individual is still alive at age a when it has experienced $\tilde{R}$. An equilibrium must satisfy two conditions. First, the total number of offspring produced by a individual during its entire lifetime (commonly indicated by R_0) should equal 1. Second, the total consumption rate of resource by the individuals should equal the production rate of the resource. The first equilibrium condition corresponds to

$$\int_0^\infty b(s(\tilde{R},a),\tilde{R})\,H(\tilde{R},a)\,\mathrm{d}a = 1. \tag{2.24}$$

If we denote the total population birth rate by $\tilde{B}$, the second equilibrium condition corresponds to

$$\tilde{B}\int_0^\infty I(s(\tilde{R},a),\tilde{R})\,H(\tilde{R},a)\,\mathrm{d}a = G(\tilde{R}). \tag{2.25}$$

The central idea of the equilibrium computation approach in [23, 53, 54, 22] is that, given the functions $I(s,R)$, $g(s,R)$, $b(s,R)$ and $\mu(s,R)$, the integrals in (2.24) and (2.25) can be computed by numerically solving a coupled set of ODEs. Given a

constant resource density $\tilde{R}$, $s(\tilde{R},a)$ and $H(\tilde{R},a)$ are the solutions of the following system of ODEs:

$$\frac{\mathrm{d}s(\tilde{R},a)}{\mathrm{d}a} = g(s,\tilde{R}), \quad s(\tilde{R},0) = s_b, \tag{2.26}$$

$$\frac{\mathrm{d}H(\tilde{R},a)}{\mathrm{d}a} = -\mu(s,\tilde{R})\,H(\tilde{R},a), \quad H(\tilde{R},0) = 1. \tag{2.27}$$

If we denote the expected cumulative reproduction by all individuals up to age a as $\Theta(\tilde{R},a)$ and the expected cumulative consumption by all individuals up to age a as $\Psi(\tilde{R},a)$, then:

$$\Theta(\tilde{R},a) = \int_0^a b(s(\tilde{R},\omega),\tilde{R})\,H(\tilde{R},\omega)\,\mathrm{d}\omega,$$

$$\Psi(\tilde{R},a) = \int_0^a I(s(\tilde{R},\omega),\tilde{R})\,H(\tilde{R},\omega)\,\mathrm{d}\omega.$$

$\Theta(\tilde{R},a)$ and $\Psi(\tilde{R},a)$ are solutions of the following system of ODEs:

$$\frac{\mathrm{d}\Theta(\tilde{R},a)}{\mathrm{d}a} = b(s(\tilde{R},a),\tilde{R})\,H(\tilde{R},a), \quad \Theta(\tilde{R},0) = 0, \tag{2.28}$$

$$\frac{\mathrm{d}\Psi(\tilde{R},a)}{\mathrm{d}a} = I(s(\tilde{R},a),\tilde{R})\,H(\tilde{R},a), \quad \Psi(\tilde{R},0) = 0. \tag{2.29}$$

The equilibrium conditions (2.24) and (2.25) can be represented as

$$\Theta(\tilde{R},\infty) = 1, \tag{2.30}$$

$$\tilde{B}\,\Psi(\tilde{R},a) = G(\tilde{R}). \tag{2.31}$$

Standard numerical techniques can be used to locate the roots of this system of equations. To compute the left-hand side of the equations, the set of ODEs (2.26), (2.27), (2.28) and (2.29) has to be integrated numerically from zero to infinite age. In practice the integration is done until the survival probability $H(\tilde{R},a)$ has reached some chosen lower threshold or until a chosen maximum value for the age is obtained. (2.30) does not depend on $\tilde{B}$, so the value of $\tilde{B}$ can be obtained by (2.31) once $\tilde{R}$ is known from (2.30). It follows that the equilibrium $(\tilde{R},\tilde{B})$ of a size-structured population model can be calculated in an iterative manner. Starting with an initial estimate $\tilde{R}^{(0)}$ for $\tilde{R}$, the set of ODEs (2.26), (2.27), (2.28) and (2.29) is integrated and a new estimate $\tilde{R}^{(1)}$ is obtained from (2.30). This cycle is repeated using the

new estimate $\tilde{R}^{(i)}$, until $\tilde{R}^{(i)}$ converges and $\tilde{R}$ is found. From (2.31) follows the corresponding $\tilde{B}$ of the equilibrium.

Extensions of this method include continuation of stability boundaries as a function of two model parameters, for more details see [17, 53, 54].

2.3 Mathematical methods

2.3.1 Background on bifurcation theory of ODEs

A dynamical system can be a continuous-time system described by Ordinary Differential Equations (ODEs) or a discrete-time system described by a map. In this section we give a brief summary of possible bifurcations in the case of a continuous-time system. In the next Section 2.3.2 the bifurcations of a discrete-time system that we will meet in Chapter 5, are briefly described. For more background on bifurcation theory we refer to [3] and [56]. As in [2, 14, 39, 66, 79, 80], our work in Chapter 3 relies heavily on bifurcation theory of ODEs.

Generally, we consider the following system of ODEs

$$\dot{x}(t) = f(x(t), \alpha), \tag{2.32}$$

with $x \in \mathcal{R}^n = (x_1, \ldots, x_n)$ the vector of the system variables, $\alpha \in \mathcal{R}^p = (\alpha_1, \ldots, \alpha_p)$ the parameter vector and $f : \mathcal{R}^n \times \mathcal{R}^p \to \mathcal{R}^n$ a non-linear sufficiently smooth function dependent on x and α. An equilibrium of (2.32) is a point $x_0 \in \mathcal{R}^n$ for which $f(x_0, \alpha) = 0$ so that $x(t) \equiv x_0$ is a solution of (2.32). The Jacobian matrix A of the system at x_0 is then defined as $\left(\frac{\partial f}{\partial x}\right)_{x=x_0}$:

$$A = \begin{pmatrix} \frac{\partial f_1}{\partial x_1} & \cdots & \frac{\partial f_1}{\partial x_n} \\ \vdots & & \vdots \\ \frac{\partial f_n}{\partial x_1} & \cdots & \frac{\partial f_n}{\partial x_n} \end{pmatrix}_{x=x_0}. \tag{2.33}$$

The equilibrium x_0 is linearly asymptotically stable if all eigenvalues λ of A have a negative real part, which implies that there exists a certain neighbourhood so that all solutions that start in it converge to the equilibrium. If at least one eigenvalue has a positive real part, the equilibrium is unstable.

A limit cycle of (2.32) is a periodic orbit (also called cycle) $x(t)$ with a neighbourhood in which there are no other periodic orbits.

A bifurcation of (2.32) occurs when an arbitrarily small change of one of the parameter values α_i (the bifurcation parameter) causes a change in the qualitative nature of the solutions of (2.32), for example the appearance or disappearance of equilibria or changes in the stability of the equilibria. We will briefly describe the different types of codimension-1 bifurcations that we will encounter in Chapter 3. Codimension 1 means that they can generically be expected in systems with one free parameter. Consequently, curves of such bifurcations can be expected in two-parameter problems.

- A Hopf point H is characterized by a Jacobian matrix with a pair of purely imaginary eigenvalues $\pm i\omega$. Depending on other eigenvalues and higher-order terms, stable or unstable periodic orbits are born in a Hopf point. A Hopf bifurcation is called supercritical when a stable equilibrium loses stability and stable periodic orbits are born. When the equilibrium becomes unstable and unstable periodic orbits coexist with the stable equilibria, the Hopf bifurcation is called subcritical.

- A Limit Point bifurcation LP is the bifurcation associated with the appearance of an eigenvalue $\lambda_1 = 0$. When crossing the bifurcation parameter value, two equilibria with different stability properties collide and disappear.

- A Limit Point of Cycles bifurcation (LPC) is a limit point for limit cycles. Generically, at such a parameter value two cycles with different stability properties collide and disappear.

In Chapter 3 we will also encounter homoclinic orbits. An orbit corresponding to a solution $x(t)$ is called homoclinic to the equilibrium point x_0 if $x(t) \to x_0$ as $t \to \pm\infty$. There are two types of such orbits with codimension 1, namely orbits homoclinic-to-hyperbolic-saddle (HHS, also known as saddle-loop SL) if x_0 is a hyperbolic saddle[3], and orbits homoclinic-to-saddle-node (HSN, also known as SNIC and SNIPER) if x_0 is a saddle-node[4].

In the bifurcation studies we use MatCont, which is a numerical bifurcation software

[3] A hyperbolic saddle is an equilibrium with no eigenvalues on the imaginary axis and a positive and negative real eigenvalue.

[4] A saddle-node is an equilibrium which is a LP, i.e. has an eigenvalue 0.

package in Matlab for the interactive study of continuous-time dynamical systems and its bifurcations. It is freely available at [20]. We use MatCont repeatedly in Chapter 3.

2.3.2 Background on bifurcation theory of maps

Consider the following discrete-time dynamical system

$$x \mapsto f(x, \alpha), \tag{2.34}$$

with $x \in \mathcal{R}^n$ the system vector, $\alpha \in \mathcal{R}^p$ the parameter vector and $f : \mathcal{R}^n \times \mathcal{R}^p \to \mathcal{R}^n$ a non-linear map which is sufficiently smooth with respect to x and α. A fixed point of the system (2.34) for $\alpha = \alpha_0$ is a point x_0 that is mapped to itself, i.e. $f(x_0, \alpha_0) = x_0$. The eigenvalues of the Jacobian matrix evaluated at a fixed point x_0 are called multipliers. If the absolute values of the multipliers are all smaller than 1, x_0 is asymptotically stable. If for at least one multiplier the absolute value is bigger than 1, x_0 is unstable. In discrete-time dynamical systems with $n = 1$, two types of bifurcations occur generically: the Period Doubling bifurcation and the Limit Point bifurcation. We will illustrate this by means of two basic one-dimensional maps.

The figures in this section are made using MatContM. MatContM is an interactive Matlab toolbox for numerical analysis of bifurcations of fixed points and periodic orbits of maps, developed by W. Govaerts, R. Khoshiar Ghaziani, Yu. A. Kuznetsov and H. Meijer who released the first version in 2008 [40]. It is freely available at `http://sourceforge.net/projects/matcont/`.

First, consider the one-dimensional map

$$x \mapsto -(1+\alpha)x - x^3, \tag{2.35}$$

with one parameter α [56]. The bifurcation diagram of (2.35) for free α is depicted in Figure 2.8. For $\alpha < 0$, the fixed point $x_0 = 0$ is stable. For α equal to 0, a Period Doubling (PD) bifurcation (also called flip bifurcation) occurs: the fixed point changes stability and a 2-cycle emerges. A 2-cycle for $\alpha = \alpha_0$ is a pair (x_1, x_2) for which $f(x_1, \alpha_0) = x_2$ and $f(x_2, \alpha_0) = x_1$. The PD bifurcation in Figure 2.8 is subcritical: for $\alpha < 0$ the fixed point is stable and there exists an unstable 2-cycle,

for $\alpha > 0$ the fixed point is unstable. A supercritical PD corresponds with a stable fixed point for parameter values smaller than the critical one, and with an unstable fixed point and a stable 2-cycle for parameter values bigger than the critical value. The one-dimensional map

$$x \mapsto -(1+\alpha)x + x^3, \tag{2.36}$$

has a supercritical PD for $\alpha = 0$ (see [56]). In both the subcritical and supercritcial cases, a Period Doubling bifurcation occurs when one of the multipliers crosses -1.

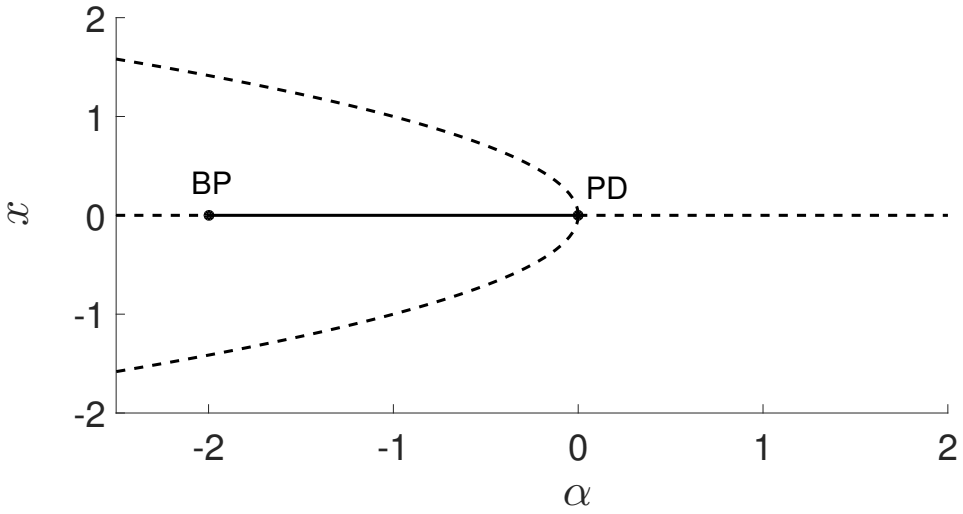

Figure 2.8: Bifurcation diagram of the discrete-time system (2.35) for free α. Solid curves represent stable fixed points and dotted curves unstable fixed points.

Next, consider the one-dimensional map

$$x \mapsto -(1+\alpha)x - x^3 + x^5, \tag{2.37}$$

as an extension of (2.35). In Figure 2.9 the bifurcation diagram of (2.37) for free α is depicted. For $\alpha = 0$ there is a subcritical PD bifurcation, as for (2.35). Additionally, for $\alpha = -\frac{1}{4}$ the system has two Limit Point bifurcations (also called Saddle-Nodes or fold bifurcations). This occurs generically when a multiplier equals 1 and results in 2 fixed points (a stable and an unstable) that "collide" and disappear. The symmetry-breaking branch points (BP) in Figures 2.8 and 2.9 are of no consequence for the present thesis.

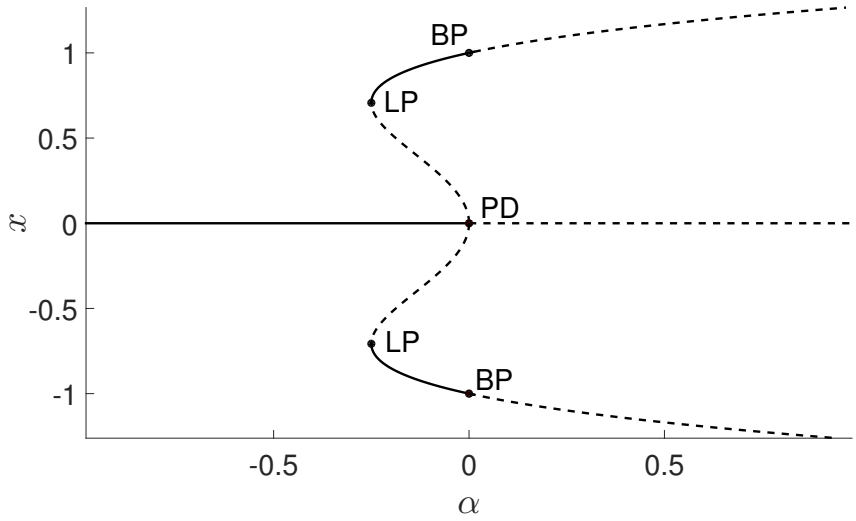

Figure 2.9: Bifurcation diagram of the discrete-time system (2.37) for free α. Solid curves represent stable fixed points and dotted curves unstable fixed points.

For a discrete-time dynamical system with $n \geq 2$, besides PD and LP bifurcations, Neimark-Sacker bifurcations can occur. A Neimark-Sacker (NS) bifurcation occurs when a pair of multipliers $e^{\pm i\theta}$ with $0 < \theta < \pi$ crosses the unit circle for a parameter value α_c. When α passes α_c the fixed point loses stability. If the bifurcation is supercritical, then a unique closed invariant curve bifurcates from it. All orbits starting near the closed invariant curve, except for orbits starting exactly at the unstable fixed point, tend to the curve under iterations of the map. An example of a 2-dimensional map with a supercritical NS bifurcation (see [56]) is

$$\begin{aligned}\begin{pmatrix} x_1 \\ x_2 \end{pmatrix} \mapsto (1+\alpha) \begin{pmatrix} 0.1 & -\sqrt{0.99} \\ \sqrt{0.99} & 0.1 \end{pmatrix} \begin{pmatrix} x_1 \\ x_2 \end{pmatrix} \\ + (x_1^2 + x_2^2) \begin{pmatrix} 0.1 & -\sqrt{0.99} \\ \sqrt{0.99} & 0.1 \end{pmatrix} \begin{pmatrix} -1 & -2 \\ 2 & -1 \end{pmatrix} \begin{pmatrix} x_1 \\ x_2 \end{pmatrix}.\end{aligned} \tag{2.38}$$

The bifurcation diagram of (2.38) for free α is depicted in Figure 2.10. For $\alpha < 0$, the fixed point $(x_0, x_1) = (0,0)$ is stable. A supercritical NS bifurcation occurs for $\alpha = 0$, so the fixed point is unstable for $\alpha > 0$. In Figure 2.11 the closed invariant curves for positive α are depicted for α equal to 0.0001, 0.001, 0.01 and 0.1. The invariant curves become larger as α moves further away from the NS bifurcation

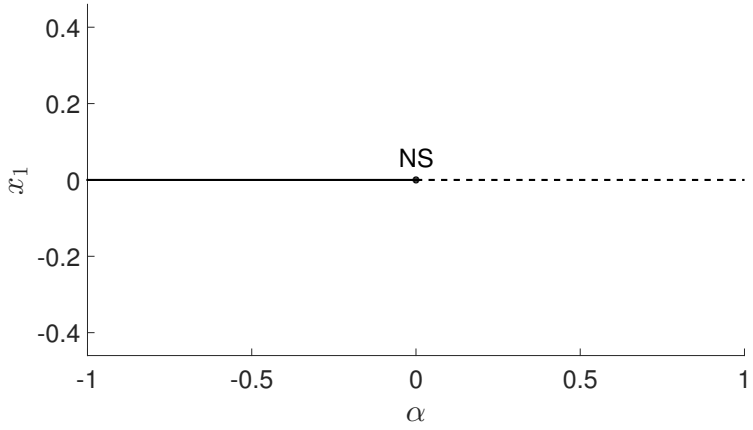

Figure 2.10: Bifurcation diagram of the discrete-time system (2.38) for free α. Solid curves represent stable fixed points and dotted curves unstable fixed points.

parameter, which is a typical behaviour of a NS bifurcation. There also exists a subcritical NS bifurcation in which unstable closed invariant curves coexist with stable fixed points.

In [51, 52] are more advanced bifurcation studies of discrete-time dynamical systems representing predator-prey systems.

2.3.3 Pseudo-arclength continuation

Consider the general problem of computing a curve implicitly defined by

$$F(X,a) = 0, \tag{2.39}$$

with $X \in \mathcal{R}^n$, $a \in \mathcal{R}$ the parameter of the problem, $F(X,a) \in \mathcal{R}^n$ and F a non-linear function. A numerical continuation problem is the problem to compute a branch of solutions to (2.39). Studies about numerical continuation can be found in [48, 72, 73, 49, 74, 1, 50, 38, 29].

The simplest strategy to solve continuation problems is using a prediction-correction algorithm, for which there are several options. Suppose that we know one solution point (X_1, a_1). A possible procedure to calculate the next solution point for $a = a_2$ is by taking (X_1, a_2) as the starting point for a Newton iteration for the system (2.39) as a system of n nonlinear equations in the n unknown components of X. The following

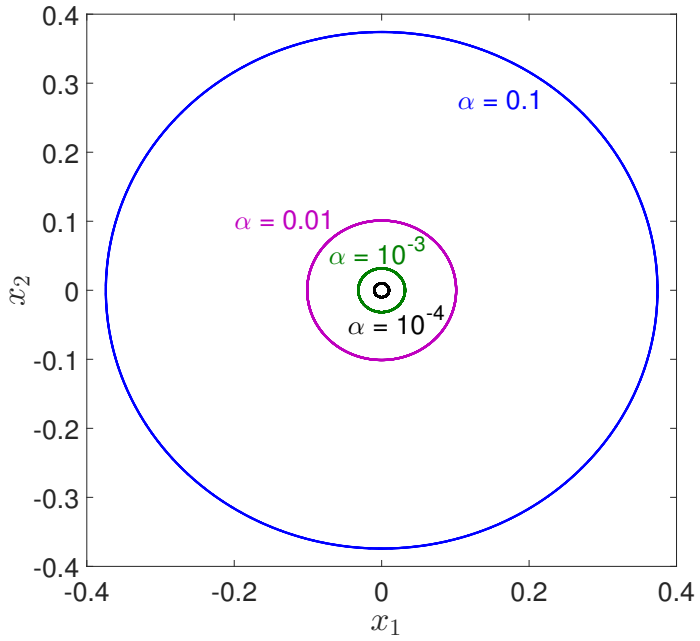

Figure 2.11: Closed invariant curves in (x_1, x_2)-plane for different values of $\alpha > 0$ for (2.38).

algoritm is then used:

$$X_2^{(0)} := X_1,$$

with for $n = 1, 2, \ldots$

$$\begin{aligned} \Delta X_2^{(n-1)} &:= -F_X^{-1}(X_2^{(n-1)}, a_2) \cdot F(X_2^{(n-1)}, a_2), \\ X_2^{(n)} &:= X_2^{(n-1)} + \Delta X_2^{(n-1)}, \end{aligned}$$

where $F_X(X_2^{(n-1)}, a_2)$ is the $n \times n$ Jacobian matrix $\left(\frac{\partial F_i}{\partial X_j}\right)$, evaluated in $(X_2^{(n-1)}, a_2)$. This is an example of a prediction-correction algorithm where $X_2^{(0)}$ is the prediction for X_2 and the Newton iteration is the correction, and is called parameter continuation. Convergence of $X_2^{(k)}$ to the solution point for $a = a_2$ may be defined by two parameter values $VarTolerance$ and $FunTolerance$. Convergence is achieved by $X_2^{(k)}$ if simultaneously $\|\Delta X_2^{(k-1)}\| < VarTolerance$ and $\|F(X_2^{(k)}, a_2)\| < FunTolerance$. For this elementary prediction-correction algorithm the step length h is $|a_k - a_{k-1}|$. A typical stepsize strategy is based on the use of four other parameters: $MinStepsize$, $MaxStepsize$, $InitStepsize$ and $MaxNewton$. One starts a continuation with the initial choice $h = InitStepsize$ and applies the following rules:

- If the number of Newton iterations needed for convergence to a point is smaller than or equal to $MaxNewton$, then h is multiplied by a constant factor (usually 1.3). If this value exceeds $MaxStepsize$, then it is decreased to $MaxStepsize$.
- If convergence is not obtained after $MaxNewton$ Newton iterations, or if something else goes wrong (for example, a singular Jacobian) then h is divided by two and the iteration is started again.
- If $h < MinStepsize$, then the algorithm is declared to have failed.

The applicability of parameter continuation is limited by the possible presence of limit points (points where the curve turns with respect to the parameter). Parameter continuation typically has convergence problems when a tends to the parameter value of the limit point.

The pseudo-arclength continuation, first published in the 1970s by H.B. Keller [48, 49], allows continuation of a solution branch past a limit point. Suppose that we know the solution point (X_1, a_1) and the unit tangent vector v_1 along the curve in this point. To compute the next point (X_2, a_2) and the corresponding tangent vector v_2, one predicts X_2 along the tangent line as follows (see Figure 2.12):

$$(X_2^{(0)}, a_2^{(0)}) = (X_1, a_1) + h_1 v_1,$$

and the Newton correction is based on the solution of the system

$$\left\{ \begin{array}{rcl} F(X,a) & = & 0 \\ < \begin{pmatrix} X - X_2^{(0)} \\ a - a_2^{(0)} \end{pmatrix}, v_1 > & = & 0 \end{array} \right. \tag{2.40}$$

with Jacobian matrix

$$\begin{bmatrix} F_X & F_a \\ v_1^T & \end{bmatrix}.$$

The system (2.40) has a clear geometric meaning: one looks for a point on the curve that lies in the hyperplane through the predicted $(X_2^{(0)}, a_2^{(0)})$ orthogonal to v_1. In this way the difficulties associated to turning points are resolved, cf. Figure 2.12. The strategy for adapting the steplength h_i is the same as for the natural parameter

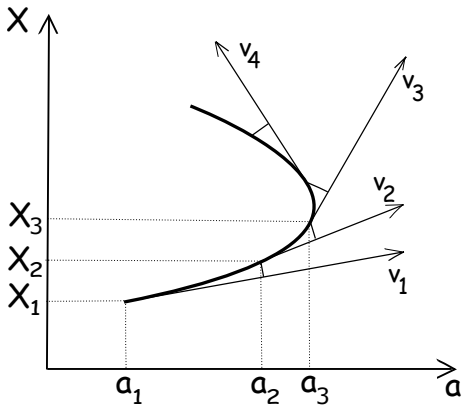

Figure 2.12: Pseudo-arclength continuation.

continuation. The new tangent vector v_2 can be calculated as a null vector of the $n \times (n+1)$ extended Jacobian matrix

$$[F_X(X_2, a_2), F_a(X_2, a_2)].$$

We normalize v_2 so that $\|v_2\| = 1$ and $< v_1, v_2 >$ is positive. The latter condition ensures that the orientation along the curve is preserved from point to point.

Pseudo-arclength continuation is used in the software package AUTO, originally developed by Eusebius Doedel, for continuation and bifurcation problems in ordinary differential equations [27, 28, 30, 31]. It is also used in MatCont [20], a Matlab successor package to AUTO, for the continuation of equilibria curves and bifurcation curves.

CHAPTER 3

Computational study of a budding yeast model of Tyson and Novák

The main results in this Chapter are published in [41].

Introduction

The cell cycle is the series of events that take place in a cell leading to the duplication of its components (in particular its DNA) and the splitting of the cell into two daughter cells. More information about the different phases of the cell cycle and the molecular mechanisms that play an important role in it, is given in Section 2.1.1 and 2.1.2. Many mathematical models have been proposed for the cell cycle. In Section 2.1.3 the equations of a model for the cell cycle of budding yeast developed by John Tyson and Béla Novák [81] are explained. In a series of papers and book chapters Tyson and Novák and their collaborators studied the cell cycle of various organisms as an alternation between two stable steady states of a system of kinetic equations (see e.g. [2, 14, 66, 67, 81, 79, 80]). The basic principles are already present in the simple model ("Toy model") proposed by Tyson & Novák [80]. In the same paper, Tyson & Novák also propose more realistic models for the cell cycle in the case of yeast cells and frog egg cells. A generic model of eukaryotic cell cycle regulation is described in [14] and linked to existing models, such as the budding yeast model in [10]. For more detail about the design principles of biological control systems

such as the cell cycle, we refer to [35, 79, 82]. The focus of this chapter is on the bifurcation analysis of the budding yeast model introduced in Section 2.1.3. Related work for the fission yeast cell cycle is in [36, 66]. The earliest and one of the most detailed papers that link bifurcation theory and cell cycle models is [4]; this paper deals with mitotic control in frog eggs. In [2] a bifurcation analysis of a similar (but different) budding yeast model is considered. It will be stressed in the text where our results match and differ from this related work.

Overview

In Section 3.1, we perform a bifurcation analysis of the budding yeast model in [81]. Our computational results were obtained by using the numerical bifurcation software MatCont [20]. We find that, unlike in [2], both the G1 phase and the S-G2-M phase contain stable steady states and stable periodic orbits. A further difference with the model in [2] is that the branch of equilibria loses stability through a Hopf point and not through an orbit homoclinic to saddle node or a limit point. A closer investigation of the periodic orbits in the model is done. The large stable periodic orbits (that are of particular interest for the interpretation of the model) lose their stability at a limit point of cycles and not through a homoclinic orbit as in [2].

In Section 3.2 the corresponding dynamic mass cell model is discussed. We investigate the model as a slow-fast system and compute the cell cycle efficiently as the fixed point of a map. In §3.2.4 we discuss the found relationship between the growth rate of the cell and the mass increase after DNA-replication. We relate this to a constant phase fraction of a periodic orbit traversed during S-G2-M phase and derive a relation between the growth rate and time spent in S-G2-M space. This relation is consistent with experimental results but was so far not found in other models. In §3.2.5 we investigate the robustness of the model under the change of the parameter k'_{13}, which is chosen as zero in [81] and whose presence is the only difference with the original model in [80]. We find that a non-zero k'_{13} not only leads to a premature transition from G1 to S phase and smaller cells (as is experimentally known and confirmed by other models) but can in this model also lead to nonviable cells.

Finally, in Section 3.3 we introduce the Toy model of Tyson and Novák, a sim-

plified model for the cell cycle. This model will be used to describe the internal structure of cells in the structured cell population model that we propose in Chapter 4.

3.1 The constant mass cell model of Tyson and Novák

The budding yeast equations for a constant cell mass m, as established in [81], are given in (2.1) and the values of its parameters are given in Table 2.1 in Section 2.1.3.

3.1.1 Equilibria in the constant mass model

The main equilibria of the constant mass cell equations are presented in Figure 3.1. For values of m below that of the Hopf point[1] H1 where $m = m_{REP} \approx 0.6546307$, the system has stable equilibria with $[CycB]_T$ below 0.1. This branch of equilibria loses stability at the supercritical Hopf point H1 where stable periodic orbits are born. We note that this bifurcation behaviour is different from the Toy model discussed in [81] (this Toy model is presented in Section 3.3), where stability is lost through an HSN orbit, and also from the models for budding yeast discussed in [2], where stability is lost either through an HSN orbit or through a limit point. The now unstable branch of equilibria turns at the limit point LP1 where $m \approx 0.67256764$ and turns again at the limit point LP2 where $m \approx 0.15237731$, where it regains stability. It further loses stability at the supercritical Hopf point H2 where $m \approx 0.58438062$ and regains it at the supercritical Hopf point H3 where $m \approx 1.0118642$. The other points marked with stars are all neutral saddle points, i.e. points where two real eigenvalues have sum zero. In most applications such points are not relevant but they become so if they are saddle equilibria of homoclinic orbits. The above described equilibrium curve hence contains three disjoint stable parts, namely before H1, between LP2 and H2, and beyond H3. The equilibria on the first branch correspond to G1 phase (low cyclin activity) and the second to S-G2-M phase (high cyclin activity). The third branch does not seem to be biologically relevant.

We note that the S-shaped curve in Figure 3.1 was also found in §IV of [2]. The authors also showed that in their model a switch between the two stable steady

[1] In Section 2.3.1 the necessary background on bifurcation theory of ODEs is given.

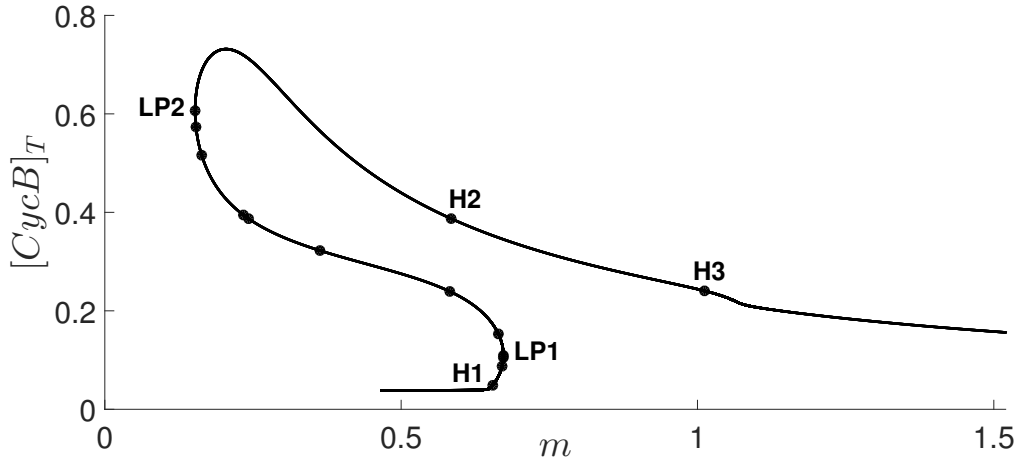

Figure 3.1: Equilibria curve of the constant mass cell equations (2.1).

states is possible. Moreover, they brought this in relation to experimentally found bistability in [12].

3.1.2 Periodic orbits in the constant mass model

A close investigation shows that the stable periodic orbits born at H1 are really short-lived. They die at an orbit homoclinic to saddle for $m = m_{Hom1} \approx 0.65506647$, see Figure 3.2. In the computer model they can be seen as oscillations in the G1 phase of the cell cycle. Of course, their region of existence is so small that we do not expect to see them in a cell.

The stable periodic orbits born at H2 have a longer life. They lose stability at a limit point of cycles for $m = m_{LPC1} \approx 0.67243138$, after which they return as unstable periodic orbits and move to a region which is irrelevant for the application, see Figure 3.3. They can be seen as oscillations in the S-G2-M phase of the cell cycle. In this situation, i.e. for the parameter values in Table 2.1, these orbits do not play a role in the normal cell cycle. However, we will see in §3.2.5 that for $k'_{13} = 0.2$ these cycles connect to the cycles born at H3. The cycles then exist throughout the region where the "normal" periodic orbits also exist and even for considerably larger values of m and so potentially have a big effect on the behaviour of the cell.

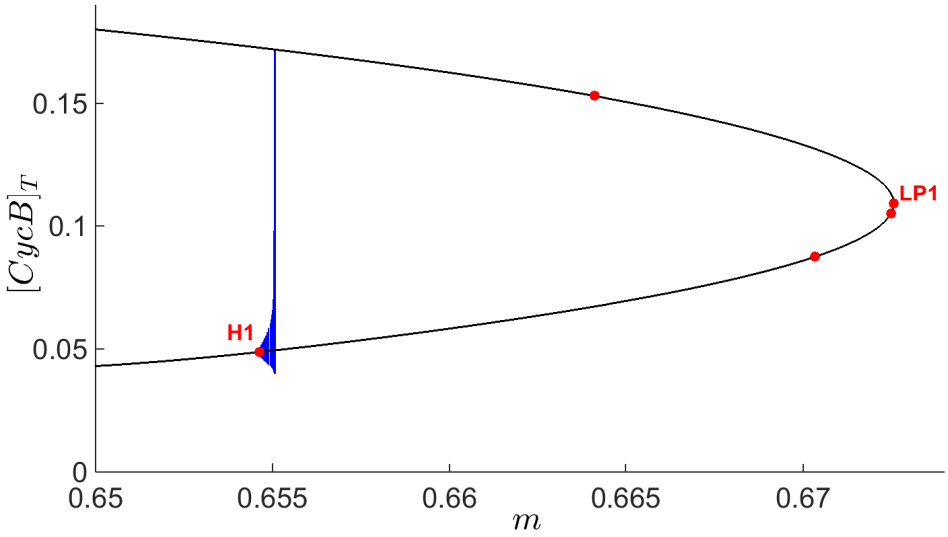

Figure 3.2: Periodic orbits born at the Hopf point H1 and dying at an orbit homoclinic to saddle.

The stable limit cycles born at H3 are the most important ones for the interpretation of the model. They first turn and become unstable at a limit point of cycles LPC2 for $m = m_{LPC2} \approx 0.86187777$, then turn again at another limit point of cycles LPC3 for $m = m_{LPC3} \approx 0.92913359$. Then m further decreases until the stable limit cycles turn again and become unstable at a limit point of cycles LPC4 for $m = m_{LPC4} \approx 0.65521623$, see Figure 3.4. These instable limit cycles die at another homoclinic orbit for $m = m_{Hom2} \approx 0.65521728$, see Figure 3.5, and thus only exist for a very small range of mass values. Note that for the parameter values in Table 2.1 the large stable limit cycles born at H3 lose stability through a limit point of cycles and not through a homoclinic orbit, as is the case for the models in [2] (more precisely, Chen's nine-variable model through a HHS orbit and the reduced three-variable model through a HSN orbit) and for the Toy model in [81] where stability is lost through a HSN orbit.

We note that $m_{Hom1} < m_{Hom2}$, but both are very close. Also, the region for which the periodic orbits born at H2 are stable overlaps both regions where the orbits born at H1 and H3 exist and are stable (see Figure 3.6). In Figure 3.7 we present in $([Cdh1], [CycB]_T)$-space the orbits close to the homoclinics born at H1 and H3 and the limit point of cycle orbit on the limit cycle curve born at H2. Interestingly, this

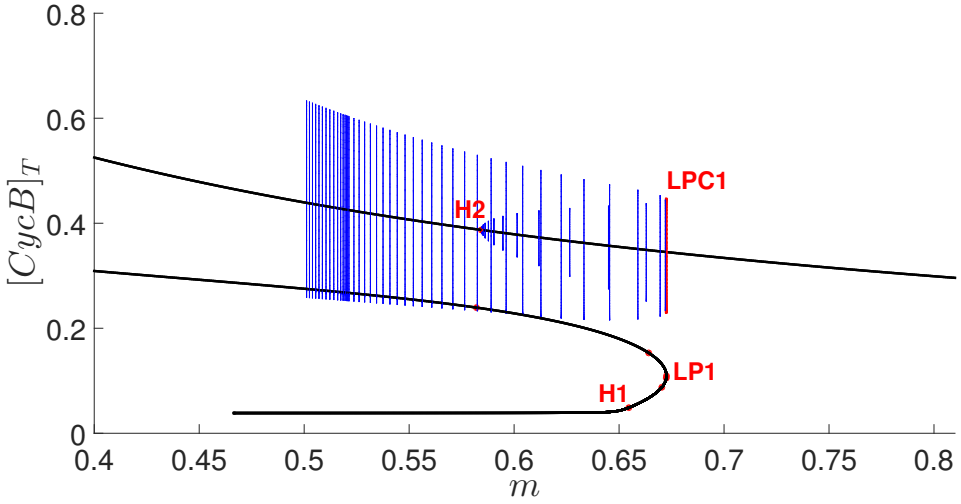

Figure 3.3: Periodic orbits born at the Hopf point H2 and losing stability at a limit point of cycles.

picture suggests that in a loose sense two periodic orbits, living in the G1 and in the S-G2-M state region respectively, merge to become a bigger orbit that lives in both states. It even suggests that the three orbits live in the same two-dimensional manifold and arise from a single higher codimension bifurcation of periodic orbits. We have not investigated this further since it is numerically very hard and probably not relevant for the biological interpretation of the model.

The constant mass cell model (2.1) contains more stable and unstable periodic orbits. For values $m > m_{LPC5} \approx 1.2945067$ stable and unstable orbits exist which collide and disappear in a limit point of cycles for $m = m_{LPC5}$. These orbits live in both G1 and in S-G2-M space but are not relevant to the physical modeling.

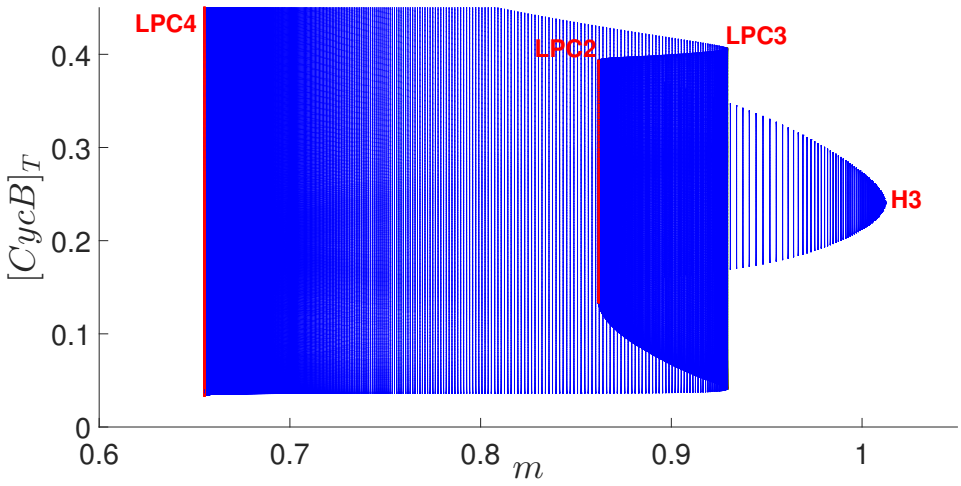

Figure 3.4: Periodic orbits born at the Hopf point H3, resp. losing, regaining and losing stability at the three limit points of cycles LPC2, LPC3 and LPC4.

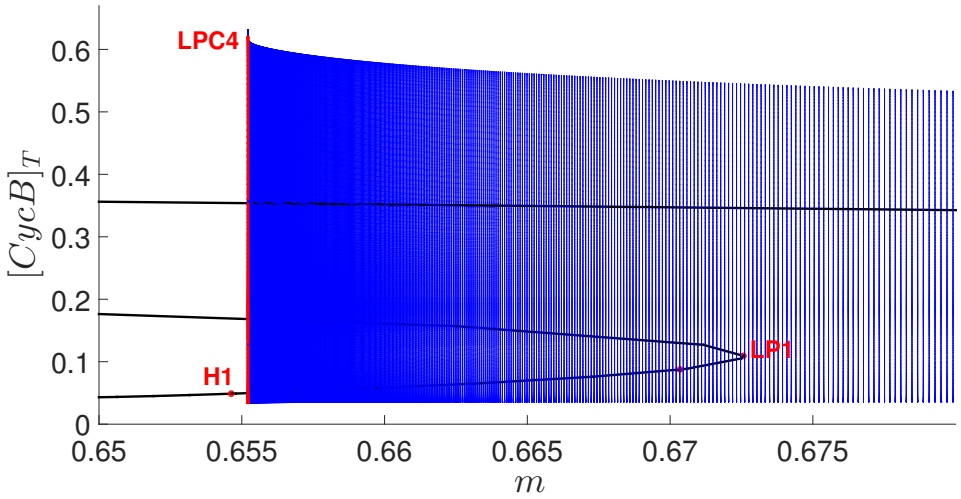

Figure 3.5: Periodic orbits born at the Hopf point H3 become unstable at the limit point of cycles LPC4 and then disappear through a homoclinic orbit.

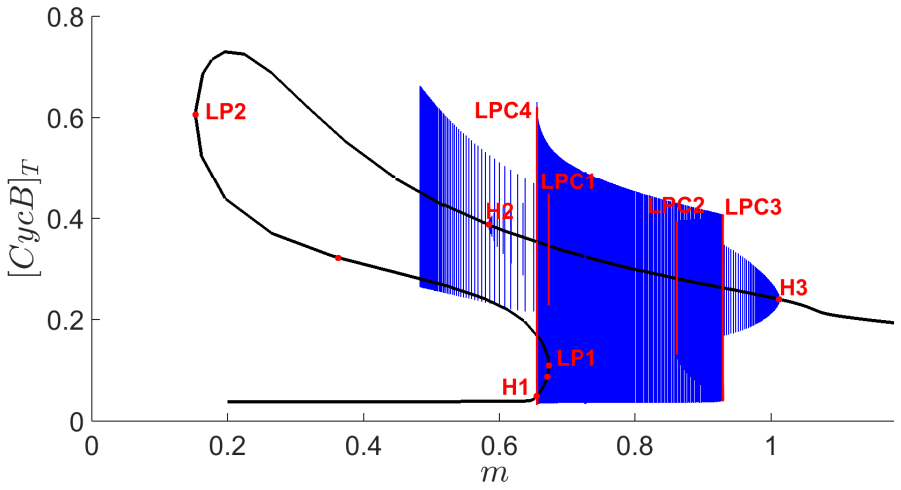

Figure 3.6: Equilibrium bifurcation diagram of the constant mass model for the parameter values in Table 2.1.

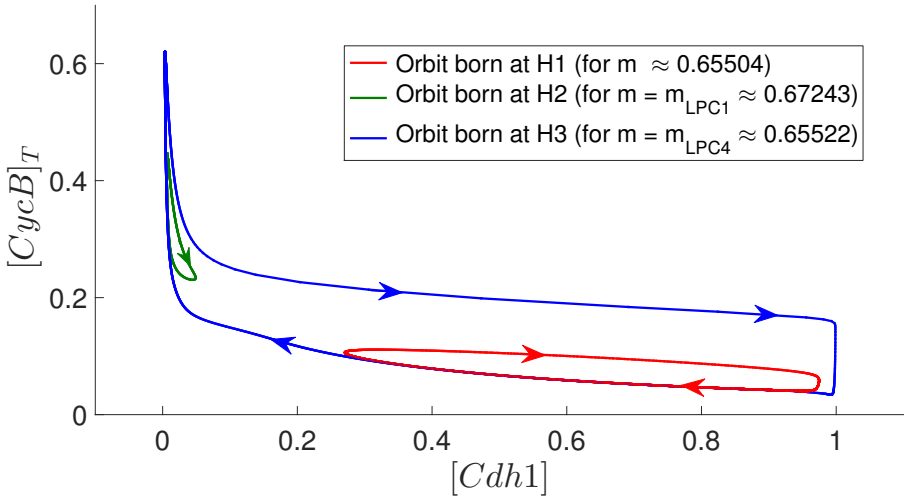

Figure 3.7: Periodic orbits born at H1, H2 and H3 with indication of the flow along the orbits.

3.2 The dynamic mass cell model of Tyson and Novák

3.2.1 The basic equations

For a growing cell, one equation is added to (2.1):

$$\frac{\mathrm{d}m}{\mathrm{d}t} = \mu m, \tag{3.1}$$

where μ is a parameter with dimension min^{-1} that represents the growth rate. The exact solution to (3.1) is, of course, given by $m(t) \equiv m(0)e^{\mu t}$. Let I be the elapsed time (expressed in minutes) between the birth of a cell and its division and let $\frac{1}{\nu}$ be the ratio $\frac{m_{NEW}}{m_{DIV}}$ where m_{DIV} is the mass of the mother cell at division and m_{NEW} the mass of the newborn cell. In combination with $m_{DIV} = m_{NEW}e^{\mu I}$, we get that

$$I = \frac{\ln \nu}{\mu}\,\mathrm{min}. \tag{3.2}$$

As budding yeast cells divide asymmetrically, we use $\nu = \frac{1}{0.443}$ as proposed in [11]. The period is thus given by

$$I = \frac{0.814}{\mu}\,\mathrm{min}. \tag{3.3}$$

We note that in [81] and many other papers (3.1) is replaced by the logistic (Verhulst-Pearl) equation (2.3). Equation (2.3) can also be solved analytically. However, in practice the cell divides for mass values much smaller than m_{max}, so the factor $(1 - \frac{m}{m_{max}})$ can be ignored in some applications.

3.2.2 The dynamic mass cell system as a slow-fast dynamical system

A newborn cell must first grow in the G1 phase, which corresponds to the lower left branch of stable equilibria in Figure 3.1. This phase loses its equilibrium stability in the constant mass cell system when m grows beyond m_{REP} and the state of the cell is then attracted by the stable periodic orbits that exist for larger values of m, mainly the orbits born at H3 since the others disappear either when $m \geq m_{Hom1}$ (those born at H1) or when $m \geq m_{LPC1}$ (those born at H2). We take m_{REP} as the onset of DNA-replication. It follows that the moment when $m = m_{REP}$ corresponds to the beginning of the S-G2-M phase, the Start transition. The large stable limit

cycles born at H3 correspond to the oscillations in S-G2-M phase.

To gain quantitative insight in the interplay between the constant and dynamic mass cell models, we compute several orbits of the dynamic mass model. We choose $\mu = 0.005$ min^{-1}, start with $m = 0.5$ and integrate over a time interval $I = \frac{\ln \nu}{\mu} = 162.837101787$ min. We start a basic orbit with initial value 0.1 for all state variables other than m. The orbit is presented in Figure 3.8. It is clear that the

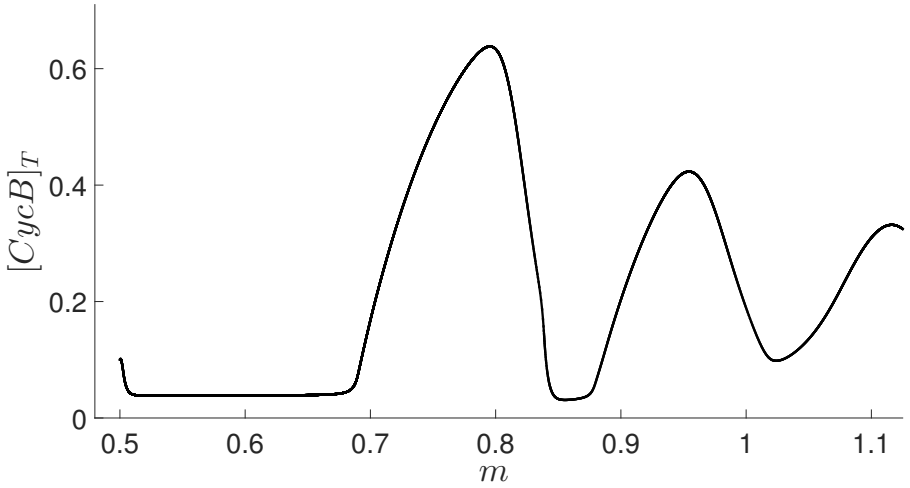

Figure 3.8: An orbit of the dynamic mass cell system for parameter values in Table 2.1, $\mu = 0.005$ min^{-1} and starting value 0.1 for all state variables with exception of $m = 0.5$.

initial point of this orbit is in the attraction domain of the stable equilibrium at the lower left branch of equilibria of the constant mass cell system (Figure 3.6). For increasing m the orbit follows closely the equilibrium branch in Figure 3.1, passes close to H1 and then gets attracted by the stable periodic orbits. Note that the convergence to the branch of stable equilibria for mass values larger than $m_{H3} \approx 1.012$ is not yet visible in Figure 3.8 since this convergence is quite slow and only shows when integrating over a larger time interval.

For a large range of initial values of m and the concentration variables, the initial segment of the orbit has the same behaviour. We illustrate this in Figure 3.9. The system behaves as a slow-fast system with m as the slow variable and the concentration variables as fast ones. This phenomenon is called the "funnel effect" of the system.

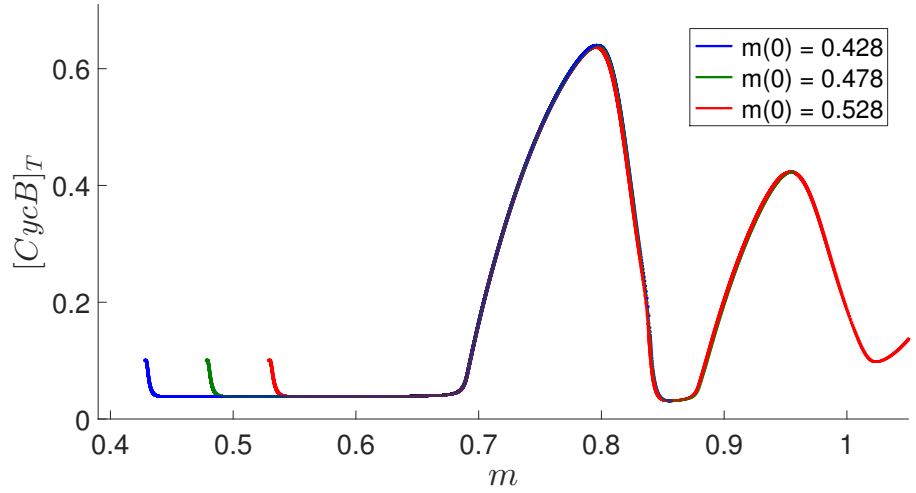

Figure 3.9: Three orbits of the dynamic mass cell system for different starting values for $m = 0.428, 0.478$ and 0.528 and other state variabeles equal to 0.1 (parameter values as in Table 1 and $\mu = 0.005$ min^{-1}).

To estimate how sensitive this orbit is to perturbations in the initial conditions of the concentration variables, we compute 16 orbits in which one of the initial values is replaced by either 0.11 or 0.09. Taking finite differences, we find an approximation to the linearization J of the map defined by time integration over I near the initial orbit, i.e. of the fundamental matrix solution to the dynamic mass cell equations, evaluated at time I. The norms of the columns of J are, respectively, $4.3606e-4$, $1.0952e-5$, $5.4429e-6$, $2.3940e-5$, 0.2089, $1.9474e-4$, $1.5671e-4$, $3.9309e-5$. It is therefore clear that the sensitivity to perturbations in the fifth variable $[IEP]$ is much higher than to the other variables, but the map is still contracting. The biggest singular value of J is 0.208906 with all the other singular values smaller than 10^{-5}. We note that IE is an "imaginary" enzym invented by the modelers to introduce a time-delay between $[CycB]$ and $[Cdc20]_A$ (see [80]). A high sensitivity to IEP in the model therefore suggests that the modeling of this time-delay (which was done differently in other models) is a sensitive issue.

3.2.3 Computation of the dividing point in the cell cycle

We model the cell cycle as an orbit $([CycB]_T(t),\ldots,[TF](t),m(t))$ with the property that $[CycB]_T(I) = [CycB]_T(0)$, …, $[TF](I) = [TF](0)$, $m(I) = m_{DIV} = m(0)\nu$ where I is the cell cycle duration. Cell division then reduces the value of m at time I to $m(0) = m_{NEW}$. If all parameters, including the growth rate μ are fixed (let $\mu = 0.005\ \text{min}^{-1}$), then the solution to this problem is determined by the choice of the point where the cell actually divides. Following the choice in [81], we assume that a cell divides at the moment when $[CycB]_T$ crosses 0.1 from above. The choice of $[CycB]_T$ as the "leading" variable is motivated by the biological interpretation of the model (see §2.1.3) but the chosen threshold value is approximative. In Section 5.10 we will investigate other choices for the point of division.

We will show numerically that the problem can be reduced to the computation of the fixed point of the map which is defined by shooting to the point where $[CycB]_T$ crosses 0.1 from above, followed by a division of the m-component by ν. Even a very crude initial guess is sufficient and the convergence is fast. In a way, this is not surprising since in this case the mathematical algorithm (shooting and dividing) mimics the biological process (growing and dividing) and we must expect that the latter is fairly robust. Consider again the basic orbit computed in §3.2.2. Let the iterates of order $0,1,2,\ldots$ of the map be called $x_0,x_1,x_2,\ldots$ respectively. We find that

$$x_0 = \begin{bmatrix} 0.1 \\ 0.1 \\ 0.1 \\ 0.1 \\ 0.1 \\ 0.1 \\ 0.1 \\ 0.1 \\ 0.1 \\ 0.5 \end{bmatrix}, \quad x_6 = \begin{bmatrix} 0.1 \\ 0.997465672008502 \\ 1.093211613628905 \\ 0.316659450964317 \\ 0.541516533594340 \\ 0.179844535437557 \\ 0.112391031803462 \\ 0.252722767468698 \\ 0.371775316102405 \end{bmatrix}. \tag{3.4}$$

After about 4 iterations, the norm of the difference between two successive iterates no longer decreases, so we take $x_\infty = x_6$ as the approximation to the exact fixed point.

To establish the stability of the found fixed point of the shoot-and-divide map, we compute the 16 orbits in which one of the components of the initial vector $([Cdh1],[Cdc20]_T,\ \ldots,\ m)$ is either increased or decreased by a small amount ε.

We took $\varepsilon = 0.01$. We exclude the component $[CycB]_T$ since this concentration is fixed as 0.1 through the definition of the map. Taking finite differences, we find an approximation to the Jacobian J of the map. The eigenvalues of J are given by

$$\begin{bmatrix} -0.013813641207812 \\ -0.001045514411775 \\ -0.000474497695339 \\ 0.000012182956256 \\ 0.000001478974507 \\ 0.000000032717216 + 0.000000088987369i \\ 0.000000032717216 - 0.000000088987369i \\ 0.000000009346214 \end{bmatrix}. \tag{3.5}$$

All eigenvalues are small in modulus and the spectral radius is of the order 0.013814. Since it is much smaller than 1, we conclude that the fixed point is indeed stable and strongly attracting.

As a check, we compute the errors in the first few iterates and find $\|x_0 - x_\infty\| = 1.4423$, $\|x_1 - x_\infty\| = 0.0093$, $\|x_2 - x_\infty\| = 1.2974e-4$, $\|x_3 - x_\infty\| = 7.7279e-5$, $\|x_4 - x_\infty\| = 1.2659e-4$, $\|x_5 - x_\infty\| = 5.5349e-5$. The ratios between the successive errors are the following: $1.5487e2$, 71.7783, 1.6789, ... The last ratio (1.6789) is close to 1 which indicates that no further improvement is possible, due to numerical errors in the shooting process. The preceding ratio (71.7783) is close to the inverse of the spectral radius of J, thus confirming linear convergence.

3.2.4 Growth rate versus time between DNA-replication and cell division

To study the effect of the growth rate μ, we compute another group of orbits. The computations all start with the same values for all state variables, in particular with $m = 0.5$ in all cases (i.e. a value definitely below m_{REP}). The values of the other state variables do not matter, if at least they are in the attraction domain of the stable equilibrium at the lower left branch of equilibria of the constant mass system (Figure 3.1). We compute the orbits for $\mu = 0.02$, 0.01, 0.005, 0.0025, 0.00125, 0.000625, 0.0003125 and 0.00015625 min^{-1}.

In Figure 3.10 we present the time evolution of $[CycB]_T$ for $\mu = 0.01$, 0.005 and 0.0025 min^{-1}. As expected, all orbits first converge to quasi-steady state solutions, corresponding to the steady states of the constant mass cell model. When the cell mass exceeds m_{REP}, the system starts oscillating with a damped amplitude.

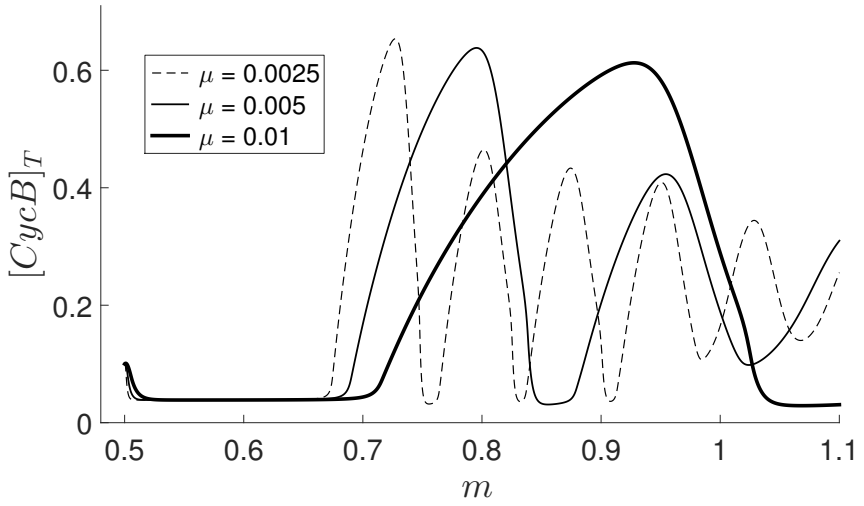

Figure 3.10: Three orbits of the dynamic mass cell system for different values of μ (in min^{-1}) and with the other parameter values as in Table 2.1.

Table 3.1: Values of the growth rate μ in (3.1) and corresponding values m_{REP} and m_{DIV} of the cell mass at DNA replication and division, time in S-G2-M phase $\Delta_2 t$ and the ratio $\frac{m_{DIV} - m_{REP}}{\mu}$.

μ (min^{-1})	$\mathbf{m_{REP}}$	$\mathbf{m_{DIV}}$	$\Delta_2\mathbf{t}$ (min)	$\frac{\mathbf{m_{DIV} - m_{REP}}}{\mu}$
0.02	0.6546307	1.4439561	39.5535089	39.4663
0.01	0.6546307	1.0267880	45.0119476	37.2157
0.005	0.6546307	0.8401373	49.8988046	37.1013
0.0025	0.6546307	0.7486099	53.6587133	37.5917
0.00125	0.6546307	0.7020505	55.9472195	37.9358
0.000625	0.6546307	0.6782075	56.6111394	37.7228
0.0003125	0.6546307	0.6666489	58.2150869	38.4581
0.00015625	0.6546307	0.6641031	91.9437708	60.6236

In Table 3.1 we give for each of the computed orbits (each corresponding with a certain μ ranging from 0.00015625 to 0.02 min^{-1}) the value m_{REP} of the cell mass at DNA replication, the value of the cell mass at division m_{DIV} (so, as previously

defined, when $[CycB]_T$ crosses 0.1 from above) and the time in S-G2-M phase $\Delta_2 t$ (the time elapsed when m increases from m_{REP} to m_{DIV}). Note that by (3.1) follows that

$$m_{DIV} = m_{REP} e^{\mu \Delta_2 t}.$$

A striking feature of Figure 3.10 is that the mass increase of the cell in S-G2-M phase is apparently proportional to μ. To make this more precise we also present in Table 3.1 the ratio of $m_{DIV} - m_{REP}$ to μ for the different μ values. The remarkable observation is that for the whole range of reasonable values of μ between 0.0003125 and 0.01 min^{-1}, the ratio of $m_{DIV} - m_{REP}$ to μ is nearly constant. We illustrate this graphically in Figure 3.11 and note that it is not an isolated phenomenon since it was also observed in [39] in the case of the Toy model of [81]. We note that this could in principle be checked experimentally if μ can be manipulated without changing the other parameters. Taking averages we find that

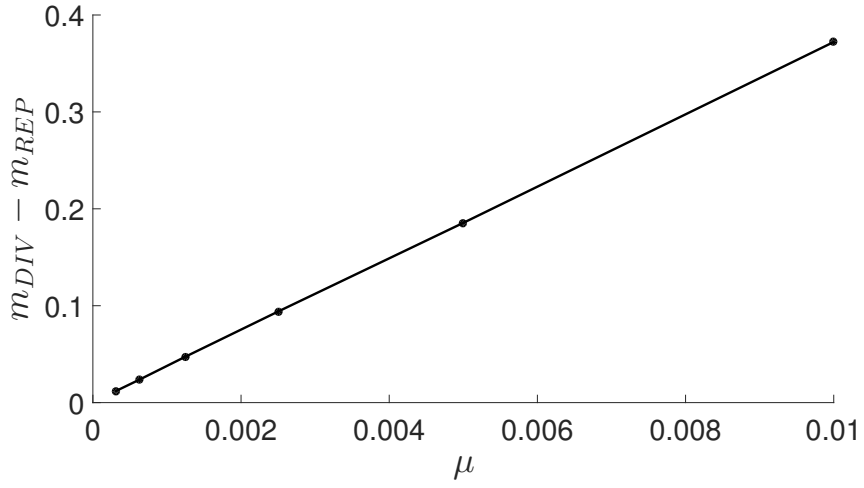

Figure 3.11: Graphical interpretation of Table 3.1: $m_{DIV} - m_{REP}$ versus μ (in min^{-1}).

$$\frac{m_{DIV} - m_{REP}}{\mu} \approx C = 37.67\,\text{min}. \tag{3.6}$$

To interpret the existence of a constant C for which (3.6) holds for a wide range of values of μ, we first consider Figure 3.12 in which we plot $mT(m)$ versus m with m in the range of the stable periodic orbits born at H3 and where $T(m)$ is the period of the periodic orbit at m. The remarkable feature is that $mT(m)$ is nearly constant in

this range (with an exception only very close to the homoclinic orbit at $m = m_{Hom2}$). Let $C_1 \approx 30$ denote this constant value.

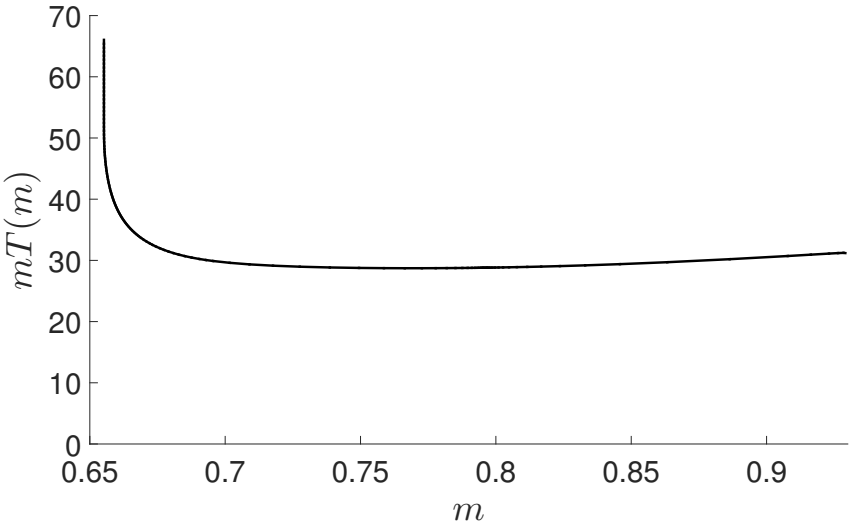

Figure 3.12: Representation of $mT(m)$ (in minutes) versus m for the stable orbits born at H3 (with T the period of the orbit).

We further suppose that the periodic orbits in the fast manifold during the S-G2-M phase have essentially the same shape and can globally be parameterized by the same phase variable $\phi \in [0,1]$. During a time dt a fraction $\frac{dt}{T(m(t))}$ is traversed by the isochron in the space of the fast state variables (see Figure 3.13). Let ρ be the total fraction of a periodic orbit traversed during S-G2-M phase. We then have

$$\int_0^{\Delta_2 t} \frac{dt}{T(m(t))} = \rho.$$

By multiplying with $m(t)$ in the numerator and the denominator and taking into account that $m(t)T(m(t)) \approx C_1$ min, we get that

$$\begin{aligned}
& \int_0^{\Delta_2 t} m(t)dt \approx C_1\rho \\
\iff & \int_0^{\Delta_2 t} m_{REP}e^{\mu t}dt \approx C_1\rho \\
\iff & \frac{m_{REP}}{\mu}\left(e^{\mu\Delta_2 t}-1\right) \approx C_1\rho \\
\iff & \frac{m_{DIV}-m_{REP}}{\mu} \approx C_1\rho.
\end{aligned}$$

From the observed relationship (3.6), we get that $C \approx C_1 \rho$. This means that the total phase fraction of a periodic orbit traversed during S-G2-M phase is constant, i.e. independent of μ:

$$\rho \approx \frac{C}{C_1} \approx 1.26. \tag{3.7}$$

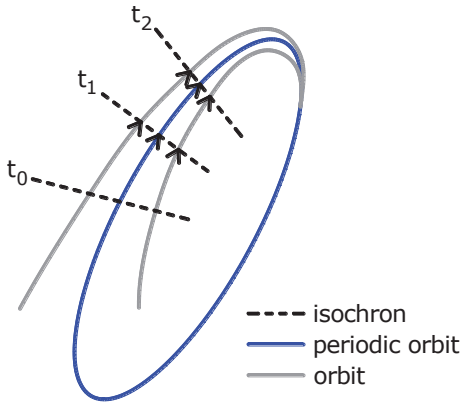

Figure 3.13: Schematic illustration of a periodic orbit (blue orbit) which attracts two approaching orbits (solid grey lines) and the isochrons at time t_0, t_1 and t_2 (dashed black lines).

It is also clear why the argument fails if either μ is very small (then an important part of the orbit is in the region where m is close to m_{LPC4}, where $mT(m)$ is large) or very large (then an important part of the orbit is in a region where no periodic orbits exist).

From the above, it follows that the duration of the different phases of the cell cycle can be calculated as follows. Let $\Delta_1 t$ be the time in minutes between the birth of a cell and the onset of DNA-replication (time in G1 phase), $\Delta_2 t$ the time in minutes between the onset of DNA-replication and cell division (time in S-G2-M phase) and I the time in minutes between birth of the cell and cell division. We have (see (3.2) for the last equality)

$$I = \Delta_1 t + \Delta_2 t = \frac{\ln \nu}{\mu}. \tag{3.8}$$

We also have from (3.6)

$$m_{DIV} = m_{REP} e^{\mu \Delta_2 t} \approx m_{REP} + C\mu, \tag{3.9}$$

which leads to

$$\Delta_2 t = \frac{1}{\mu} \ln \frac{m_{DIV}}{m_{REP}} \approx \frac{1}{\mu} \ln \left(1 + \frac{C\mu}{m_{REP}} \right). \tag{3.10}$$

The time in G1 phase is then

$$\Delta_1 t \approx \frac{\ln \nu}{\mu} - \frac{1}{\mu} \ln \left(1 + \frac{C\mu}{m_{REP}} \right). \tag{3.11}$$

Since $\frac{C\mu}{m_{REP}}$ is small, we can use the Taylor series for $\ln \left(1 + \frac{C\mu}{m_{REP}} \right)$ and get as approximation for (3.10):

$$\Delta_2 t \approx \frac{1}{\mu} \left(\frac{C\mu}{m_{REP}} - \frac{1}{2} \frac{C^2\mu^2}{m_{REP}^2} \right) = \frac{C}{m_{REP}} - \frac{1}{2} \frac{C^2\mu}{m_{REP}^2}. \tag{3.12}$$

It follows that for small μ, the time in S-G2-M phase is nearly independent of μ and slowly decreases for increasing values of μ. It is interesting to note that the model in [11] (Figure 1) predicts a practically constant time in S-G2-M phase for all values of μ. However, the experimental results in [58], also presented in Figure 1 of [11], indicate that the time in S-G2-M space is slightly decreasing for increasing μ, a fact that is consistent with (3.12).

By (3.8), (3.10) and (3.11) the cell division cycle therefore is determined by one parameter in the sense that if one of the four quantities $\Delta_1 t$, $\Delta_2 t$, I or μ is given, then the three others can be computed (assuming that μ is in the admissible range, say $0.0003125\,\text{min}^{-1} \leq \mu \leq 0.01\ \text{min}^{-1}$ and that ν is known).

In §3.2.3 we showed that the cell cycle is determined by fixing the value of $[CycB]_T$ at cell division and can be computed as the fixed point of a map.

3.2.5 Robustness under a parameter change

The only difference between the models in [81] and [80] is the introduction in [81] of the parameter k'_{13} which, however, is put to zero in [81] and in our discussion so far. We now briefly study the consequences of a nonzero k'_{13}.

This situation reflects the experiment described in [26] where it was found that a premature expression of Cln2 (analogous to SK in (2.1)) had no particular effect on cell growth but advanced the entry in S-phase and the budding. This was confirmed in the model in [11] where the authors also found that the resulting cells are smaller than normal but still viable.

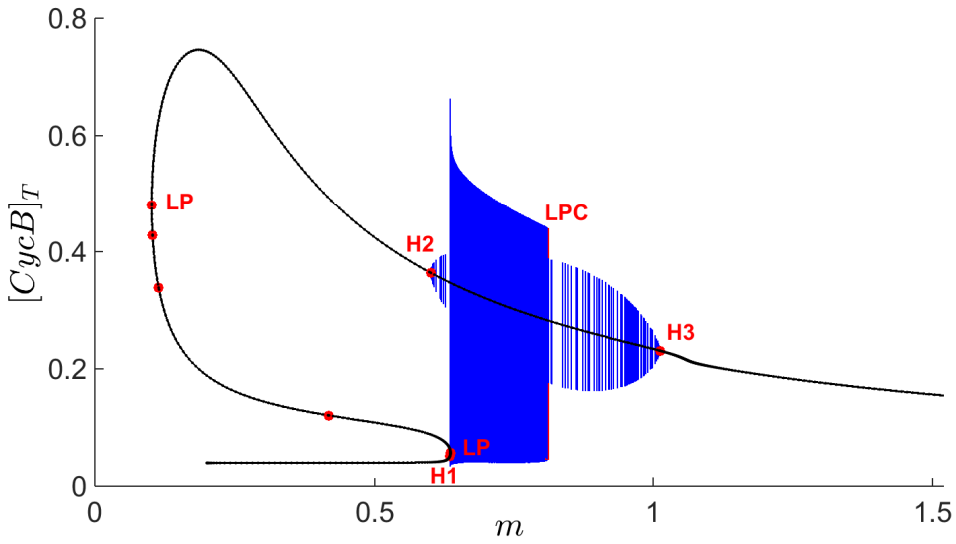

Figure 3.14: Equilibrium bifurcation diagram for the constant mass model for the parameter values in Table 2.1 except for $k'_{13} = 0.2$.

If we change k'_{13} to 0.2, we get the equilibrium bifurcation behaviour of the constant mass model as shown in Figure 3.14. For values of m below that of the subcritical Hopf point H1, the system has stable equilibria with low $[CycB]_T$. This branch of equilibria becomes unstable at H1 and then turns at a first limit point where $m \approx 0.636024$. The branch of unstable equilibria turns again at a second limit point and regains stability. It further loses stability a the supercritical Hopf point H2 and regains it at the supercritical Hopf point H3. So the equilibrium bifurcation curve has qualitatively the same stable parts as for zero k'_{13}, namely a stable part before

H1, a stable part between the second limit point and H2 and a stable part beyond H3.

For the periodic orbits we get a slightly different situation. The stable periodic orbits born at H2 die at H3 and hence for m-values between 0.58438076 and 1.0118642 "small" stable periodic orbits exist. "Large" stable periodic orbits exist for m-values between 0.63581534 and 0.8087945, where they respectively lose stability through a period doubling and a limit point of cycles. The "large" stable periodic orbits are unrelated to H1, H2 and H3. For the whole region where the "large" stable periodic orbits exist (which are the most important for the model, as explained before) there also exist "small" stable periodic orbits. It is possible to find orbits that are attracted to a "small" stable period orbit and hence, under the previously mentioned assumptions of division, never reach low enough values of $[CycB]_T$ to divide. Such cells would not be viable and this suggests that natural selection might work to keep k'_{13} small. In Figure 3.15 an orbit for $m = 0.65$ (a value slightly larger than that of H1) is shown as illustration.

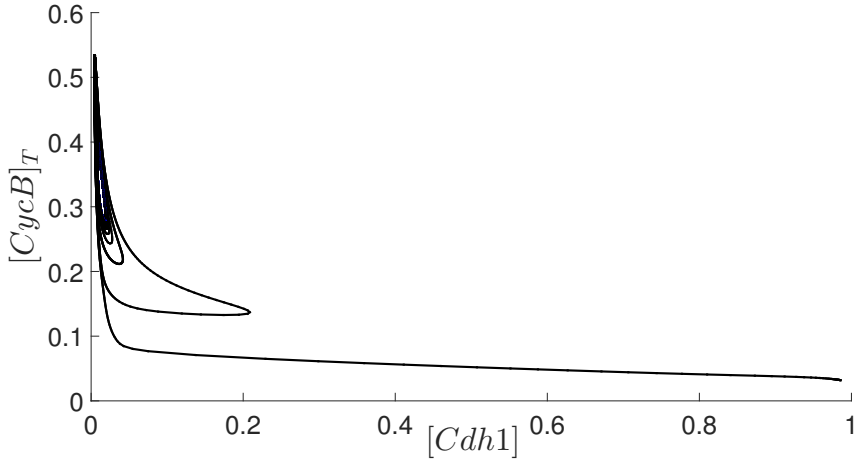

Figure 3.15: Orbit of the dynamic mass cell model converging to a "small" stable periodic orbit ($k'_{13} = 0.2$ and $m = 0.65$).

We find that the domain of bistability of the periodic orbits becomes initially wider for rising values of k'_{13}. In Figure 3.16 the continuation of the different bifurcation points for the original constant mass model (with zero k'_{13} - see Figure 3.6) is illustrated in $\left(m, k'_{13}\right)$-space. The green curve represents the continuation of H2 and H3 and the black curve the continuation of H1. The blue curve represents the

continuation of LPC1 (the limit point of cycles where the stable periodic orbits born at H2 lose stability) and LPC2 (the first limit point of cycles where the periodic orbits born at H3 lose stability). The light blue line represents the continuation of LPC3 (the limit point of cycles where the periodic orbits born at H3 regain stability) and the pink curve the continuation of LPC4 (where the periodic orbits born at H3 finally lose stability). We note that the pink curve is hardly visible in Figure 3.16 because it is so close to the H1 curve. A zoom is provided in Figure 3.18 (top figure).

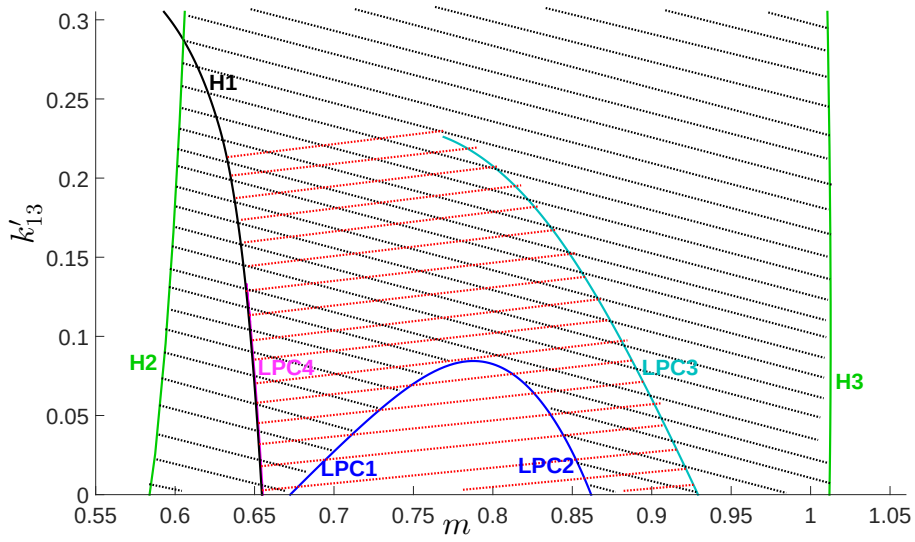

Figure 3.16: Continuation of resp. H2 and H3 (green curve), H1 (black curve), LPC4 (pink curve), LPC1 and LPC2 (blue curve) and LPC3 (light blue line) in $\left(m, k'_{13}\right)$-space. The "small" stable periodic orbits exist in the black shaded region and the "large" stable periodic orbits in the red shaded region.

The form of the H1 curve shows that for increasing values of k'_{13} the cells enter S-phase at lower values of m. This is consistent with the results in [26, 11]. The cells also divide at a smaller mass as shown in Figure 3.17.

The "large" stable periodic orbits are born at LPC3 and lose their stability at LPC4, so the red shaded region in the figure is the corresponding stability region. The curve LPC4 ends at a cusp of cycles (CPC in Figure 3.18 at the top with a zoom at the bottom) for $k'_{13} = 0.13346724$. It is difficult to determine how the large periodic orbits disappear for $k'_{13} > 0.13346724$, but the periods become very large and are, in

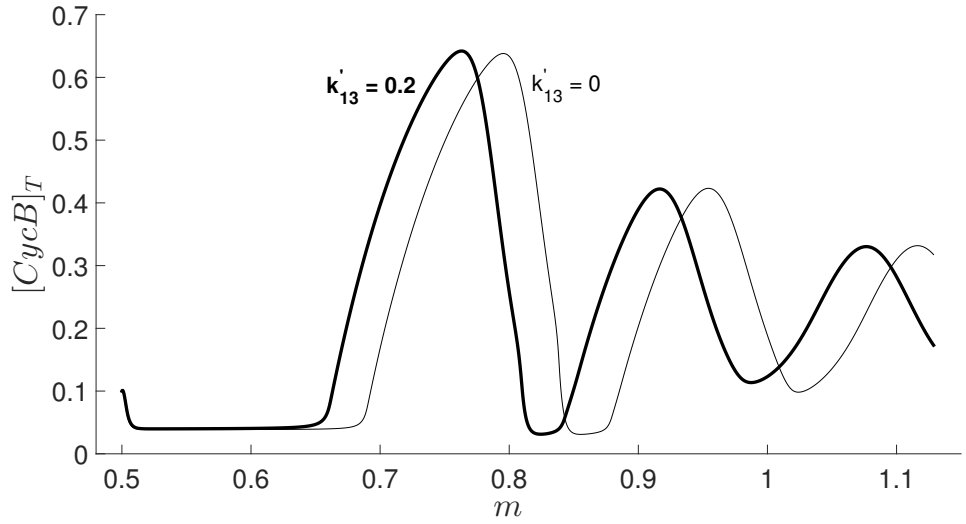

Figure 3.17: Two orbits of the dynamic mass cell model for different values of k'_{13} (the orbit for $k'_{13} = 0$ is identical to that in Figure 3.8).

practice, hardly distinguishable from homoclinic orbits. The "small" stable periodic orbits exist between H2 and H3, with an exception for the part between LPC1 and LPC2 and hence the black shaded region in the figure is the stability region of these "small" periodic orbits. The domain of bistability is the double-shaded region in Figure 3.16, which becomes wider for rising values of k'_{13}. To check if the existence of this bistability region has a great impact on the model, the attraction domains of the different stable periodic orbits should be investigated in more detail. But clearly a non-zero k'_{13} leads to a large region of birhythmicity.

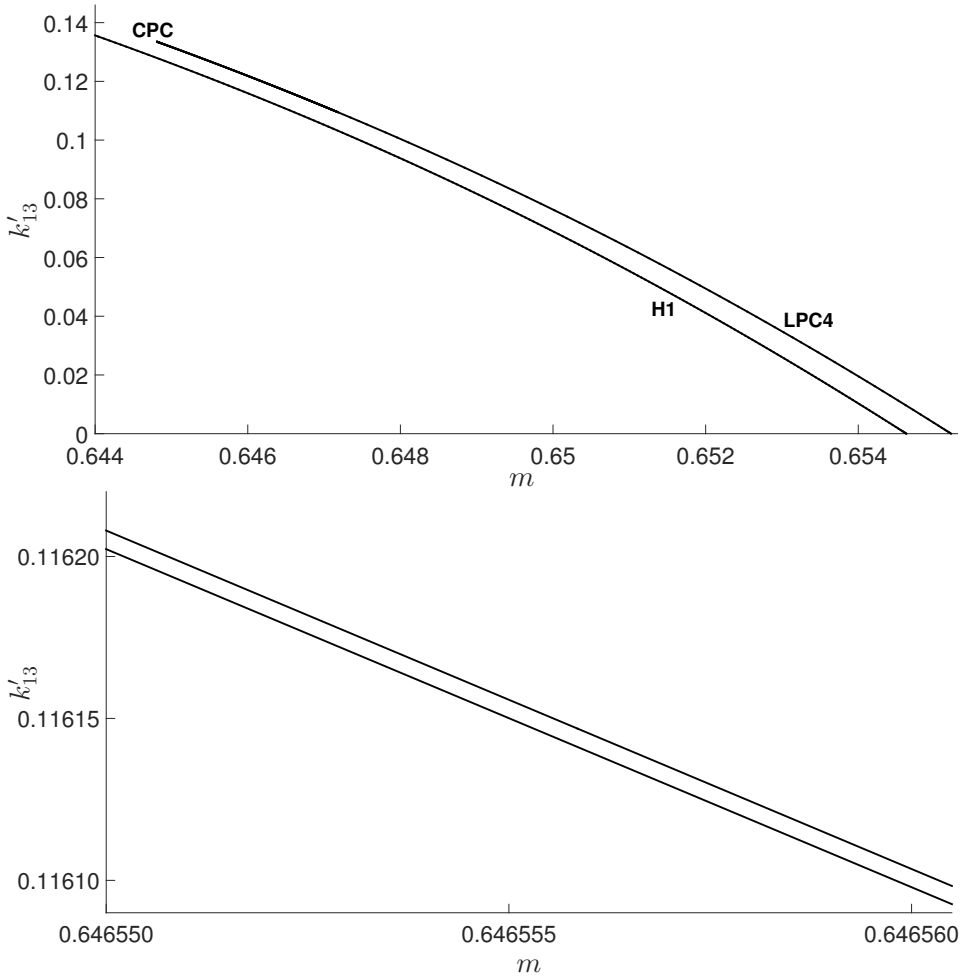

Figure 3.18: Continuation of H1 and LPC4 in $\left(m, k'_{13}\right)$-space (top figure). The LPC4 curve ends in a cusp of cycles CPC. The two nearly parallel LPC curves are presented in the zoom in the bottom figure.

Table 3.2: Parametervalues Toy model of Tyson and Novák (3.13)

parameter	value	parameter	value
k_1	0.04/min	k_5'	0.005/min
k_2'	0.04/min	k_5''	0.2/min
k_2''	1/min	k_6	0.1/min
k_3'	1/min	J_5	0.3
k_3''	10/min	n	4
k_4	35/min	μ	0.01/min
J_3	0.04	m_{max}	10
J_4	0.04		

3.3 Toy model of Tyson and Novák

Tyson and Novák also propose a simplified model for the cell cycle, the Toy model, in [81, 44], which we briefly introduce here. This model is further studied in more detail in [39]. The model consists of 4 state components: the mass m, the concentration of Cdk-cyclin dimers X, the concentration of active Cdh1-APC complexes Y and the concentration of a protein that activates Cdh1 at Finish A. Tyson and Novák assume that a cell starts dividing if the concentration X crosses $X_{DIV} = 0.1$ from above. The equations are

$$\begin{aligned} \frac{dm}{dt} &= \mu m\left(1-\frac{m}{m_{max}}\right), \\ \frac{dX}{dt} &= k_1-(k_2'+k_2''Y)X, \\ \frac{dY}{dt} &= \frac{(k_3'+k_3''A)(1-Y)}{J_3+1-Y}-\frac{k_4mXY}{J_4+Y}, \\ \frac{dA}{dt} &= k_5'+k_5''\frac{(mX)^n}{J_5^n+(mX)^n}-k_6A. \end{aligned} \tag{3.13}$$

All parameters in these equations are positive and the parameter values, as introduced in [81], are listed in Table 3.2. X takes the role of $[CycB]_T$ in (2.1), Y the role of $[Cdh1]$ in (2.1) and A the role of $[Cdc20]_T$ in (2.1). The concentrations X, Y and A are dimensionless quantities (expressed as grams of the protein per grams of total cell mass), as well as the cell mass m.

A bifurcation study of this model is done in [39]. The main equilibria of the Toy model for a constant mass (so without the first equation in (3.13)) are depicted in Figure 3.19. The bottom part of the equilibrium curve represents stable equilibria with X below 0.1, corresponding to the G1 phase of the cell cycle. This branch

of equilibria loses stability at a Limit Point for $m \approx 0.79$. The two further points denoted by H (of which one is very close to the first LP) are in fact neutral saddles and do not change the stability. The equilibria regain stability at the second LP for $X \approx 0.437$ and lose stability again at the subcritical Hopf point for $X \approx 0.35$ and $m \approx 0.6$. The unstable periodic orbits born at this Hopf point die at a HHS orbit and are not relevant from the modelling perspective. The authors of [39] find stable periodic orbits for mass values larger than 0.79. These periodic orbits tend to a HSN orbit for $m \approx 0.79$, with the lower LP in Figure 3.19 as saddle-node. The stable periodic orbits have part of their period in a region with low X (below 0.1), but also have part of their period in the region with higher X. This means that they correspond to the "large" stable periodic orbits of the budding yeast model of Tyson and Novák and that they provide the cycling behaviour in the S-G2-M phase.

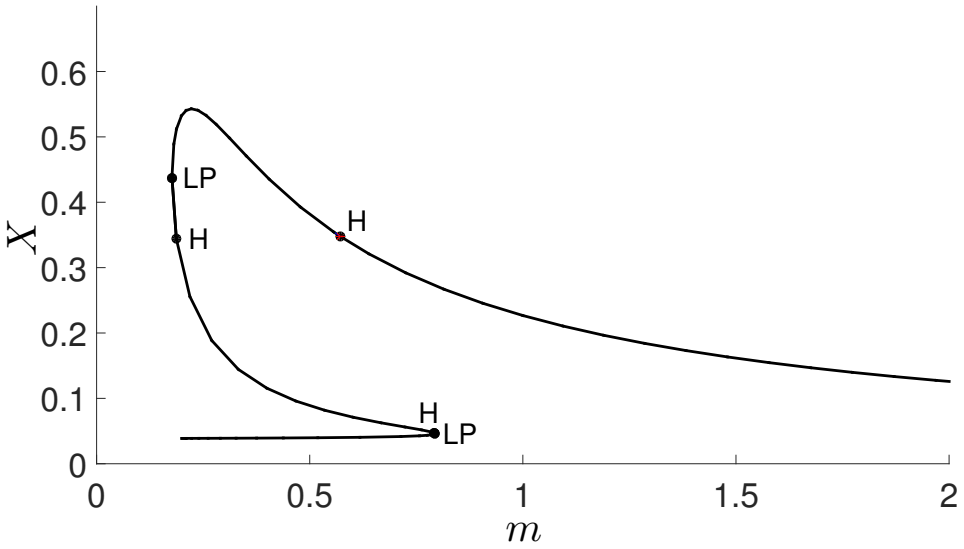

Figure 3.19: Equilibria curve of the Toy model (3.13) for a constant mass.

In Figure 3.20 six orbits of the Toy model (with a dynamic mass) are depicted in (m,X)-space for different starter values of m (starter values for X, Y and A are respectively 0.1, 0.5 and 0.5, and the parameter values are listed in Table 3.2, except that we use $\mu = \frac{4}{300}$ min^{-1}). For small mass starter values (see the orbits for $m(0) = 0.2$ and $m(0) = 0.6$) the orbits converge to the same, initially oscillating, orbit in (m,X)-space. The Toy model thus shows the same "funnel effect" for small mass starter values as the budding yeast model (see §3.2.2). For birth mass values

$m(0) < 2.138325$ the orbit will still oscillate initially in the X component. From the assumption that cells divide when X crosses 0.1 from above, it follows that cells with birth mass $m(0) \geq 2.138325$ will not divide since the X value will never decrease to 0.1 (see Figure 3.20).

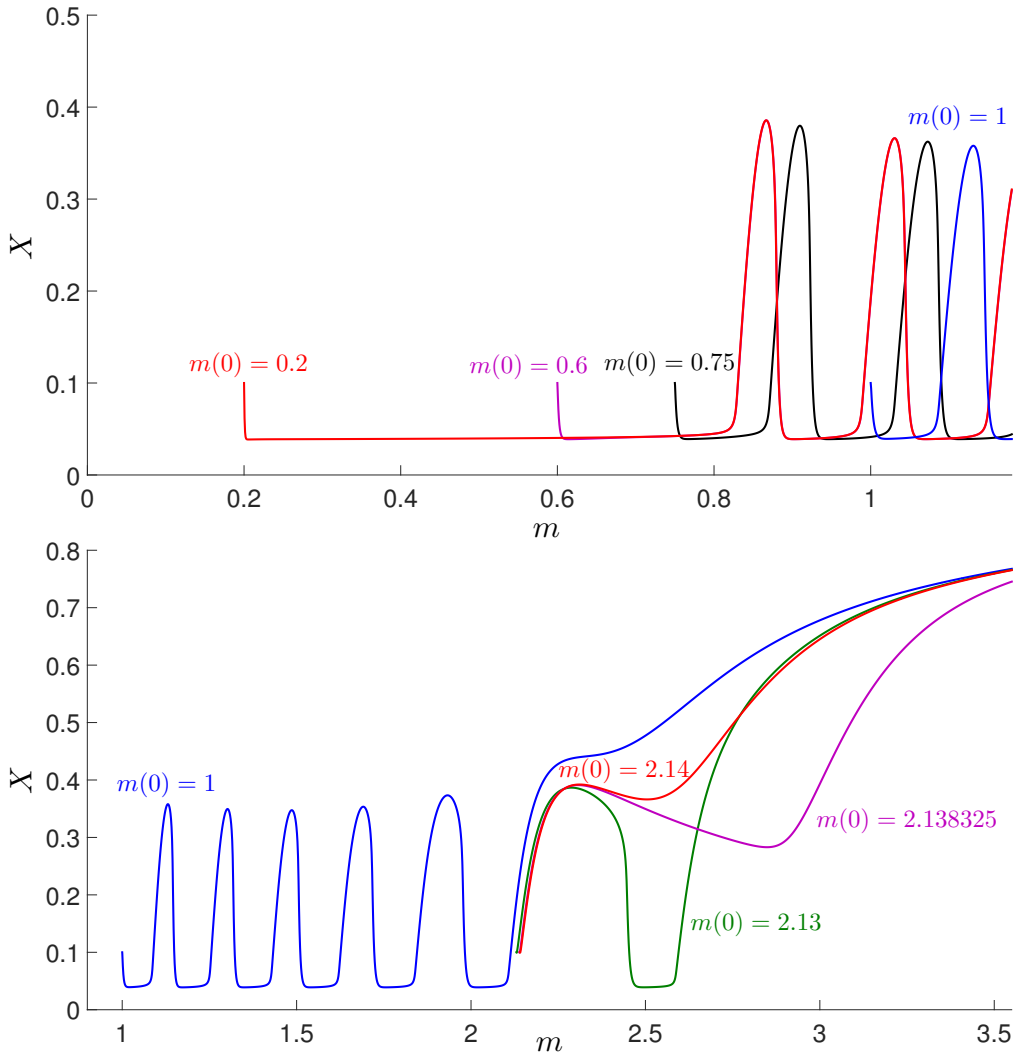

Figure 3.20: Orbits of the Toy model of Tyson and Novák (4.3) for different starter values of m (starter values for X, Y and A resp. 0.1, 0.5 and 0.5 and parameter values as in Table 3.2 except $\mu = \frac{4}{300}$ min^{-1}).

CHAPTER 4

Modelling structured population models with internal cell cycle

Overview

We introduce a chemostat model describing a population of unicellular organisms living in a continuous culture. We attach a physiological structure to these cells which describes their internal cell cycle. The cycling through the cell cycle depends on the environment, which in this case is the concentration of the limiting nutrient in the bioreactor. In Section 4.1 the model is described in general terms, with attention for the notation and including the general system equations that consist of a renewal equation coupled to a delay differential equation. The i-state of the cells describes their progression through the cell cycle by using well-studied mathematical models for the cell cycle. In the major part of this chapter, an adjusted form (that incorporates nutrient dependency) of the Toy model of Tyson and Novák is used. In Section 4.2, we give the equations for the cell cycle and explain the cell division conditions. We make the distinction between population models where cells can only divide when their mass satisfies a minimal mass criterion (Minal-Mass models MM1 and MM2) and a model without minimal mass criterion (No-Minimal-Mass model NMM). The only difference between the MM1 and MM2 model is the way the maximal mass is incorporated in the models. In Section 4.3 the equations for the equilibrium $(\bar{S}, \bar{b}(x))$ are given.

To enable the computation of the equilibrium, the birth space has to be discretised which results in a finite number of birth cohorts. In Section 4.4 we discuss a general discretisation of the birth space, using a uniform meshing, and give the equations for the discretised population model and the equilibrium. The internal state of each birth cohort, together with the nutrient consumption by the cells in the cohort, is integrated over age until the survival probability of the cells in the cohort becomes very small. In Section 5.1 we simplify the discretisation of the birth space relying on the funnel effect which the Toy model, and more extensive cell cycle models, display. We only discretise the mass component of the cell using an adaptive discretisation. The location of the birth cohorts in birth space is not fixed: the age integration is performed on an initial list of birth cohorts resulting in a new list of birth cohorts. This new list of birth cohorts depends on which cells are born from mother cells in the initial list of cohorts and two parameters δ and ε. δ represents the "inhibition zone" of an existing cohort, so the masses in a list of birth cohorts differ at least δ from each other. ε is a lower threshold for the fraction of cells born in a cohort. The resulting equations for the population model with the adaptive discretisation are given and we motivate how the equilibrium equations can be rewritten as the fixed point of a map. In Chapter 5 we will discuss the computational results for the structured population models that are introduced in this chapter.

4.1 The model

4.1.1 Chemostat model

The chemostat (see Figure 4.1), also known as the continuous stirred tank bioreactor, was invented in 1950 independently by Jacques Monod [63] and by Novick and Szilard [68] as a suitable way to study a bacterial population in the steady state (see [42]). The experimenters could easily adjust the growth rate and external parameters such as the temperature. Monod was particulary interested in which regulation mechanisms operate within cells when there are nutrient-limited conditions. The chemostat has been omnipresent in the study of microbial physiology and metabolism since its invention [47]. Also for the study of microbial ecology and more general population dynamics, it has proven its use [75].

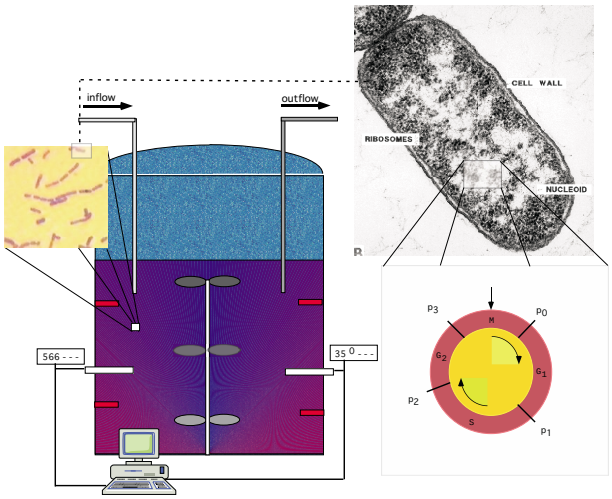

Figure 4.1: Sketch of a chemostat: a stirred bioreactor to which fresh nutrient is continuously added (the inflow), while the culture liquid is continuously removed (the outflow) at the same rate to keep the culture volume constant.

All cells in the bioreactor experience the same limiting nutrient concentration as we assume the reactor is well-mixed, see Fig. 4.1. Let us denote this nutrient concentration inside the reactor by $S(t)$, the available resource concentration at time t. Our way of bookkeeping at the population level leads us to introduce histories, first as functions defined on $(-\infty,0]$. For the resource S, we introduce the notation

$$S_t(\sigma) := S(t+\sigma), \sigma \in (-\infty,0],$$

which is common in the theory of functional differential equations (see [43]). Then S_t is the history of the resource at time t. The dimension of the nutrient concentration is [mass]·[size]$^{-3}$. Since the mass of the cell is a dimensionless quantity in the cell cycle models (see the comments to (2.1)), the nutrient concentration is only expressed per unit of volume so we assume $[S]$=m^{-3}.

4.1.2 Introduction of the vital rates

We introduce $x(a,x_0,\Psi)$ as the individual state of a cell at age a, given it had state x_0 at birth and has experienced history Ψ during its lifetime. Then $x(a,x_0,S_t)$ is the state that a cell has at age a and time t, given it had birth state x_0 and has experienced resource concentration S_t in the time interval $[t-a,t]$.

Likewise, we introduce $\mathcal{F}(a,x_0,\Psi)$ as the survival probability to age a of a cell, given it had birth state x_0 and has experienced history Ψ during its lifetime. Then $\mathcal{F}(a,x_0,S_t)$ is the probability for a cell to reach age a at time t given it had birth state x_0 and has experienced resource concentration S_t in the time interval $[t-a,t]$.

We further denote by $\beta(x,E)$ the rate of division of a cell at state x under environmental condition E, and by $\gamma(x,E)$ the rate of food consumption of such a cell at state x under environmental condition E. So, for example, $\beta(x(a,x_0,S_t),S(t))$ is the rate of division of a cell at time t of age a (the cell is born from a mother cell which divided a time units ago) with birth state x_0.

Finally, $f(S)$ denotes the intrinsic rate of change of the resource, meaning the rate of change in absence of the consumer. We will assume the so-called chemostat condition

$$f(S) = D(S^0 - S), \tag{4.1}$$

where D is a positive constant, representing the dilution rate, and $S^0 > 0$ is the concentration of the limiting nutrient contained in the feeding bottle of the chemostat, before it is pumped into the bioreactor and consumed by the cells floating in the tank.

4.1.3 Evolution of the *i*-state and the survival probability

The internal state x attached to each cell is a vector of which the dimension depends on the details with which each cell is represented in the model. We will assume that the dimension is $\nu \in \mathbb{N}$ with $\nu \geq 2$. A special *i*-state component of the cells is mass, which we assume to always be the first component of x and denote by m. We will make several assumptions about the cell division mechanisms (see Section 4.2.2), of which some are related to the mass of the cell. The other components of x will be concentrations of certain chemicals associated to and necessary to formulate the cell's cell cycle. The division of the cell will be determined or triggered by a threshold concentration reached by one of these molecules, by default this molecular species concentration will be the second component of x, denoted by δ. As m and δ are the minimal components needed to establish such a model, this explains why $\nu \geq 2$. The other state vector components besides m and δ are denoted by α_i, $i = 1,\ldots,\nu-2$ (i.e. the α_i are not present in case the *i*-state has dimension 2).

We also introduce the i-state space Ω_i as the space of all i-states in which any cell inside the bioreactor can be. As besides mass, the other state vector components have interpretations as concentrations clearly $\Omega_i \subseteq \mathbb{R}_+ \times \mathbb{R}_+ \times \ldots \times \mathbb{R}_+$, where the Cartesian product is taken $\nu - 1$ times. This space can be restricted further with respect to its m component, as we will explain in Section 4.1.4. We define Ω_b as the space of all states in which a newly born cell inside the bioreactor can be.

We can establish equations for $x(a,x_0,S_t)$ and $\mathcal{F}(a,x_0,S_t)$ in terms of the individual evolution rate $g(x,E)$ and the mortality rate $\mu_d(x,E)$. We assume that $g : \Omega_i \times \mathbb{R}_+ \to \mathbb{R}^\nu$ is C^1 on $\Omega_i \times \mathbb{R}_+$ and $\mu_d : \Omega_i \times \mathbb{R}_+ \to \mathbb{R}_+$ is C^1 on $\Omega_i \times \mathbb{R}_+$. We then assume the following evolution laws for $x(a,x_0,S_t)$ and $\mathcal{F}(a,x_0,S_t)$:

$$\begin{aligned} \frac{\partial}{\partial a} x(a,x_0,S_{t+a}) &= g(x(a,x_0,S_{t+a}),S(t+a)), \\ x(0,x_0,S_t) &= x_0,\ x_0 \in \Omega_b, \end{aligned}$$

and

$$\begin{aligned} \frac{\partial}{\partial a} \mathcal{F}(a,x_0,S_{t+a}) &= -[\mu_d(x(a,x_0,S_{t+a}),S(t+a)) + \beta(x(a,x_0,S_{t+a}),S(t+a))] \\ &\quad \cdot \mathcal{F}(a,x_0,S_{t+a}), \\ \mathcal{F}(0,x_0,S_t) &= 1, \text{ for all } x_0 \in \Omega_b. \end{aligned}$$

The latter condition means that a cell eventually either dies (which means in our chemostat model that it is washed out of the bioreactor) or it divides and leaves the size cohort $(x(a,x_0,S_{t+a}),S(t+a))$ of cells having age a. These equations are valid for cells born at time t, having age a at time $t+a$.

4.1.4 Cell division

We will assume that a cell always splits into two parts during a division event, and that it can only divide when it has maximally mass m_{max}. Furthermore, we define a number ϕ with $0 < \phi \leq 0.5$. We assume that a cell with mass m always splits into a cell with mass ϕm and a cell with mass $(1-\phi)m$. The largest possible size of a newborn cell is clearly $(1-\phi)m_{max}$. We will consider two different cases for a lower boundary for the mass at division: in the first case there is no lower boundary and in the second case a cell can only divide when it has at least mass m_{min}. In the first case we have that

$\Omega_b|_m :=]0,(1-\phi)m_{max}]$ and in the second case that $\Omega_b|_m := [\phi m_{min},(1-\phi)m_{max}]$. In Figure 4.2 the i-state space restricted to the mass is illustrated for the second case. For this case, it follows that $\Omega_i = [\phi m_{min}, m_{max}] \times \mathbb{R}_+ \times \ldots \times \mathbb{R}_+$.

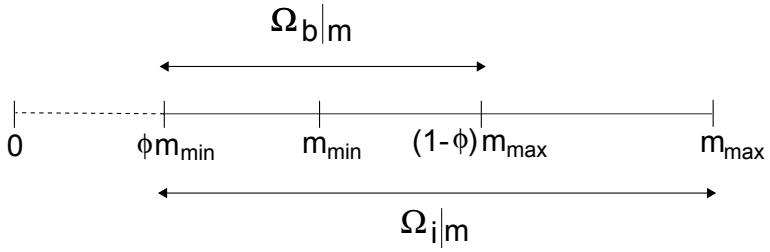

Figure 4.2: The i-state space Ω_i restricted to the first component, the cells' sizes or masses.

These settings describe a deterministic splitting in always the same fractions, which is a rough approximation of a stochastic splitting. For values of $\phi \approx 0.5$ this describes sufficiently well bacterial populations such as E. coli (see [77]), and for smaller ϕ ($\phi \approx 0.4$) it describes a population dividing by budding, such as brewer's yeast *S. cerevisiae* (see Figure 2.4, [44]).

We assume that when the cell divides the mass changes as described above and the other components of the *i*-state variabele x are unaltered. So the state variables of the new cells differ only in the m component from the mother cell's state.

4.1.5 The complete model

Let us finally denote by $b(t,x)$ the population birth rate, i.e., the number of new individuals created per unit of time and volume in the bioreactor with *i*-state x at time t. Then we can describe the population dynamics by the system of equations

$$\begin{aligned}
\frac{dS}{dt} &= f(S(t)) \\
&\quad - \int_0^\infty \int_{\Omega_b} \gamma(x(a,x_0,S_t),S(t))\, \mathcal{F}(a,x_0,S_t)\, b(t-a,x_0)\, dx_0\, da, \\
b(t,x) &= \int_0^\infty \Big[\beta\left(\tfrac{x}{[\phi\ 1\ldots 1]},S(t)\right) \mathcal{F}\left(a,\xi(\tfrac{x}{[\phi\ 1\ldots 1]},a,S_t),S_t\right) \\
&\qquad\qquad b\left(t-a,\xi(\tfrac{x}{[\phi\ 1\ldots 1]},a,S_t)\right) \\
&\qquad + \beta\left(\tfrac{x}{[1-\phi\ 1\ldots 1]},S(t)\right) \mathcal{F}\left(a,\xi(\tfrac{x}{[1-\phi\ 1\ldots 1]},a,S_t),S_t\right) \\
&\qquad\qquad b\left(t-a,\xi(\tfrac{x}{[1-\phi\ 1\ldots 1]},a,S_t)\right)\Big]\, da,
\end{aligned} \tag{4.2}$$

where the system is already running from time $-\infty$ up to present time t. This explains why we have not imposed any initial conditions. Of course this is experimentally unrealistic, but as we will only consider equilibria of the system, this point-of-view is actually the most natural.

The nutrient concentration changes due to the intrinsic rate of change (the inflow and outflow of nutrient) and due to the consumption of nutrient by the living cells. The rate of nutrient consumption by all living cells at time t is calculated by considering the cells that originate from all possible birth states x_0 (the integral over Ω_b in the first equation of (4.2)) and by considering for every possible birth state x_0 the consumption rate of a cell of age a (factor $\gamma(x(a,x_0,S_t),S(t))$ in the first equation of (4.2)) times the number of living cells per unit of time at time t with age a (factor $b(t-a,x_0)\cdot\mathcal{F}(a,x_0,S_t)$ in the first equation of (4.2)), for all possible ages (the integral from 0 to ∞ in the first equation of (4.2)).

The equation for the number of newborn cells with i-state x at time t per unit of time consists of two parts. A newborn cell with i-state x and more precisely mass m, can either be the small daughter cell of a cell that divides when it has the same i-state x except for the mass (which then must equal $\frac{m}{\phi}$), or the large daughter cell of a cell that divides when it has i-state x except for the mass (which then must equal $\frac{m}{1-\phi}$). We use the notation $\frac{x}{[\phi\,1\ldots1]}$ for the pointwise vector division (so only the m component is divided by ϕ) in (4.2). The number of cells born with i-state x at time t per unit of time equals the sum of the number of cells born with i-state x at time t per unit of time from mother cells with age a (for all possible ages) and state $\frac{x}{[\phi\,1\ldots1]}$ at time t, and the number of cells born with i-state x at time t per unit of time from mother cells with age a (for all possible ages) and state $\frac{x}{[1-\phi\,1\ldots1]}$ at time t. We define the function $\xi(y,a,S_t)$ in (4.2) as the birth state vector of a cell which was born at time $t-a$ and has at time t state y while experiencing resource concentration S_t in the time interval $[t-a,t]$ (under the assumption that it did not die). If no such vector exists then the corresponding birth rate is set to zero. The number of cells born with i-state x at time t per unit of time from mother cells with age a and state $\frac{x}{[\phi\,1\ldots1]}$ at time t then equals the division rate of such a mother cell times the number of living mother cells of this type per unit of time at time t with age a (factor $b\left(t-a,\xi(\frac{x}{[\phi\,1\ldots1]},a,S_t)\right)\cdot\mathcal{F}\left(a,\xi(\frac{x}{[\phi\,1\ldots1]},a,S_t),S_t\right)$ in the second equation of (4.2)). Together this gives the second equation of (4.2).

Table 4.1: Parameter values $h(S)$ in (4.3)

parameter	value
c_1	2
ζ_1	0.5/m^3

The population equations (4.2) form a system of a renewal equation coupled to a delay differential equation.

4.2 The cell cycle

4.2.1 Toy model adjusted

To describe the cell cycle, we start with a simple model, namely the Toy model of Tyson and Novák, which we introduced in Section 3.3 with equations (3.13). The i-state variable x then equals the vector with m, X, Y and A as components. We adjust the original equation for the mass by Tyson and Novák to incorporate a dependency on the nutrient concentration. The equations then are

$$\begin{aligned}
\frac{dm}{dt} &= g_m(x,S) = \mu m\left(1-\frac{m}{m_{max}}\right)h(S),\\
\frac{dX}{dt} &= g_X(x,S) = k_1-(k_2'+k_2''Y)X,\\
\frac{dY}{dt} &= g_Y(x,S) = \frac{(k_3'+k_3''A)(1-Y)}{J_3+1-Y}-\frac{k_4mXY}{J_4+Y},\\
\frac{dA}{dt} &= g_A(x,S) = k_5'+k_5''\frac{(mX)^n}{J_5^n+(mX)^n}-k_6A,
\end{aligned} \tag{4.3}$$

where we choose a Holling type II functional response [8] for $h(S)$:

$$h(S) = \frac{c_1S}{\zeta_1+S},$$

with c_1 and ζ_1 positive parameters. We use the parameter values in Table 3.2 for the original parameter values and the values in Table 4.1 for c_1 and ζ_1. The rationale for the choice for c_1 and ζ_1 is that we choose $h(S)\to 2$ for $S\to+\infty$ and $h(\frac{1}{2})=1$ for $S^0=1$.

Table 4.2: Overview of the deterministic cell division assumptions for the different models

No-Minimal-Mass model	*Minimal-Mass model*
NMM deterministic division: cells divide when $X = X_{DIV}$ and $\frac{dX}{dt} < 0$ (with m_{max} in equation of $\frac{dm}{dt}$)	**MM1** deterministic division: cells divide when $X = X_{DIV}$, $\frac{dX}{dt} < 0$ and $m \geq m_{min}$ (with m_{max} in equation of $\frac{dm}{dt}$)
	MM2 deterministic division: cells divide when $X = X_{DIV}$, $\frac{dX}{dt} < 0$, $m \geq m_{min}$ and $m \leq m_{max}$ (without m_{max} in equation of $\frac{dm}{dt}$)

4.2.2 Conditions for cell division

We will study the effect that different assumptions about the mechanisms triggering cell division have. We can subdivide the corresponding cell population models in two classes, based on whether or not the cells can only divide when the reach a minimal mass value. More precisely we will study the models with deterministic cell division mechanisms as described in Table 4.2. We can interpret deterministic division as the limit cases of probabilistic division.

No-Minimal-Mass model with deterministic division NMM

The rate of reproduction is the following Dirac function:

$$\beta(m,X,Y) := \begin{cases} 0 & \text{if } X \neq X_{DIV} \text{ or } \frac{dX}{dt} \geq 0, \\ +\infty & \text{if } X = X_{DIV} \text{ and } \frac{dX}{dt} < 0. \end{cases}$$

Minimal-Mass model with deterministic division MM1

The rate of reproduction is for this model the following Dirac function:

$$\beta(m,X,Y) := \begin{cases} 0 & \text{if } m < m_{min} \text{ or } X \neq X_{DIV} \text{ or } \frac{dX}{dt} \geq 0, \\ +\infty & \text{if } m_{min} \leq m \text{ and } X = X_{DIV} \text{ and } \frac{dX}{dt} < 0. \end{cases}$$

Minimal-Mass model with deterministic division MM2

The rate of reproduction for this model is the following Dirac function:

$$\beta(m,X,Y) := \begin{cases} 0 & \text{if } m < m_{min} \text{ or } m > m_{max} \text{ or } X \neq X_{DIV} \text{ or } \frac{dX}{dt} \geq 0, \\ +\infty & \text{if } m_{min} \leq m \leq m_{max} \text{ and } X = X_{DIV} \text{ and } \frac{dX}{dt} < 0. \end{cases}$$

In MM2, we use $\frac{dm}{dt} = \mu m h(S)$ as equation for the mass increase instead of the equation in (4.3).

4

As value for X_{DIV} we will use 0.1, as proposed by Tyson and Novák. In Section 5.10 we will discuss other cell division criteria for X.

In the following Sections 4.3 and 4.4 we will use the general notation for the components of the state vector x and from Section 4.5 onwards we will use the specific notation for model (4.3).

4.3 The equilibrium condition

An equilibrium is a pair of a constant number and a time-invariant distribution $(\bar{S},\bar{b}(x))$ satisfying the renewal and delay equation (4.2) simultaneously. If $\bar{b}(x) = 0$ for all $x \in \Omega_b$, $\bar{S}$ must be such that $f(\bar{S}) = 0$. In this case, we have a trivial equilibrium $(S^0,0)$, which is not very interesting. A nontrivial equilibrium is given by a pair $(\bar{S},\bar{b}(x))$ satisfying

$$\begin{array}{rcl} f(\bar{S}) - \int_{\Omega_b} \Theta(x_0,\bar{S}) \cdot \bar{b}(x_0) dx_0 & = & 0, \\ R_0(x_0,\bar{S}) - \bar{b}(x_0) & = & 0, \text{ for all } x_0 \in \Omega_b, \end{array} \tag{4.4}$$

with

$$\begin{aligned} \Theta(x_0,\bar{S}) &:= \int_0^\infty \gamma(x(a,x_0,\bar{S}),\bar{S})\, \mathcal{F}(a,x_0,\bar{S})\, da, \text{ with } x_0 \in \Omega_b, \\ R_0(x_0,\bar{S}) &:= \int_0^\infty \beta\left(\frac{x_0}{[\phi\ 1\ldots 1]},\bar{S}\right) \mathcal{F}\left(a,\xi(\frac{x_0}{[\phi\ 1\ldots 1]},a,\bar{S}),\bar{S}\right) \bar{b}\left(\xi(\frac{x_0}{[\phi\ 1\ldots 1]},a,\bar{S})\right) da \\ &+ \int_0^\infty \beta\left(\frac{x_0}{[1-\phi\ 1\ldots 1]},\bar{S}\right) \mathcal{F}\left(a,\xi(\frac{x_0}{[1-\phi\ 1\ldots 1]},a,\bar{S}),\bar{S}\right) \\ &\quad \bar{b}\left(\xi(\frac{x_0}{[1-\phi\ 1\ldots 1]},a,\bar{S})\right) da. \end{aligned}$$

$\Theta(x_0,\bar{S})$ can be interpreted as the total nutrient consumption of a cell that started with birth state x_0 over its entire life-time when there is a constant nutrient concentration $\bar{S}$ and $R_0(x_0,\bar{S})$ as the number of cells born per unit of time with birth state x_0 when there is a constant nutrient concentration $\bar{S}$.

We compute $x(a,x_0,\bar{S})$ and $\mathcal{F}(a,x_0,\bar{S})$ by solving the following system of non-autonomous ODEs in which the derivative is taken with respect to age a:

$$\begin{aligned} x'(a,x_0,\bar{S}) &= g(x(a,x_0,\bar{S}),\bar{S}), \\ x(0,x_0,\bar{S}) &= x_0, \quad x_0 \in \Omega_b, \end{aligned}$$

and

$$\begin{aligned} \mathcal{F}'(a,x_0,\bar{S}) &= -(\mu_d(x(a,x_0,\bar{S}),\bar{S}) + \beta(x(a,x_0,\bar{S}),\bar{S}))\mathcal{F}(a,x_0,\bar{S}), \\ \mathcal{F}(0,x_0,\bar{S}) &= 1, \quad x_0 \in \Omega_b. \end{aligned}$$

4.4 Discretisation of Ω_b by a uniform mesh

4.4.1 First view on the discretisation of Ω_b

In order to make the computation of a population equilibrium possible, we will need to discretise the multidimensional birth state space Ω_b and make biologically reasonable assumptions about the mechanisms triggering cell division. Numerically this leads to a system with tremendous complexity, so in Section 4.5 we will simplify this general discretisation. In order to understand the discretisation of Ω_b we first expand the vector notation of $x(a,x_0,\bar{S})$:

$$x(a,x_0,\bar{S}) = \begin{pmatrix} m(a,x_0,\bar{S}) \\ \delta(a,x_0,\bar{S}) \\ \alpha_1(a,x_0,\bar{S}) \\ \alpha_2(a,x_0,\bar{S}) \end{pmatrix},$$

where we have assumed that there are 3 internal concentrations we need to follow to know the state of the cell cycle of a cell. We start by looking at $\Omega_b|_m$, the restriction of Ω_b to its first component, the mass-state of the cell population.

We discretise $\Omega_b|_m$ in the simplest possible way, with a uniform meshing. Let $N_m \in \mathbb{N}$ be the number of intervals into which we divide $\Omega_b|_m$. We have to make the distinction between the No-Minimal-Mass model, where $\Omega_b|_m =]0,(1-\phi)m_{max}]$, and the Minimal-Mass models, where $\Omega_b|_m = [\phi m_{min},(1-\phi)m_{max}]$ (see section 4.1.4 and Table 4.2). For NMM, let $\Delta m = \frac{(1-\phi)m_{max}}{N_m}$ be the discretisation step. We then have N_m+1 mesh points in $\Omega_b|_m$, whose values we can address in a simple way:

$$m_{0i} := i\Delta m \quad \text{for} \quad i = 1,\ldots,N_m.$$

The discretisation points in $\Omega_b|_m$ are then:

$$d_{0i} := \left(i - \frac{1}{2}\right)\Delta m \quad \text{for} \quad i = 1,\ldots,N_m. \tag{4.5}$$

For the Minimal-Mass models, let $\Delta m = \frac{((1-\phi)m_{max}-\phi m_{min})}{N_m}$ be the discretisation step, we then have the following N_m+1 mesh points:

$$m_{0i} := \phi m_{min} + i\Delta m \quad \text{for} \quad i = 1,\ldots,N_m.$$

The discretisation points then are:

$$d_{0i} := \phi m_{min} + \left(i - \frac{1}{2}\right)\Delta m \quad \text{for} \quad i = 1,\ldots,N_m. \tag{4.6}$$

The discretisation of $\Omega_b|_\delta$, $\Omega_b|_{\alpha_1}$ and $\Omega_b|_{\alpha_2}$ can be done analogously to $\Omega_b|_m$ with N_δ, N_{α_1} and $N_{\alpha_2} \in \mathbb{N}$ the respective number of intervals of the discretisation. Whether a cell divides or not depends on its value $\delta(a,x_0,\bar{S})$ and the choices that are made for the cell division mechanism in the model, so this means that $\Omega_b|_\delta$ will correspond to a certain interval depending on the chosen cell division mechanism. Assume that $\Omega_b|_\delta = [\delta_m,\delta_M]$, then $\Delta\delta = \frac{\delta_M-\delta_m}{N_\delta}$ is the discretisation step of $\Omega_b|_\delta$. Assume $\Omega_b|_{\alpha_1} = [a_{1m},a_{1M}]$ and $\Omega_b|_{\alpha_2} = [a_{2m},a_{2M}]$ (these ranges can be found by experiments with the cell cycle model), then $\Delta\alpha_1 = \frac{a_{1M}-a_{1m}}{N_{\alpha_1}}$ and $\Delta\alpha_2 = \frac{a_{2M}-a_{2m}}{N_{\alpha_2}}$ are the respective discretisation steps of $\Omega_b|_{\alpha_1}$ and $\Omega_b|_{\alpha_2}$. We then have the following discretisation points:

$$\delta_{0j} \quad = \quad \delta_m + \left(j - \frac{1}{2}\right)\Delta\delta \quad \text{for} \quad j = 1,...,N_\delta,$$

$$\begin{aligned}\alpha_{10k} &= a_{1m} + \left(k - \frac{1}{2}\right)\Delta\alpha_1 \quad \text{for} \quad k = 1,...,N_{\alpha_1},\\ \alpha_{20l} &= a_{2m} + \left(l - \frac{1}{2}\right)\Delta\alpha_2 \quad \text{for} \quad l = 1,...,N_{\alpha_2}.\end{aligned}$$

We will use the notation x_{0ijkl} for $\begin{pmatrix} d_{0i} \\ \delta_{0j} \\ \alpha_{10k} \\ \alpha_{20l} \end{pmatrix}$ ($i = 1,...,N_m,\ j = 1,...,N_\delta,\ k = 1,...,N_{\alpha_1}$ and $l = 1,...,N_{\alpha_2}$), which represents the discretisation points of the different birth cohorts. This general discretisation leads to a high number of possible birth states, which will make the computations for the system complex. In Section 4.5 we will motivate certain simplifications, specifically for the kind of internal cell cycle models we implement.

4.4.2 The equilibrium conditions of the discretised model

The discretised population model is now governed by the following equations, in which the derivative is taken with respect to age a:

$$\begin{aligned}
m'(a,x_{0ijkl},\bar{S}) &= g_m\left(m(a,x_{0ijkl},\bar{S}),\delta(a,x_{0ijkl},\bar{S}),\alpha_1(a,x_{0ijkl},\bar{S}),\alpha_2(a,x_{0ijkl},\bar{S}),\bar{S}\right),\\
m(0,x_{0ijkl},\bar{S}) &= d_{0i},\\
\delta'(a,x_{0ijkl},\bar{S}) &= g_\delta\left(m(a,x_{0ijkl},\bar{S}),\delta(a,x_{0ijkl},\bar{S}),\alpha_1(a,x_{0ijkl},\bar{S}),\alpha_2(a,x_{0ijkl},\bar{S}),\bar{S}\right),\\
\delta(0,x_{0ijkl},\bar{S}) &= \delta_{0j},\\
\alpha_1'(a,x_{0ijkl},\bar{S}) &= g_{\alpha_1}\left(m(a,x_{0ijkl},\bar{S}),\delta(a,x_{0ijkl},\bar{S}),\alpha_1(a,x_{0ijkl},\bar{S}),\alpha_2(a,x_{0ijkl},\bar{S}),\bar{S}\right),\\
\alpha_1(0,x_{0ijkl},\bar{S}) &= \alpha_{10k},\\
\alpha_2'(a,x_{0ijkl},\bar{S}) &= g_{\alpha_2}\left(m(a,x_{0ijkl},\bar{S}),\delta(a,x_{0ijkl},\bar{S}),\alpha_1(a,x_{0ijkl},\bar{S}),\alpha_2(a,x_{0ijkl},\bar{S}),\bar{S}\right),\\
\alpha_2(0,x_{0ijkl},\bar{S}) &= \alpha_{20l},\\
\mathcal{F}'(a,x_{0ijkl},\bar{S}) &= -\left(\mu_d(x(a,x_{0ijkl},\bar{S}),\bar{S}) + \beta(m(a,x_{0ijkl},\bar{S}),\delta(a,x_{0ijkl},\bar{S}))\right)\\
&\quad \cdot\mathcal{F}(a,x_{0ijkl},\bar{S}),\\
\mathcal{F}(0,x_{0ijkl},\bar{S}) &= 1,\\
r_0'(a,x_{0ijkl},\bar{S}) &= \beta\left(\frac{m_{0i}}{\phi},\delta_{0j}\right)\cdot\mathcal{F}\left(a,\xi(\frac{x_{0ijkl}}{[\phi\ 1\ldots 1]},a,\bar{S}),\bar{S}\right)\cdot\bar{b}\left(\xi(\frac{x_{0ijkl}}{[\phi\ 1\ldots 1]},a,\bar{S})\right)\\
&+ \beta\left(\frac{m_{0i}}{1-\phi},\delta_{0j}\right)\cdot\mathcal{F}\left(a,\xi(\frac{x_{0ijkl}}{[1-\phi\ 1\ldots 1]},a,\bar{S}),\bar{S}\right)\\
&\quad \cdot\bar{b}\left(\xi(\frac{x_{0ijkl}}{[1-\phi\ 1\ldots 1]},a,\bar{S})\right),
\end{aligned}$$

$$
\begin{aligned}
r_0(0, x_{0ijkl}, \bar{S}) &= 0, \\
\theta'(a, x_{0ijkl}, \bar{S}) &= \gamma\big(x(a, x_{0ijkl}, \bar{S}), \bar{S}\big) \cdot \mathcal{F}(a, x_{0ijkl}, \bar{S}), \\
\theta(0, x_{0ijkl}, \bar{S}) &= 0.
\end{aligned}
$$

These equations define the cohort solutions as a function of age a. For a given fixed $\bar{S}$ they compute the cohort behaviour, i.e. the evolution of all cells that are born with a size $m_{0i} \in \Omega_b|_m$ ($0 \leq i \leq N_m$) and with concentration $\delta_{0j}, \alpha_{10k}$ and α_{20l} ($0 \leq j \leq N_\delta$, $0 \leq k \leq N_{\alpha_1}$ and $0 \leq l \leq N_{\alpha_2}$). $r_0(a, x_{0ijkl}, \bar{S})$ can be interpreted as the number of cells born per unit of time with birth state x_{0ijkl} as a result from mother cells with ages up to a when there is a constant nutrient concentration $\bar{S}$. $\theta(a, x_{0ijkl}, \bar{S})$ can be interpreted as the total nutrient consumption of a cell that had birth state x_{0ijkl} over its life-time up to age a when the nutrient concentration is the constant $\bar{S}$. The equations are solved for every cohort until a cell age $\bar{a}$ for which $\mathcal{F}(\bar{a}, x_{0ijkl}, \bar{S}) < \varepsilon_a$ for a given small $\varepsilon_a > 0$. We start with a value of $\bar{S}$ and a fixed parameter set, and solve the above system of ODEs for sufficiently long age a until the stop criterion is met. The result is plugged into the equilibrium condition (4.4), with

$$R_0(x_{0ijkl}, \bar{S}) = r_0(\bar{a}, x_{0ijkl}, \bar{S})$$

and

$$\Theta(x_{0ijkl}, \bar{S}) = \theta(\bar{a}, x_{0ijkl}, \bar{S}).$$

for all $x_{0ijkl} \in \Omega_b$. The integral over Ω_b in (4.4) is replaced by a discrete sum, which must be solved to obtain the pair $(\bar{S}, \bar{b})$. If we free one parameter λ, we have obtained a map

$$F(\bar{S}, \bar{b}, \lambda) = 0,$$

which in principle can be used for continuation of the cell population equilibria. We can investigate how changes in the environment or in the cell cycle trigger different equilibrium cell state distributions.

4.5 Adaptive discretisation and choices for the vital rates

In the previous section, we described the general discretisation of Ω_b which results in $N_m \times N_\delta \times N_{\alpha_1} \times N_{\alpha_2}$ possible states at birth and which thus implies heavy computations. If we consider the Toy model of Tyson and Novák (4.3), we can simplify this discretisation because of the funneling effect the model displays. There is namely a strict coupling between m, X, Y and A at the moment of division if the birth mass is not too large (see the top figure of Figure 3.20). This means that the value of X at division determines the values of m, Y and A to a large extent. Since the mother cells divide in two daughter cells that can be unequal in size (if $\phi < 0.5$), a newborn cell with a given mass can originate from two possible mother cell's masses, that have different corresponding X, Y and A values. So with a certain newborn cell mass m_i that is small enough so that the funneling effect plays, can correspond two different sets of values for (X,Y,A). We do not have to consider these values explicitly since because of the funneling effect, the two initial stages converge fast to the same orbit. We note that the funneling effect is also observed in more realistic models, e.g. the budding yeast model in [80], see Section 3.2.2. We therefore choose, as an approximation motivated by the funneling effect for small newborn cells, to only discretise $\Omega_b|_m$ in N intervals and take the initial discretisation points as the center of the meshes (see Section 4.4.1). The inital discretisation points of Ω_b then are

$$x_{0i} = \begin{pmatrix} d_{0i} \\ 0.1 \\ 0.5 \\ 0.5 \end{pmatrix} \quad \text{for} \quad i = 1,\ldots,N, \tag{4.7}$$

with d_{0i} as in (4.5) for the No-Minimal-Mass model and (4.6) for the Minimal-Mass models MM1–MM2. We have chosen the values for X, Y and A such that the convergence to the funneled orbit is achieved long before the concentration values are in the neighbourhood where division is possible.

Instead of fixing the discretisation points of Ω_b, and thus the number of birth cohorts N, we use adaptive meshing. More precisely, we let the choice of the discretisation points depend on the cells that are born and on two parameters δ and ε. For the initial discretisation points we use the values (4.7) and this is the starting list of birth

cohorts for the first age integration. The idea is that for every age integration, we have a list of birth cohorts (resulting from the previous step) and by going through this list, we create a new list of birth cohorts (so while doing an age integration, we work with two seperate lists of cohorts). The calculation of the new list of birth cohorts is done by going through the input list of birth cohorts and checking for every division if this gives rise to a new discretisation point (in addition to the ones already created) and thus an extra cohort in the new list of birth cohorts. We only create a new discretisation point if the mass of the newborn cells is not in the "inhibition zone" of an existing discretisation point, meaning within a distance δ of it. This new discretisation point then has the m, X, Y and A values of the corresponding newborn cells. If the mass of the newborn cells is closer than δ to the mass of an already existing discretisation point, we merge the newborn cells with those in the existing discretisation point by using weighted means for the m, X, Y and A values. In the special case that the newborn cells are in the "inhibition zone" of two discretisation points, the cells are merged with the closest cohort (in m-distance), but afterwards we check if the adjusted discretisation point is not too close to the other one (in which case, they are also merged together). At the end of the loop, we check if there are discretisation points (and corresponding birth cohorts) that can be ignored in the newly created list of birth cohorts because of too little cells. We use ε as a lower threshold for the fraction of cells born in a birth cohort.

We then have for a birth cohort i ($i = 1,...,N$) with birth state $x_{0i} = \begin{pmatrix} m_i \\ X_i \\ Y_i \\ A_i \end{pmatrix}$, the following age equations (the derivatives are taken with respect to age a) and initial conditions in the equilibrium state:

$$
\begin{aligned}
m'(a,x_{0i},\bar{S}) &= g_m(m(a,x_{0i},\bar{S}),X(a,x_{0i},\bar{S}),Y(a,x_{0i},\bar{S}),A(a,x_{0i},\bar{S}),\bar{S}), && (4.8)\\
m(0,x_{0i},\bar{S}) &= m_i, \\
X'(a,x_{0i},\bar{S}) &= g_X(m(a,x_{0i},\bar{S}),X(a,x_{0i},\bar{S}),Y(a,x_{0i},\bar{S}),A(a,x_{0i},\bar{S}),\bar{S}), && (4.9)\\
X(0,x_{0i},\bar{S}) &= X_i, \\
Y'(a,x_{0i},\bar{S}) &= g_Y(m(a,x_{0i},\bar{S}),X(a,x_{0i},\bar{S}),Y(a,x_{0i},\bar{S}),A(a,x_{0i},\bar{S}),\bar{S}), && (4.10)\\
Y(0,x_{0i},\bar{S}) &= Y_i, \\
A'(a,x_{0i},\bar{S}) &= g_A(m(a,x_{0i},\bar{S}),X(a,x_{0i},\bar{S}),Y(a,x_{0i},\bar{S}),A(a,x_{0i},\bar{S}),\bar{S}), && (4.11)\\
A(0,x_{0i},\bar{S}) &= A_i,
\end{aligned}
$$

$$\begin{aligned}
\mathcal{F}'(a,x_{0i},\bar{S}) &= -(\mu_d(x(a,x_{0i},\bar{S}),\bar{S})+\beta(m(a,x_{0i},\bar{S}),X(a,x_{0i},\bar{S})))\\
&\quad \cdot\mathcal{F}(a,x_{0i},\bar{S}), \qquad (4.12)\\
\mathcal{F}(0,x_{0i},\bar{S}) &= 1,\\
\theta'(a,x_{0i},\bar{S}) &= \gamma(m(a,x_{0i},\bar{S}),X(a,x_{0i},\bar{S}),Y(a,x_{0i},\bar{S}),A(a,x_{0i},\bar{S}),\bar{S})\\
&\quad \cdot\mathcal{F}(a,x_{0i},\bar{S}), \qquad (4.13)\\
\theta(0,x_{0i},\bar{S}) &= 0.
\end{aligned}$$

The equations for r_0 are omitted because the number of cells that are born in the new list of birth cohorts is automatically calculated during each age integration. For every $x_{0i} \in \Omega_b$ the equations (4.8)-(4.13) are solved until age $\bar{a}_i$, where we have that $\mathcal{F}(\bar{a}_i,x_{0i},\bar{S}) < \varepsilon_{\mathcal{F}}$ for a given small positive $\varepsilon_{\mathcal{F}}$. When this stop criterion is met, we can calculate $\Theta(x_{0i},\bar{S}) = \theta(\bar{a}_i,x_{0i},\bar{S})$.

We note that it is in principle possible that a newborn cell divides immediately (see Figure 4.2), namely if it is born with a mass $m \in [m_{min},(1-\phi)m_{max}]$ for the Minimal-Mass models MM1–MM2 (if this interval is nonempty), and it is always the case for cells in the No-Minimal-Mass model NMM (see Section 4.2.2). We expect for the simulation of the NMM model, that the cells will divide immediately after they are born, so we expect a situation where the number of newborn cells increases, while the mass of the cells is decreasing. In the simulation of the Minimal-Mass models it might happen that (for a good choice of δ) there are only 2 intervals of masses where $\bar{b}(x) \neq 0$, namely an interval around ϕm^* and an interval around $(1-\phi)m^*$, where m^* is the mass that corresponds with the X-value 0.1 at division (because of the funneling effect this mass value is uniquely determined).

The equilibrium $(\bar{S},\bar{b}(x_{0i}))$ is the $(N+1)$-vector that fulfills the following $N+1$ equations:

$$\begin{aligned}
&f(\bar{S}) - \sum_{i=1}^{N} \Theta(x_{0i},\bar{S})\,\bar{b}(x_{0i}) = 0,\\
&R_0(x_{0i},\bar{S}) - \bar{b}(x_{0i}) = 0, \quad \forall i = 1,\cdots,N.
\end{aligned}$$

Here we assume implicitly that the number of birth cohorts N and their birth states converge when the system converges to an equilibrium. To solve these equations, we

rewrite them as the fixed point of the following map M:

$$M : \begin{pmatrix} \bar{S} \\ \bar{b}(x_{0i}) \end{pmatrix} \longrightarrow \begin{pmatrix} S^0 - \frac{1}{D}\sum_{i=1}^{N} \Theta(x_{0i}, \bar{S})\, \bar{b}(x_{0i}) \\ R_0(x_{0i}, \bar{S}) \end{pmatrix}, \tag{4.14}$$

using $f(S) = D(S^0 - S)$, see (4.1). To make sure that the resulting $\bar{S}$ is non-negative, we define it as the maximum of $S^0 - \frac{1}{D}\sum_{i=1}^{N} \Theta(x_{0i}, \bar{S})\, \bar{b}(x_{0i})$ and 0.000001. The map M is a mathematical construction to calculate equilibria of the cell population model. A map iteration has no biological meaning, except when it leads to a fixed point. By starting a map iteration with a certain number of cells born per unit of time in certain birth cohorts, we implicitly also consider all the older cells that originate from one of these birth cohorts, so in fact start with a (discretised form of the) population distribution over Ω. Note that although there is a correspondence between fixed points of this map and equilibria of the cell population model, stability has a different meaning in the two contexts and the relation between the two is unclear. Also important to note is that $\bar{b}(x_{0i})$ is scalable. It is expressed as the number of cells born per unit of time and per unit of volume in a certain birth cohort x_{0i}. From the equilibrium equations it is easy to note that we can multiply the number of cells born per unit of time in every birth cohort with a certain factor and still get a solution to the equilibrium equations, as long as the nutrient concentration in the bioreactor $\bar{S}$, the nutrient concentration in the feeding bottle S^0 (see (4.1)) and the parameter ζ_1 (see h(S) in (4.3)) are multiplied with the same factor. This can be interpreted as a change to the volume of the chemostat.

Some vital rates still have to be chosen. The rates g_m, g_X, g_Y and g_A are defined in (4.3). We assume that the death rate of the cells is constant and equal to the dilution rate: $\mu_d(x,S) = D$. The rate of division $\beta(m,X)$ is defined in Section 4.2.2 and for the consumption rate $\gamma(x,S)$ we choose:

$$\gamma(x,S) = c_2 \frac{dm}{dt} = c_2\, \mu\, m \left(1 - \frac{m}{m_{max}}\right) \frac{c_1 S}{\zeta_1 + S},$$

with $c_2 \leq 1$ a positive parameter.

In Table 4.3 the remaining parameters in the cell population models NMM, MM1 and MM2 are listed. We further have to choose the initial N to start the map iterations

Table 4.3: Parameter values of population models NMM, MM1 and MM2

parameter	value
X_{DIV}	0.1
ϕ	0.4
m_{min}	0.75
S^0	$1/m^3$
c_2	1
D	0.01/min
$\varepsilon_{\mathcal{F}}$	0.0000001
δ	0.001
ε	0.0000000001

in search of a fixed point. In Chapter 5 we will discuss the computational results for the structured population models that are introduced in this chapter.

CHAPTER 5

Computational results for structured population models with internal cell cycle

Overview

In this chapter we discuss the computational results for the structured population models with internal cell cycle, as introduced in Chapter 4. In Section 5.1.1 we briefly discuss how we implement the map (introduced in §4.5) and in Section 5.1.2 the convergence results for the models NMM, MM1 and MM2 (see §4.2.2) are discussed. In the NMM model, all cells divide immediately after birth, which is not very realistic. For the MM1 model, we find a non-trivial fixed point with 41 birth cohorts for the initial parameter values, which we discuss in more detail with e.g. a cohort-to-cohort representation that indicates for every birth cohort to which birth cohorts the daughter cells of dividing cells that were born in this certain birth cohort, contribute. For the MM2 model, a similar non-trivial fixed point is found. We will focus on the MM1 model for the calculations in the rest of this chapter.

In Section 5.2 we discuss the numerical effects that have to be taken into account when calculating the fixed point by iterating the map. First, numerical noise may result in a higher number of birth cohorts when `reltol` (the scalar relative tolerance in the age integration) is not small enough for the used value of δ. Second, the total amount of cells born per minute in the fixed point $\bar{b}_{tot}$ decreases and the nutrient value

of the fixed point $\bar{S}$ increases, when `reltol` decreases. And finally, the variation of $\bar{b}_{tot}$ and $\bar{S}$ during the map iterations decreases when `reltol` decreases. We further compare the impact of changing δ and `reltol` on the speed and precision of the calculation of the fixed point and conclude that the best choice for δ and `reltol` can only be motivated locally in parameter space by considering the robustness of the found fixed point, the number of cohorts and the computation time.

In Section 5.3 we investigate how the convergence behaviour changes under variation of the parameter S^0 (the nutrient concentration in the feeding bottle of the chemostat). For some values of S^0 non-trivial fixed points coexist with cycles of the map, both stable in terms of the map. This might be due to the combination of a subcritical period doubling bifurcation and a limit point bifurcation. In Section 5.4 we investigate how sensitive the fixed point is to perturbations for a parameter value for which there also exists a stable cycle. We consider a random shift of the mass of the cohorts, a fixed shift of the mass of the cohorts, doubling of the number of cohorts and a perturbation of the nutrient concentration and number of cells of the fixed point. In Section 5.5 we use the observed cyclic behaviour for several S^0 values to make an "educated" guess for the fixed point. This gives good results for some values, but it only works if the attraction region of the fixed point is big enough and the values of the points of the cycle are located quite symmetrical around the fixed point.

In Section 5.6 three different fixed point continuation methods for free S^0 are discussed. A very simple method is used in §5.6.1, which we call the zero-order prediction method. The fixed point of the previous S^0 value is used as prediction. In §5.6.2 the prediction of the new fixed point is based on the 2 previously computed fixed points, using linear extrapolation, which we call the chord prediction. Finally, in §5.6.3 a modified version of the pseudo-arclength continuation method is used. The resulting fixed point curves are given for every method. The fixed points of the non-trivial fixed point curve all have the same 41 birth cohorts and the same $\bar{S}$, and $\bar{b}_{tot}$ increases linearly with increasing S^0. We explain this result using the equilibrium equations. In Section 5.7 we discuss the results of the same fixed point continuation methods of the previous section, but applied to a free dilution rate D. D plays a more complex role in the system since it both influences the nutrient level and the death rate of the cells. This results in a more complex shape of the

fixed point curve. The continuation method with chord prediction gives the best results for free D, meaning that it enables us to find the fixed points for the widest range of parameter values. We observe behaviour that is typical for a supercritical Neimark-Sacker bifurcation at $D = 0.0052$ min^{-1}. In Section 5.8 we discuss which D value is optimal to maximize the yield and in Section 5.9 we study the non-trivial fixed points with very few cohorts for small D values.

As a generalisation of our population model, we consider two adaptations in the last sections. In Section 5.10 we adapt one of the cell division criteria proposed by Tyson and Novák and study the effect on the resulting fixed point. We make the distinction between the case where the value of a critical chemical concentration for division is imprinted at birth and the case where the value is established during the progression through the cell cycle. For both cases, we study an example. Finally, in Section 5.11 we incorporate a more extended model for the cell cycle as internal structure for the cells, namely the budding yeast model of Tyson and Novák. We discuss the found non-trivial fixed point and compare the fixed points for several D values.

5.1 Computational study of the Toy model with variable number of cohorts

5.1.1 Implementation: class cohort and age integration

A birth cohort corresponds to an object of the class cohort. We create N cohorts for the birth mass, as explained in Section 4.5. The function `integrate_cohort` calculates for a given cohort m, X, Y, A, $\mathcal{F}$ and θ for the cells in the cohort at ages $a_i = T_1 + i * T_{IN}$ with $i \in \mathbb{N}$. The calculations stop when the survival probability for cells in the cohort at that age is smaller than $\varepsilon_{\mathcal{F}}$. For the age integration, we use the CVODE-solver of the SUNDIALS (SUite of Nonlinear and DIfferential/ALgebraic equation Solvers) package (see [45, 46]). The CVODE-solver is designed to solve initial value problems for ordinary differential equation systems. We use the recommended options for non-stiff problems: the Adams-Moulton linear multistep method with functional iteration for each integration step. The function `integrate_cohort` also determines for a given birth cohort which cells are born from mother cells in this cohort throughout their life-time.

The function `integrate_allcohorts` makes a loop over a given list of birth cohorts and initial number of cells born per minute in each birth cohort and uses the function `integrate_cohort` to determine the new list of birth cohorts with all the cells that are born per minute from cells originating from the original birth cohorts. When constructing this new list of cohorts, we use the tactics of an "inhibition zone" for the mass and the minimal fraction of cells in a cohort, as explained in Section 4.5.

The function `loopMap` iterates the map (4.14) a given fixed number of times.

More detailed information about the implementation can be found in Chapter 6.

5.1.2 Convergence results for three models of cell division

The results in this section were obtained for the parameter values in Table 4.3.

No-Minimal-Mass model with deterministic division NMM

For this model we assume that the cells in a cohort divide when $X = X_{DIV}$ and $\frac{dX}{dt} < 0$, so all cells alive at the age when $X = X_{DIV}$ and $\frac{dX}{dt} < 0$ in a cohort divide. The function `integrate_cohort` gives an extra output value when $X = X_{DIV}$ using the rootfinding feature of the CVODE-solver. We use the following simple algorithm in `integrate_cohort`:

```
if(X = X_DIV and X is decreasing)
  print message "Conditions for division are immediately fulfilled";
  determine the values of m, X, Y and A of the small part;
  determine the values of m, X, Y and A of the large part;
  calculation of number of cells born;
else
  take age-step T_IN in age integration of m, X, Y, A, F and θ;
  while((X ≠ X_DIV and F > ε_F) or (X = X_DIV and X is not decreasing))
    take age-step T_IN in age integration of m, X, Y, A, F and θ;
  if(X ≠ X_DIV and F ≤ ε_F)
    print message "Survival probability too small in cohort, cells
                   in cohort do not divide";
  else
    if(X = X_DIV and X is decreasing)
      print message "Conditions for division are immediately
                     fulfilled";
```

Table 5.1: Orbit of the map for NMM with at start $\bar{S} = 1$ and 10^{-7} cells born per minute in every of the 100 birth cohorts (with the initial m through uniform meshing, $X = 0.1$, $Y = A = 0.5$). Parameter values as in Tables 3.2, 4.1 and 4.3.

iteration	N	total number of cells born per minute	birth mass in cohort 1	new $\bar{S}$
1	200	$2.00000 \cdot 10^{-5}$	$1.20000 \cdot 10^{-2}$	1
2	300	$4.00000 \cdot 10^{-5}$	$4.80000 \cdot 10^{-3}$	1
3	304	$8.00000 \cdot 10^{-5}$	$2.64000 \cdot 10^{-3}$	1
4	246	$1.60000 \cdot 10^{-4}$	$1.43127 \cdot 10^{-3}$	1
5	186	$3.20000 \cdot 10^{-4}$	$9.74653 \cdot 10^{-4}$	1
6	155	$6.40000 \cdot 10^{-4}$	$8.31065 \cdot 10^{-4}$	1
7	116	$1.28000 \cdot 10^{-3}$	$1.00603 \cdot 10^{-3}$	1
8	72	$2.56000 \cdot 10^{-3}$	$1.06964 \cdot 10^{-3}$	1
9	42	$5.12000 \cdot 10^{-3}$	$7.37686 \cdot 10^{-4}$	1
10	27	$1.02400 \cdot 10^{-2}$	$8.94714 \cdot 10^{-4}$	1
100	1	$1.26765 \cdot 10^{25}$	$2.36658 \cdot 10^{-30}$	1
200	1	$1.60694 \cdot 10^{55}$	$1.86690 \cdot 10^{-60}$	1
300	1	$2.03704 \cdot 10^{85}$	$1.47273 \cdot 10^{-90}$	1

```
    determine the values of m, X, Y and A of the small part;
    determine the values of m, X, Y and A of the large part;
    calculation of number of cells born;
  else
    print message "Problem with age integration";
```

We start with $\bar{S} = 1$, $N = 100$, 10^{-7} cells born per minute in every birth cohort and the discretisation points x_{0i} as described in Section 4.5 (with parameter values as in Tables 3.2, 4.1 and 4.3). The cells in every birth cohort divide immediately. The newborn cells have smaller masses at every iteration of the map. An overview of the results is given in Table 5.1. Note that in this case the total number of cells born per minute in iteration i equals $10^{-5} \cdot 2^i$. Also the total mass of all the cells born per minute remains constant, namely

$$\sum_{i=1}^{100} 10^{-7} \cdot (i - \frac{1}{2}) \cdot 0.06 = 3 \cdot 10^{-5},$$

since $\Omega_b|_m =]\,0,6\,]$.

It is important to note that the initial discretisation points for Y have a strong influence on the outcome of the map iterations. We namely have two division

Table 5.2: Orbit of the map for NMM with at start $\bar{S} = 1$ and 10^{-7} cells born per minute in every of the 100 birth cohorts (with the initial m through uniform meshing, $X = 0.1$, $Y = 0.35$ and $A = 0.5$). Parameter values as in Tables 3.2, 4.1 and 4.3.

iteration	N	total number of cells born per minute	birth mass in cohort 1	new $\bar{S}$
1	35	$2.15135 \cdot 10^{-6}$	$4.50401 \cdot 10^{-1}$	0.99489
2	51	$2.15135 \cdot 10^{-6} \cdot 2$	$1.80160 \cdot 10^{-1}$	1
3	64	$2.15135 \cdot 10^{-6} \cdot 2^2$	$7.21673 \cdot 10^{-2}$	1
4	66	$2.15135 \cdot 10^{-6} \cdot 2^3$	$2.91461 \cdot 10^{-2}$	1
5	56	$2.15135 \cdot 10^{-6} \cdot 2^4$	$1.17719 \cdot 10^{-2}$	1
6	43	$2.15135 \cdot 10^{-6} \cdot 2^5$	$4.93629 \cdot 10^{-3}$	1
7	33	$2.15135 \cdot 10^{-6} \cdot 2^6$	$2.75066 \cdot 10^{-3}$	1
8	22	$2.15135 \cdot 10^{-6} \cdot 2^7$	$2.22381 \cdot 10^{-3}$	1
9	15	$2.15135 \cdot 10^{-6} \cdot 2^8$	$1.29792 \cdot 10^{-3}$	1
10	10	$2.15135 \cdot 10^{-6} \cdot 2^9$	$9.44866 \cdot 10^{-4}$	1
100	1	$2.15135 \cdot 10^{-6} \cdot 2^{99}$	$1.18780 \cdot 10^{-30}$	1
200	1	$2.15135 \cdot 10^{-6} \cdot 2^{199}$	$9.37008 \cdot 10^{-61}$	1
300	1	$2.15135 \cdot 10^{-6} \cdot 2^{299}$	$7.39169 \cdot 10^{-91}$	1

conditions for NMM: $X = 0.1$ (which is automatically fulfilled for newborn cells) and $\frac{dX}{dt} = k_1 - (k_2^{'} + k_2^{''}Y)X < 0$. For the parameter values in Tables 3.2, 4.1 and 4.3 and the discretisation points for $Y = 0.5$, the latter condition is fulfilled and the cells divide immediately. For e.g. $Y = 0.35$ this is not the case and we will obtain different results for the first map iteration (see Table 5.2). After this first iteration the discretisation points in the birth cohorts are such that the latter condition for division is immediately fulfilled and we get the same behaviour as in Table 5.1.

First Minimal-Mass model with deterministic division MM1

In this model we assume that the cells in a cohort divide when $X = X_{DIV}$, $\frac{dX}{dt} < 0$ and $m \geq m_{min}$, so the only difference with the model NMM is the requirement of a minimal mass for division. We use the following algorithm in `integrate_cohort`:

```
if(X = X_DIV and X is decreasing and m ≥ m_min)
  print message "Conditions for division are immediately fulfilled";
  determine the values of m, X, Y and A of the small part;
  determine the values of m, X, Y and A of the large part;
  calculation of number of cells born;
else
```

```
take age-step T_IN in age integration of m, X, Y, A, F and θ;
while((X ≠ X_DIV and F > ε_F) or (X = X_DIV and X is not decreasing)
                              or (X = X_DIV and m < m_min))
  take age-step T_IN in age integration of m, X, Y, A, F and θ;
if(X ≠ X_DIV and F ≤ ε_F)
  print message "Survival probability too small in cohort, cells
                 in cohort do not divide";
else
  if(X = X_DIV and X is decreasing and m ≥ m_min)
    print message "Conditions for division are immediately
                       fulfilled";
    determine the values of m, X, Y and A of the small part;
    determine the values of m, X, Y and A of the large part;
    calculation of number of cells born;
  else
    print message "Problem with age integration";
```


We start again with $\bar{S} = 1$, $N = 100$, 10^{-7} cells born per minute in every birth cohort and the initial discretisation points x_{0i} as in (4.7). The results are in Table 5.3. For these parameter values, the map converges to a non-trivial fixed point. The number of birth cohorts is constant from map iteration 65 to 300 (see Figure 5.1). We observe that the amount of cells born in total per minute in the 41 birth cohorts only varies slightly after an initial number of map iterations. More precisely, from map iteration 200 to 300 $\sum_{i=1}^{41} \bar{b}(x_{0i}) = \bar{b}_{tot}$ varies between 0.007202849249 and 0.007202858108, and the nutrient concentration $\bar{S}$ varies between 0.5948903581 and 0.5948913497. This is illustrated in Figure 5.2 in the $(\bar{b}_{tot}, \bar{S})$-plane.

When starting the iterations of the map with cells born in only one birth cohort (with $m = 0.301425$, $X = 0.1$, $Y = A = 0.5$) with 10^{-5} cells born per minute and with $\bar{S} = 1$, we obtain convergence to the same fixed point. Also, if we start with the same birth cohort with a higher amount of cells born per minute such as 10^{-3} and 10^{-2}, we obtain convergence to the same fixed point. The only difference is that we are sooner (i.e., after less age iterations) in the neighbourhood of the fixed point. For example, if we start the map iterations with 10^{-2} cells born per minute, we already have 41 cohorts after 26 map iterations. If the initial amount of cells born per minute is too high, there is usually no convergence to the non-trivial fixed point. For example, if we start the iterations of the map with only one birth cohort (with $m = 0.301425$, $X = 0.1$, $Y = A = 0.5$) with 0.1 cells born per minute and with $\bar{S} = 1$, we obtain convergence to the trivial fixed point with no cells and $\bar{S} = S^0 = 1$ (see Table 5.4).

Table 5.3: Orbit of the map for MM1 with at start $\bar{S} = 1$ and 10^{-7} cells born per minute in every of the 100 birth cohorts (with the initial m through uniform meshing, $X = 0.1$, $Y = A = 0.5$).

iteration	N	total number of cells born per minute	birth mass in cohort 1	new $\bar{S}$
1	196	$1.92067 \cdot 10^{-5}$	0.31380	0.99995
2	265	$3.49635 \cdot 10^{-5}$	0.30792	0.99976
3	236	$5.54086 \cdot 10^{-5}$	0.30168	0.99899
4	187	$6.66228 \cdot 10^{-5}$	0.30128	0.99697
5	165	$7.22470 \cdot 10^{-5}$	0.30053	0.99576
6	161	$8.24619 \cdot 10^{-5}$	0.30093	0.99563
7	150	$9.37082 \cdot 10^{-5}$	0.30086	0.99501
8	135	$1.04292 \cdot 10^{-4}$	0.30089	0.99417
9	122	$1.18415 \cdot 10^{-4}$	0.30081	0.99366
10	113	$1.34802 \cdot 10^{-4}$	0.30061	0.99285
100	41	$7.72029 \cdot 10^{-3}$	0.30440	0.59489
200	41	$7.72029 \cdot 10^{-3}$	0.30440	0.59489
300	41	$7.72029 \cdot 10^{-3}$	0.30440	0.59489

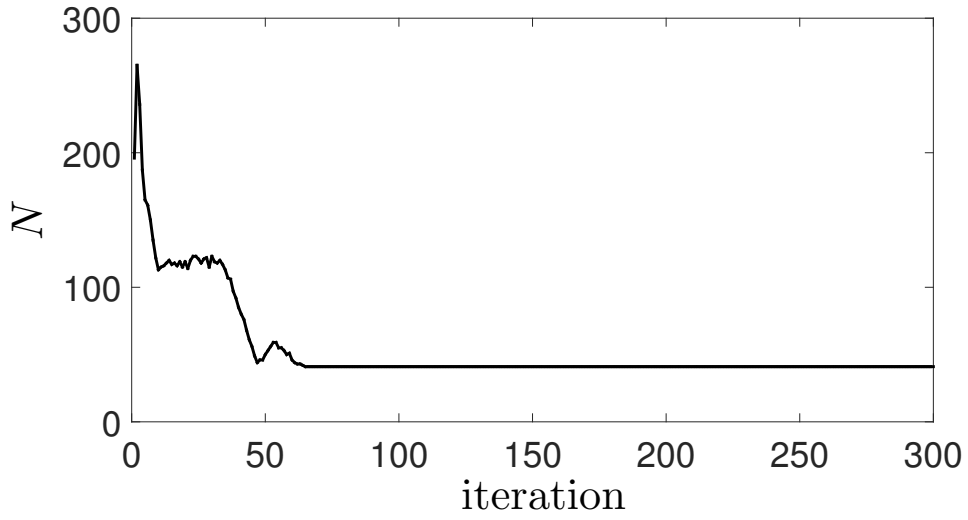

Figure 5.1: (iteration, N)-plot of MM1 with at start $\bar{S} = 1$ and 10^{-7} cells born per minute in every of the 100 birth cohorts (with the initial m through uniform meshing, $X = 0.1$, $Y = A = 0.5$). N settles at the value 41.

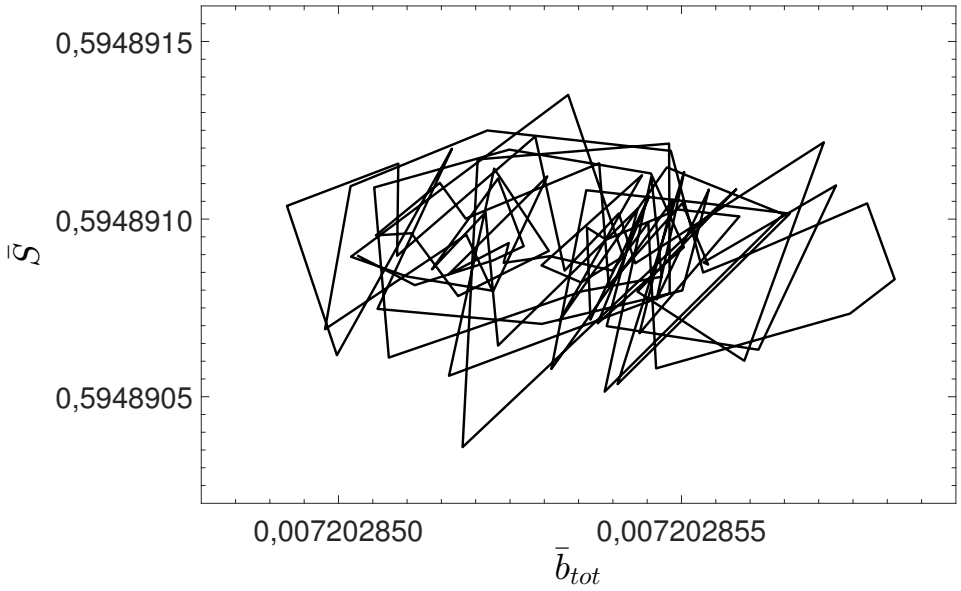

Figure 5.2: $(\bar{b}_{tot}, \bar{S})$-plot of the 200^{th} to 300^{th} iterates of MM1 with at start $\bar{S} = 1$ and 10^{-7} cells born per minute in every of the 100 birth cohorts (with the initial m through uniform meshing, $X = 0.1$, $Y = A = 0.5$).

The non-trivial fixed point has 41 birth cohorts for $\delta = 10^{-3}$ and `reltol`$= 10^{-6}$. In Table 5.5, the internal state of the 41 birth cohorts of the fixed point is given. The fixed point corresponds to a certain number of cells born per minute (see $\bar{b}$ in Table 5.5) in every of the birth cohorts. At any given time, cohorts with older cells originating from one of the birth cohorts at an earlier time also exist in the population. More precisely at a given time t, cohorts with cells of age a exist, each corresponding to one of the birth cohorts (born at time $t - a$). Such a cohort with cells of a certain

Table 5.4: Orbit of the map for MM1 with at start $\bar{S} = 1$ and only 1 birth cohort with 0.01 cells born per minute ($m = 0.301425$, $X = 0.1$, $Y = A = 0.5$).

iteration	**N**	**total number of cells born per minute**	**new $\bar{S}$**
1	2	0.0696146	0.000001
2	0	0	0.999762
3	0	0	1
4	0	0	1
5	0	0	1

Table 5.5: The internal state of the 41 birth cohorts of the fixed point of MM1 for $S^0 = 1$ (with $\bar{b}_{tot} = 7.720285 \cdot 10^{-3}$ and $\bar{S} = 0.59489$).

cohort	m	X	Y	A	$\bar{b}$
1	0.30440	0.1	0.97696	1.07222	3.13811 e-04
2	0.30578	0.1	0.97695	1.07704	1.20839 e-04
3	0.30731	0.1	0.97693	1.08235	7.11201 e-05
4	0.42506	0.1	0.97753	0.89846	1.48854 e-04
5	0.42870	0.1	0.97750	0.90625	6.84562 e-04
6	0.43205	0.1	0.97748	0.91343	2.15702 e-04
7	0.43437	0.1	0.97746	0.91839	3.44225 e-04
8	0.43543	0.1	0.97746	0.92065	5.66550 e-05
9	0.44053	0.1	0.97742	0.93154	2.34084 e-04
10	0.45523	0.1	0.97697	1.06903	4.42883 e-05
11	0.45653	0.1	0.97696	1.07206	2.04719 e-04
12	0.45836	0.1	0.97695	1.07630	1.85643 e-04
13	0.46096	0.1	0.97693	1.08235	7.11201 e-05
14	0.47448	0.1	0.97718	1.00333	7.95283 e-05
15	0.47661	0.1	0.97717	1.00781	3.67090 e-04
16	0.47860	0.1	0.97716	1.01200	1.16051 e-04
17	0.48009	0.1	0.97715	1.01512	2.16190 e-04
18	0.48376	0.1	0.97712	1.02284	1.26944 e-04
19	0.50587	0.1	0.97697	1.06903	4.42883 e-05
20	0.50726	0.1	0.97696	1.07206	2.04719 e-04
21	0.50862	0.1	0.97696	1.07491	6.48040 e-05
22	0.50964	0.1	0.97695	1.07704	1.20839 e-04
23	0.51218	0.1	0.97693	1.08235	7.11201 e-05
24	0.63760	0.1	0.97753	0.89846	1.48854 e-04
25	0.64285	0.1	0.97750	0.90598	5.87746 e-04
26	0.64421	0.1	0.97750	0.90792	9.68156 e-05
27	0.64807	0.1	0.97748	0.91343	2.15702 e-04
28	0.65155	0.1	0.97746	0.91839	3.44225 e-04
29	0.65314	0.1	0.97746	0.92065	5.66550 e-05
30	0.66059	0.1	0.97742	0.93124	2.01007 e-04
31	0.66207	0.1	0.97742	0.93334	3.30773 e-05
32	0.71172	0.1	0.97718	1.00333	7.95283 e-05
33	0.71491	0.1	0.97717	1.00781	3.67090 e-04
34	0.71790	0.1	0.97716	1.01200	1.16051 e-04
35	0.72013	0.1	0.97715	1.01512	2.16190 e-04
36	0.72565	0.1	0.97712	1.02284	1.26944 e-04
37	0.75871	0.1	0.97697	1.06903	4.42883 e-05
38	0.76089	0.1	0.97696	1.07206	2.04719 e-04
39	0.76293	0.1	0.97696	1.07491	6.48040 e-05
40	0.76446	0.1	0.97695	1.07704	1.20839 e-04
41	0.76827	0.1	0.97693	1.08235	7.11201 e-05

age exists as long as the survival probability of the cells at that age is bigger than a certain small positive threshold $\varepsilon_{\mathcal{F}}$ (see §4.5). The number of cells in a cohort decreases when the cells age, due to the constant dilution rate D. In Figure 5.3 the number of living cells (cells of all ages arising from the birth cohorts) at any given time is depicted as a function of the mass. Since this is a fixed point, the distribution stays constant in time. A more visually appealing representation is shown in Figure 5.4 where the living cells at any given moment in time are represented in 30 different uniformly distributed sizes. In the picture the cells are well-mixed, as we use a chemostat model. The size of the circles is proportional to the mass of the cells and the number of the circles is proportional to the amount of cells of a certain size. The cells of the same size are in the same color.

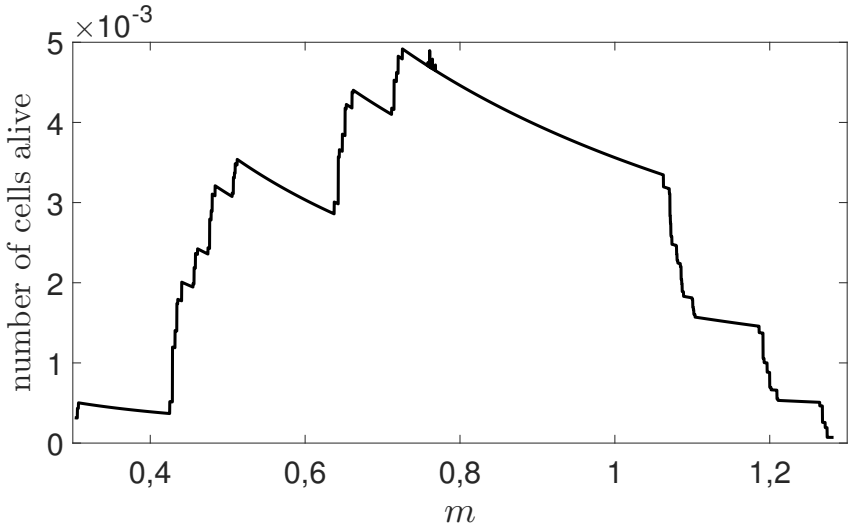

Figure 5.3: Representation of the fixed point in Table 5.5 as the number of cells alive at any time as a function of the mass.

In Figure 5.5 lines indicate to which birth cohorts the cells originating from every of the birth cohorts of the fixed point contribute when they divide at a certain age. This representation is implemented by Bart Mesuere using the D3 JavaScript library. The circles correspond to the birth cohorts, each located at its respective birth mass. The size of the circle gives an indication of the amount of cells that are born in the birth cohort. The blue lines correspond with the small newborn cells after division (40% of the mass at division) and the orange lines with the large newborn cells after division (60% of the mass at division). The cells born in the 5 largest birth cohorts

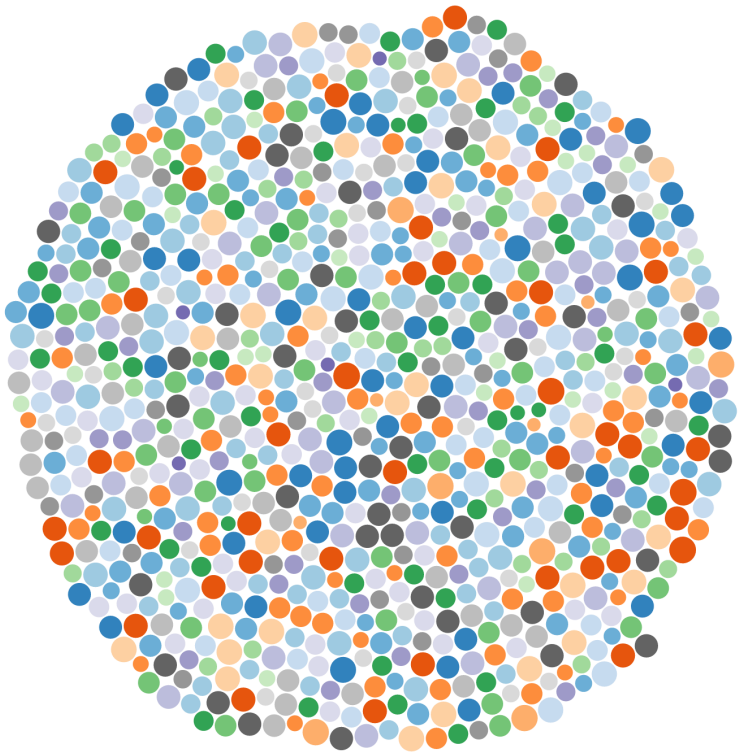

Figure 5.4: Visual representation of the fixed point in Table 5.5 consisting of cells of 30 different sizes alive at a given time point.

behave differently from the other cohorts. The birth mass of the cells in these cohorts is large enough to divide immediately (so larger than $m_{min} = 0.75$), which makes the mass of these cells at division smaller than the mass at division of the cells in the other cohorts. The cells in the other cohorts namely have to grow to the minimal mass for division and then grow further until the other division criteria are fulfilled again. Note that the birth cohorts at the top and bottom of the figure are the same since this is the representation of a fixed point of the map.

The most natural way to represent a fixed point of the map is to depict the cumulative birth mass distribution. In Figure 5.6 this is done for the found non-trivial fixed point with 41 cohorts. An equilibrium of the population model corresponds to a frequency distribution over the i-state space, which follows directly from the frequency distribution over the birth state space in our case. Since we assume that the birth mass is the most important characteristic of the i-state in our models, we

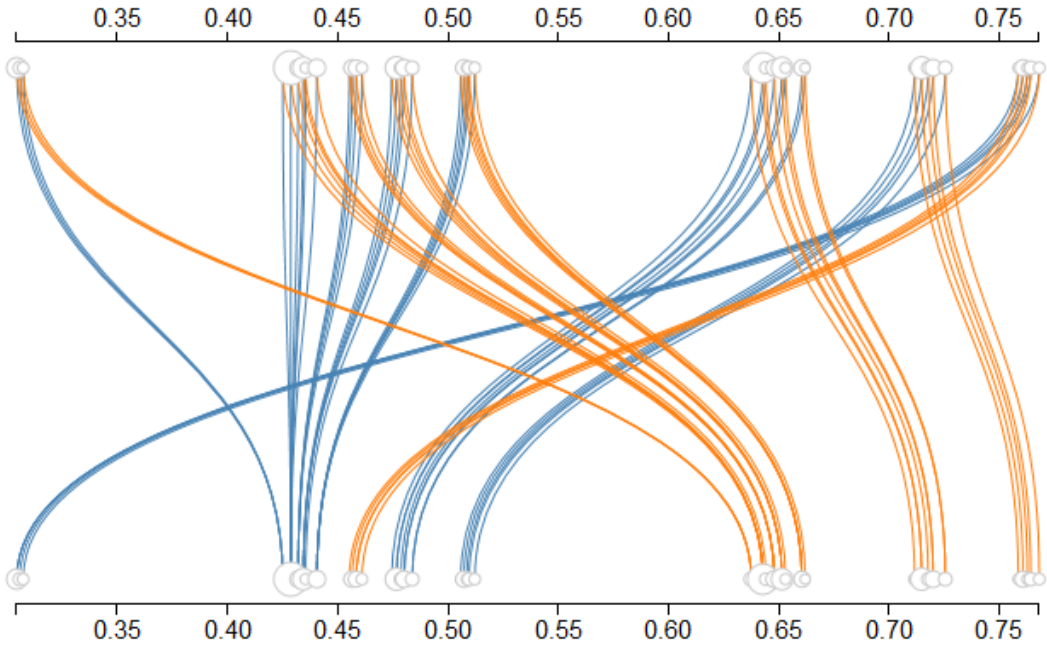

Figure 5.5: Cohort-to-cohort representation of the fixed point in Table 5.5: the blue (resp. orange) line indicates to which birth cohort the small (resp. large) newborn cells (originating from dividing cells that were originally born in the indicated birth cohort) contribute.

use the cumulative birth mass distribution as a representation of the equilibrium. The effect of the number of discretisation points, i.e. the number of birth cohorts, on this representation is investigated in Section 5.2. The dots in Figure 5.6 indicate the birth mass locations of the 41 cohorts.

To sketch a more complete picture, the evolution of the i-state (due to their internal cell cycle mechanism) of the cells originating from newborn cells in a certain birth cohort is depicted for cells born in birth cohort 1, 10 and 32 as the orbit of the adjusted Toy model (4.3). The cells that originate from cells born in birth cohort 1, 10 and 32 divide at respectively age ≈ 122.54 min, age ≈ 85.66 min and age ≈ 58.54 min (when X crosses $X_{DIV} = 0.1$ from above). How bigger the mass at birth, how sooner (at a smaller age) the cells will divide. The special cases are the cells that are born in birth cohorts 37-41, which all divide immediately after birth.

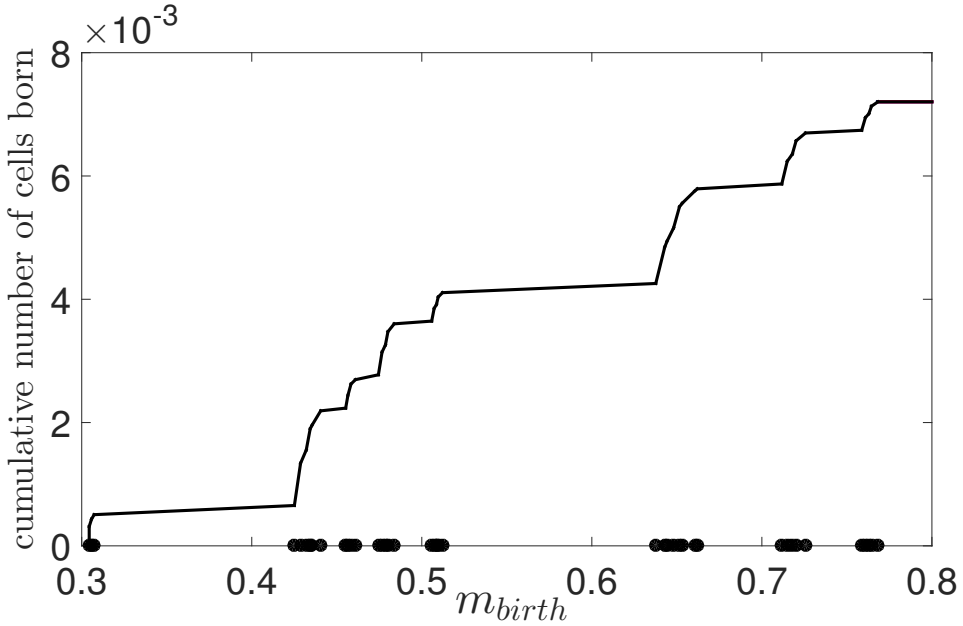

Figure 5.6: Cumulative birth mass distribution of the non-trivial fixed point of MM1 in Table 5.5. The dots indicate the birth mass locations of the 41 cohorts.

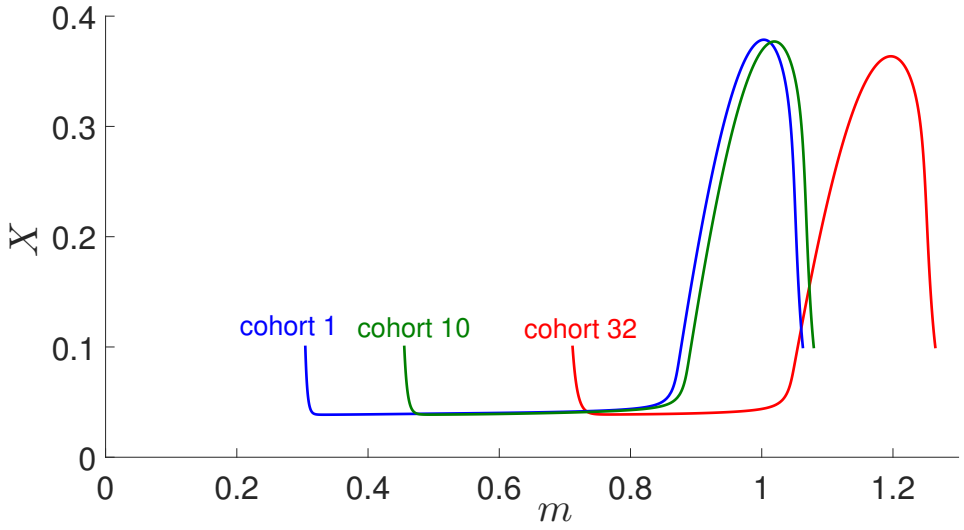

Figure 5.7: Orbits of the adjusted Toy model (4.3) for the parameter values in Tables 3.2 and 4.1 starting from 3 of the birth cohorts of the fixed point of MM1 in Table 5.5.

Second Minimal-Mass model with deterministic division MM2

The difference with the model MM1 is the assumption concerning the maximal mass value m_{max}. In this model, we assume that cells cannot divide when their mass is larger than the maximal mass value m_{max} and that the cells with a larger mass will simply grow further until they die, i.e. are washed away. This means that we use the following equation for m:

$$\frac{dm}{dt} = \mu m \frac{S}{\zeta_1 + S},$$

the following equation for the consumption rate:

$$\gamma(x,S) = c_2 \mu m \frac{c_1 S}{\zeta_1 + S},$$

and the following algorithm in `integrate_cohort`:

```
if(X = X_DIV and X is decreasing and m_min ≤ m ≤ m_max)
  print message "Conditions for division are immediately fulfilled";
  determine the values of m, X, Y and A of the small part;
  determine the values of m, X, Y and A of the large part;
  calculation of number of cells born;
else
  take age-step T_IN in age integration of m, X, Y, A, F and θ;
  while((X ≠ X_DIV and F > ε_F) or (X = X_DIV and X is not decreasing)
        or (X = X_DIV and m < m_min) or (X = X_DIV and m > m_max))
    take age-step T_IN in age integration of m, X, Y, A, F and θ;
  if(X ≠ X_DIV and F ≤ ε_F)
    print message "Survival probability too small in cohort,
                   cells in cohort do not divide";
  else
    if(X = X_DIV and X is decreasing and m_min ≤ m ≤ m_max)
      print message "Conditions for division are immediately
                     fulfilled";
      determine the values of m, X, Y and A of the small part;
      determine the values of m, X, Y and A of the large part;
      calculation of number of cells born;
    else
      print message "Problem with age integration";
```

Starting the calculations for this model with $\bar{S} = 1$ and one birth cohort (with $m = 0.301425, X = 0.1, Y = A = 0.5$) with 10^{-2} cells born per minute as for MM1, we get the results in Table 5.6. We see that the map converges to a fixed point with different values from the one for MM1 for the same original birth cohort and

Table 5.6: Orbit of the map for MM2 with at start $\bar{S} = 1$ and 10^{-2} cells born per minute in one birth cohort (with $m = 0.301425$, $X = 0.1$, $Y = A = 0.5$).

iteration	N	total number of cells born per minute	birth mass in cohort 1	new $\bar{S}$
1	2	$7.24858 \cdot 10^{-3}$	0.46660	0.13493
2	4	$4.92466 \cdot 10^{-3}$	0.36548	0.74313
3	8	$4.56075 \cdot 10^{-3}$	0.45132	0.65285
4	13	$4.66909 \cdot 10^{-3}$	0.45193	0.76997
5	22	$5.99430 \cdot 10^{-3}$	0.31592	0.77245
6	34	$6.26583 \cdot 10^{-3}$	0.32078	0.60727
7	50	$6.71620 \cdot 10^{-3}$	0.33118	0.63225
8	63	$7.55219 \cdot 10^{-3}$	0.31106	0.62630
9	72	$8.00593 \cdot 10^{-3}$	0.30744	0.55544
10	79	$8.43653 \cdot 10^{-3}$	0.30802	0.55138
100	51	$8.82368 \cdot 10^{-3}$	0.30936	0.50000
200	51	$8.82368 \cdot 10^{-3}$	0.30936	0.50000
300	51	$8.82368 \cdot 10^{-3}$	0.30936	0.50000

parameter values. For map iteration 200 to 300, the number of birth cohorts is 51, the total amount of cells born per minute $\bar{b}_{tot}$ varies between $8.82367604 \cdot 10^{-3}$ and $8.82368695 \cdot 10^{-3}$, and $\bar{S}$ varies between 0.54999993906 and 0.5000004491. The found fixed point is very similar to the one of MM1 where we started with the same birth cohort, so we will restrict ourselves to further investigating the MM1 case.

5.2 MM1-calculations: numerical effects and optimal (δ,reltol)

5.2.1 Numerical effects

Several numerical effects have to be taken into account in the type of computation done in Section 5.1.2. The first effect is that of numerical noise. In the following calculations we will always start with one birth cohort (with $m = 0.301425$, $X = 0.1$, $Y = A = 0.5$) with 10^{-2} cells born per minute and with $\bar{S} = 1$. If we decrease δ from 10^{-3} to 10^{-6} (with all other parameter values unchanged), we get a different result with the number of cohorts varying between 2384 and 2530 for map iteration 200 to 300. But if we compare the values of $\bar{b}_{tot}$ and $\bar{S}$ for these map iterations (Figure 5.8 in blue) with these for $\delta = 10^{-3}$ (Figure 5.8 in red), we see that the results are in fact not that different. This larger number of cohorts is partly an effect of numerical noise as we will show. Indeed, if we repeat these calculations for $\delta = 10^{-6}$ but with a smaller scalar relative tolerance for the CVODE integration (`reltol` equal to 10^{-9} instead of 10^{-6}), we get a smaller amount of birth cohorts for map iteration 200 to 300 (namely between 2222 and 2239 cohorts, see Figure 5.8 in green). The scalar relative tolerance for the CVODE integration `reltol` is set to control relative errors and it is recommended by the CVODE developers to not use a value larger than 10^{-3} or smaller than 10^{-15}. If we further decrease `reltol` to 10^{-10}, there is no further impact on the number of birth cohorts (see Figure 5.8 in brown). This means that the increase in the number of birth cohorts for a smaller value of δ is not only an effect of numerical noise, but this larger number of birth cohorts also seems to be a more accurate representation of the fixed point. Note that the effect of numerical noise increases if a smaller δ is chosen. For δ equal to 10^{-3}, a decrease of `reltol` to 10^{-9} also gives rise to 41 birth cohorts from map iteration 200 until 300 (see Figure 5.8 in purple), whereas for δ equal to 10^{-6}, we could already see the effect of the numerical noise for `reltol` = 10^{-6}.

Second, there is a another numerical effect whose explanation is less obvious. If we repeat the calculations for $\delta = 10^{-3}$ for several values of `reltol`, we observe a trend in the fixed point values $\left(\bar{b}_{tot}, \bar{S}\right)$. In Figure 5.9 the results are shown from map iteration 200 to 300 for `reltol` equal to 10^{-6} (the value we normally use) in blue

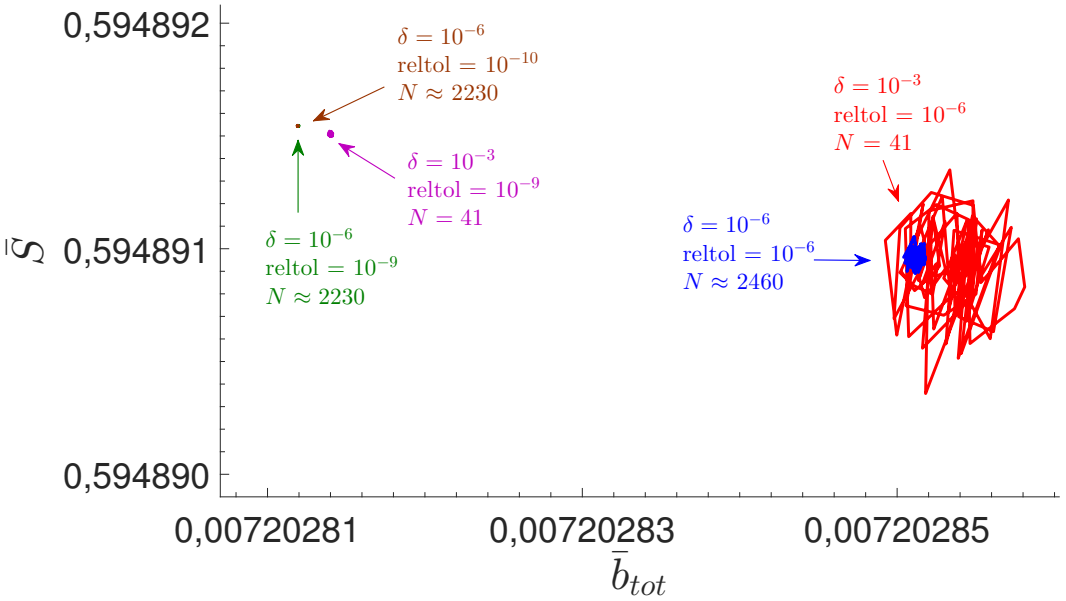

Figure 5.8: $(\bar{b}_{tot}, \bar{S})$-plot of the 200^{th} to 300^{th} iterates of MM1 for different combinations of δ and `reltol` (for unchanged parameter values and the same initial birth cohort). The number of birth cohorts N is given for every combination.

and 10^{-5} in green. For the larger value of `reltol` the results seem to be centered around a fixed point with a larger $\bar{b}_{tot}$ and a smaller $\bar{S}$.

If we repeat the calculations for a wider range of values for `reltol` (all for $\delta = 10^{-3}$) as depicted in Figure 5.10, this trend continues to hold. For a clearer visualisation of the trend, the corresponding centers of gravity for each of the scalar relative tolerances are depicted in Figure 5.11. The trend that $\bar{b}_{tot}$ decreases and $\bar{S}$ increases if `reltol` decreases is clear. Two observations can be made that help to understand the trend, although we do not claim to have a full explanation. First, when `reltol` decreases, we observe that the number of cells born per unit of time decreases or more precisely the age at which the cells divide increases. Since there is a constant dilution rate, a later division age corresponds to a smaller survival probability, so less cells are born. We made this observation by comparing the age at division at the first iteration of the map (where all the calculations started with the same initial birth cohort) for the different values of `reltol`, see Table 5.7. The reason for this must be the shape of the functions for m, X, Y and A in interaction with how the integration in the CVODE solver precisely works. For other differential equations for the internal state of the cells, this may not hold. The second observation

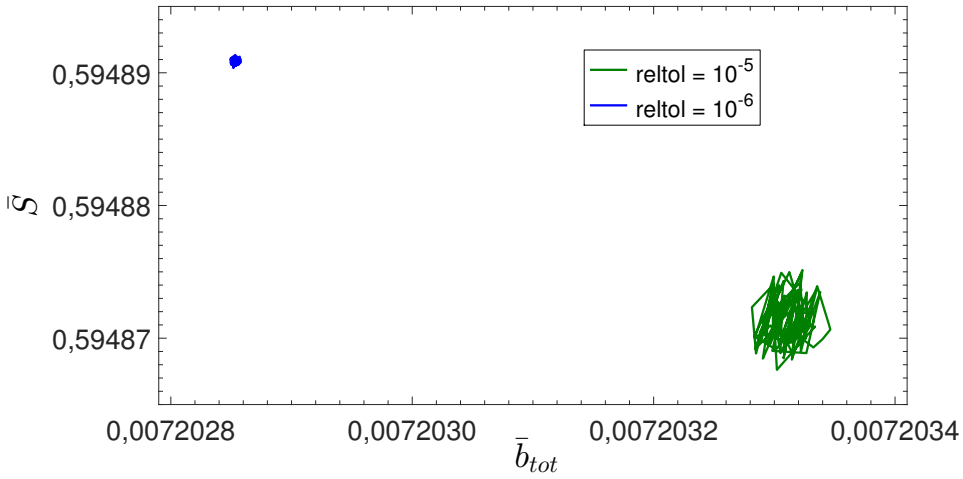

Figure 5.9: $(\bar{b}_{tot}, \bar{S})$-plot of map iteration 200 until 300 for $\delta = 10^{-3}$ and for reltol resp. equal to 10^{-5} (in green) and 10^{-6} (in blue) (for unchanged parameter values and the same initial birth cohort).

Table 5.7: Age at division (expressed in minutes) for the first iteration of the map for MM1 with at start $\bar{S} = 1$ and only 1 birth cohort where 0.01 cells are born per minute ($m = 0.301425$, $X = 0.1$, $Y = A = 0.5$) for different values of reltol.

reltol	age at division
10^{-4}	105.4940645
10^{-5}	105.5324800
10^{-6}	105.5342260
10^{-7}	105.5345477
10^{-8}	105.5345947
10^{-9}	105.5346039
10^{-10}	105.5345995

is that the relation (see (4.14))

$$\bar{S} = S^0 - \frac{1}{D}\sum_{i=1}^{N} \theta(x_{0i}, \bar{S}) \cdot \bar{b}(x_{0i})$$

suggests that a lower number of cells born per unit of time is connected to a higher residual nutrient concentration. So we hypothesize that the decrease in the number of newborn cells when reltol decreases is a numerical effect, while the increase in nutrient concentration follows from this by the properties of the model.

Finally, in Figure 5.10 another effect of changing the value of reltol is visible:

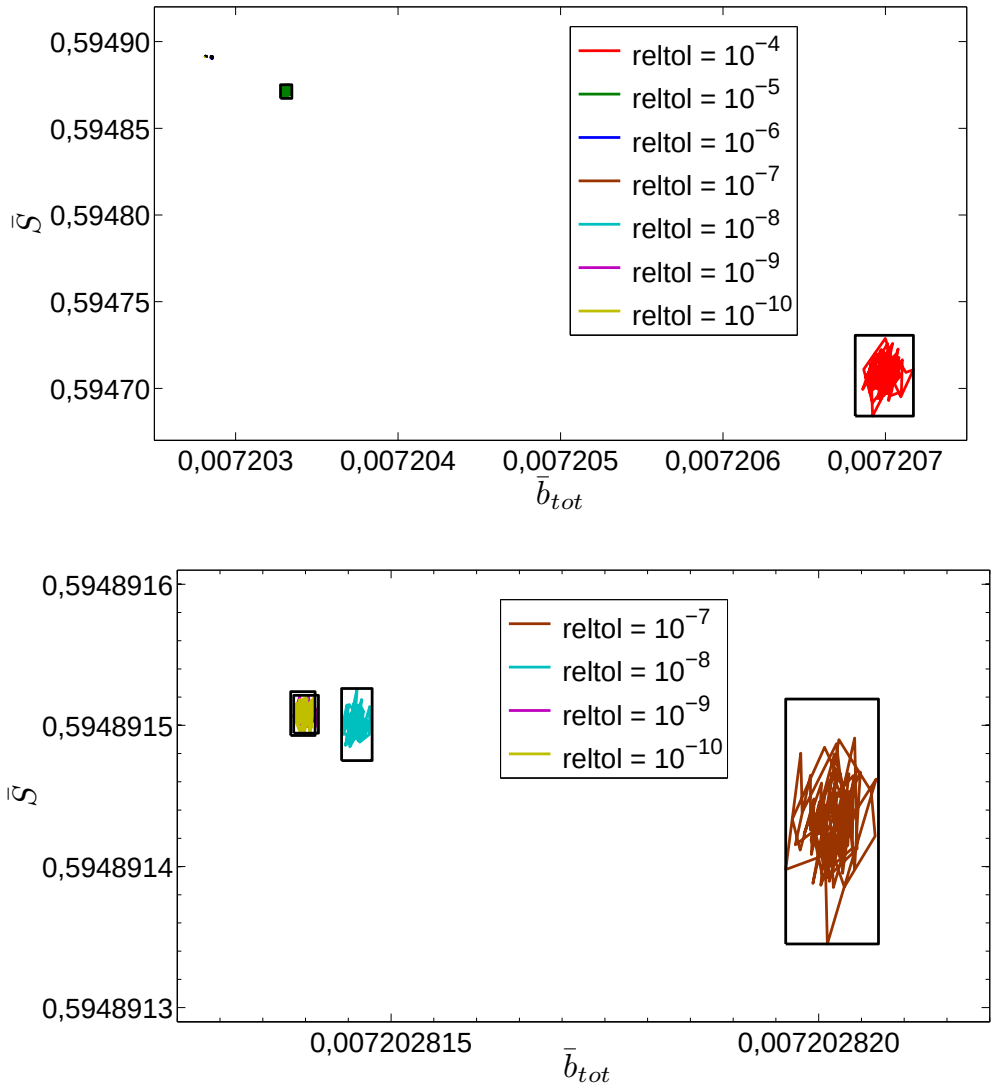

Figure 5.10: $(\bar{b}_{tot}, \bar{S})$-plot of map iteration 200 until 300 for $\delta = 10^{-3}$ and for several values of `reltol` (for unchanged parameter values and the same initial birth cohort). The figure at the bottom is a zoom-in of the figure at the top for the smaller values of `reltol`.

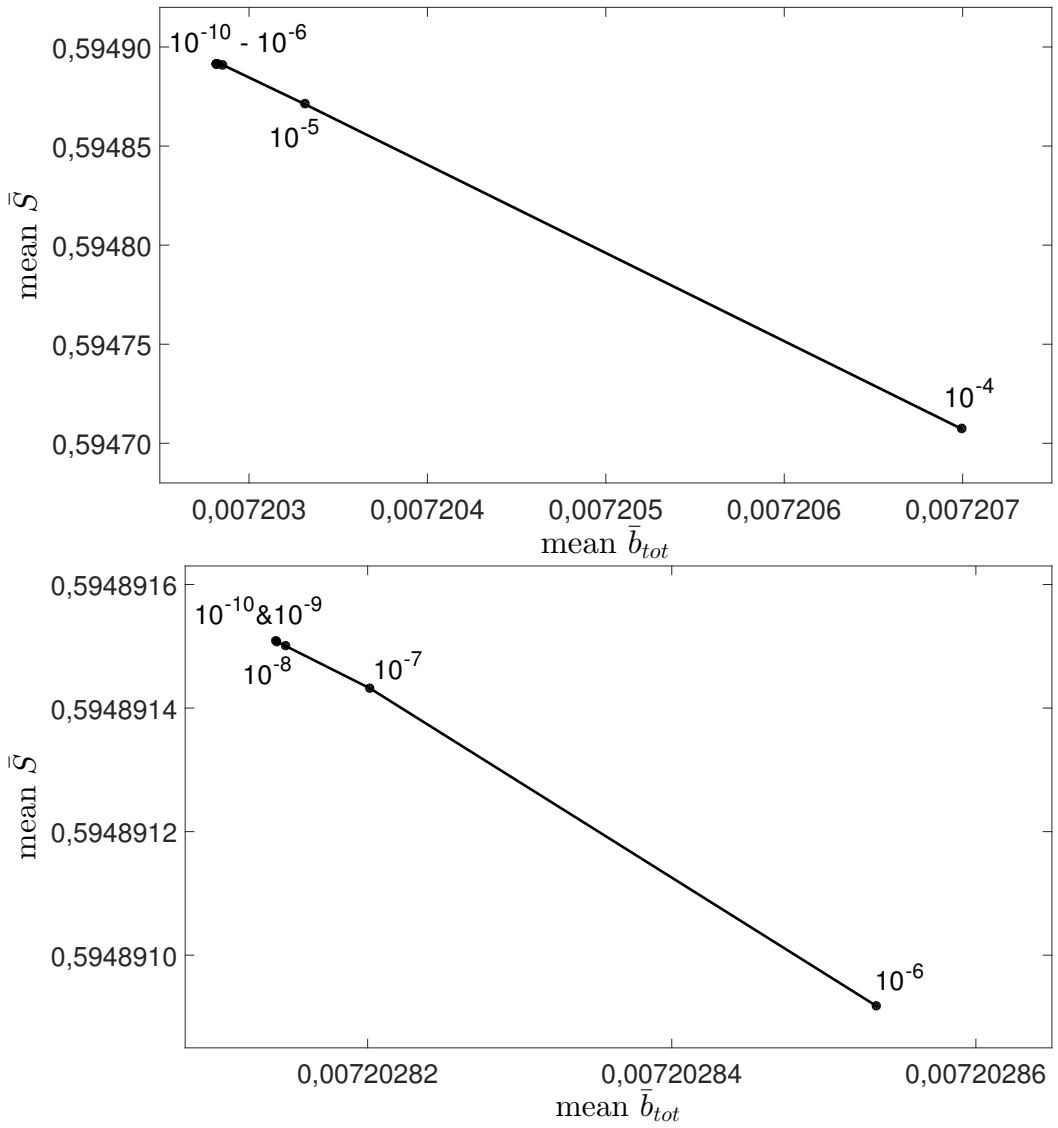

Figure 5.11: $(\bar{b}_{tot}, \bar{S})$-plot of the centers of gravity of map iteration 200 until 300 for several values of `reltol` (for unchanged parameter values and the same initial birth cohort). The figure at the bottom is a zoom-in of the figure at the top for the smaller values of `reltol`.

the variation of $\bar{b}_{tot}$ and $\bar{S}$ in the map iterations decreases when `reltol` decreases. In the next subsection, we investigate the impact of changing δ and `reltol` on both the precision and the speed of the calculations of the fixed point.

5.2.2 (δ,`reltol`)-calculations

In this subsection we compare the impact of changing δ and `reltol` on the speed and precision of the calculation of the fixed point. We always start with 1 birth cohort with $m = 0.301425$, $X = 0.1$, $Y = A = 0.5$, where 10^{-2} cells are born per minute and $\bar{S} = 1$ (for the fixed parameter value $S^0 = 1$). For every combination of δ and `reltol` the map is iterated until convergence or until 500 map iterations. Parameter values used for the convergence of the map are a maximum relative change in $\bar{S}$ of 10^{-7}, a maximum relative change in $\bar{b}_{tot}$ of 10^{-7} and maximally 1% change in the number of cohorts. For every (δ,`reltol`)-combination, the following summary can be found in Table 5.8:

- convergence: yes (after how many map iterations) or no
- N of fixed point (range of N in 20 map iterations after convergence)
- relative average difference of $\bar{S}$ in 20 map iterations after convergence compared to the mean value of $\bar{S}$ during these 20 map iterations
- relative average difference of $\bar{b}_{tot}$ in 20 map iterations after convergence compared to the mean value of $\bar{b}_{tot}$ during these 20 map iterations
- L_2-norm of the relative differences of $\bar{S}$ and $\bar{b}_{tot}$ of the fixed point in 20 map iterations after convergence
- error in cumulative mass distribution compared to the case with $\delta = 10^{-6}$ and `reltol` $= 10^{-8}$ with the representation of the fixed point with 2231 birth cohorts (calculated as the sum of the absolute values of the differences of the cumulative number of cells per unit of time for each mass value of the 2231 birth cohorts with the -estimated through linear interpolation- cumulative number of cells per unit of time of the compared fixed point, divided by 2231)
- computation time until convergence (maximum 500 iterations of the map) including storing the output files NSb.txt and data.txt. NSb.txt contains for every map iteration a line with the number of the iteration, N, $\bar{S}$ and $\bar{b}_{tot}$.

data.txt contains the results in more detail, namely for every iteration a line with the number of the iteration, N, $\bar{S}$, m_{01}, X_{01}, Y_{01}, A_{01}, $\bar{b}(x_{01})$,..., $\bar{b}(x_{0N})$, $\bar{b}_{tot}$. The reported time is the real computation time, meaning the wall clock time from start to finish of the call.

Decreasing δ creates a representation of the fixed point with a higher amount of birth cohorts, as is to be expected. If reltol is too big, the map does not converge to the required thresholds to the fixed point (see for example the results for reltol $= 10^{-4}$). Decreasing reltol does not have any impact on the number of birth cohorts of the fixed point for the larger values of δ, but for the smaller values of δ it does.

The precision of the fixed point can be represented by the L_2-norm of the relative differences of $\bar{S}$ and $\bar{b}_{tot}$ (compared to the mean values of $\bar{S}$ and $\bar{b}_{tot}$) during 20 map iterations on the fixed point (square root of the sum of the squares of the relative differences of $\bar{S}$ and $\bar{b}_{tot}$). The precision is improved when reltol is decreased up to a value of 10^{-8}, further decreasing of the relative tolerance of the age integration doesn't help the precision any more. The most precise representation of the fixed point is for $\delta = 10^{-8}$ and reltol=10^{-8}. The cumulative mass distribution of the other representations of the fixed point is compared to this one. Especially the number of birth cohorts, so δ, plays a role in how good the cumulative mass distribution of the fixed point for another (δ,reltol)-combination resembles the most precise one.

In order to decide which (δ,reltol)-combination is precise enough, but also fast enough to use for the continuation calculations of the fixed point, we also compare the computation time to find the fixed point in Table 5.8 including storing the essential output files NSb.txt and data.txt. The real computation time is minimal for $\delta = 10^{-2}$ and reltol$= 10^{-7}$, but the error in the cumulative mass distribution is quite big. So we look for a (δ,reltol)-combination that is satisfactory on both the precision of the calculated fixed point and the computation time. In Table 5.9 the product of the precision (L_2-norm of the relative differences of $\bar{S}$ and $\bar{b}_{tot}$ during 20 map iterations on the fixed point) and the real computation time is given, which has a minimal value for $\delta = 10^{-2}$ and reltol$= 10^{-10}$. In Table 5.10 the product of the error of the cumulative mass distribution and the real computation time is given, which on the other hand has a minimal value for $\delta = 10^{-6}$ and reltol$= 10^{-10}$.

Table 5.8: Summary of the $(\delta, \texttt{reltol})$-calculations

`reltol` \ δ	10^{-2}	10^{-3}	10^{-4}	10^{-5}	10^{-6}
10^{-4}	*no* *(10)* *1.15933e-04* *7.41498e-05* *1.37617e-04* *58.576s*	*no* *(40-43)* *5.18342e-05* *2.24622e-05* *5.64919e-05* *3m46.15s*	*no* *(156-174)* *2.68960e-05* *1.39579e-05* *3.03021e-05* *13m38.295s*	*no* *(856-906)* *1.31836e-05* *9.11812e-06* *1.60296e-05* *86m9.915s*	yes (385) 7851 (7807-7996) 5.22929e-06 3.24283e-06 6.15316e-06 1.856432e-04 682m45.730s
10^{-5}	yes (223) 10 2.46674e-05 1.55080e-05 2.91372e-05 2.95455e-04 26.327s	*no* *(41)* *1.30448e-05* *7.51767e-06* *1.50560e-05* *3m58.721s*	yes (206) 160 (160-165) 8.6963e-06 4.57776e-06 9.82762e-06 2.08718e-05 6m18.562s	yes (102) 641 (640-667) 2.98149e-06 2.17178e-06 3.68862e-06 8.07127e-06 11m46.648s	yes (59) 4303 (4241-4410) 1.44519e-06 6.74551e-07 1.59486e-06 5.20170e-06 47m15.734s
10^{-6}	yes (110) 10 2.54418e-06 1.67859e-06 3.04804e-06 2.95814e-04 12.038s	yes (86) 41 1.23636e-06 6.30861e-07 1.38801e-06 7.52129e-05 36.280s	yes (60) 162 (160-164) 5.17910e-07 2.79611e-07 5.88569e-07 1.93353e-05 1m36.524s	yes (59) 599 (594-607) 4.01250e-07 2.01448e-07 4.48980e-07 5.71000e-06 5m53.555s	yes (68) 2457 (2393-2548) 1.57172e-07 1.09401e-07 1.91498e-07 2.19453e-06 30m30.920s
10^{-7}	yes (58) 10 1.89111e-07 1.66319e-07 2.51843e-07 2.95401e-04 6.744s	yes (57) 41 2.27941e-07 2.30188e-07 3.23950e-07 7.50789e-05 25.976s	yes (57) 162 1.09264e-07 1.19814e-07 1.62154e-07 1.89978e-05 1m44.043s	yes (58) 596 (596-601) 7.69888e-08 8.01075e-08 1.11106e-07 4.86867e-06 5m55.967s	yes (57) 2251 (2230-2258) 6.43815e-08 8.80211e-08 1.09054e-07 4.39263e-07 26m19.670s
10^{-8}	yes (58) 10 1.54483e-07 1.51464e-07 2.16348e-07 2.95392e-04 6.911s	yes (57) 41 7.39631e-08 9.53794e-08 1.20697e-07 7.50560e-05 27.280s	yes (57) 162 5.63128e-08 9.16309e-08 1.07552e-07 1.89404e-05 1m39.765s	yes (57) 597 (597-600) 5.12699e-08 7.95523e-08 9.46423e-08 4.71134e-06 5m52.150s	yes (57) 2231 (2223-2238) 4.43778e-08 8.01076e-08 9.15785e-08 reference 24m15.334s
10^{-9}	yes (56) 10 9.29587e-08 9.35719e-08 1.31898e-07 2.95392e-04 7.304s	yes (57) 41 6.06833e-08 9.02425e-08 1.08748e-07 7.50515e-05 26s	yes (57) 162 6.67349e-08 8.56610e-08 1.08588e-07 1.89337e-05 1m42.761s	yes (57) 600 (597-600) 5.22784e-08 8.41338e-08 9.90532e-08 4.67907e-06 6m19.911s	yes (57) 2230 (2221-2238) 4.85803e-08 8.13571e-08 9.47577e-08 7.88427e-08 24m10.949s
10^{-10}	yes (56) 10 8.58986e-08 8.91293e-08 1.23784e-07 2.95392e-04 6.985s	yes (57) 41 6.65668e-08 9.45464e-08 1.15629e-07 7.50515e-05 27.737s	yes (57) 162 5.19422e-08 8.49668e-08 9.95859e-08 1.89332e-05 1m48.909s	yes (57) 598 (597-600) 5.26146e-08 7.96911e-08 9.54933e-08 4.68893e-06 6m42.156s	yes (57) 2240 (2223-2238) 4.77398e-08 7.99688e-08 9.31348e-08 7.43967e-08 24m28.725s

Table 5.9: $(\delta, \texttt{reltol})$-calculations: product of the L_2-norm of the relative differences of $\bar{S}$ and $\bar{b}_{tot}$ of the fixed point and the real computation time

reltol \ δ	10^{-2}	10^{-3}	10^{-4}	10^{-5}	10^{-6}
10^{-5}	7.67095 e-04		3.72036 e-03	2.60656 e-03	0.00452
10^{-6}	3.66923 e-05	5.03570 e-05	5.68110 e-05	1.58739 e-04	0.00035
10^{-7}	1.69843 e-06	8.55636 e-06	1.68710 e-05	3.95501 e-05	0.00017
10^{-8}	1.49518 e-06	3.29261 e-06	1.07299 e-05	3.33283 e-05	0.00013
10^{-9}	9.63383 e-07	2.82745 e-06	1.11586 e-05	3.76314 e-05	0.00014
10^{-10}	8.64631 e-07	3.20720 e-06	1.08458 e-05	3.84032 e-05	0.00014

Table 5.10: $(\delta, \texttt{reltol})$-calculations: product of the error of the cumulative mass distribution and the real computation time

reltol \ δ	10^{-2}	10^{-3}	10^{-4}	10^{-5}	10^{-6}
10^{-5}	7.77844 e-03		7.90127 e-03	5.70355 e-03	1.47506 e-03
10^{-6}	3.56101 e-03	2.72872 e-03	1.86632 e-03	2.01880 e-03	4.01801 e-03
10^{-7}	1.99218 e-03	1.95025 e-03	1.97659 e-03	1.73309 e-03	6.93891 e-04
10^{-8}	2.04145 e-03	2.04753 e-03	1.88959 e-03	1.65910 e-03	ref
10^{-9}	2.15754 e-03	1.95134 e-03	1.94565 e-03	1.77763 e-03	1.14397 e-04
10^{-10}	2.06331 e-03	2.08170 e-03	2.06200 e-03	1.88568 e-03	1.09268 e-04

It is clear that there is no universal ideal combination and that this choice depends on which aspect of the computations is considered to be the most important. Note that the given computation time could be decreased if we use parallel computing for the age integration of the different birth cohorts. The matching procedure of the cohorts of newborns would be slightly different, but this should not have a big effect on the outcome of the calculations. If the calculations were run on a processor with a core for every birth cohort, the amount of birth cohorts would have little influence on the computation time. Since we do the continuation calculations with a single processor, the number of birth cohorts plays a role in our choice for δ and reltol. For $\delta = 10^{-2}$ the fixed point is represented with 10 birth cohorts, which is not precise enough, but the representation with 41 birth cohorts for $\delta = 10^{-3}$ already seems to be quite close to the real fixed point. From reltol$= 10^{-6}$ on, there is convergence to the fixed point. In Figure 5.12 the cumulative mass distributions of the fixed point is depicted for $\delta = 10^{-6}$ and reltol$= 10^{-8}$ (the "most precise" one) and for $\delta = 10^{-3}$ and reltol$= 10^{-6}$. It is clear that the most important jumps in the mass distribution are already present in the representation with 41 birth cohorts. We will mainly use $\delta = 10^{-3}$ and reltol$= 10^{-6}$ for our further

calculations, but for some calculations will compare the results with the results for the "most precise" combination ($\delta = 10^{-6}$ and $\texttt{reltol} = 10^{-8}$) and for $\delta = 10^{-3}$ and $\texttt{reltol} = 10^{-7}$ to make sure that the obtained computational results are no ghost results.

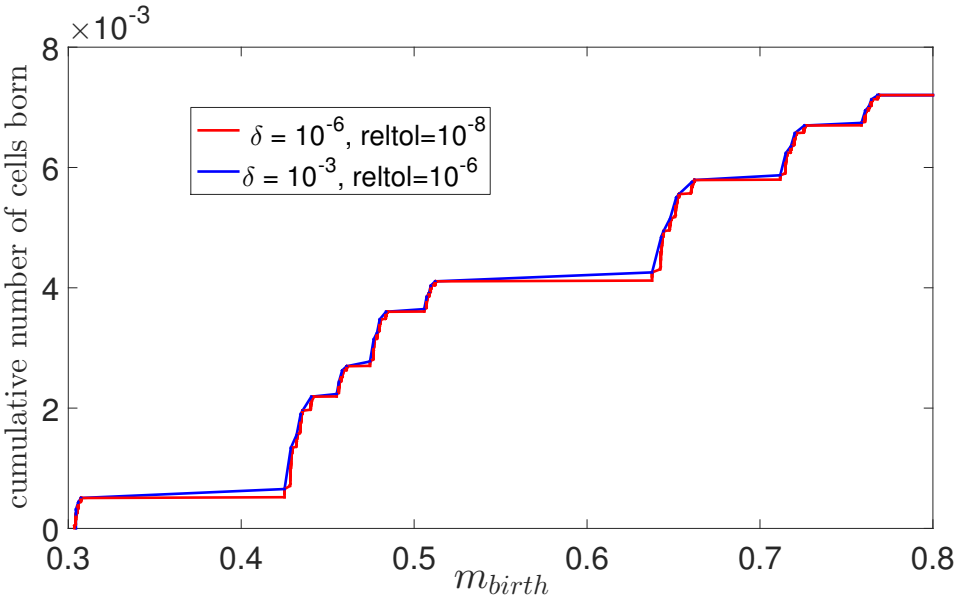

Figure 5.12: Cumulative mass distribution of the fixed point for $S^0 = 1$ for two different (δ,reltol)-combinations.

In order to sketch a more complete picture, we compare the results for two other fixed points for the above mentioned 3 different (δ,reltol)-combinations: the fixed point for $D = 0.009$ min^{-1} and the fixed point for $D = 0.0115$ min^{-1} (both with fixed $S^0 = 1$). All the calculations start with 1 birth cohort with $m = 0.301425$, $X = 0.1$, $Y = A = 0.5$, 10^{-2} cells born per minute and $\bar{S} = 1$. Like before, for every (δ,reltol)-combination the map is iterated until convergence (with convergence parameter value for $\bar{S}$ of 10^{-7}, for $\bar{b}_{tot}$ of 10^{-7} and maximally 1% change in the number of cohorts) or until 500 map iterations. The results can be found in Table 5.11. If we compare the results for the two different fixed points, it is clear that the best (δ,reltol)-combination can be different for different fixed points. For $D = 0.009$ min^{-1} the real computation time is the lowest for $\delta = 10^{-3}$ and $\texttt{reltol} = 10^{-7}$, and for $D = 0.0115$ min^{-1} it is the lowest for $\delta = 10^{-3}$ and $\texttt{reltol} = 10^{-6}$. If we look at the precision of the fixed point for the different combinations (the L_2-norm

Table 5.11: Summary of the (δ, reltol)-calculations for $D = 0.0115$ min^{-1} and $D = 0.009$ min^{-1}.

δ & reltol \ D	0.0115 min^{-1}	0.009 min^{-1}
$\delta = 10^{-3}$ & reltol$= 10^{-6}$	yes (224)	yes (94)
	69	43
	4.27834 e-07	3.52545 e-06
	1.85584 e-06	9.01165 e-07
	1.90452 e-06	3.63880 e-06
	3m42.155s	0m42.939s
$\delta = 10^{-3}$ & reltol$= 10^{-7}$	yes (223)	yes (54)
	69	43
	2.17919 e-07	7.75172 e-07
	1.02584 e-06	4.41584 e-07
	1.04873 e-06	8.92125 e-07
	4m31.469s	0m23.542s
$\delta = 10^{-6}$ & reltol$= 10^{-8}$	yes (230)	yes (60)
	12739 (12616-12829)	2196 (2189-2206)
	3.81478 e-07	7.35076 e-08
	1.36789 e-06	8.17014 e-08
	1.42009 e-06	1.09902 e-07
	702m6.785s	21m9.06s

of the relative differences of $\bar{S}$ and $\bar{b}_{tot}$), $\delta = 10^{-6}$ and reltol$= 10^{-8}$ is the best for $D = 0.009$ min^{-1} and $\delta = 10^{-3}$ and reltol$= 10^{-7}$ for $D = 0.0115$ min^{-1}. In Figures 5.13 and 5.14 a comparison of the cumulative mass distribution of the fixed point is made.

We conclude that the best choice of δ and reltol can differ for different parameter values, although it can be motivated locally in parameter space by considering the robustness of the found fixed point, the number of birth cohorts and the computation time. Anyway, there is always the possibility that discovered phenomena are artefacts of the chosen δ and reltol, so this should be cross-checked by repeating the computations with different (δ,reltol).

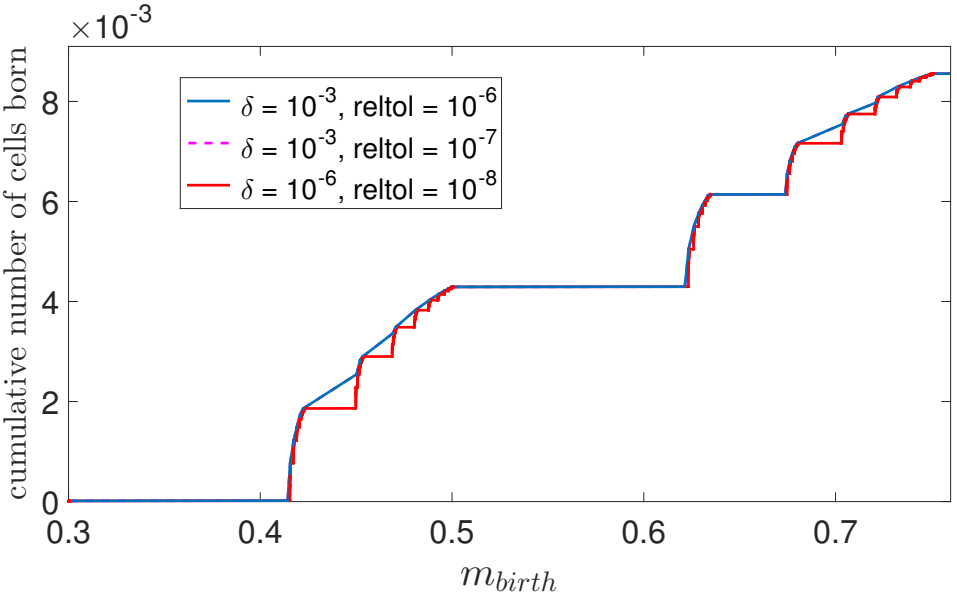

Figure 5.13: Cumulative mass distribution of the fixed point for $D = 0.009$ min^{-1} for three different (δ,`reltol`)-combinations.

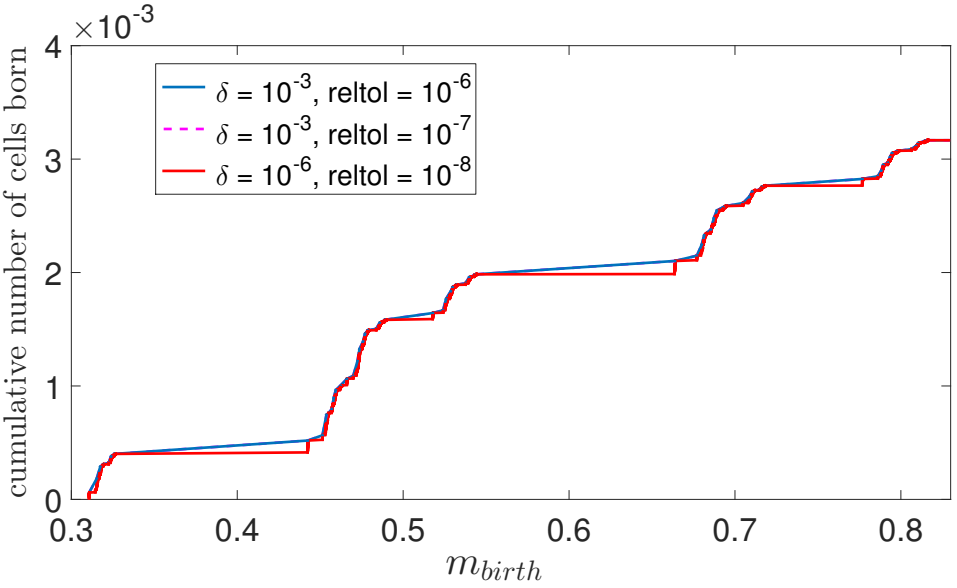

Figure 5.14: Cumulative mass distribution of the fixed point for $D = 0.0115$ min^{-1} for three different (δ,`reltol`)-combinations.

5.3 Convergence behaviour of MM1 under variation of S^0

In this section a preliminary investigation of the convergence behaviour of MM1 for different values of S^0 is done. The fixed point for $S^0 = 1$ in Table 5.5 (see Section 5.1.2 for MM1) is used as a starting point for map iterations for other values of S^0. In Table 5.12 a summary of the results is given for different values of S^0. For S^0 values 0.8, 1.05, 1.1 and 1.3 the map converges, after a transient, to a fixed point with the same 41 birth cohorts. More surprisingly, for S^0 values 1.5, 1.7 and 2 the map shows cyclic behaviour (after a transient) and converges to a 2-cycle.

If we start the map iterations from a different point, namely the birth cohort with $m = 0.301425$, $X = 0.1$, $Y = 0.5$ and $A = 0.5$ with 0.01 cells born per minute (the starting point from which we found the fixed point for $S^0 = 1$), we get different results for some values of S^0. An overview of the results for this starting point can be found in Table 5.13. For example, for $S^0 = 0.8$ we have convergence to the trivial fixed point instead of a non-trivial fixed point with 41 birth cohorts (see Table 5.12), which is understandable since the trivial fixed point exists for all S^0 values. For $S^0 = 1.7$ we now have convergence to a non-trivial fixed point with 41 birth cohorts instead of the 2-cycle (see Table 5.12), so this means that for certain ranges of S^0 the non-trivial fixed point coexists with cyclic behaviour. In Figure 5.15 at the top both the fixed point and the 2-cycle are depicted. For $S^0 = 1.5$ the map converges to a 10-cycle when we start with the one birth cohort instead of the 2-cycle we had before, so different cyclic behaviour must also coexist. In Figure 5.15 at the bottom the cycles for $S^0 = 1.5$ are compared.

An overview of the results and the found coexistence for the test cases can be found in Figure 5.16. Although the map can show cyclic behaviour, the found cycles do not have any biological meaning in the model. Note that the found 28-cycle for $S^0 = 1.53$ is partly due to the precision of the calculations. If we repeat the calculations (again starting from the one initial birth cohort as above) with $\delta = 10^{-3}$ and `reltol`$= 10^{-7}$ we find the same 28-cycle, but if we use $\delta = 10^{-4}$ and `reltol`$= 10^{-7}$ or $\delta = 10^{-6}$ and `reltol`$= 10^{-8}$, we find an 8-cycle. In Figure 5.17 both the 28-cycle and the 8-cycle for $S^0 = 1.53$ are depicted in $(\bar{b}_{tot},\bar{S})$-space. So the cyclic behaviour is rarely an artefact of the chosen precision of the calculations, but the period can be.

Table 5.12: Statistics of 300 map iterations starting from the fixed point for $S^0 = 1$ (Table 5.5) for several other S^0 values. The 2-cycles have no biological meaning in our model.

S^0	result	after how many iterations	values
0.8	fixed point	$\pm$ 50	$N = 41$ $\bar{S} \approx 0.594891$ $\bar{b}_{tot} \approx 0.003646846$
1.05	fixed point	$\pm$ 40	$N = 41$ $\bar{S} \approx 0.594891$ $\bar{b}_{tot} \approx 0.008091854$
1.1	fixed point	$\pm$ 50	$N = 41$ $\bar{S} \approx 0.5948909$ $\bar{b}_{tot} \approx 0.00898086$
1.3	fixed point	$\pm$ 50	$N = 41$ $\bar{S} \approx 0.594891$ $\bar{b}_{tot} \approx 0.01253686$
1.5	2-cycle	$\pm$ 20	$N = 44$ $\bar{S} \approx 0.4241$ $\bar{b}_{tot} \approx 0.0152$ and $N = 47$ $\bar{S} \approx 0.8068$ $\bar{b}_{tot} \approx 0.0161$
1.7	2-cycle	$\pm$ 20	$N = 34$ $\bar{S} \approx 1.0261$ $\bar{b}_{tot} \approx 0.0191$ and $N = 34$ (different location of the cohorts) $\bar{S} \approx 0.3125$ $\bar{b}_{tot} \approx 0.0178$
2	2-cycle	$\pm$ 80	$N = 38$ $\bar{S} \approx 1.2313$ $\bar{b}_{tot} \approx 0.0229$ and $N = 41$ $\bar{S} \approx 0.2659$ $\bar{b}_{tot} \approx 0.0218$

Table 5.13: Outcome of 1000 map iterations starting from 0.01 cells born per minute in one birth cohort (with $m = 0.301425$, $X = 0.1$, $Y = 0.5$, $A = 0.5$) for different values of the parameter S^0.

S^0	result	S^0	result
0.7	trivial fixed point	**1.53**	28-cycle
0.8	trivial fixed point	**1.55**	8-cycle
0.82	trivial fixed point	**1.6**	8-cycle
0.85	fixed point	**1.65**	8-cycle
0.9	fixed point	**1.66**	8-cycle
1	fixed point	**1.665**	8-cycle
1.1	fixed point	**1.6655**	8-cycle
1.2	fixed point	**1.6656**	8-cycle
1.3	fixed point	**1.6657**	8-cycle
1.4	fixed point	**1.66571**	fixed point
1.45	fixed point	**1.66573**	fixed point
1.48	fixed point	**1.66575**	fixed point
1.482	fixed point	**1.6658**	fixed point
1.483	fixed point	**1.666**	fixed point
1.4835	fixed point	**1.668**	fixed point
1.4837	2-cycle	**1.67**	fixed point
1.4838	2-cycle	**1.68**	fixed point
1.4839	10-cycle	**1.7**	fixed point
1.49	10-cycle	**2**	2-cycle
1.5	10-cycle	**2.5**	4-cycle
1.51	10-cycle	**3**	no convergence

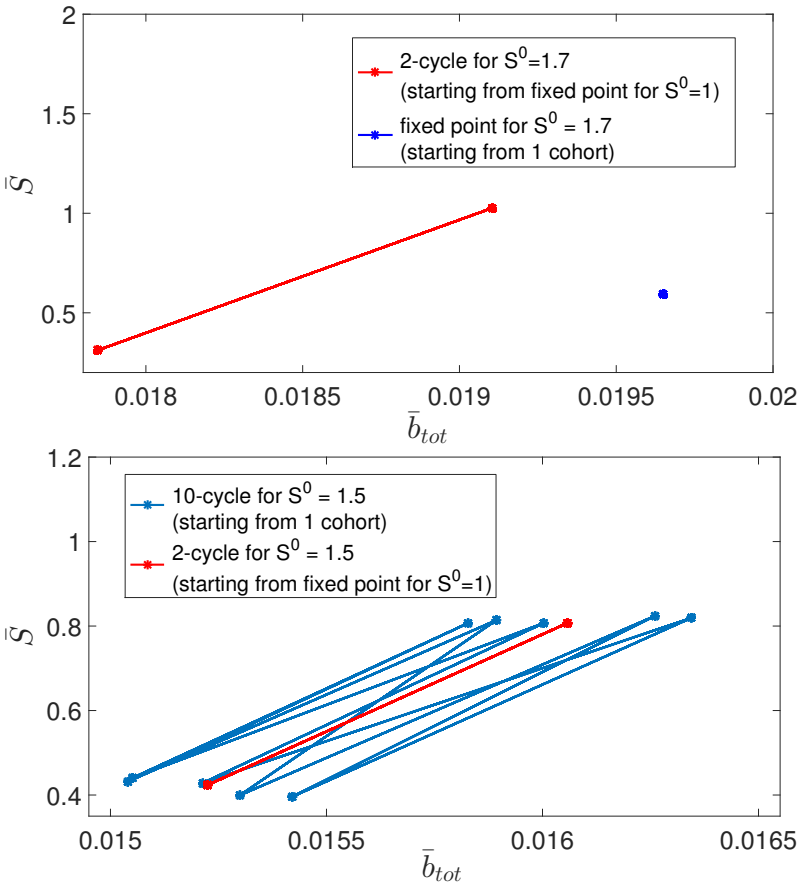

Figure 5.15: Comparison of the results for different starting points of the map for the same S^0 value. The fixed point for $S^0 = 1$ (Table 5.5) was the starting point for the red curve. The blue curve was started from 1 birth cohort with 0.01 cells born per minute (with $m = 0.301425$, $X = 0.1$, $Y = 0.5$, $A = 0.5$). The top figure is for $S^0 = 1.7$ and the bottom figure is for $S^0 = 1.5$.

5.3.1 Bifurcations of the map for free S^0

The coexistence of stable fixed points and stable cycles (see Figure 5.16) might be due to a combination of a subcritical Period Doubling bifurcation and a Limit Point bifurcation as in the model map (2.37) in Figure 2.9. The branches of the stable cycles are for small values of S^0 quite symmetrical, but become more asymmetrical for larger values of S^0, which is also common in models more complicated than (2.37).

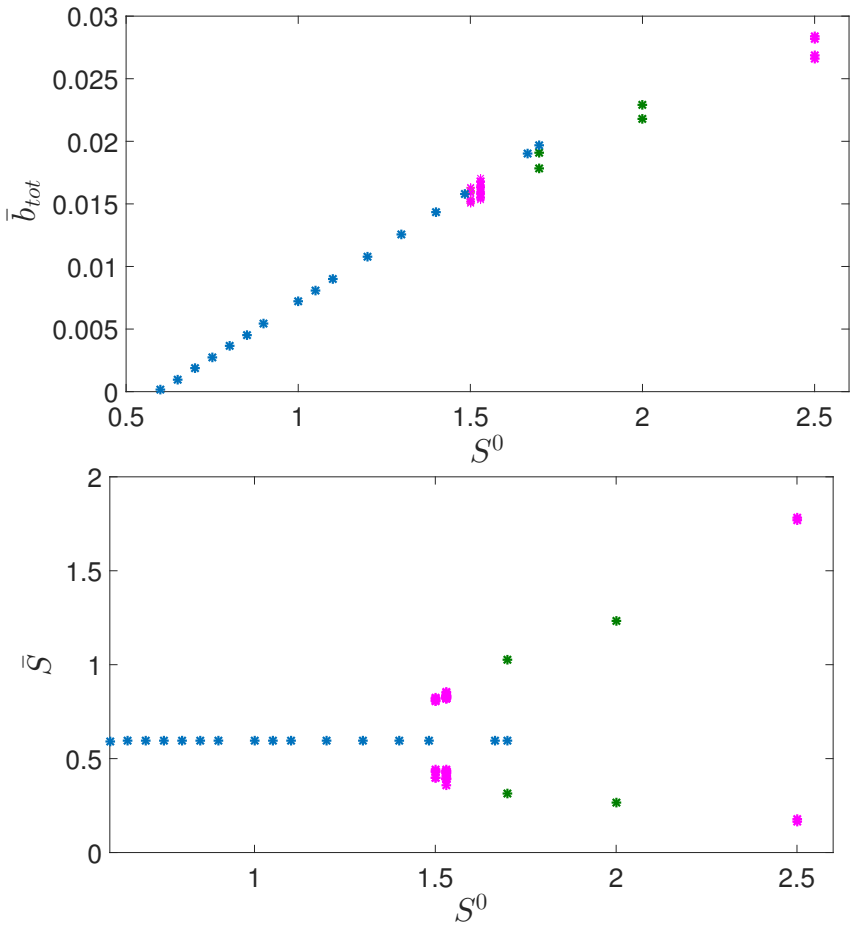

Figure 5.16: Representation of the results of the map iterations in $(S^0, \bar{b}_{tot})$-space and in (S^0,$\bar{S}$)-space. The found fixed points for different values of S^0 are given in blue. In green the cycles found by iterating the map starting from the fixed point for $S^0 = 1$ (Table 5.5) are shown, and in pink the cycles found by iterating the map starting from one birth cohort with 0.01 cells born per minute (with $m = 0.301425$, $X = 0.1$, $Y = 0.5$ and $A = 0.5$) are shown.

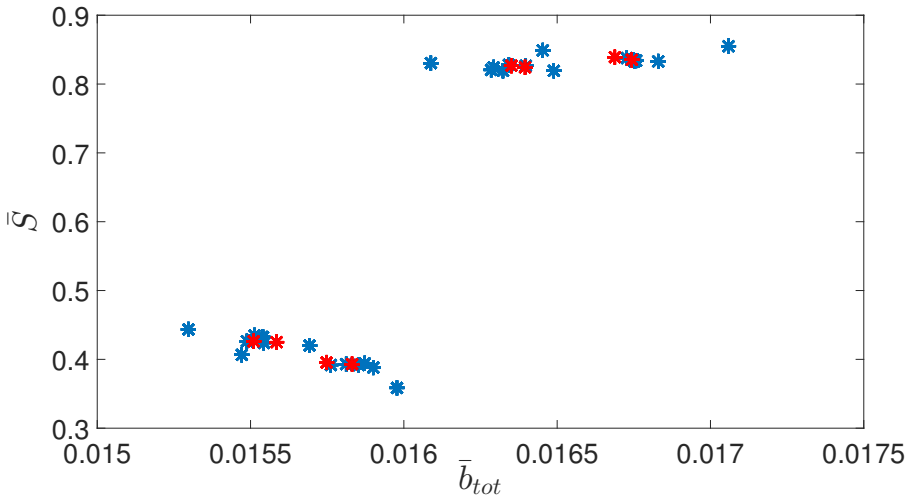

Figure 5.17: In blue the 28-cycle for $S^0 = 1.53$ for $\delta = 10^{-3}$ and `reltol`$= 10^{-6}$ and in red the 8-cycle for $S^0 = 1.53$ for $\delta = 10^{-4}$ and `reltol`$= 10^{-7}$ in ($\bar{b}_{tot}$,$\bar{S}$)-space.

5.4 Stability of the fixed point of MM1 under perturbation

We found cyclic behaviour of the map for S^0 between 1.4837 and 2.5. There are regions where both stable cycles and a stable fixed point exist. For $S^0 = 1.4837$ a 2-cycle coexists with a fixed point. The 2-cycle was found by starting the map iterations with the one birth cohort ($m = 0.301425$, $X = 0.1$, $Y = 0.5$ and $A = 0.5$) with 0.01 cells born per minute (see Table 5.13) and the fixed point by starting from the found fixed point for $S^0 = 1.4835$ (see Table 5.13). We investigate how sensitive the fixed point is to perturbations for this S^0 parameter value.

First to make sure that the 2-cycle is no artefact of the chosen precision of the calculations ($\delta = 10^{-3}$ and `reltol` = 10^{-6}), the map is iterated starting from one of the points of the 2-cycle for $\delta = 10^{-6}$ and `reltol` = 10^{-8}. The results are unchanged, we still find the 2-cycle, now with a higher amount of birth cohorts in each of the two points. Also if we start the map iterations with the one birth cohort, as before, $\delta = 10^{-6}$ and `reltol` = 10^{-8} we find the 2-cycle with the higher amount of birth cohorts in each of the two points. In Figure 5.18 the cumulative mass distributions are shown for the two (δ,`reltol`)-combinations for the 2 points of the 2-cycle. It is clear that this is the same 2-cycle, but with a finer discretisation of the birth mass space.

In Figure 5.19 the 2-cycle for $S^0 = 1.4837$ is represented ($\delta = 10^{-3}$ and `reltol`= 10^{-6}). The lines indicate to which birth cohorts the daughter cells of cells that were originally born in a certain birth cohort contribute when they divide. On top is the point of the 2-cycle with 45 birth cohorts ($\bar{S} \approx 0.015797$) and in the middle the other point of the 2-cyle with 44 birth cohorts ($\bar{S} \approx 0.014967$). Because it is a representation of a 2-cycle, the point at the bottom of the figure is the same point as on the top of the figure. The blue lines correspond with the small newborn cells (40% of the mass at division) and the orange lines with the large newborn cells (60% of the mass at division). The size of the circle gives an indication of the amount of cells that are born per unit of time in the birth cohort.

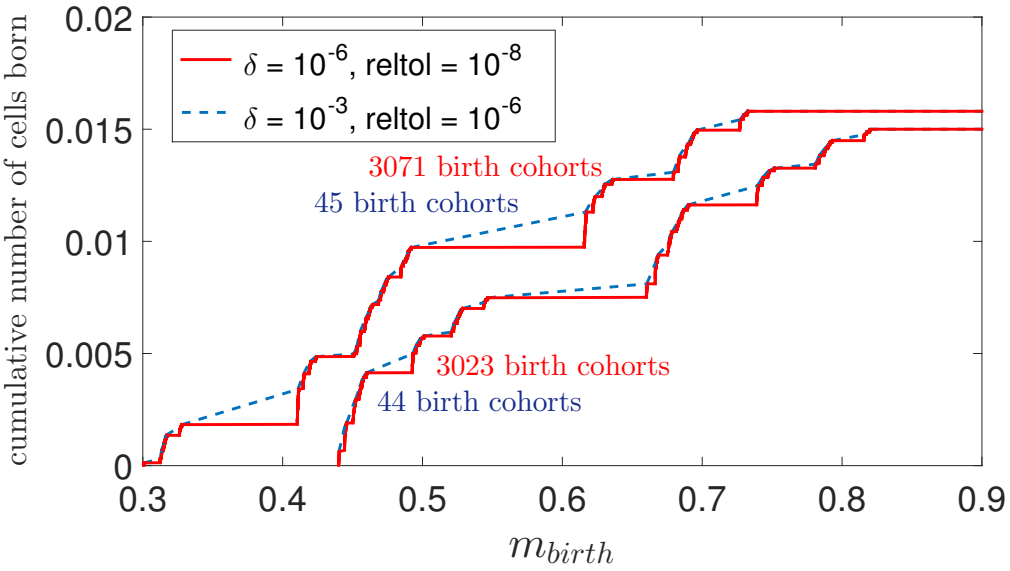

Figure 5.18: Cumulative mass distribution of the 2 points of the 2-cycle for $S^0 = 1.4837$, for two different (δ,`reltol`)-combinations. For the point with the largest number of birth cohorts (and the largest $\bar{b}_{tot}$) $\bar{S} = 0.799803$ and for the other point $\bar{S} = 0.427896$.

5.4.1 Shift of the birth cohorts

We investigate how sensitive the fixed point of the map is to a change in the location of the cohorts. We start with the fixed point for $S^0 = 1.4837$.

First, we let the mass in every birth cohort change by adding a uniformly distributed random number over $[-a,a]$ and then iterate the map. In Table 5.14 the results can be found, where for every range of the random number 20 test cases were performed. The map converges to either the fixed point or the 2-cycle. The larger the change of the birth mass locations, the higher the percentage that converges to the 2-cycle, as could be expected. It could be useful to keep these results in mind when we are considering a continuation strategy for the fixed point. During a continuation step, the change in birth mass for the cohorts of the fixed point should not be too big compared to the attraction region of the fixed point, since we then could get periodic behaviour of the map.

If we repeat this test with the fixed point for $S^0 = 1$, where we did not observe any cyclic behaviour of the map, we find indeed a larger convergence region of the fixed

Table 5.14: Results of the map iterations starting with a perturbation of the fixed point for $S^0 = 1.4837$: the mass of every cohort is changed by adding a uniformly distributed random number over $[-a, a]$. The percentage is for 20 test cases.

change \ result	**fixed point**	**2-cycle**
$[-\mathbf{0.01}, \mathbf{0.01}]$	100%	0%
$[-\mathbf{0.05}, \mathbf{0.05}]$	90%	10%
$[-\mathbf{0.1}, \mathbf{0.1}]$	50%	50%
$[-\mathbf{0.2}, \mathbf{0.2}]$	35%	65%

point. Of the 20 test cases with a random shift of the mass in every birth cohort of the fixed point between -0.2 and 0.2, the map converges in all the cases to the fixed point.

To have a clearer idea of what happens precisely to the location of the cohorts, we also did a fixed shift of the mass of every birth cohort to the right. A fixed shift to the right of all the birth cohorts with 0.0001, 0.0002, 0.0005, 0.001, 0.005 and 0.01 gives convergence to the fixed point. A larger shift with sizes 0.05 and 0.1 gives convergence to the 2-cycle, but a shift with 0.2 gives convergence to the fixed point.

5.4.2 Doubling of the birth cohorts

The doubling of the birth cohorts is performed so that the original birth cohorts are "doubled" to themselves and a nearby new birth cohort. The number of cells born per minute in the birth cohort is equally divided between both and the chemical concentrations X, Y and A are the same as in the original birth cohort. The mass location of the new birth cohort is chosen taking the results of the shift-experiments into account.

If we let the location of each doubled birth cohort be determined randomly at a distance between $-a$ and a to the original birth cohort, it makes sense to take $a = 0.01$ because we know shifting the birth cohort did not affect the convergence to the fixed point for this size of shift and so we can really see the effect of the number of birth cohorts. 20 tests all give convergence to the initial fixed point (with the same location of the birth cohorts), so the doubling does not seem to have a long-term effect on the convergence.

If we combine the doubling of the birth cohorts with a fixed shift to the right,

Table 5.15: Results of the map iterations starting with a perturbation of the fixed point for $S^0 = 1.4837$: for every birth cohort the number of cells born per minute is changed with a factor $1+b$ where b is a uniformly distributed random number over $[-a,a]$, and the nutrient concentration is changed with a factor $1+c$ where c is a random number out of the uniform distribution over $[-a,a]$. The percentage is for 20 test cases.

change \ result	**fixed point**	**2-cycle**
$[-\mathbf{1}\%,\mathbf{1}\%]$	100%	0%
$[-\mathbf{5}\%,\mathbf{5}\%]$	100%	0%
$[-\mathbf{10}\%,\mathbf{10}\%]$	90%	10%
$[-\mathbf{20}\%,\mathbf{20}\%]$	70%	30%
$[-\mathbf{30}\%,\mathbf{30}\%]$	35%	65%

at fixed distance 0.0001, 0.0002 and 0.0005 for every birth cohort to its doubled birth cohort, we always get convergence to the same fixed point. Even a larger shift of 0.001, 0.002, 0.003, 0.004, 0.005 and 0.01 for every doubled birth cohort gives convergence to the fixed point. Note that the "order" of the birth cohorts is not preserved for the larger shifts (instead of having birth cohort 1a, 1b, 2a, 2b and so on, we could have 1a, 2a, 1b, 2b, ...), but this does not affect the convergence.

5.4.3 Perturbation of nutrient concentration and number of cells

To investigate how sensitive the fixed point for $S^0 = 1.4837$ is to changes in the nutrient concentration and the number of cells born per unit of time, we change both $\bar{S}$ and $\bar{b}(x_{0i})$ with a factor $1+b$. b is a number chosen randomly in the uniformly distribution over $[-a,a]$, independently chosen for $\bar{S}$ and each of the $\bar{b}(x_{0i})$'s. A summary of the results is given in Table 5.15. For random perturbations up to 5% the map still converges to the fixed point, but for larger perturbations the map may converge to the 2-cycle.

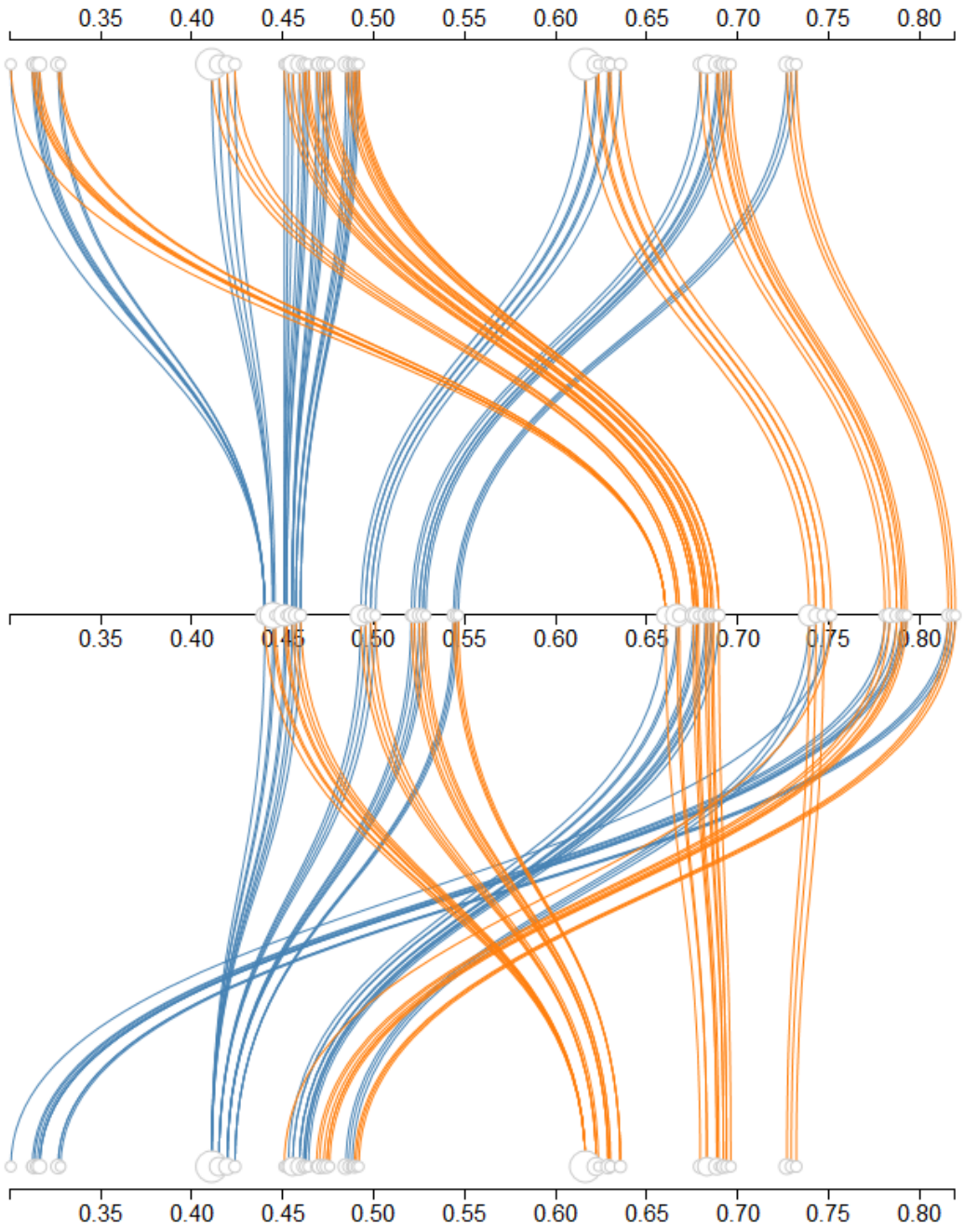

Figure 5.19: Cohort-to-cohort representation of the 2-cycle for $S^0 = 1.4837$ ($\delta = 10^{-3}$ and `reltol`$= 10^{-6}$): on the top and bottom the point with 45 birth cohorts ($\bar{S} \approx 0.015797$) and in the middle the point with 44 birth cohorts ($\bar{S} \approx 0.014967$). The blue (resp. orange) line indicates to which birth cohort the small (resp. large) newborn cells (originating from dividing cells that were originally born in the indicated birth cohort) contribute.

5.5 Using a cycle to make an "educated" guess for the fixed point of MM1

We investigate if cyclic behaviour can help find the fixed point for the same parameter value of S^0. Given a n-cycle, we can make an "educated" guess for the fixed point by using all the birth cohorts of the n different points in the cycle while adjusting the number of cells born per minute in each birth cohort through a division by n. The estimated nutrient level is the mean value of the nutrient levels of the n different points in the cycle. In the case of the 2-cycle for $S^0 = 1.4837$, the map indeed converges to the fixed point for this parameter value. It works also to find the fixed point for $S^0 = 1.6$, using the corresponding 8-cycle. A comparison of the $\bar{S}$ values and the cumulative number of cells born per minute in the prediction and in the actual fixed point can be found in Figure 5.20.

However, when trying to find a fixed point for $S^0 = 2.5$ by using the found 4-cycle the map still converges to the 4-cycle. So presumably the fixed point of the map for $S^0 = 2.5$ has a smaller attraction region. This method could obviously only help to find the fixed point in regions where both cyclic behaviour and a fixed point exist, and the attraction region of the fixed point is big enough. To check how sensitive the fixed point for $S^0 = 2.5$ is to changes in the mass location of the birth cohorts, we repeat the random shift of the birth cohorts experiment (see Section 5.4.1) for this fixed point. For a random shift between -0.01 and 0.01, all the 20 test cases converge to the fixed point. But for a random shift between -0.05 and 0.05, only 1 out of the 20 test cases converge to the fixed point (18 converge to the 4-cycle and 1 to a 2-cycle). So the fixed point for $S^0 = 2.5$ indeed is more sensitive to changes in the mass location of the birth cohorts than the fixed point for $S^0 = 1.4873$ (see Table 5.14). We can also check how sensitive the fixed point is to perturbations in the amount of cells born per minute in the birth cohorts and to a perturbation of the nutrient concentration. We repeat the experiment we did for the fixed point for $S^0 = 1.4837$ (see Section 5.4.3 and Table 5.15). The results are summarized in Table 5.16. This also confirms that the fixed point for $S^0 = 2.5$ has a smaller attraction region than the fixed point for $S^0 = 1.4837$.

Note that the prediction for $\bar{S}$ as the mean of the different points of the 4-cycle for $S^0 = 2.5$ is poor: the mean $\bar{S}$ is 0.97261 which is quite different from the value of

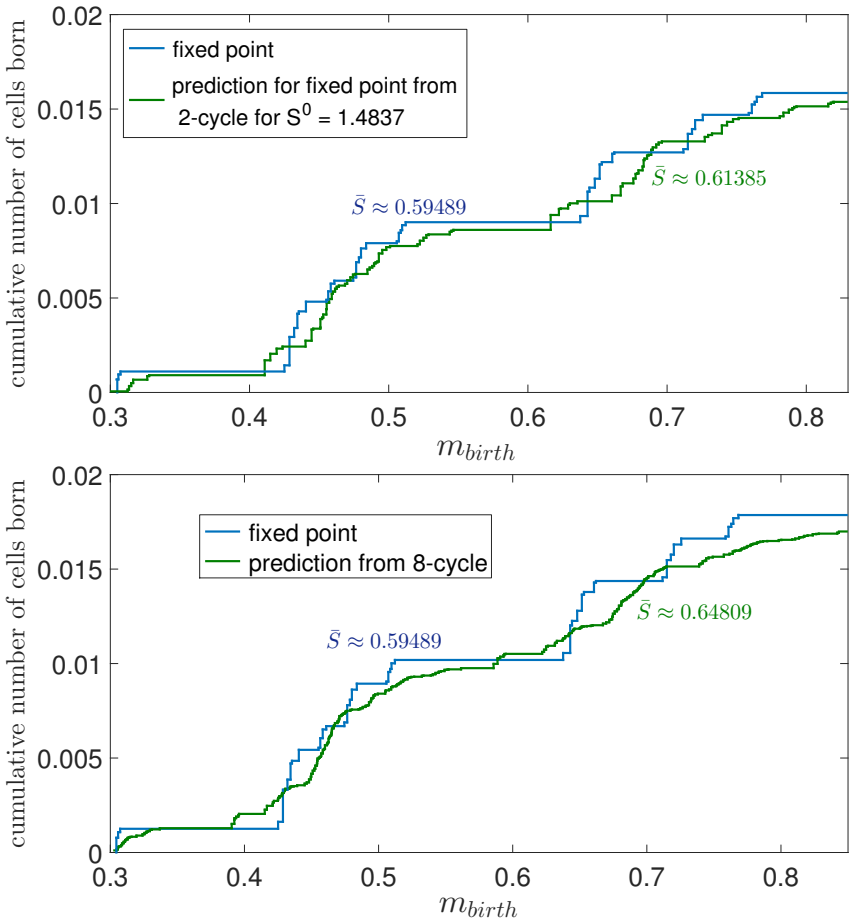

Figure 5.20: Comparison between the predicted fixed point based on the cycle for $S^0 = 1.4837$ (top) and 1.6 (bottom), and the actual fixed point.

$\bar{S}$ for the fixed point 0.59489. A comparison of the distributions of the cumulative number of cells born per minute is presented in Figure 5.21. This larger deviation from the prediction to the actual fixed point most certainly also plays a role in whether or not the fixed point can be found starting from the cyclic behaviour.

Table 5.16: Results of the map iterations starting with a perturbation of the fixed point for $S^0 = 2.5$: for every birth cohort the number of cells born per minute is changed with a factor $1+b$ where b is a uniformly distributed random number over $[-a,a]$, and the nutrient concentration is changed with a factor $1+c$ where c is a random number out of the uniform distribution over $[-a,a]$. The percentage is for 20 test cases.

change \ result	**fixed point**	**4-cycle**
$[-\mathbf{1}\%,\mathbf{1}\%]$	100%	0%
$[-\mathbf{10}\%,\mathbf{10}\%]$	70%	30%
$[-\mathbf{20}\%,\mathbf{20}\%]$	20%	80%
$[-\mathbf{30}\%,\mathbf{30}\%]$	95%	5%

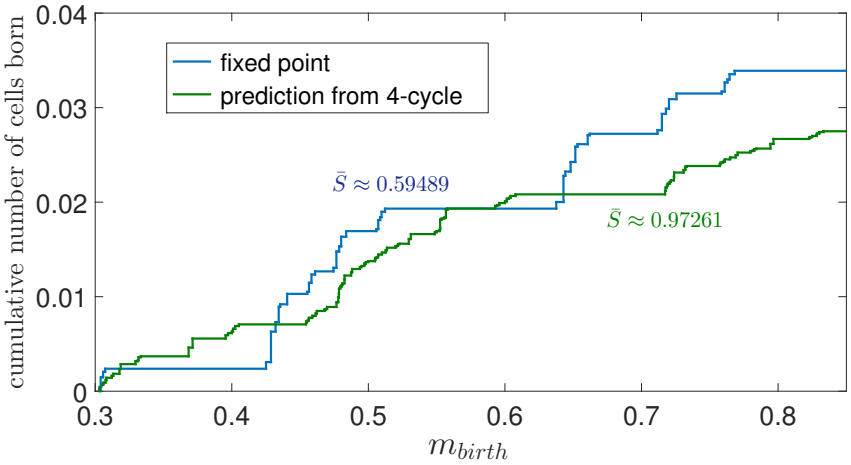

Figure 5.21: Comparison of the predicted fixed point based on the 4-cycle and the actual fixed point for $S^0 = 2.5$.

5.6 Continuation of a MM1 fixed point with S^0 free

5.6.1 Zero-order prediction

A very simple case of fixed point continuation is implemented. We start from a fixed point for a certain value of S^0 and then use this fixed point as a prediction for the fixed point for a different value of S^0. The fixed points are calculated up to a chosen value of S^0. The change of S^0 is regulated by a step size control procedure: a start value step_{start}, a minimal step size step_{min} and a maximal step size step_{max} are chosen. The structure of the continuation is as follows:

```
fixed point given with coh_fp, S0_fp and S_fp and wanted S0_dest
set step = step_start
if(S0_dest < S0_fp)
  set step = -step_start
make prediction for new fixed point: set coh_pred =  coh_fp, S_pred = S_fp
                                     and S0_pred  =  S0_fp + step
while((step>0 and S0_pred-step<S0_dest) or (step<0 and S0_pred-step>S0_dest))
  map is iterated starting from predicted fixed point, until
        convergence or the maximum number of iterations is reached
  if(maximum number of iterations was reached)
    S0_pred  =  S0_fp - step/2
    step = step/2
    if(|step|<step_min)
      stop continuation
  else
    if(number of iterations<50)
      step = step*1.3
      if(step>0)
        step = min(step*1.3,step_max)
      else
        step = max(step*1.3,-step_max)
    print information about new fixed point
    update S_pred and coh_pred to new fixed point
    S0_pred += step
```

The results are shown in Figure 5.22, where we start with the fixed point for $S^0 = 1$. The starting step size is 0.1, the minimal step size is 10^{-5} and the maximal step size is 1. Parameter values used for the convergence of the map are a maximum relative change in $\bar{S}$ of 10^{-7} and a maximum relative change in $\bar{b}_{tot}$ of 10^{-7}. At most 300 map iterations are performed to check the convergence of the map. We tried to calculate the fixed points from 1 until 3, but there was no convergence (according to our chosen convergence parameters) for S^0 values larger than 2.25280. For a larger S^0 value there is no sign of cyclic behaviour, N stays the constant 41 and $\bar{S}$ and $\bar{b}_{tot}$

do not vary that much, so we continue the continuation with less strict convergence parameters ($5 \cdot 10^{-6}$ for the relative variation in $\bar{S}$ and $\bar{b}_{tot}$ and maximum 500 map iterations). The continuation now gives results up to $S^0 = 2.55$ and probably fixed points for higher parameter values could still be found if we further "loosened" the convergence parameters. When decreasing S^0 starting from $S^0 = 1$ (with the convergence parameters $5 \cdot 10^{-6}$ for the relative variation in $\bar{S}$ and $\bar{b}_{tot}$ and maximum 500 map iterations), the fixed points could be calculated up to $S^0 = 0.59866$.

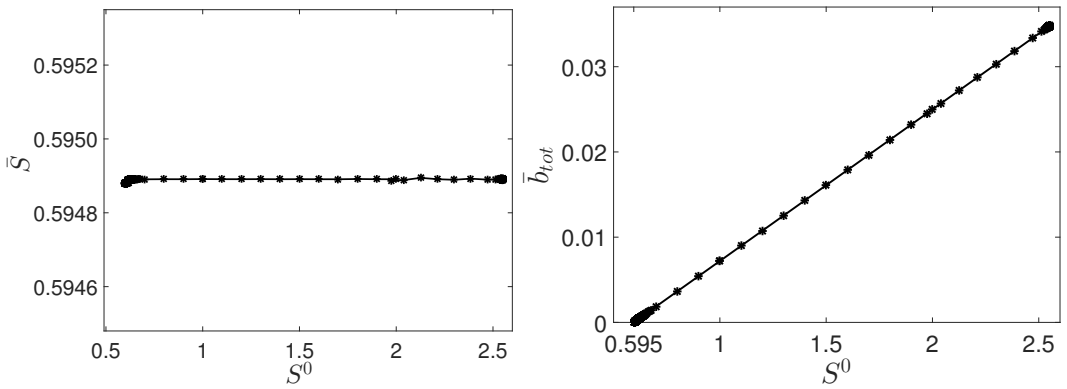

Figure 5.22: Fixed point continuation with zero-order prediction for free S^0, starting from $S^0 = 1$.

For the different S^0 values, the fixed point has always the same 41 birth cohorts and $\bar{S}$ is constant. The increase of $\bar{b}_{tot}$ is linear with S^0, as could be expected for a constant $\bar{S}$ and unchanged internal state of the cells in the birth cohorts. In Figure 5.23 the cumulative birth mass distribution of the fixed point for $S^0 = 1$, $S^0 = 2$ and $S^0 = 0.7$ can be seen as multiples of each other.

In Figure 5.24 the bifurcation diagram of the fixed point of the map for free S^0 is shown. The trivial fixed point (red) corresponds to the situation with no cells in the chemostat and a nutrient concentration that equals the nutrient concentration in the feeding bottle. The non-trivial fixed points, all with the same 41 birth cohorts, are depicted in blue.

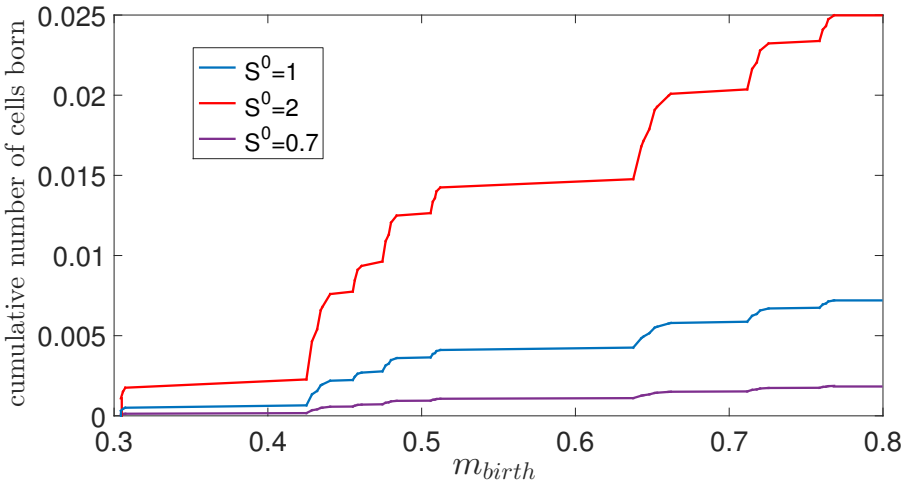

Figure 5.23: The cumulative mass distribution of the fixed point for $S^0 = 1$, $S^0 = 2$ and $S^0 = 0.7$.

5.6.2 Chord prediction

In this subsection we apply a continuation method in which the prediction of the fixed point is based on 2 previously computed fixed points. The number of cells born per unit of time is predicted using linear extrapolation from the $\bar{b}_{tot}$ values of the 2 previous fixed points. For the list of birth cohorts of the predicted fixed point, the list of the last fixed point is used, where only the number of cells born per unit of time in the birth cohorts is rescaled according to the predicted $\bar{b}_{tot}$. $\bar{S}$ is predicted using linear extrapolation from the $\bar{S}$ values of the 2 previous fixed points. As before, step size control is used with a start value step_{start}, a minimal step size step_{min} and a maximal step size step_{max}. The method includes a check that the predicted values of $\bar{b}_{tot}$ and $\bar{S}$ are not negative. If the predicted $\bar{b}_{tot}$ is negative, it is set to zero, and if the predicted $\bar{S}$ is negative, it is set to 0.000001. The structure of the continuation is as follows:

2 fixed points given with coh_{fp1}, $b_{tot,fp1}$, $S0_{fp1}$, S_{fp1}, coh_{fp2}, $b_{tot,fp2}$, $S0_{fp2}$, S_{fp2} and wanted $S0_{dest}$

set step = step_{start}

if ($S0_{dest} < S0_{fp}$)

  set step = -step_{start}

make prediction for new fixed point:

$S0_{pred}$ = $S0_{fp2}$ + step

$$b_{tot,pred} = \max\left(b_{tot,fp1} + \frac{S0_{pred} - S0_{fp1}}{S0_{fp2} - S0_{fp1}} \cdot \left(b_{tot,fp2} - b_{tot,fp1}\right),\ 0\right)$$

coh_{pred} = coh_{fp2} with amount of cells in every cohort adjusted by

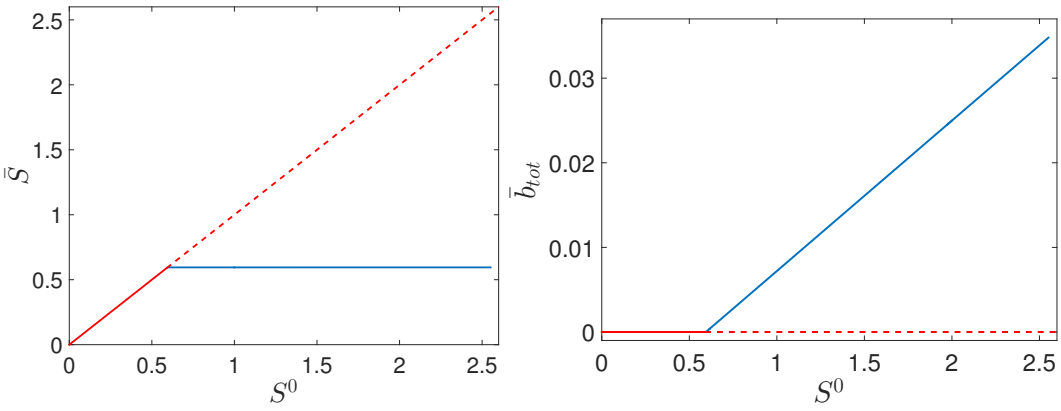

Figure 5.24: Bifurcation diagram of the fixed point of the map for free S^0. The trivial fixed point is depicted in red and the non-trivial fixed points with the 41 birth cohorts in blue.

5

the factor $\frac{b_{tot,pred}}{b_{tot,fp2}}$

$S_{pred} = \max\left(S_{fp1} + \frac{S0_{pred} - S0_{fp1}}{S0_{fp2} - S0_{fp1}} \cdot \left(S_{fp2} - S_{fp1}\right),\ 10^{-6}\right)$

while((step>0 and $S0_{pred}$-step<$S0_{dest}$) or (step<0 and $S0_{pred}$-step>$S0_{dest}$))
  map is iterated starting from predicted fixed point, until
    convergence or the maximum number of iterations is reached
  if(maximum number of iterations was reached)
    $S0_{pred}$ = $S0_{fp}$ - step/2
    step = step/2
    if(|step|<$step_{min}$)
      stop continuation
    else
      adjust S_{pred}, $b_{tot,pred}$ and amount of cells in coh_{pred}
  else
    if(number of iterations<50)
      step = step*1.3
      if(step>0)
        step = min(step*1.3,$step_{max}$)
      else
        step = max(step*1.3,-$step_{max}$)
    print information about new fixed point
    $S0_{pred}$ += step
    coh_{fp1} = coh_{fp2}, $b_{tot,fp1}$ = $b_{tot,fp2}$, $S0_{fp1}$ = $S0_{fp2}$, S_{fp1} = S_{fp2}
    coh_{fp2} = coh_{pred}, $b_{tot,fp2}$ = $b_{tot,pred}$, $S0_{fp2}$ = $S0_{pred}$, S_{fp2} = S_{pred}
    make prediction for new fixed point using the formulas above

The results of the continuation for increasing S^0 starting from $S^0 = 1$ and $S^0 = 1.1$ are presented in Figure 5.25. If we use 10^{-7} as convergence parameter for $\bar{b}_{tot}$ and $\bar{S}$ and a maximum of 300 map iterations to achieve convergence, we find fixed points up to $S^0 = 2.52366$, so for larger S^0 values than with the zero-order continuation

method (for the same convergence parameters). By allowing maximally 500 map iterations and increasing the parameters for relative convergence of $\bar{b}_{tot}$ and $\bar{S}$ to $5 \cdot 10^{-6}$, we could go up to $S^0 = 3.16780$. For larger values of S^0 the map does not converge, but iterates between several points of which one has a negative $\bar{S}$ (which is then set to 10^{-6}).

The results of the continuation for decreasing S^0 starting from the fixed points for $S^0 = 1$ and $S^0 = 0.9$ can also be found in Figure 5.25. With 10^{-7} as convergence parameter for $\bar{b}_{tot}$ and $\bar{S}$ and a maximum of 300 map iterations to achieve convergence, we calculate non-trivial fixed points up to $S^0 = 0.595$ and find the trivial fixed points for smaller S^0 values. If we decrease the step size, non-trivial fixed points can be found up to a S^0 value very close to $\bar{S} \approx 0.59489$. With the zero-order continuation method, we could only find the non-trivial fixed points up to 0.59866.

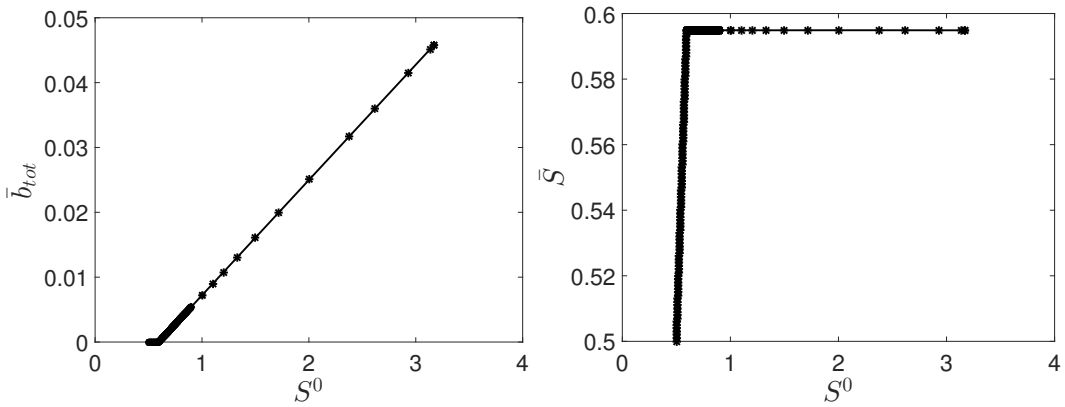

Figure 5.25: Chord fixed point continuation for free S^0, starting from $S^0 = 1$ and $S^0 = 1.1$ for increasing S^0, and $S^0 = 1$ and $S^0 = 0.9$ for decreasing S^0.

In fact, we would expect that the chord prediction method works very well for free S^0 since once we know the existence of a fixed point with a certain set of birth cohorts and $\bar{S}$, we know that for every $S^0 > \bar{S}$ a fixed point exists with the same $\bar{S}$ and the same birth cohorts with only a rescaling of the number of cells born per minute in the birth cohorts. The rescaling factor for the number of cells born per minute can be obtained from the equilibrium equation for the nutrient:

$$D(S^0 - \bar{S}) = \sum_{i=1}^{N} \theta(a_i, x_{0i}, \bar{S}) \cdot \bar{b}(x_{0i}), \tag{5.1}$$

where $\bar{S}$ and $\theta(a_i, x_{0i}, \bar{S})$ are in this case constant. Since only a rescaling of the number of cells born per minute in the birth cohorts is done, $\sum_{i=1}^{N} \theta(a_i, x_{0i}, \bar{S}) \cdot \bar{b}(x_{0i})$ can only change with a factor dependent on $\bar{b}_{tot}$. Since the relationship between S^0 and $\bar{b}_{tot}$ of the corresponding fixed point is linear and this continuation method is based on linear extrapolation, the method should give very good estimates for the fixed points for other values of S^0 (in fact, the estimates are exact except for numerical errors). Why it fails for values of S^0 smaller than $\bar{S}$ is clear as the nutrient concentration in the feeding bottle should be at least the nutrient concentration inside the bioreactor (see (5.1)). Why the continuation fails for large values of S^0 is not obvious. It is probably related to a change in stability of the fixed point. To get a better understanding of the stability of the fixed point, we repeat the experiment with a random shift of the mass of the birth cohorts for $S^0 = 3.16780$ (the last found fixed point in the continuation). The results can be found in Table 5.17, where for every range of the random number 20 test cases were considered. There is convergence of the map to either the fixed point or the 4-cycle with negative $\bar{S}$ (changed to 0.000001) in one of the points. Compared to the fixed points for $S^0 = 1.4873$ and $S^0 = 2.5$, the fixed point for $S^0 = 3.16780$ is much more sensitive to small changes in the mass location of the birth cohorts. To check how sensitive the fixed point is to perturbations in the amount of cells born per minute in the birth cohorts and the nutrient concentration, we repeat the experiment we did for the fixed point for $S^0 = 1.4837$ (see Table 5.15) and for $S^0 = 2.5$ (see Table 5.16). Already for a random perturbation between -1% and 1% the map converged to the 4-cycle in all 20 test cases. This confirms that the fixed point for $S^0 = 3.16780$ has a small attraction region and so we can postulate that the fixed point loses stability near this S^0 value, although we can not prove this. This is at least consistent with the bifurcation behaviour we propose (see Figure 2.9).

5.6.3 Pseudo-arclength continuation

In this subsection we numerically continue the fixed point with S^0, the concentration of nutrient influx, as free parameter. We use a modified version of pseudo-arclength continuation (see the original pseudo-arclength continuation in Section 2.3.3). A

Table 5.17: Results of the map iterations starting with a perturbation of the fixed point for $S^0 = 3.16780$: the mass of every birth cohort is changed by adding a uniformly distributed random number over $[-a,a]$. The percentage is for 20 test cases.

change \ result	**fixed point**	**4-cycle**
$[-\mathbf{10^{-6}}, \mathbf{10^{-6}}]$	100%	0%
$[-\mathbf{10^{-5}}, \mathbf{10^{-5}}]$	65%	35%
$[-\mathbf{10^{-4}}, \mathbf{10^{-4}}]$	10%	90%
$[-\mathbf{10^{-3}}, \mathbf{10^{-3}}]$	0%	100%
$[-\mathbf{10^{-2}}, \mathbf{10^{-2}}]$	0%	100%

fixed point with N cohorts $\left(\bar{S}, \bar{b}(x_{01}), \ldots, \bar{b}(x_{0N}), S^0\right)$ satisfies

$$\begin{aligned} G\left(\bar{S}, \bar{b}(x_{01}), \ldots, \bar{b}(x_{0N}), S^0\right) &= \begin{pmatrix} G_1\left(\bar{S}, \bar{b}(x_{01}), \ldots, \bar{b}(x_{0N}), S^0\right) \\ G_2\left(\bar{S}, \bar{b}(x_{01}), \ldots, \bar{b}(x_{0N}), S^0\right) \\ \vdots \\ G_{N+1}\left(\bar{S}, \bar{b}(x_{01}), \ldots, \bar{b}(x_{0N}), S^0\right) \end{pmatrix} \\ &:= M^1(S^0) \begin{pmatrix} \bar{S} \\ \bar{b}(x_{01}) \\ \vdots \\ \bar{b}(x_{0N}) \end{pmatrix} - \begin{pmatrix} \bar{S} \\ \bar{b}(x_{01}) \\ \vdots \\ \bar{b}(x_{0N}) \end{pmatrix} = \begin{pmatrix} 0 \\ 0 \\ \vdots \\ 0 \end{pmatrix}, \end{aligned} \tag{5.2}$$

where $M^1(S^0)$ is the map obtained by first applying the map M in (4.14) on $\left(\bar{S}, \bar{b}(x_{01}), \ldots, \bar{b}(x_{0N})\right)$ and then mapping the birth values in the new cohorts back to the original N cohorts. More precisely, $M^1(S^0) = \begin{pmatrix} M_1^1(S^0) \\ M_2^1(S^0) \\ \vdots \\ M_{N+1}^1(S^0) \end{pmatrix} = M_B \circ M(S^0)$,

where:

$$M_B : \begin{pmatrix} \bar{S} \\ \bar{b}(\tilde{x}_{01}) \\ \bar{b}(\tilde{x}_{02}) \\ \vdots \\ \bar{b}(\tilde{x}_{0N_B}) \end{pmatrix} \longrightarrow \begin{pmatrix} \bar{S} \\ \sum\limits_{i \in A_1} \bar{b}(\tilde{x}_{0i}) \\ \sum\limits_{i \in A_2} \bar{b}(\tilde{x}_{0i}) \\ \vdots \\ \sum\limits_{i \in A_N} \bar{b}(\tilde{x}_{0i}) \end{pmatrix}, \tag{5.3}$$

with

$$\begin{aligned} A_1 &= \left\{ i \in \{1,\ldots,N_B\} \,|\, \tilde{m}_{0i} \leq \frac{m_{01}+m_{02}}{2} \right\}, \\ A_2 &= \left\{ i \in \{1,\ldots,N_B\} \,|\, \frac{m_{01}+m_{02}}{2} < \tilde{m}_{0i} \leq \frac{m_{02}+m_{03}}{2} \right\}, \\ &\vdots \\ A_N &= \left\{ i \in \{1,\ldots,N_B\} \,|\, \frac{m_{0(N-1)}+m_{0N}}{2} < \tilde{m}_{0i} \right\}. \end{aligned}$$

Freeing S^0 in (5.2) defines a fixed point curve in $\left(\bar{S}, \bar{b}(\bar{x}_{01}), \ldots, \bar{b}(\bar{x}_{0N}), S^0\right)$-space.

5

We calculate the fixed point curve for increasing or decreasing S^0 using the following procedure. We start with (an approximation of) a fixed point:

$$fix = \begin{pmatrix} \bar{S} \\ \bar{b}(x_{01}) \\ \vdots \\ \bar{b}(x_{0N}) \\ S^0 \end{pmatrix}$$

with initial conditions m_{0i}, X_{0i}, Y_{0i}, A_{0i} and $\bar{b}(x_{0i})$ for every cohort, and first calculate the tangent vector to the curve in this fixed point. The Jacobian matrix of G evaluated in the fixed point is a $(N+1)\times(N+2)$-matrix J_G. We calculate the tangent vector v by solving

$$\begin{pmatrix} J_G \\ 1\ldots1 \end{pmatrix} \cdot v = \begin{pmatrix} 0 \\ \vdots \\ 0 \\ 1 \end{pmatrix},$$

and then normalizing v. To predict the next fixed point, we first check the direction of v and if necessary reverse it. The next fixed point is then predicted as $\left(\bar{S}^p, \bar{b}(\bar{x}_{01})^p, \ldots, \bar{b}(\bar{x}_{0N})^p, S^{0p}\right) = fix + step \cdot v$, with $step$ the stepsize of the continuation. The value of $step$ is adjusted during the continuation and is dependent on the previous stepsize, the number of Newton steps, the minimal stepsize $step_{min}$ and the maximal stepsize $step_{max}$. For the first continuation step $step$ is set to $step_{start}$. We use the continuation values in Table 5.18.

Table 5.18: Parameter values used in the pseudo-arclength continuation of the fixed point.

parameter	value
$step_{start}$	10^{-1}
$step_{min}$	10^{-5}
$step_{max}$	1
N_{max}	10
$VarTolerance$	10^{-6}
$FunTolerance$	10^{-6}

If one of the values of the predicted fixed point is negative (either $\bar{S}^p$, one of the $\bar{b}(\bar{x}_{0i})^p$ or S^{0p}), we repeat the calculation with half the stepsize (bounded from below by $step_{min}$). If this is not the case, we adjust the prediction by applying one map iteration on the predicted point: this can change $\bar{S}^p$, $\bar{b}(\bar{x}_{0i})^p$ and also the number of cohorts and their initial values. Note that we continue to denote the number of cohorts as N, but that it can be different from the initial N. This new prediction is corrected using a Newton iteration. During the calculation of the Newton-correction step the mesh and number of cohorts of the predicted fixed point are kept constant. First the Jacobian J_G is calculated and then the normalised tangent vector v_P. We then use a Newton correction step of the following system of equations to correct this new prediction:

$$\begin{cases} G\left(\bar{S},\bar{b}(x_{01}),\ldots,\bar{b}(x_{0N}),S^0\right)=0, \\ \begin{pmatrix}\bar{S}-\bar{S}^p & \bar{b}(x_{01})-\bar{b}(x_{01})^p & \ldots & \bar{b}(x_{0N})-\bar{b}(x_{0N})^p & S^0-S^{0p}\end{pmatrix}\cdot v_p^T=0. \end{cases}$$

The Newton correction cor is obtained by solving

$$\begin{pmatrix} J_G \\ v_p \end{pmatrix}\cdot cor = R = \begin{pmatrix} \bar{S}^p - M_1^1(S^{0p})\left(\bar{S}^p,\bar{b}(x_{01})^p,\ldots,\bar{b}(x_{0N})^p\right) \\ \bar{b}(x_{01})^p - M_2^1(S^{0p})\left(\bar{S}^p,\bar{b}(x_{01})^p,\ldots,\bar{b}(x_{0N})^p\right) \\ \vdots \\ \bar{b}(x_{0N})^p - M_{N+1}^1(S^{0p})\left(\bar{S}^p,\bar{b}(x_{01})^p,\ldots,\bar{b}(x_{0N})^p\right) \\ 0 \end{pmatrix}.$$

For every Newton step, we check if the norm of the correction cor and the norm of R are small enough. $VarTolerance$ is the threshold of $\|cor\|$ and $FunTolerance$ is the threshold for $\|R\|$. The norm is the L_1-norm. If one or both of $\|cor\|$ and $\|R\|$

are not small enough, we add *cor* to the predicted point vector to obtain an update. If one of the predicted number of cells born per minute in a cohort is negative, it is set to zero, and if $\bar{S}^p \leq 0$, it is set to 10^{-6}. Before repeating the Newton step, the predicted fixed point is adjusted by applying one map iteration. This means that the number of cohorts may change. This procedure is repeated until the norms are small enough which means we have found a new fixed point. The stepsize is then adjusted, i.e. divided by 2 if 4 or more Newton steps were needed and multiplied by 1.3 if less than 4 Newton steps were needed. If the maximum number of Newton steps N_{max} was taken, we divide the stepsize by 2 and start again from the previous fixed point.

This Moore-Penrose-like continuation method works for MM1. Starting with the fixed point for $S^0 = 1$ with the continuation parameters as in Table 5.18 for increasing values of S^0, the method calculates the fixed points up to $S^0 = 1.60107$. If we increase $VarTolerance$ and $FunTolerance$ to 10^{-5}, fixed points are found up to $S^0 = 7.83502$. If we decrease S^0 starting from $S^0 = 1$ for $VarTolerance$ and $FunTolerance$ equal to 10^{-5}, fixed points are found down to $S^0 = 0.59490$. The results are depicted in Figure 5.26. Note that the stability of the found fixed points of the map is unknown, contrary to the continuation methods in Sections 5.6.1 and 5.6.2, since the convergence of the map iteration is not checked. For the found fixed point for $S^0 = 4.20148$ for example, the map iteration indeed does not converge, so this fixed point is unstable as a fixed point of the map (cf. the previous continuation results in Section 5.6.2).

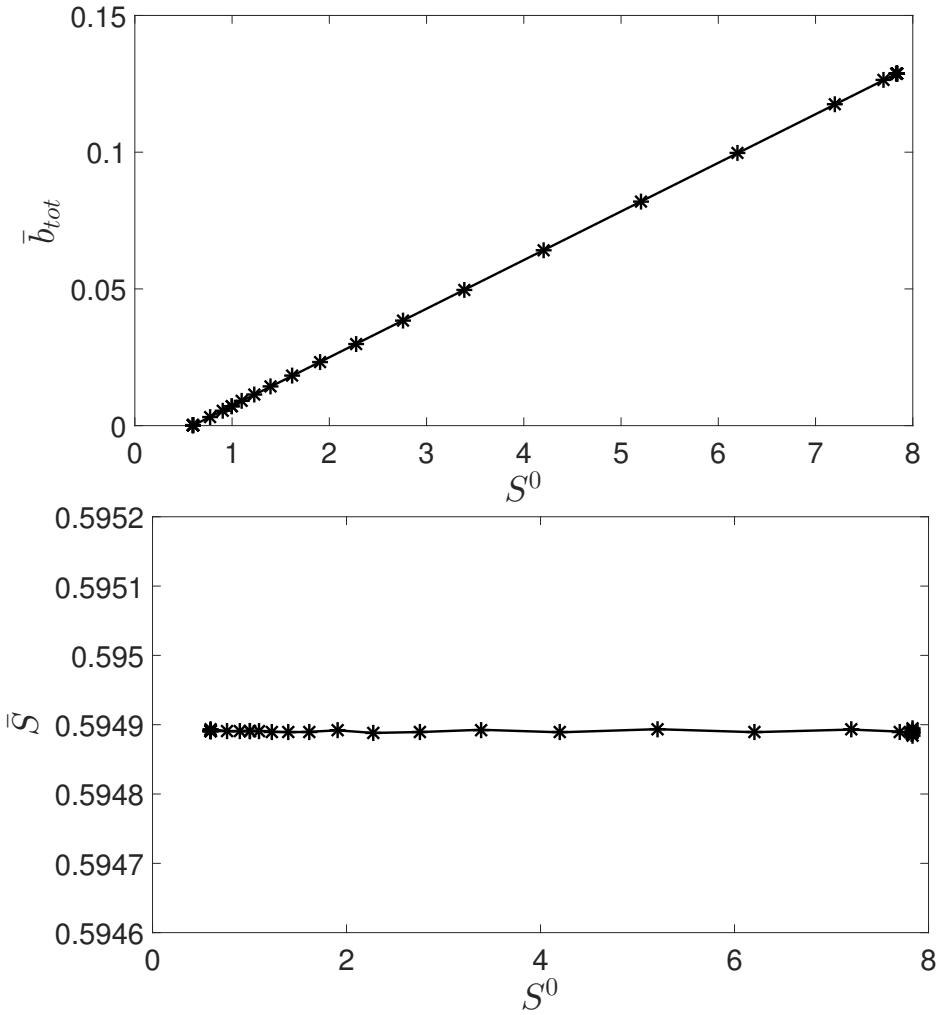

Figure 5.26: The results of the pseudo-arclength continuation with free S^0 starting from $S^0 = 1$.

5.7 Continuation of a MM1 fixed point for free D

5.7.1 Zero-order prediction

The parameter D plays a more complex role in the system than S^0. It represents the dilution rate of the nutrient, as well as the death rate of the cells.

A very simple case of fixed point continuation is implemented: starting from a found fixed point for a certain value of D, the fixed points are calculated up to a chosen value of D, as we did for S^0 in Section 5.6.1. The results are shown in Figures 5.27 and 5.29, where we start with the fixed point for $D = 0.01$ min^{-1}. The starting step size is 10^{-3}, the minimal step size 10^{-7} and the maximal step size 10^{-2}, maximally 300 map iterations are performed to check the convergence of the map and the convergence parameters for $\bar{S}$ and $\bar{b}_{tot}$ were 10^{-7}. We tried to calculate the fixed points from 0.01 until 0.011, but only could calculate the fixed point up to 0.010696. For larger values of D there is too much variation on $\bar{S}$ (values approximately between 0.68 and 0.707) and on $\bar{b}_{tot}$ (values approximately between 0.00558 and 0.00568), the number of cohorts also varies between 57 and 61 and there is no cyclic behaviour of the map.

When decreasing D, we could calculate the fixed points up to $D = 0.00689$ min^{-1}. For a smaller value of D, the convergence parameters seemed to be too strict for the found point. We then started the continuation with the fixed point for $D = 0.00689$ min^{-1}, but loosened the convergence conditions to $5 \cdot 10^{-6}$ for the parameter for both $\bar{S}$ and $\bar{b}_{tot}$ and allowed maximally 500 map iterations instead of 300 to check convergence. As a result we could find further fixed points for D down to 0.0059. If D is smaller than this value, there is again too much variation in $\bar{S}$ and $\bar{b}_{tot}$ (values respectively between 0.233274 and 0.233282, and between 0.00948017 and 0.00948024), and the number of cohorts switches between 4 and 5. As a test, we did the same continuation with a smaller relative tolerance (10^{-7} instead of 10^{-6}), but this has no big effect on the results and the map still oscillates between 4 and 5 cohorts for D values smaller than 0.0059. We want to consider this result with the alternating number of cohorts as a fixed point, so continue the continuation for decreasing D starting from the fixed point for $D = 0.0059$ min^{-1} with loosened convergence conditions (10^{-5} for the parameter for both $\bar{S}$ and $\bar{b}_{tot}$, maximally 500 map iterations allowed and

the number of cohorts can change maximally 100% instead of 1% during one map iteration for a fixed point). Fixed points were found up to $D = 0.00525$ min^{-1}, for smaller D values the variation in $\bar{S}$ and $\bar{b}_{tot}$ was again a bit too big (N was however a constant 4). Further increasing the convergence parameters (10^{-4} for the parameter for both $\bar{S}$ and $\bar{b}_{tot}$), allows to calculate the fixed points up to $D = 0.00522$ min^{-1}. Even further increasing of the convergence parameters (10^{-3} for the parameter for both $\bar{S}$ and $\bar{b}_{tot}$), allows to calculate the fixed points up to $D = 0.00519$ min^{-1}, but this appears to be the limit since for smaller D values there is too much variation on $\bar{S}$ (values approximately between 0.168 and 0.199) and on $\bar{b}_{tot}$ (values approximately between 0.0088 and 0.0091). For D values between 0.0085 and 0.01, extra fixed points were calculated using smaller step sizes in the continuation.

In Figure 5.27 the number of birth cohorts of the fixed points for the different values of D is depicted. The number of birth cohorts is no longer fixed for the different parameter values (as was the case for S^0). The different fixed points also do not have the same shape of the cummulative mass distribution per unit of time at birth, as can be seen in Figure 5.28.

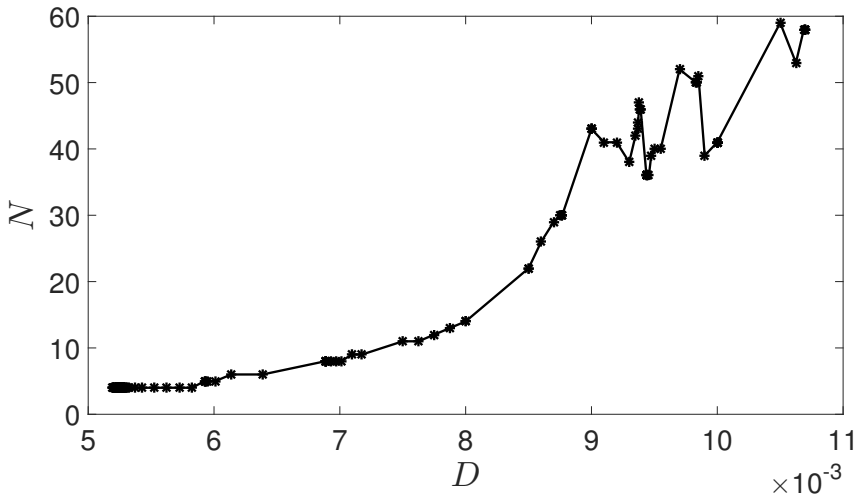

Figure 5.27: The zero-order prediction continuation starting from $D = 0.01$ min^{-1}: the number of birth cohorts of the fixed point in function of D.

In Figure 5.29 the values of $\bar{S}$ and $\bar{b}_{tot}$ of the fixed points are depicted for different values of D: $\bar{S}$ is increasing with increasing D, the relation between $\bar{b}_{tot}$ and D is more complex.

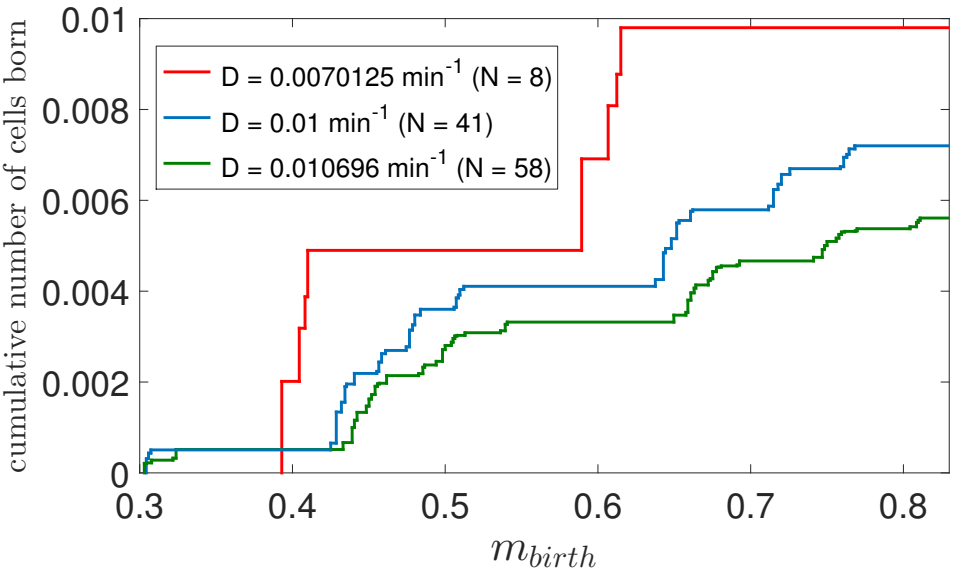

Figure 5.28: The cumulative mass distribution of the fixed point for $D = 0.0070125$ min^{-1}, $D = 0.01$ min^{-1} and $D = 0.010696$ min^{-1}.

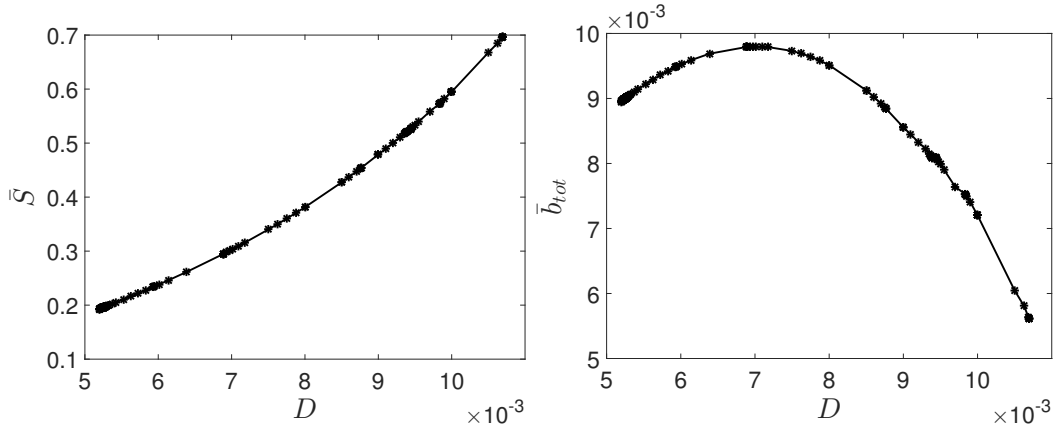

Figure 5.29: Continuation with zero-order prediction starting from the fixed point for $D = 0.01$ min^{-1}: $\bar{S}$ (left figure) and $\bar{b}_{tot}$ (right figure) as a function of D.

5.7.2 Chord prediction

We now apply the continuation method with chord prediction for free D. Details of the method are as in Section 5.6.2 for the case of free S^0.

The results of the continuation for increasing D starting from the fixed points for $D = 0.01$ min^{-1} and $D = 0.0105$ min^{-1} are given in Figure 5.30 and Figure 5.31. We start with the same continuation parameters as for the "simple" continuation (10^{-7} as convergence parameter for $\bar{b}_{tot}$ and $\bar{S}$ and a maximum of 300 map iterations to achieve convergence) and the same values for the step size (starting step size 10^{-3}, minimal step size 10^{-7} and maximal step size 10^{-2}). Non-trivial fixed points are found up to $D = 0.01194$ min^{-1}, so this method seems to work better than the zero-order continuation method in Section 5.7.1 (fixed points found up to 0.01070). By allowing maximally 500 map iterations, increasing the parameters for relative convergence of $\bar{b}_{tot}$ and $\bar{S}$ to 10^{-4}, allowing a variation of 100% in N (instead of 1% before) and taking smaller steps (starting step size 10^{-5}, minimal step size 10^{-7} and maximal step size 10^{-5}), we could find non-trivial fixed points up to $D = 0.012194$ min^{-1}. For larger values of D, we find the trivial fixed point.

Decreasing D when we start from the fixed points for $D = 0.01$ min^{-1} and $D = 0.009$ min^{-1} (with the same initial convergence parameter values and step sizes as before), we could calculate the non-trivial fixed points up to $D = 0.00709$ min^{-1}. For smaller values of D, the convergence parameters appear to be too strict. We repeated the same continuation (starting from $D = 0.01$ min^{-1} and $D = 0.009$ min^{-1}) with a smaller relative tolerance of 10^{-8} instead of 10^{-6} for the age integration, an allowed change of 100% instead of 1% for the number of cohorts during one map iteration for a fixed point, 10^{-5} as convergence parameter for $\bar{b}_{tot}$ and $\bar{S}$, a maximum of 500 map iterations to achieve convergence and smaller step sizes (starting step size 10^{-4}, minimal step size 10^{-7} and maximal step size 10^{-3}). The non-trivial fixed points were found up to $D = 0.00539$ min^{-1} and from $D = 0.00473$ min^{-1} downwards trivial fixed points were found. To find the transition from the non-trivial fixed points to the trivial fixed points, we are interested in the region of D values between 0.00539 and 0.00473. If we start from the 2 last found fixed points and play with different step sizes, convergence parameters and relative tolerances, we find non-trivial fixed points up to $D = 0.0052$ min^{-1}. For smaller values of D, the map does not converge to a

fixed point but it wanders along a closed invariant curve (see Figure 5.32). Changing the precision of the calculations does not have a real effect on the results: map iteration 400 to 500 for $D = 0.00523$ min^{-1} for $\delta = 10^{-3}$, 10^{-4} and 10^{-5}, all with $\texttt{reltol} = 10^{-9}$, show the same closed invariant curve (completely overlapping in Figure 5.32). For $\delta = 10^{-3}$ the points have 4 birth cohorts, for $\delta = 10^{-4}$ 6 birth cohorts and for $\delta = 10^{-5}$ 7 birth cohorts, but they clearly reflect the same invariant curve so the result is no numerical artefact. Such a closed invariant curve is typical for a supercritical Neimark-Sacker bifurcation (see Section 2.3.2) at $D = 0.0052$ min^{-1} where the fixed point loses stability. In Figure 5.33 the behaviour of the closed invariant curve is shown for a decrease in D (all calculated for $\delta = 10^{-3}$ and $\texttt{reltol}= 10^{-8}$). The increase of the size of the invariant curve corresponds with the typical behaviour for a supercritical Neimark-Sacker bifurcation (see Figure 2.11).

Note that the special case $D = 0$ min^{-1} corresponds to a batch culture where no nutrient is added to the bioreactor and the cells only have the initial amount of nutrient at their disposal. Since cells only die by being washed out of the bioreactor, cells can never die when $D = 0$ min^{-1}. Our model is therefore not a good representation for a batch culture and we can expect some problems for small D values.

In Figure 5.34 the bifurcation diagram of the fixed point of the map for free D is shown. The trivial fixed points are depicted in red and the non-trivial fixed points in blue.

The effect of D upon the number of cells born is complicated. More food in the bioreactor as D increases gives rise to an increase in births, and more outflow of cells as D increases gives rise to an increase of deaths. This results in almost no cells born for low D because of the very low nutrient inflow, and also for high D because the cells rapidly flow out of the bioreactor. This explains the shape of the fixed point curve in Figure 5.34. If D increases, then $\bar{S}$ also increases until $\bar{S} = S^0$ when no living cells are left. If D decreases, then the inflow of nutrient is decreased and the nutrient is taken up by cells faster than provided, so $\bar{S}$ converges to 0.

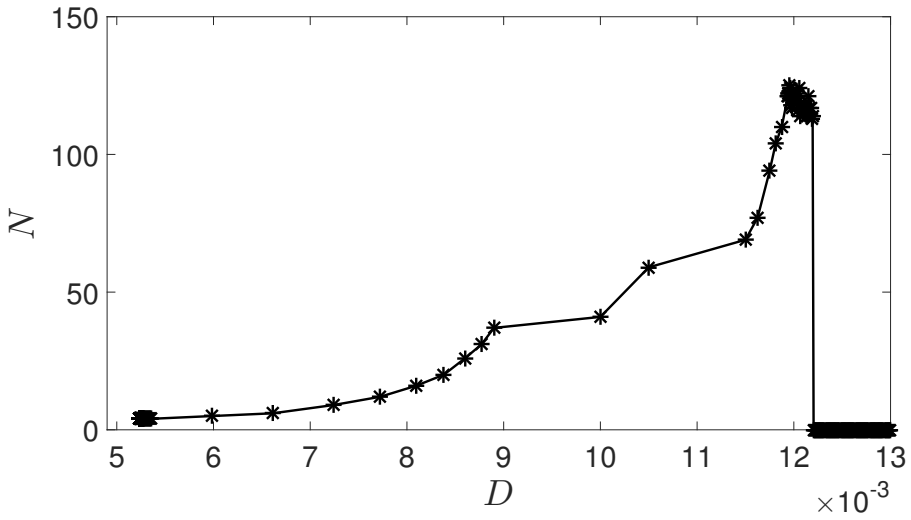

Figure 5.30: Continuation with chord prediction starting from $D = 0.01$ min^{-1} and $D = 0.0105$ min^{-1} for increasing values of D and starting from $D = 0.01$ min^{-1} and $D = 0.009$ min^{-1} for decreasing D: the number of cohorts of the fixed point as a function of D.

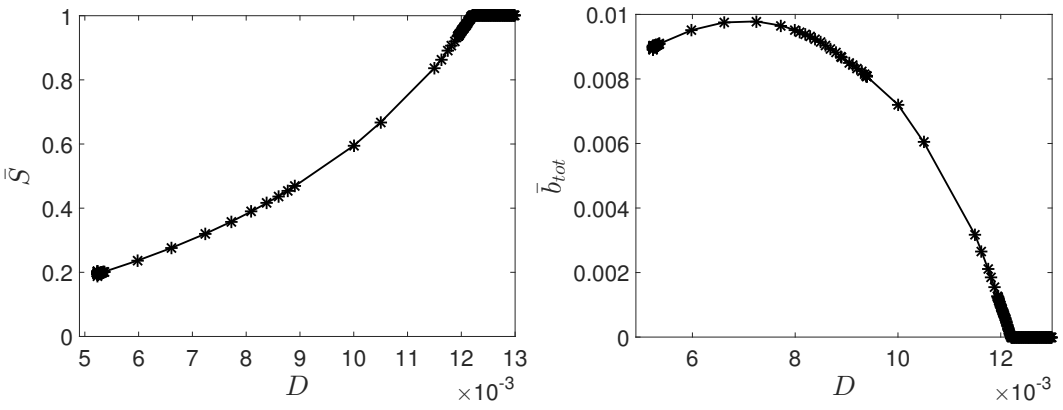

Figure 5.31: Continuation with chord prediction starting from $D = 0.01$ min^{-1} and $D = 0.0105$ min^{-1} for increasing values of D and starting from $D = 0.01$ min^{-1} and $D = 0.009$ min^{-1} for decreasing D: $\bar{S}$ (left figure) and $\bar{b}_{tot}$ (right figure) of the fixed points in function of D.

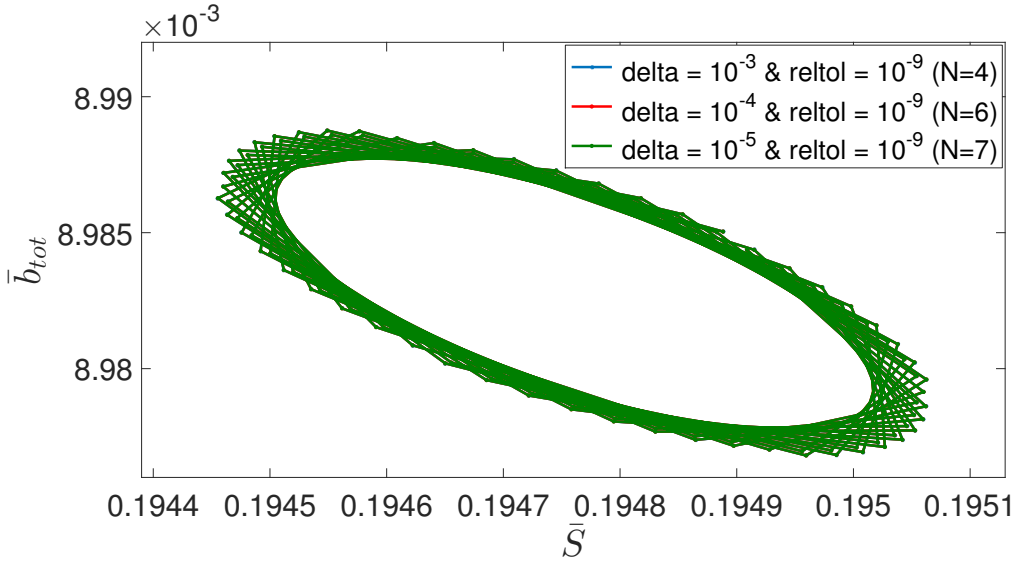

Figure 5.32: Map iteration 400 to 500 for $D = 0.00523$ min^{-1} for 3 different δ values for `reltol`$= 10^{-9}$. The 3 invariant closed curves completely overlap.

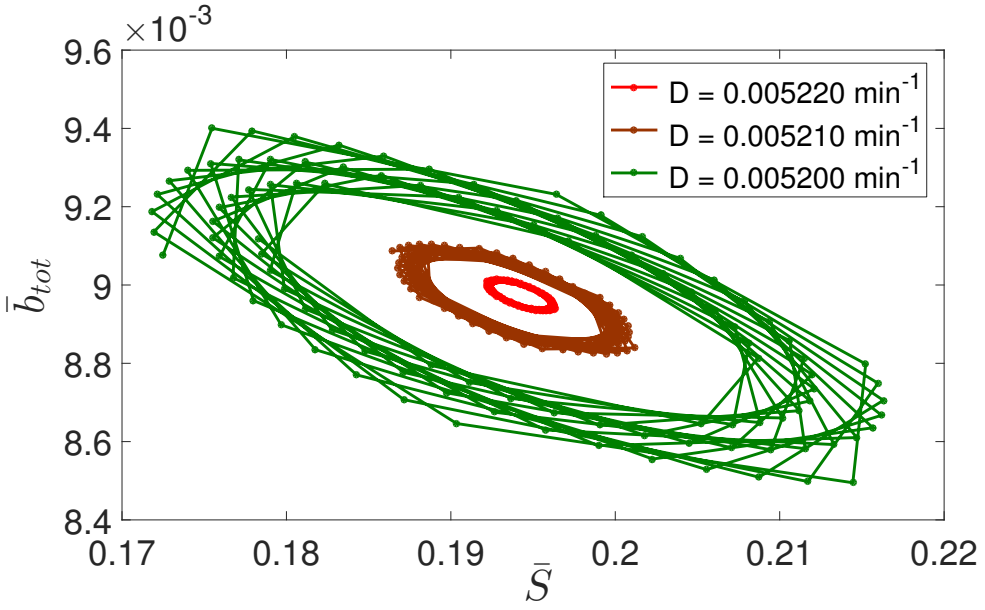

Figure 5.33: Map iteration 400 to 500 for different D values for $\delta = 10^{-3}$ and `reltol`$= 10^{-8}$ show the invariant curves beyond the supercritical Neimark-Sacker bifurcation.

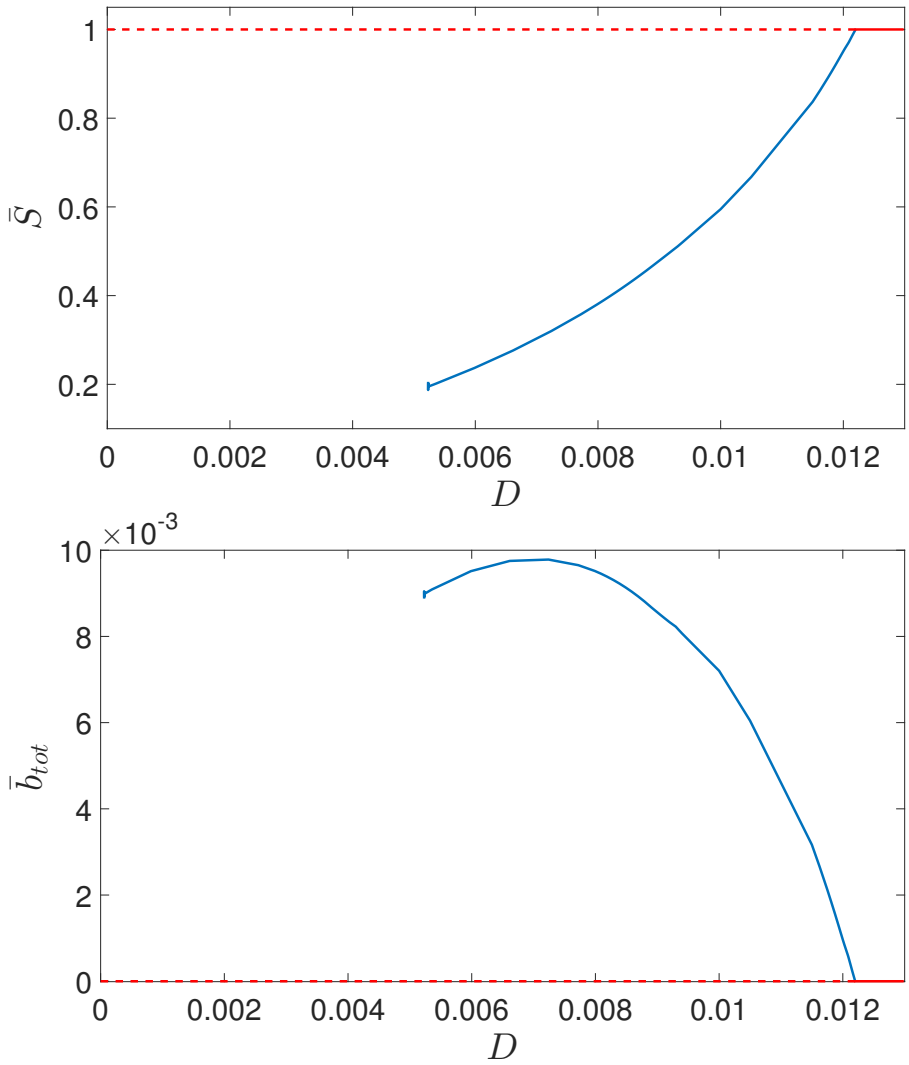

Figure 5.34: Bifurcation diagram of the fixed point of the map (4.14) for free D. The trivial fixed points are depicted in red and the non-trivial fixed points in blue.

5.7.3 Pseudo-arclength continuation

For free D, the same pseudo-arclength continuation method is used as the one for free S^0 in Section 5.6.3.

We start the continuation for increasing D from the fixed point for $D = 0.01$ min^{-1} with $FunTolerance$ and $VarTolerance$ equal to 10^{-5}. The continuation only converges for increasing D until $D = 0.010968$ min^{-1}. The norms of cor and R (see Section 5.6.3) are too large for larger D values, even when the stepsize is decreased to the minimal stepsize of 10^{-5}. For decreasing D starting from the fixed point for $D = 0.01$ min^{-1}, fixed points could only be calculated down to $D = 0.0098195$ min^{-1}. The continuation code then jumps to the fixed point for $D = 0.0099181$ min^{-1}, after which the D parameter of the calculated fixed points decreases again. At the jump the initial predicted fixed point is for a smaller value of D, but the Newton-correction is so big that the resulting fixed point has a larger D value. In Figure 5.35 the found fixed points are depicted in green.

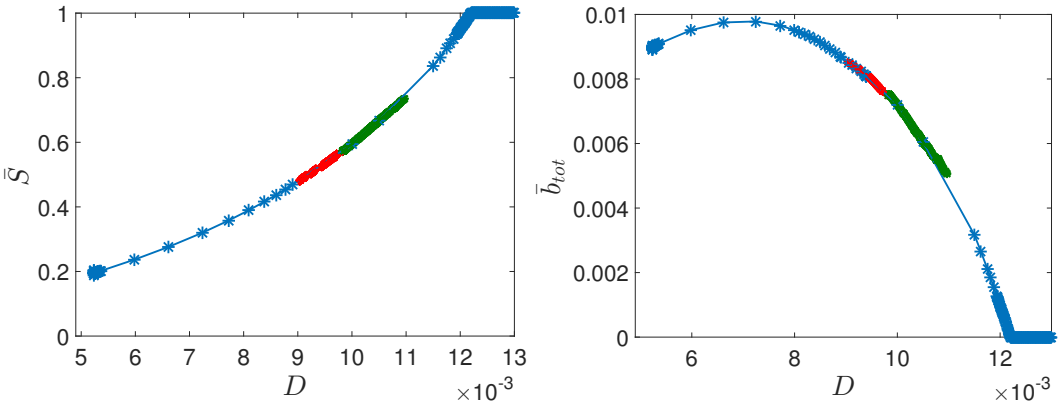

Figure 5.35: Green: fixed points obtained by the pseudo-arclength continuation method starting from $D = 0.01$ min^{-1}. Blue: fixed points obtained by the continuation method with chord prediction. Red: fixed points obtained by the pseudo-arclength continuation method with damped Newton corrections of 20% starting from $D = 0.0098195$ min^{-1}. $\bar{S}$ (left) and $\bar{b}_{tot}$ (right) are depicted as functions of D.

To improve the convergence behaviour of the pseudo-arclength continuation for decreasing D, we try damped Newton-corrections. We start from the calculated fixed point for $D = 0.0098195$ min^{-1} (where the "jump" occurred) and instead of adding cor to update the predicted fixed point, we add $\frac{cor}{5}$. We allow 100 Newton steps ($N_{max} = 100$) instead of 10. By using these damped Newton steps, fixed points were

calculated down to $D = 0.0090314$ min^{-1}. For smaller D values, the continuation no longer converges. The calculated fixed points using this method are depicted in red in Figure 5.35.

We conclude that the pseudo-arclength continuation method for free D has a smaller range of convergence than the continuation method with chord prediction in Section 5.7.2 (in blue in Figure 5.35). This is possibly due to the change in number of cohorts between the fixed points and the rough estimation of the Jacobian using finite differences.

5.7.4 Cyclic behaviour

The map also shows cyclic behaviour for some values of D. If we iterate the map starting from the birth cohort with $m = 0.301425$, $X = 0.1$, $Y = 0.5$ and $A = 0.5$ with 0.01 cells born per minute (the same birth cohort we used for the S^0 calculations) we find cycles for certain D values. The obtained results for fixed $S^0 = 1$ and with $\delta = 10^{-3}$ and `reltol`$= 10^{-6}$ are summarized in Table 5.19. To be certain that the cyclic behaviour is no numerical effect, we repeated the calculations for $D = 0.0105$ min^{-1} with a higher precision ($\delta = 10^{-6}$ and `reltol`$= 10^{-8}$) and anew found the 2-cycle, so the cylic behaviour is "real".

Table 5.19: Results of 500 map iterations starting from 0.01 cells born per minute in one birth cohort (with $m = 0.301425$, $X = 0.1$, $Y = 0.5$ and $A = 0.5$) for different D values with $\delta = 10^{-3}$ and `reltol`$= 10^{-6}$.

D (min^{-1})	**result**	**D (min^{-1})**	**result**
0.007	trivial fixed point	**0.0104**	6-cycle
0.008	trivial fixed point	**0.0105**	2-cycle
0.009	non-trivial fixed point	**0.0106**	6-cycle
0.0103	non-trivial fixed point	**0.011**	non-trivial fixed point

5.8 Yield of the chemostat for MM1

We can consider the chemostat as a machine that produces an outflow of cells. The yield of the chemostat is then proportional to $D \cdot \bar{b}_{tot}$. An interesting question is for which dilution rate D there is a maximal yield per unit of time for a fixed S^0. For $S^0 = 1$, $D \cdot \bar{b}_{tot}$ is plotted as a function of D in Figure 5.36. The optimal value of D for $S^0 = 1$ in terms of time efficiency, is approximately 0.0086 min^{-1}.

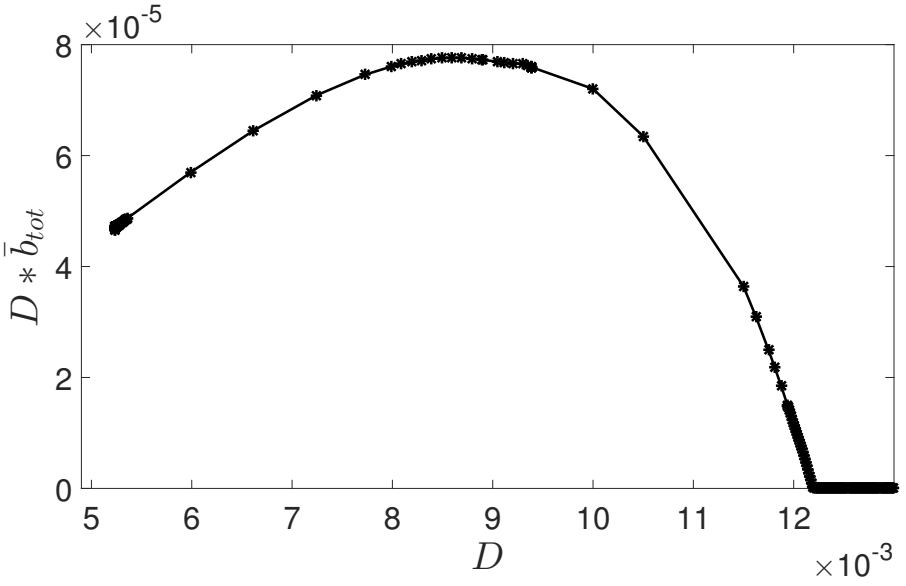

Figure 5.36: Plot of $D \cdot \bar{b}_{tot}$ (proportional to the yield of the chemostat) as a function of D for the fixed points found for $S^0 = 1$.

We could also take as the optimal value of D the one that has the highest yield relative to the amount of nutrient needed per unit of time, so for which the ratio of $D \cdot \bar{b}_{tot}$ to $S^0 \cdot D$ is maximal. Since S^0 is constant, this corresponds to the D value for which $\bar{b}_{tot}$ is maximal. So the optimal D value for $S^0 = 1$ in terms of cost efficiency, is around 0.007 min^{-1} (see Figure 5.31).

5.9 Non-trivial fixed points of MM1 for small D

We found non-trivial fixed points for decreasing D down to around $D = 0.00523$ min^{-1}. In the region of D between approximately 0.00523 and 0.00536 the non-trivial fixed points have few birth cohorts. For the used $\delta = 10^{-3}$ and `reltol`$= 10^{-6}$, the fixed point has only 4 birth cohorts. Birth cohorts 1 and 2 both contribute to birth cohorts 1 and 3 at division, birth cohorts 3 and 4 both contribute to birth cohorts 2 and 4 at division. To see the impact of a smaller δ on the representation of the fixed point, we repeat the calculations for different δ. For $\delta = 10^{-4}$ and `reltol`$= 10^{-8}$, the fixed point has 6 birth cohorts. For $\delta = 10^{-5}$ and `reltol`$= 10^{-8}$ 7 birth cohorts and for $\delta = 10^{-6}$ and `reltol`$= 10^{-8}$ 9 birth cohorts. So the number of birth cohorts to represent a fixed point for $D \approx 0.00523$ min^{-1} stays low. For a larger δ of 10^{-2} the fixed point has only 2 birth cohorts. In Figure 5.37 the cumulative mass distribution at birth is given for different representations. The representation with 2 birth cohorts already is quite accurate when compared to the ones with more birth cohorts.

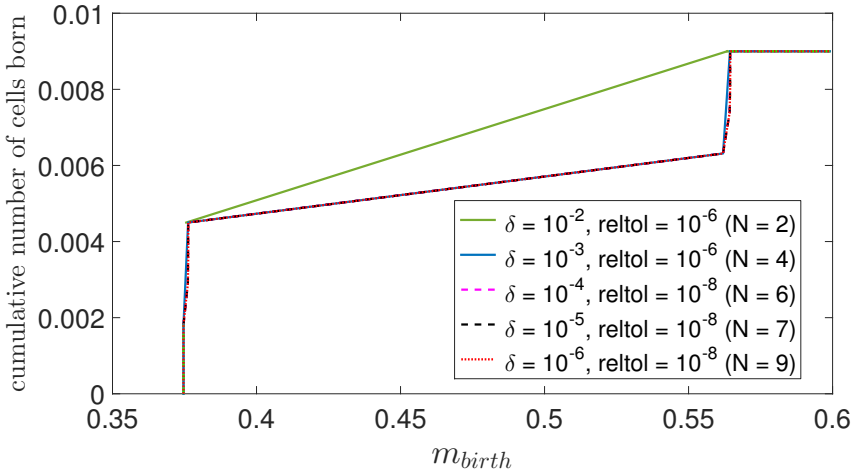

Figure 5.37: The cumulative mass distribution of the fixed point for $D = 0.00525013559$ min^{-1} for 5 different (δ,`reltol`)-combinations.

This is confirmed by investigating to which birth cohorts the dividing cells contribute that were originally born in a certain birth cohort. In Figure 5.38 the cohort-to-cohort representation of the fixed point for $D = 0.00525013559$ min^{-1} is given for 3 different (δ, `reltol`)-combinations. At the top of Figure 5.38 the cohort-to-cohort representation is given for $\delta = 10^{-2}$ and `reltol`$= 10^{-6}$ (2 birth cohorts), in the middle of Figure 5.38 it is given for $\delta = 10^{-4}$ and `reltol`$= 10^{-8}$ (6 birth cohorts),

and at the bottom in Figure 5.38 it is given for $\delta = 10^{-6}$ and `reltol`$= 10^{-8}$ (9 birth cohorts).

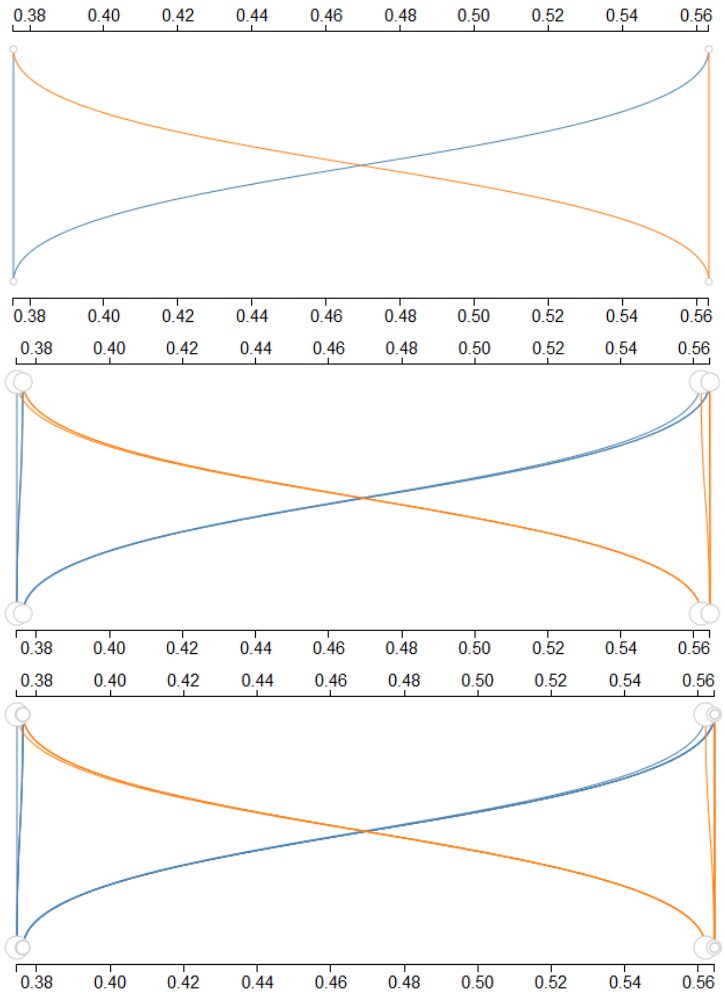

Figure 5.38: Cohort-to-cohort representation of the fixed point for $D = 0.00525013559$ min^{-1} for $\delta = 10^{-2}$ and `reltol`$= 10^{-6}$ ($N = 2$) at the top, for $\delta = 10^{-4}$ and `reltol`$= 10^{-8}$ ($N = 6$) in the middle and for $\delta = 10^{-6}$ and `reltol`$= 10^{-8}$ ($N = 9$) at the bottom. The blue (resp. orange) line indicates to which birth cohort the small (resp. large) newborn cells (originating from dividing cells that were originally born in the indicated birth cohort) contribute.

5.10 Other cell division criteria for X

So far, throughout Chapter 4, we assume that all cells divide when X is equal to a fixed X value X_{DIV}, chosen as 0.1 following Tyson and Novák [81], if the side criteria for division are satisfied (see Table 4.2). We can distinguish two classes of other options for X_{DIV}. The value of X_{DIV} for a certain cell can either be imprinted at birth or it can be established during the progression through the cell cycle (see [62]). In the latter case X_{DIV} can be dependent on external parameters such as the available nutrient level at different check points when the cell is growing. For both classes, we consider in this section an example for the adaptation of X_{DIV}.

5.10.1 X_{DIV} imprinted at birth

If the value of X_{DIV} is imprinted at birth, it can either be dependent on one or more of the i-state variables of the cell at birth, or it can be dependent on an environmental factor at the moment of birth. As an example, we assume that the birth mass determines X_{DIV} deterministically in a discrete manner.

We use a deterministic mapping from intervals of m_{birth} to a set of X_{DIV} values. From $m_{min} = 0.75$, $m_{max} = 10$ and $\phi = 0.4$, it follows that the possible masses at birth are between 0.3 and 6. Using $\{0.086, 0.087, \ldots, 0.113, 0.114\}$ for the X_{DIV} values, we define the following map:

$$
\begin{aligned}
m_{birth} \mapsto X_{DIV}: \quad & [0.3, 0.4966] && \to \quad 0.086, \\
&]0.4966, 0.6932] && \to \quad 0.087, \\
&]0.6932, 0.8898] && \to \quad 0.088, \\
& && \vdots \\
&]5.6082, 5.8048] && \to \quad 0.113, \\
&]5.8048, 6.0014] && \to \quad 0.114.
\end{aligned}
\tag{5.4}
$$

For the usual parameter values and starting from the fixed point for $S^0 = 1$ and $D = 0.01$ min^{-1} with 41 birth cohorts ($\bar{S} \approx 0.59489$ and $\bar{b}_{tot} \approx 7.720285 \cdot 10^{-3}$), the map (4.14) converges to a fixed point with 41 birth cohorts with $\bar{S} \approx 0.59516$ and $\bar{b}_{tot} \approx 7.180457 \cdot 10^{-3}$. So the use of (5.4) instead of a fixed $X_{DIV} = 0.1$ does not have a major influence on the fixed point and this is understandable since the birth

cohorts of the fixed point when $X_{DIV} = 0.1$ have m_{birth} values only between 0.30440 and 0.76827 (see Table 5.5), so X_{DIV} is either 0.086, 0.087 or 0.088. In Figure 5.39 the cumulative mass distribution of the fixed point is depicted in blue and compared with the one in purple for the fixed point when $X_{DIV} = 0.1$. The cumulative mass distributions are very similar.

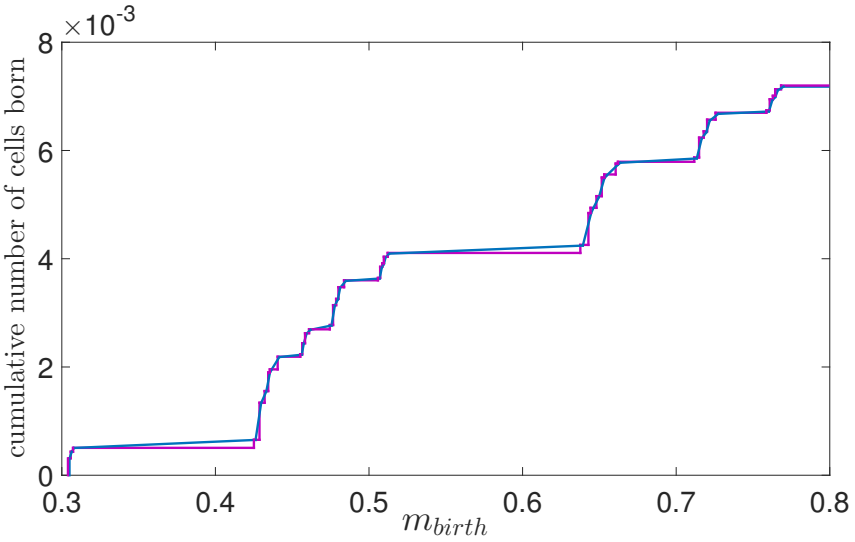

Figure 5.39: Blue: cumulative mass distribution of the fixed point when the map (5.4) is used for the determination of X_{DIV} for every cohort. Purple: distribution of the fixed point when $X_{DIV} = 0.1$ for all cells (for the same parameter values).

To get more variation in X_{DIV} for the actual range of m_{birth} values of the fixed point for $S^0 = 1$ (see Table 5.5), we use the following map:

$$
\begin{aligned}
m_{birth} \mapsto X_{DIV}: \quad & [0.3, 0.31] && \to \quad 0.08000, \\
&]0.31, 0.32] && \to \quad 0.08055, \\
&]0.32, 0.33] && \to \quad 0.08110, \\
& && \vdots \\
&]0.99, 1] && \to \quad 0.11850, \\
&]1, +\infty] && \to \quad 0.11905.
\end{aligned}
\tag{5.5}
$$

The resulting fixed point has 243 birth cohorts with $\bar{S} \approx 0.60504$ and $\bar{b}_{tot} \approx 6.7155 \cdot 10^{-3}$. The mass distribution of the resulting fixed point is quite different from the one when $X_{DIV} = 0.1$. The cumulative mass distribution is depicted in Figure 5.40

in blue, where it is compared with the fixed point when X_{DIV} is fixed to 0.1 for all cells, in purple.

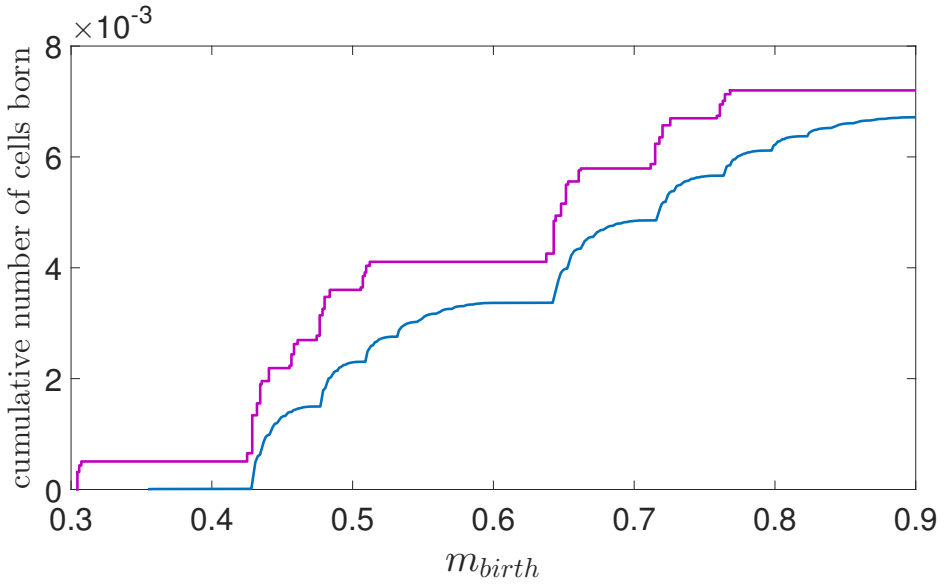

Figure 5.40: Blue: cumulative mass distribution of the fixed point when the map (5.5) is used for the determination of X_{DIV} for every cohort. Purple: distribution of the fixed point when $X_{DIV} = 0.1$ for all cells (for the same parameter values, Table 5.5).

5.10.2 X_{DIV} decided during cell cycle

As an example for the case that the value of X_{DIV} is decided during the life-time of the cell, we consider a probability density for X_{DIV} denoted by ϕ_D. This means that if we consider a large population of cells, the fraction of cells that will divide with X_{DIV} between X_1 and X_2 equals

$$\int_{X_1}^{X_2} \phi_D(x)\,\mathrm{d}x, \tag{5.6}$$

under the assumption that cells did not flow out of the bioreactor before they divide. In this example, we assume that ϕ_D is independent of the internal characteristics of the cell and the environment.

We use a normal density distribution for ϕ_D with mean 0.1. For the standard deviation

we compare two choices: a standard deviation of 0.007 resp. 0.02, such that 95% of the X_{DIV} values are expected between 0.086 and 0.114, resp. between 0.061 and 0.139. In Figure 5.41 the two corresponding ϕ_D functions are depicted.

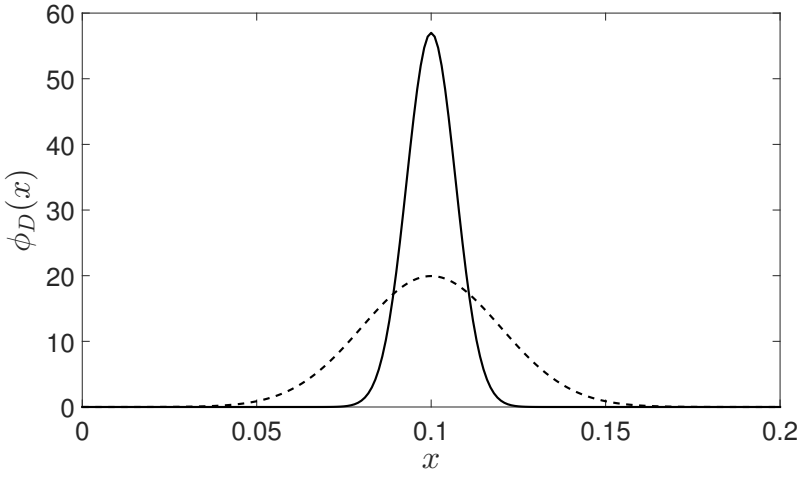

Figure 5.41: The probability density distribution for X_{DIV} as normal density distribution with mean 0.1 and standard deviation 0.007 (full line) resp. 0.02 (dashed line).

We use a discretised version of the corresponding cumulative distribution function: for x values from 0 to 0.2 with step 0.001, the corresponding

$$K(x) = \int_x^\infty \phi_D(z)\,\mathrm{d}z \tag{5.7}$$

is calculated (see Figure 5.42). The first idea to use the probability density is to check after every age integration step for every birth cohort (if the side criteria for division are fulfilled - see Table 4.2) whether the present X value will be X_{DIV} for this cohort. Whether all remaining cells in the cohort will divide at this age, is determined by generating a random number between 0 and 1. If the random number is smaller than $K(x)$ (with x the smallest value for which we calculated $K(x)$ and for which $x \geq X$), the cells in the cohort divide. The problem with generating a random number after every age integration step is that the size of the step influences the eventually used X_{DIV}. For a smaller age integration step size, the random number generator will be evoked more often to check if the cells will divide, division will happen "sooner", so X_{DIV} will be larger. To avoid this, we consider the number of times the random number generator is evoked in an age interval of size s_a as a Poisson process with parameter $\lambda_a \cdot s_a$. This means that the time (or age) between evoking the random

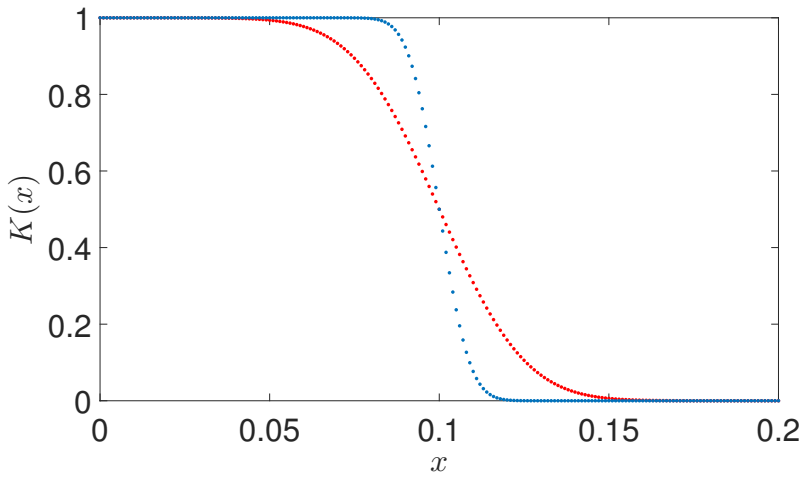

Figure 5.42: The cumulative distribution function (5.7) for ϕ_D corresponding to a normal density distribution with mean 0.1 and standard deviation 0.007 (blue) resp. 0.02 (red).

number generator is exponentially distributed with parameter λ_a. We denote the age when the random number generator is evoked as a_{rg} and determine it as a random number of an exponential distribution with parameter λ_a. During the age integration of a cohort, after each step it is checked whether the side criteria for division are satisfied. If this is the case and the current age is larger than a_{rg}, the random number generator is evoked to check if the cells will divide. When the cells do not divide at this age, a_{rg} is replaced by the sum of the current age and a random number of the exponential distribution. There are other ways to implement the use of a_{rg} which are more precise, but as an approximation we assume that the age integration steps are small enough and that it is not necessary to stop the age integration exactly at a_{rg}. Note that for this choice for X_{DIV} cells can not divide immediately after birth, as was the case when a fixed value for X_{DIV} was used.

In the calculations we use 50 as parameter value for λ_a (meaning that the average age between two consecutive uses of the random generator for division is 0.02 min) and take age integration steps with size 0.001 min. We start the map iterations from the fixed point for $S^0 = 1$ and $D = 0.01$ min^{-1} with 41 birth cohorts (see Table 5.5) for the usual parameter values. We did the calculations 20 times, 10 times using a normal density distribution with mean 0.1 and standard deviation 0.007 for ϕ_D and 10 times using the standard deviation 0.02. For both choices for ϕ_D, the map (4.14)

does not converge for the used threshold conditions (a maximum relative change in $\bar{S}$ and $\bar{b}_{tot}$ of 10^{-7} and maximum 1% variation in the number of cohorts). In Figure 5.43 the results of map iteration 200 to 300 are depicted in $(\bar{b}_{tot}, \bar{S})$-space for 4 of the 10 calculations for both choices for ϕ_D. The results of the other 6 calculations are similar for both density distributions.

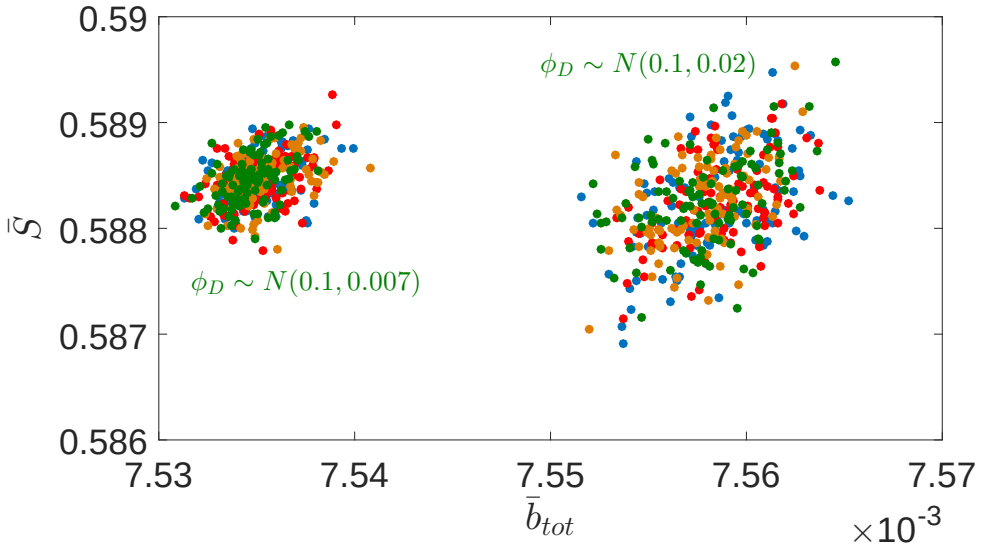

Figure 5.43: Results of map iteration 200 to 300 depicted in $(\bar{b}_{tot}, \bar{S})$-space for $\phi_D \sim N(0.1, 0.007)$ (left) and $\phi_D \sim N(0.1, 0.02)$ (right) for calculations starting from the fixed point in Table 5.5. For both density distributions the results for 4 calculations are depicted.

Although the map does not converge, the iterates stay in a bounded range of values. The number of cohorts from map iteration 200 to 300 varies between 13 and 21 for $\phi_D \sim N(0.1, 0.007)$ and between 13 and 25 for $\phi_D \sim N(0.1, 0.02)$, for the 10 performed calculations for each. We can consider the use of a probability density for X_{DIV} instead of the fixed value of X_{DIV} as a process that makes the fixed point more hazy. Comparing the results for the normal density distributions for ϕ_D results in no surprises. If the standard deviation is larger (on the right in Figure 5.43) cells have a larger chance to divide sooner, meaning for a larger X_{DIV}, resulting in more cells born per unit of time and consequently in a lower nutrient level. Note that a larger standard deviation for ϕ_D also results in a larger range of values in which the map iterates.

5.11 Budding yeast model of Tyson and Novák as internal cell cycle mechanism

We incorporate the budding yeast model of Tyson and Novák consisting of (2.1) & (2.3) as internal model for the cell cycle instead of the Toy Model (4.3). The same division conditions as in MM1 (see Table 4.2) are used with $[CycB]_T$ in the role of X. The cell cycle model parameters in Table 2.1 and the population model parameters in Table 4.3 are used. Starting with one birth cohort (with $m = 0.301425$ and $[CycB]_T = [Cdh1] = [Cdc20]_T = [Cdc20]_A = [IEP] = [CKI]_T = [SK] = [TF] = 0.1$) with 10^{-2} cells born per minute and with $\bar{S} = 1$, gives convergence to a fixed point with 8 birth cohorts with $\bar{S} \approx 0.58241$ and $\bar{b}_{tot} \approx 8.3951 \cdot 10^{-3}$. The cumulative mass distribution is depicted in Figure 5.44.

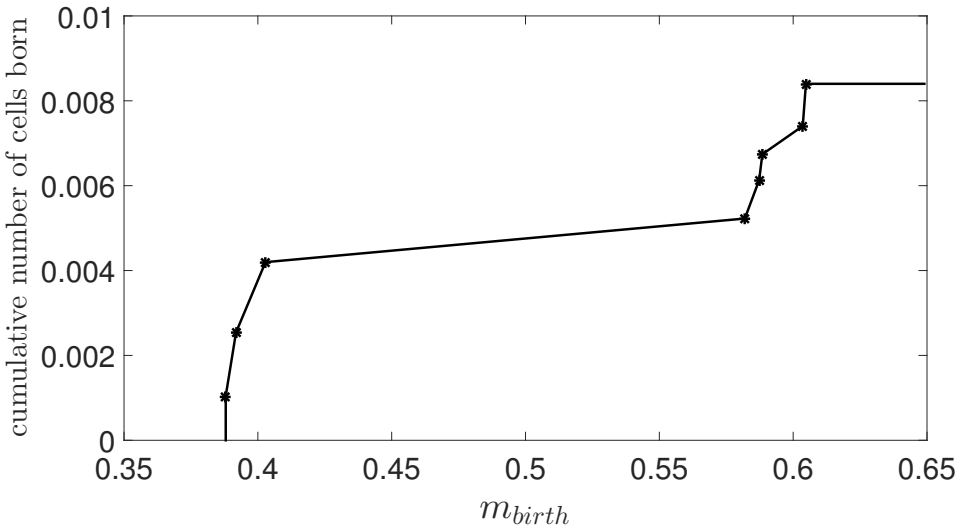

Figure 5.44: The cumulative mass distribution of the fixed point of the map for the budding yeast model of Tyson and Novák (2.1) & (2.3) as internal cell cycle model.

In Figure 5.45 the 8 birth cohorts of the fixed point are depicted with lines to indicate to which birth cohorts the cells that are originally born in a certain birth cohort contribute when they divide. The blue lines correspond with the small newborns and the orange lines with the large newborns. The 3 smaller birth cohorts with $m_{birth} \approx 0.39 - 0.4$ behave differently from the 5 larger birth cohorts with $m_{birth} \approx 0.58 - 0.6$. The latter ones divide into smaller newborns than the first ones, which may be counterintuitive, but actually can be understood easily.

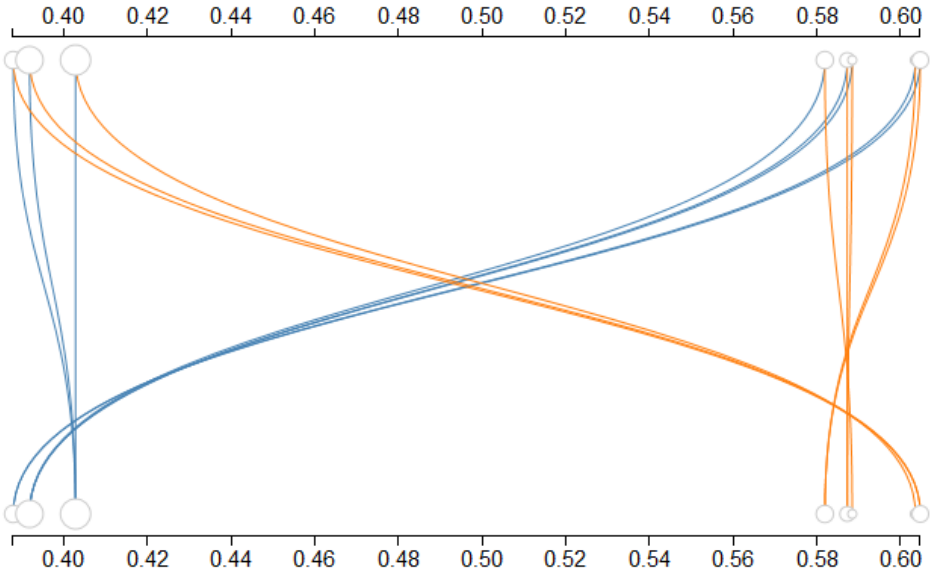

Figure 5.45: Cohort-to-cohort representation of the fixed point of the map for the budding yeast model of Tyson and Novák (2.1) & (2.3) as internal cell cycle model ($N = 8$). The blue (resp. orange) line indicates to which birth cohort the small (resp. large) newborn cells (originating from dividing cells that were originally born in the indicated birth cohort) contribute.

Cells can only divide when their mass is larger than $m_{min} = 0.75$, $[CycB]_T$ is decreasing and equal to 0.1. All the birth cohorts have $m_{birth} < m_{min}$, so none of the cells can divide immediately after birth. The cells in the birth cohorts differ in the evolution of $[CycB]_T$ during their life-time (from birth until division). In Figure 5.46 $[CycB]_T$ is depicted as a function of m for the 8 different birth cohorts. The difference in m_{birth} is not the only factor that decides the different behaviour of the smaller and larger cells. The interaction with the other chemical concentrations also influences the different shapes of the $[CycB]_T$-curves. As a result, the smaller newborns grow to a larger mass before they divide than the larger newborns do. Note that for the fixed point in Table 5.5 for the Toy Model as internal cell cycle structure, we observed similar cohort-to-cohort behaviour (see Figure 5.5), but there the reason was that $m_{birth} > m_{min}$ for the largest birth cohorts. In the budding yeast model of Tyson and Novák, we get a slightly more complex behaviour.

If we iterate the map with the same initial birth cohort as before (with $m = 0.301425$

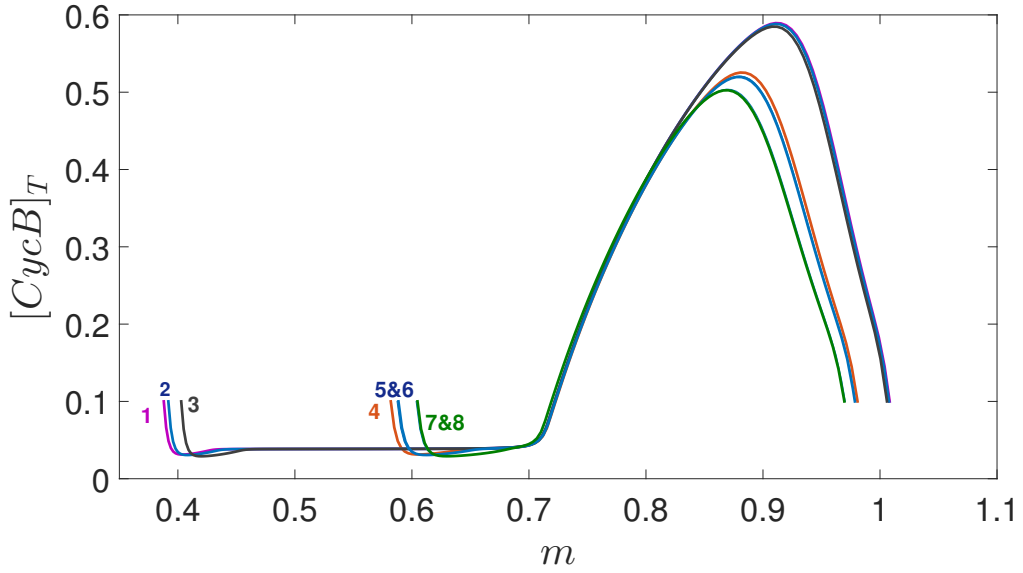

Figure 5.46: The evolution of $[CycB]_T$ as a function of the mass m of the cells in the 8 cohorts of the fixed point during their life-time (from birth to division).

and $[CycB]_T = [Cdh1] = [Cdc20]_T = [Cdc20]_A = [IEP] = [CKI]_T = [SK] = [TF] = 0.1$) with 10^{-2} cells born per minute and with $\bar{S} = 1$, but with a different D values instead of the original value of 0.01 (the other parameters are in Tables 2.1 and 4.3), the map converges to other fixed points. The results are summarized in Table 5.20 and the corresponding cumulative mass distributions of the fixed points for $D = 0.009$ min^{-1}, $D = 0.01$ min^{-1} (the fixed point of Figure 5.44), $D = 0.011$ min^{-1} and $D = 0.012$ min^{-1} are depicted in Figure 5.47. In Figure 5.48 the mass location of the birth cohorts of the fixed point for the different D values are depicted in blue for the calculation with $\delta = 10^{-3}$ and `reltol`$= 10^{-6}$. For $D = 0.01$ min^{-1}, we also calculated the fixed point with $\delta = 2 \cdot 10^{-3}$ and `reltol`$= 10^{-6}$ which resulted in the same fixed point but with 6 birth cohorts (illustrated in red in Figure 5.48). For this larger value of δ the original birth cohorts 5 and 6, and birth cohorts 7 and 8 of Figure 5.46 are merged. Note however, that the mass distributions with 6 birth cohorts for $D = 0.009$, $D = 0.01$ and $D = 0.011$ are quite different, as is clear in Figure 5.47. This means that the fixed points for the different D values are not only different in $\bar{S}$ and $\bar{b}_{tot}$, but that also the internal structure of the birth cohorts differs. For the fixed points of the population model with the Toy model as internal structure, this was not the case for free S^0 (Section 5.6), but it was for free D (Section 5.7).

Table 5.20: Convergence of the map with the Budding yeast model of Tyson and Novák (2.1)&(2.3) as internal structure, starting from 0.01 cells born per minute in one birth cohort (with $m = 0.301425$ and $[CycB]_T = [Cdh1] = [Cdc20]_T = [Cdc20]_A = [IEP] = [CKI]_T = [SK] = [TF] = 0.1$) with $\bar{S} = 1$ for different D values.

D ($\mathbf{min^{-1}}$)	**result**	**N**	$\bar{\mathbf{S}}$	$\bar{\mathbf{b}}_{\mathbf{tot}}$
0.0080	trivial fixed point	0	1.00000	0.0000000
0.0090	non-trivial fixed point	6	0.46743	0.0099433
0.0095	non-trivial fixed point	6	0.52166	0.0092766
0.0100	non-trivial fixed point	8	0.58241	0.0083951
0.0110	non-trivial fixed point	6	0.72906	0.0058156
0.0120	non-trivial fixed point	19	0.92379	0.0017279

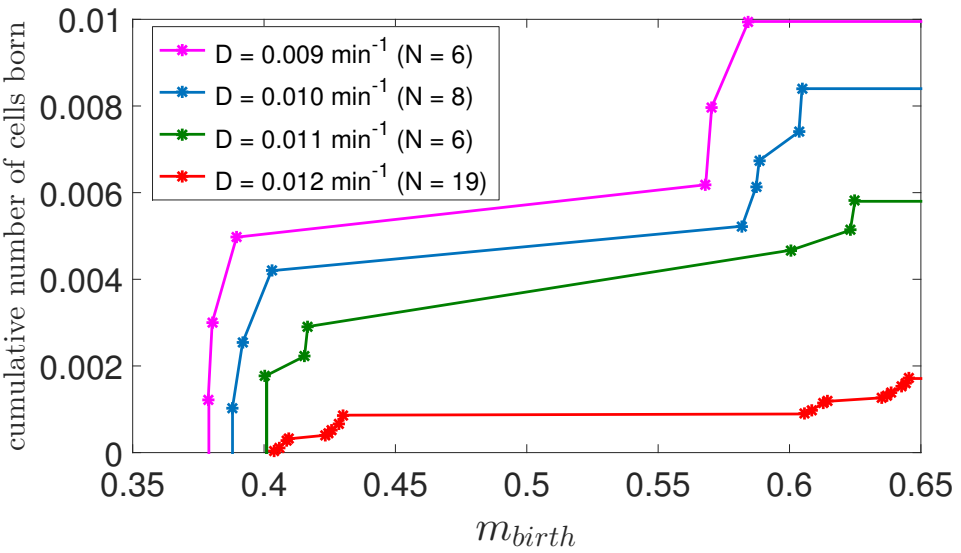

Figure 5.47: The cumulative mass distribution of the fixed point of the map for the budding yeast model of Tyson and Novák (2.1) & (2.3) as internal cell cycle model for different values of D.

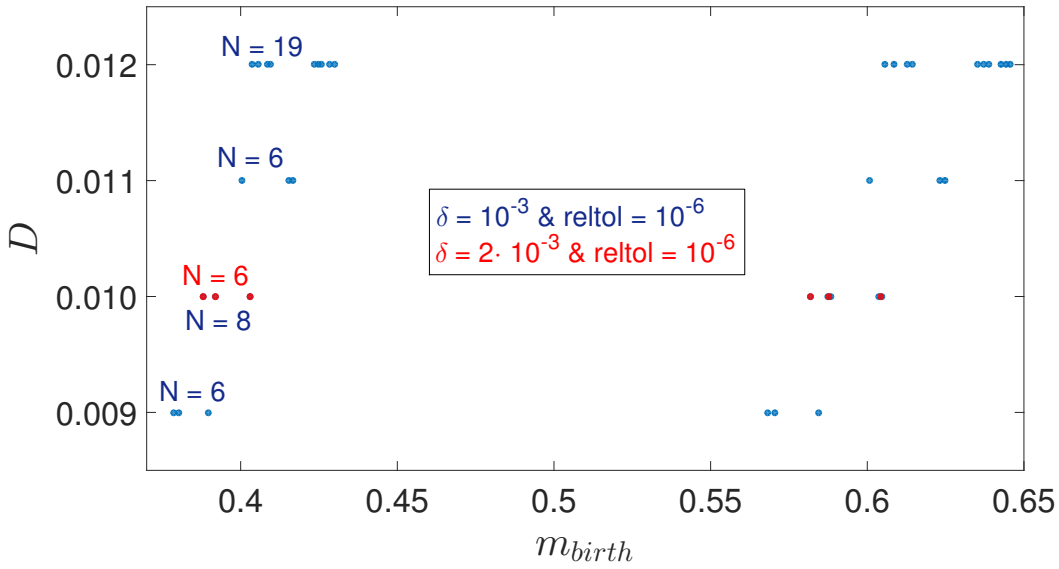

Figure 5.48: m_{birth} of the cohorts of the fixed point of the map with the budding yeast model (2.1) and (2.3) as internal cell cycle model, for D equal to 0.009, 0.01, 0.011 and 0.012 min^{-1}. In blue m_{birth} when the fixed point is calculated with $\delta = 10^{-3}$ and `reltol`$= 10^{-6}$. In red m_{birth} for the fixed point for $D = 0.01$ min^{-1} calculated with $\delta = 2 \cdot 10^{-3}$ and `reltol`$= 10^{-6}$.

CHAPTER 6

Implementation

The project source code can be downloaded at
`https://github.com/charlottesonck/StruPoMoCC`.

Overview

The code for the study of our structured population models is written in `C++` using `Microsoft Visual C++ 2010 Express`. In Section 6.1, we document how to get the code operating with `Microsoft Visual C++ 2010 Express` and which external libraries we use. An overview of the data structures, functions and global constants is given in Section 6.2. In Section 6.3 we show how to use these functions for some of the calculations in Chapter 5.

6.1 Used program and libraries

The files "StruPoMoCC_TM.cpp" and "StruPoMoCC_BY.cpp" (with resp. the Toy model and the budding yeast model as internal structure model) for the study of our structured population models is written in `C++` using the integrated development environment `Microsoft Visual C++ 2010 Express` on Windows. We use the CVODE-solver of the SUNDIALS library and the ALGLIB library. SUNDIALS (SUite of Nonlinear and DIfferential/ALgebraic equation Solvers, see [45, 46]) is

a suite of advanced computational methods for solving large-scale problems that can be modeled as a system of nonlinear algebraic equations, or as initial-value problems in ordinary differential or differential-algebraic equations. The CVODE-solver of this library can be used to solve ODE initial value problems. We use this to solve the system of equations (4.8)-(4.13). ALGLIB (`www.alglib.net`, Sergey Bochkanov) is a cross-platform open source numerical analysis and data processing library. We use the following facilities for linear algebra of ALGLIB: vectors, matrices and the solver for $A * x = b$ (with A a real matrix and b a vector).

The following should be done stepwise to get the code working in `Microsoft Visual C++ 2010 Express` (after downloading the SUNDIALS and ALGLIB packages):

1. Open a new project of the type "Win32 Console Application" and choose a name. The Win32 Application wizard opens automatically. The application type is "Console Application", tick the box "Empty project".

2. Add one of the source code files by right-clicking on the created project and choosing "Add > Existing Item".

3. Right-click on the created project and choose "Properties". Select "Configuration Properties > C/C++" and add to "Additional Include Directories" the files needed for the SUNDIALS and ALGLIB libraries. These are normally located at

   - cygwin64\home\<username>\sundials-2.4.0-install\include,
   - cygwin64\home\<username>\src alglib.

4. Right-click on "Source files" and select "Add > Existing Item...". The files of the SUNDIALS library "sundials_cvode.lib" and "sundials_nvecserial.lib" (these are normally located at cygwin64\home\<username>\sundials-2.4.0-install\lib) and the files of the ALGLIB library "alglibinternal.cpp", "alglibmisc .cpp", "ap.cpp", "dataanalysis.cpp", "diffequations.cpp", "fasttransforms .cpp", "integration.cpp", "interpolation.cpp", "linalg.cpp", "optimization.cpp", "solvers .cpp", "specialfunctions.cpp" and "statistics.cpp" (these are normally located at alglib\cpp\src) should be added.

5. Right-click on the created project, choose “Properties” and select “Linker”. Set “Enable Incremental Linking” to “No” and add the library of the SUNDIALS package (normally located at cygwin64\home\<username>\-sundials-2.4.0-install\lib) to “Additional Library Directories”.

To build the executable file for the project, right-click on the project and first select “Clean” and then “Build”. The executable file can then be executed in a directory of your choice. The output text files will be created in this directory. In Section 6.3 we will show examples of how the different functions in the project are used for the calculations in Chapter 5.

6.2 Overview of the data structures, functions and global constants

We focus in this section on the source file “StruPoMoCC_TM.cpp”. The structured population model with the budding yeast model of Tyson and Novák as internal cell structure (see Section 5.11) is implemented in a similar way in the file “StruPoMoCC_BY.cpp”.

In the project source code we frequently use the data-type “realtype”, which is defined as the data-type double in the SUNDIALS package.

The parameters in Tables 3.2, 4.1 and 4.3 are defined as constants in our program and can easily be adjusted. In Table 6.1 the remaining constants used in the implementation that may be of use to other users are listed.

Central in our code is the class `cohort` which represents the birth cohorts. An object of the class corresponds to a certain birth cohort and contains a vector `init` of dimension `NDIM`, a double `F`, a double `theta` and a double `b`. `NDIM` is the dimension of the chemical submodel for the cell cyle, so for the Toy model (4.3) `NDIM` equals 4 and `init` is (m,X,Y,A). `F` represents the survival probability of the cells in the cohort and is initally 1, `theta` represents the consumption by a cell of this cohort and is initially 0 and `b` is the initial number of cells born per minute in this cohort. A list of objects of the type cohort is defined as `clist` and the iterator of such a list as `clistit`. The class `cohort` contains several public functions: ini-

Table 6.1: Defined constants in the program, besides the ones in Tables 3.2, 4.1 and 4.3.

name	value	meaning
cond_min	0 or 1	0: condition of minimal mass is not used (NMM model) 1: condition of minimal mass is used (MM models)
cond_max	0 or 1	0: m_{max} in $\frac{dm}{dt}$ (MM1 model) 1: cells can only divide when $m \leq m_{max}$ (MM2 model)
cond_div	0 or 1	0: constant X_{DIV} 1: discrete values for X_{DIV} dependent on m_{birth} (see §5.10.1)
cond_div2	0 or 1	0: constant X_{DIV} 1: probability distribution for X_{DIV} (see §5.10.2)
NDIM	4	dimension of the cell cycle model
T0	0.0	initial age for the age integration of (4.8)-(4.13) in minutes
T1	0.5	first age output in minutes
RELTOL	10^{-6}	scalar relative tolerance of the CVODE solver
ABSTOL	10^{-8}	scalar absolute tolerance of the CVODE solver
NEQ	6	number of equations (4.8)-(4.13)
TIN	0.5	age step for the age integration of (4.8)-(4.13) in minutes
eps_m	10^{-7}	stop age integration when $m > m_{max}(1 - eps_m)$
var_N	0.01	relative amount of variation allowed in the number of cohorts at convergence, N has to change less than $var_N \cdot N$ from one iteration to the next to have convergence to a fixed point

tializers `set_init`, `setb`, `setm` and `setTheta`, functions that return an internal value `getb`, `getTheta`, `getMass`, `getX`, `getY`, `getA` and `getF`, functions that print the internal state of the cohort to an external file `PrintOutput` and `PrintOutputData`, and a function that handles CVODE errors `check_flag`. An important function for objects of the class is `integrate_cohort`: the equations (4.8)-(4.13) are integrated over age using the CVODE solver until the survival probability becomes smaller than $\varepsilon_{\mathcal{F}}$. If the cells in the cohort divide, the newborns are added to a new list of cohorts `cohnew`. After each age integration step, we check if cells divided during this step (due to the rate of reproduction `beta`) and whether the conditions are fulfilled that say that all the remaining cells in the cohort should divide. For the considered cell division criteria in §4.2.2 and §5.10, the function `beta` is zero and all the cells in the cohort divide at the same age.

The following functions are used in `cohort::integrate_cohort`:

- `merge_2Coh`: merges 2 cohorts in the list of cohorts `cohnew` at given locations by using weighted means for the values of m, X, Y and A,
- `merge_Coh`: merges $cell_b$ cells (with given m, X, Y and A) with the cohort at the given location in the list `cohnew` by using weighted means for the values of m, X, Y and A,
- `addcohort` (and subroutine `addcohort_sub`): adds the daughter cells of a given amount of dividing cells (with given m, X, Y and A) to a list of cohorts `cohnew`. Whether the two resulting daughter cohorts are simply added to `cohnew`, or if they are merged with existing cohorts depends on the δ parameter (see Section 4.5: if the distance in mass to an existing cohort $\geq \delta$, a new cohort is added, if not the daughter cohort is merged with an existing cohort).

The function `integrate_allcohorts` represents the map (4.14): a loop is made over a given list of cohorts and the function `integrate_cohort` is used to determine the new list of birth cohorts with all the cells born from the original birth cohorts. The nutrient level is adapted according to (4.14).

The functions `cohort::integrate_cohort_dest`, `addcohort_dest_sub`, `addcohort_dest` and `integrate_allcohorts_dest` are variants of the above mentioned functions with the extra functionality to print the file "data_figd3_fp.txt". "data_figd3_fp.txt" contains the information needed to make a cohort-to-cohort representation (see e.g. Figure 5.5), namely for every cohort of the initial list of cohorts a line with the birth mass, the mass of the cohort of the small daughter cells, the mass of the cohort of the large daughter cells and the number of cells originally in the cohort.

The function `cohort::integrate_cohort_bis` is an adapted form of `cohort:: integrate_cohort`, that is used in `integrate_allcohorts` when a probability distribution for X_{DIV} is used (see §5.10.2) instead of the fixed value X_{DIV}, so when `cond_div2` equals 1.

The function `loopMap` iterates the map (4.14) a given fixed number of times and the

function `loopMap_C` iterates the map until convergence to a fixed point (according to the given convergence parameters for $\bar{S}$ and $\bar{b}_{tot}$, and the value of `var_N`) or until the given maximum number of iterations is reached.

The continuation method with zero-order prediction is implemented in the functions `contfpS0_simple` and `contfpD_simple` and the continuation method with chord prediction is implemented in `contfpS0_2fp` and `contfpD_2fp`. For the adapted form of pseudo-arclength continuation several functions have to be implemented:

- `mapM_B`: maps a list of cohorts `coh_new` to another list of cohorts `coh_or`, see (5.3),
- `mapM_1`: integrates a given list of cohorts and maps the new list of cohorts `cohnew` back to the original list using `mapM_B`,
- `normalize`: normalizes a given vector,
- `signdotproduct`: calculates an approximation of the dotproduct of 2 given vectors that have a different dimension (with each a given corresponding mass distribution) and returns the sign of the dotproduct,
- `JacobianGS0` resp. `JacobianD`: calculates an approximation of the Jacobian of the map G (5.2) with parameter S^0 resp. D.

The pseudo-arclength continuation is implemented in the functions `contfpS0` and `contfpD` and the version with damped Newton-corrections for free D is implemented in `contfpD_demp`.

6.3 Examples

For the MM1-calculations in §5.1.2 corresponding to Table 5.3, the following code is used in the main function.

```
myfile_OC.precision(10);
myfile_OC.open("outputcohorts.txt", ios::app);
clist coh;
cohort a;
realtype delta_m;
int N = 100;
```

```
if(cond_min==1)
  delta_m = RCONST(((1-phi)*m_max-phi*m_min)/N);
else
  delta_m = RCONST(((1-phi)*m_max)/N);
for(int i=1; i<=N; i++){
  if(cond_min==1)
    a.set_init(phi*m_min+(i-0.5)*delta_m,0.1,0.5,0.5,0.0000001);
  else
    a.set_init((i-0.5)*delta_m,0.1,0.5,0.5,0.0000001);
  coh.push_back(a);
}
loopMap(1.0,coh,300,1,0);
myfile_OC.close();
return 0;
```

The calculations start with $\bar{S} = 1$ and 10^{-7} cells born per minute in every of the 100 birth cohorts (with the initial m through uniform meshing, $X = 0.1$, $Y = A = 0.5$). For the MM1 model, `cond_min` has to be set to 1 and `cond_max`, `cond_div` and `cond_div2` to 0 (see Table 6.1). The file outputcohorts.txt contains detailed information about the 300 map iterations (if `loopMap(1.0,coh,300,0,0)` is used, this file will not be printed and the calculations will be a lot faster). The essential output files NSb.txt (with for every map iteration a line with the number of the iteration, N, $\bar{S}$ and $\bar{b}_{tot}$) and data.txt (with for every map iteration a line with the number of the iteration, N, $\bar{S}$, m_{01}, X_{01}, Y_{01}, A_{01}, $\bar{b}(x_{01})$,..., $\bar{b}(x_{0N})$, $\bar{b}_{tot}$) are always printed.

For the MM2-calculations in §5.1.2 corresponding to Table 5.6, the following code is used in the main function.

```
myfile_OC.precision(10);
myfile_OC.open("outputcohorts.txt", ios::app);
clist coh;
cohort a;
a.set_init(0.301425,0.1,0.5,0.5,0.01);
coh.push_back(a);
loopMap(1.0,coh,300,1,0);
myfile_OC.close();
return 0;
```

300 map iterations are performed starting with $\bar{S} = 1$ and one birth cohort (with $m = 0.301425$, $X = 0.1$, $Y = A = 0.5$) with 10^{-2} cells born per minute. For the MM2 model, `cond_min` and `cond_max` have to be set to 1 and `cond_div` and `cond_div2` to 0 (see Table 6.1).

For the study in §5.2.2 of the optimal (δ,`reltol`)-combination for the MM1 calculations, the following code is used for several values of δ and `reltol`.

```
clist coh;
cohort a;
a.set_init(0.301425,0.1,0.5,0.5,0.01);
coh.push_back(a);
int k = 500;
loopMap_C(1.0,coh,k,1.0e-7,1.0e-7,0,0);
loopMap(S,coh,20,0,0);
return 0;
```

The map for the MM1 model is iterated until convergence starting with one birth cohort (with $m = 0.301425$, $X = 0.1$, $Y = A = 0.5$) with 10^{-2} cells born per minute and with $\bar{S} = 1$. The parameter values used for the convergence of the map are a maximum relative change in $\bar{S}$ of 10^{-7}, a maximum relative change in $\bar{b}_{tot}$ of 10^{-7} and maximally 1% change in the number of cohorts (see the parameter `var_N` in Table 6.1). The map is iterated maximally 500 times. The list of birth cohorts resp. $\bar{S}$ of the fixed point (or of the 500th iterate of the map) is saved in `coh` resp. `S`. Finally, 20 map iterations are performed on the fixed point for the calculations in Table 5.8.

In Section 5.3 the convergence behaviour of the MM1 model is investigated for several S^0 values. A script has been used to generate the code that initializes the list of cohorts given a matrix with the internal state of the birth cohorts. In Table 5.12 the iterations are started in the fixed point for $S^0 = 1$, for which the following code is used (in this example for $S^0 = 1.05$).

```
clist coh;
cohort a;
a.set_init(0.3044004766,0.1,0.9769631555,1.072220671,0.0003138114937);
coh.push_back(a);
a.set_init(0.3057837264,0.1,0.9769497247,1.07704208,0.0001208391583);
coh.push_back(a);
a.set_init(0.3073064296,0.1,0.9769325896,1.08234719,7.112009176e-005);
coh.push_back(a);
a.set_init(0.4250644928,0.1,0.9775276242,0.8984629322,0.0001488541793);
coh.push_back(a);
a.set_init(0.4286958898,0.1,0.9775023404,0.9062543329,0.0006845618739);
coh.push_back(a);
a.set_init(0.4320463997,0.1,0.9774791933,0.9134270349,0.0002157023706);
coh.push_back(a);
a.set_init(0.4343662815,0.1,0.977462481,0.9183861224,0.0003442251617);
coh.push_back(a);
```

```
a.set_init(0.4354251459,0.1,0.9774559972,0.9206472598,5.665502588e-005);
coh.push_back(a);
a.set_init(0.4405340308,0.1,0.9774216033,0.9315388304,0.0002340840061);
coh.push_back(a);
a.set_init(0.4552265075,0.1,0.9769742554,1.069027251,4.42882791e-005);
coh.push_back(a);
a.set_init(0.4565316306,0.1,0.976963315,1.072060504,0.0002047192669);
coh.push_back(a);
a.set_init(0.4583553196,0.1,0.9769515892,1.0762975,0.000185643106);
coh.push_back(a);
a.set_init(0.4609596444,0.1,0.9769325896,1.08234719,7.112009176e-005);
coh.push_back(a);
a.set_init(0.4744779688,0.1,0.9771846638,1.003328904,7.952826643e-005);
coh.push_back(a);
a.set_init(0.4766091003,0.1,0.9771697877,1.007810603,0.0003670901832);
coh.push_back(a);
a.set_init(0.4786014284,0.1,0.9771560318,1.011998527,0.0001160507743);
coh.push_back(a);
a.set_init(0.4800871529,0.1,0.9771480129,1.015120784,0.0002161904031);
coh.push_back(a);
a.set_init(0.4837635483,0.1,0.9771211065,1.022841042,0.0001269435127);
coh.push_back(a);
a.set_init(0.5058069794,0.1,0.9769735924,1.069025931,4.428829564e-005);
coh.push_back(a);
a.set_init(0.50725779,0.1,0.9769642709,1.072060118,0.0002047190374);
coh.push_back(a);
a.set_init(0.5086201154,0.1,0.9769563347,1.074909705,6.4803954e-005);
coh.push_back(a);
a.set_init(0.5096394629,0.1,0.9769484618,1.077039751,0.000120839163);
coh.push_back(a);
a.set_init(0.5121772113,0.1,0.9769312298,1.082347296,7.112011323e-005);
coh.push_back(a);
a.set_init(0.6375967392,0.1,0.9775276242,0.8984629322,0.0001488541793);
coh.push_back(a);
a.set_init(0.6428520507,0.1,0.977503245,0.9059803063,0.000587746251);
coh.push_back(a);
a.set_init(0.6442081133,0.1,0.977496849,0.9079178877,9.681562286e-005);
coh.push_back(a);
a.set_init(0.6480695996,0.1,0.9774791933,0.9134270349,0.0002157023706);
coh.push_back(a);
a.set_init(0.6515494222,0.1,0.977462481,0.9183861224,0.0003442251617);
coh.push_back(a);
a.set_init(0.6531377189,0.1,0.9774559972,0.9206472598,5.665502588e-005);
coh.push_back(a);
a.set_init(0.660592541,0.1,0.9774226281,0.9312429381,0.0002010067121);
coh.push_back(a);
a.set_init(0.6620681069,0.1,0.9774153752,0.9333369322,3.30772941e-005);
coh.push_back(a);
a.set_init(0.7117169532,0.1,0.9771846638,1.003328904,7.952826643e-005);
coh.push_back(a);
a.set_init(0.7149136504,0.1,0.9771697877,1.007810603,0.0003670901832);
coh.push_back(a);
```

```
a.set_init(0.7179021425,0.1,0.9771560318,1.011998527,0.0001160507743);
coh.push_back(a);
a.set_init(0.7201307294,0.1,0.9771480129,1.015120784,0.0002161904031);
coh.push_back(a);
a.set_init(0.7256453225,0.1,0.9771211065,1.022841042,0.0001269435127);
coh.push_back(a);
a.set_init(0.7587104691,0.1,0.9769735924,1.069025931,4.428829564e-005);
coh.push_back(a);
a.set_init(0.760886685,0.1,0.9769642709,1.072060118,0.0002047190374);
coh.push_back(a);
a.set_init(0.7629301732,0.1,0.9769563347,1.074909705,6.4803954e-005);
coh.push_back(a);
a.set_init(0.7644591943,0.1,0.9769484618,1.077039751,0.000120839163);
coh.push_back(a);
a.set_init(0.768265817,0.1,0.9769312298,1.082347296,7.112011323e-005);
coh.push_back(a);
S0 = 1.05;
loopMap(0.5948912593,coh,300,0,0);
return 0;
```


The following code is needed for the study in §5.4.1 for the first line in Table 5.14.

```
clist coh;
cohort a;
a.set_init(0.3044007484,0.1,0.9769638973,1.07222145,0.0006885016454);
coh.push_back(a);
a.set_init(0.3057842286,0.1,0.9769494558,1.077043997,0.0002651206152);
coh.push_back(a);
a.set_init(0.3073061661,0.1,0.9769345571,1.08234672,0.000156037579);
coh.push_back(a);
a.set_init(0.4250639351,0.1,0.9775263381,0.8984616107,0.0003265861596);
coh.push_back(a);
a.set_init(0.4286962347,0.1,0.9775018487,0.9062546461,0.001501927306);
coh.push_back(a);
a.set_init(0.4320465394,0.1,0.9774804255,0.9134273307,0.0004732505802);
coh.push_back(a);
a.set_init(0.4343669038,0.1,0.9774638031,0.9183867905,0.000755228691);
coh.push_back(a);
a.set_init(0.435425529,0.1,0.9774555805,0.9206485442,0.0001243009978);
coh.push_back(a);
a.set_init(0.4405340919,0.1,0.9774213065,0.9315386903,0.0005135800314);
coh.push_back(a);
a.set_init(0.4552264415,0.1,0.9769741552,1.069027039,9.716851262e-005);
coh.push_back(a);
a.set_init(0.4565322032,0.1,0.976964251,1.072061413,0.0004491533207);
coh.push_back(a);
a.set_init(0.4583558834,0.1,0.9769516598,1.076299113,0.0004073004273);
coh.push_back(a);
a.set_init(0.4609592492,0.1,0.9769345571,1.08234672,0.000156037579);
```

```
coh.push_back(a);
a.set_init(0.4744777563,0.1,0.9771841647,1.003329022,0.0001744851133);
coh.push_back(a);
a.set_init(0.4766086101,0.1,0.9771693239,1.007810782,0.0008053967381);
coh.push_back(a);
a.set_init(0.4786017506,0.1,0.9771582023,1.012000516,0.0002546151519);
coh.push_back(a);
a.set_init(0.4800870419,0.1,0.9771465694,1.015118949,0.0004743217566);
coh.push_back(a);
a.set_init(0.4837633357,0.1,0.9771209927,1.022840419,0.0002785141297);
coh.push_back(a);
a.set_init(0.5058073302,0.1,0.9769730116,1.069026805,9.716845824e-005);
coh.push_back(a);
a.set_init(0.5072578965,0.1,0.97696314,1.072060989,0.0004491533868);
coh.push_back(a);
a.set_init(0.5086205254,0.1,0.9769555819,1.07490901,0.0001421797224);
coh.push_back(a);
a.set_init(0.5096398312,0.1,0.9769549153,1.077041917,0.0002651208566);
coh.push_back(a);
a.set_init(0.5121769234,0.1,0.9769346704,1.082346736,0.0001560376062);
coh.push_back(a);
a.set_init(0.6375959027,0.1,0.9775263381,0.8984616107,0.0003265861596);
coh.push_back(a);
a.set_init(0.6428529304,0.1,0.977502638,0.9059811281,0.001289513299);
coh.push_back(a);
a.set_init(0.6442064263,0.1,0.9774970575,0.907915107,0.0002124140065);
coh.push_back(a);
a.set_init(0.6480698091,0.1,0.9774804255,0.9134273307,0.0004732505802);
coh.push_back(a);
a.set_init(0.6515503557,0.1,0.9774638031,0.9183867905,0.000755228691);
coh.push_back(a);
a.set_init(0.6531382936,0.1,0.9774555805,0.9206485442,0.0001243009978);
coh.push_back(a);
a.set_init(0.6605928588,0.1,0.9774221166,0.9312428732,0.0004410083308);
coh.push_back(a);
a.set_init(0.6620668208,0.1,0.9774163835,0.9333363305,7.257170063e-005);
coh.push_back(a);
a.set_init(0.7117166345,0.1,0.9771841647,1.003329022,0.0001744851133);
coh.push_back(a);
a.set_init(0.7149129152,0.1,0.9771693239,1.007810782,0.0008053967381);
coh.push_back(a);
a.set_init(0.7179026259,0.1,0.9771582023,1.012000516,0.0002546151519);
coh.push_back(a);
a.set_init(0.7201305629,0.1,0.9771465694,1.015118949,0.0004743217566);
coh.push_back(a);
a.set_init(0.7256450036,0.1,0.9771209927,1.022840419,0.0002785141297);
coh.push_back(a);
a.set_init(0.7587109952,0.1,0.9769730116,1.069026805,9.716845824e-005);
coh.push_back(a);
a.set_init(0.7608868448,0.1,0.97696314,1.072060989,0.0004491533868);
coh.push_back(a);
a.set_init(0.7629307881,0.1,0.9769555819,1.07490901,0.0001421797224);
```

```
coh.push_back(a);
a.set_init(0.7644597468,0.1,0.9769549153,1.077041917,0.0002651208566);
coh.push_back(a);
a.set_init(0.7682653851,0.1,0.9769346704,1.082346736,0.0001560376062);
coh.push_back(a);

random_device rd;
mt19937 gen(rd());
uniform_real_distribution<> dis(-0.01,0.01);
clistit cohit;
realtype newmass;
ofstream myfile;
myfile.precision(10);
myfile.open ("change_of_location_cohorts.txt", ios::app);
for(cohit=coh.begin(); cohit!=coh.end(); ++cohit){
  newmass = cohit->getMass() + dis(gen);
  myfile << cohit->getMass() << " changed to " << newmass << endl;
  cohit->setm(newmass);
}
myfile.close();

S = 0.5948910178;
S0 = 1.4837;
int k = 300;
loopMap_C(S,coh,k,1.0e-7,1.0e-7,0,0);
return 0;
```


The map iterations start on a perturbation of the fixed point for $S^0 = 1.4873$: the mass of every birth cohort is changed by adding a uniformly distributed random number over $[-0.01, 0.01]$. The resulting executable file is executed 20 times to find the percentage in Table 5.14. The output file change_of_location_cohorts.txt contains to which value the mass of every of the 41 birth cohorts of the fixed points is adjusted.

The fixed point continuation with zero-order prediction for free S^0 calculated in Section 5.6 needs the following code for increasing S^0 until $S^0 = 3$, starting in the fixed point for $S^0 = 1$.

```
clist coh;
cohort a;
a.set_init(0.3044004766,0.1,0.9769631555,1.072220671,0.0003138114937);
coh.push_back(a);
a.set_init(0.3057837264,0.1,0.9769497247,1.07704208,0.0001208391583);
coh.push_back(a);
a.set_init(0.3073064296,0.1,0.9769325896,1.08234719,7.112009176e-005);
coh.push_back(a);
a.set_init(0.4250644928,0.1,0.9775276242,0.8984629322,0.0001488541793);
coh.push_back(a);
```

```
a.set_init(0.4286958898,0.1,0.9775023404,0.9062543329,0.0006845618739);
coh.push_back(a);
a.set_init(0.4320463997,0.1,0.9774791933,0.9134270349,0.0002157023706);
coh.push_back(a);
a.set_init(0.4343662815,0.1,0.977462481,0.9183861224,0.0003442251617);
coh.push_back(a);
a.set_init(0.4354251459,0.1,0.9774559972,0.9206472598,5.665502588e-005);
coh.push_back(a);
a.set_init(0.4405340308,0.1,0.9774216033,0.9315388304,0.0002340840061);
coh.push_back(a);
a.set_init(0.4552265075,0.1,0.9769742554,1.069027251,4.42882791e-005);
coh.push_back(a);
a.set_init(0.4565316306,0.1,0.976963315,1.072060504,0.0002047192669);
coh.push_back(a);
a.set_init(0.4583553196,0.1,0.9769515892,1.0762975,0.000185643106);
coh.push_back(a);
a.set_init(0.4609596444,0.1,0.9769325896,1.08234719,7.112009176e-005);
coh.push_back(a);
a.set_init(0.4744779688,0.1,0.9771846638,1.003328904,7.952826643e-005);
coh.push_back(a);
a.set_init(0.4766091003,0.1,0.9771697877,1.007810603,0.0003670901832);
coh.push_back(a);
a.set_init(0.4786014284,0.1,0.9771560318,1.011998527,0.0001160507743);
coh.push_back(a);
a.set_init(0.4800871529,0.1,0.9771480129,1.015120784,0.0002161904031);
coh.push_back(a);
a.set_init(0.4837635483,0.1,0.9771211065,1.022841042,0.0001269435127);
coh.push_back(a);
a.set_init(0.5058069794,0.1,0.9769735924,1.069025931,4.428829564e-005);
coh.push_back(a);
a.set_init(0.50725779,0.1,0.9769642709,1.072060118,0.0002047190374);
coh.push_back(a);
a.set_init(0.5086201154,0.1,0.9769563347,1.074909705,6.4803954e-005);
coh.push_back(a);
a.set_init(0.5096394629,0.1,0.9769484618,1.077039751,0.000120839163);
coh.push_back(a);
a.set_init(0.5121772113,0.1,0.9769312298,1.082347296,7.112011323e-005);
coh.push_back(a);
a.set_init(0.6375967392,0.1,0.9775276242,0.8984629322,0.0001488541793);
coh.push_back(a);
a.set_init(0.6428520507,0.1,0.977503245,0.9059803063,0.000587746251);
coh.push_back(a);
a.set_init(0.6442081133,0.1,0.977496849,0.9079178877,9.681562286e-005);
coh.push_back(a);
a.set_init(0.6480695996,0.1,0.9774791933,0.9134270349,0.0002157023706);
coh.push_back(a);
a.set_init(0.6515494222,0.1,0.977462481,0.9183861224,0.0003442251617);
coh.push_back(a);
a.set_init(0.6531377189,0.1,0.9774559972,0.9206472598,5.665502588e-005);
coh.push_back(a);
a.set_init(0.660592541,0.1,0.9774226281,0.9312429381,0.0002010067121);
coh.push_back(a);
```

```
a.set_init(0.6620681069,0.1,0.9774153752,0.9333369322,3.30772941e-005);
coh.push_back(a);
a.set_init(0.7117169532,0.1,0.9771846638,1.003328904,7.952826643e-005);
coh.push_back(a);
a.set_init(0.7149136504,0.1,0.9771697877,1.007810603,0.0003670901832);
coh.push_back(a);
a.set_init(0.7179021425,0.1,0.9771560318,1.011998527,0.0001160507743);
coh.push_back(a);
a.set_init(0.7201307294,0.1,0.9771480129,1.015120784,0.0002161904031);
coh.push_back(a);
a.set_init(0.7256453225,0.1,0.9771211065,1.022841042,0.0001269435127);
coh.push_back(a);
a.set_init(0.7587104691,0.1,0.9769735924,1.069025931,4.428829564e-005);
coh.push_back(a);
a.set_init(0.760886685,0.1,0.9769642709,1.072060118,0.0002047190374);
coh.push_back(a);
a.set_init(0.7629301732,0.1,0.9769563347,1.074909705,6.4803954e-005);
coh.push_back(a);
a.set_init(0.7644591943,0.1,0.9769484618,1.077039751,0.000120839163);
coh.push_back(a);
a.set_init(0.768265817,0.1,0.9769312298,1.082347296,7.112011323e-005);
coh.push_back(a);
realtype Sa = 0.5948912593;
realtype S0a = RCONST(1);
contfpS0_simple(Sa,S0a,coh,3,0.1,1.0e-005,1,300,1.0e-7,1.0e-7,1);
return 0;
```

The starting step size is 0.1, the minimal step size is 10^{-5}, the maximal step size is 1, the convergence parameters for both $\bar{S}$ and $\bar{b}_{tot}$ are 10^{-7} and maximally 300 map iterations are performed to check convergence. Additional output files for the continuation methods are cont_summary.txt (containing a line for every calculated fixed point with S^0, N, $\bar{S}$, $\bar{b}_{tot}$), cont_fp.txt (containing a line for every calculated fixed point with S^0, N, $\bar{S}$, m_{01}, X_{01}, Y_{01}, A_{01}, $\bar{b}(x_{01})$,..., $\bar{b}(x_{0N})$) and cont_full.txt (containing more details about the continuation).

The fixed point continuation with chord prediction in §5.6.2, uses the following code.

```
clist coh1;
cohort a;
a.set_init(0.3044004766,0.1,0.9769631555,1.072220671,0.0003138114937);
coh1.push_back(a);
a.set_init(0.3057837264,0.1,0.9769497247,1.07704208,0.0001208391583);
coh1.push_back(a);
a.set_init(0.3073064296,0.1,0.9769325896,1.08234719,7.112009176e-005);
coh1.push_back(a);
```

```
a.set_init(0.4250644928,0.1,0.9775276242,0.8984629322,0.0001488541793);
coh1.push_back(a);
a.set_init(0.4286958898,0.1,0.9775023404,0.9062543329,0.0006845618739);
coh1.push_back(a);
a.set_init(0.4320463997,0.1,0.9774791933,0.9134270349,0.0002157023706);
coh1.push_back(a);
a.set_init(0.4343662815,0.1,0.977462481,0.9183861224,0.0003442251617);
coh1.push_back(a);
a.set_init(0.4354251459,0.1,0.9774559972,0.9206472598,5.665502588e-005);
coh1.push_back(a);
a.set_init(0.4405340308,0.1,0.9774216033,0.9315388304,0.0002340840061);
coh1.push_back(a);
a.set_init(0.4552265075,0.1,0.9769742554,1.069027251,4.42882791e-005);
coh1.push_back(a);
a.set_init(0.4565316306,0.1,0.976963315,1.072060504,0.0002047192669);
coh1.push_back(a);
a.set_init(0.4583553196,0.1,0.9769515892,1.0762975,0.000185643106);
coh1.push_back(a);
a.set_init(0.4609596444,0.1,0.9769325896,1.08234719,7.112009176e-005);
coh1.push_back(a);
a.set_init(0.4744779688,0.1,0.9771846638,1.003328904,7.952826643e-005);
coh1.push_back(a);
a.set_init(0.4766091003,0.1,0.9771697877,1.007810603,0.0003670901832);
coh1.push_back(a);
a.set_init(0.4786014284,0.1,0.9771560318,1.011998527,0.0001160507743);
coh1.push_back(a);
a.set_init(0.4800871529,0.1,0.9771480129,1.015120784,0.0002161904031);
coh1.push_back(a);
a.set_init(0.4837635483,0.1,0.9771211065,1.022841042,0.0001269435127);
coh1.push_back(a);
a.set_init(0.5058069794,0.1,0.9769735924,1.069025931,4.428829564e-005);
coh1.push_back(a);
a.set_init(0.50725779,0.1,0.9769642709,1.072060118,0.0002047190374);
coh1.push_back(a);
a.set_init(0.5086201154,0.1,0.9769563347,1.074909705,6.4803954e-005);
coh1.push_back(a);
a.set_init(0.5096394629,0.1,0.9769484618,1.077039751,0.000120839163);
coh1.push_back(a);
a.set_init(0.5121772113,0.1,0.9769312298,1.082347296,7.112011323e-005);
coh1.push_back(a);
a.set_init(0.6375967392,0.1,0.9775276242,0.8984629322,0.0001488541793);
coh1.push_back(a);
a.set_init(0.6428520507,0.1,0.977503245,0.9059803063,0.000587746251);
coh1.push_back(a);
a.set_init(0.6442081133,0.1,0.977496849,0.9079178877,9.681562286e-005);
coh1.push_back(a);
a.set_init(0.6480695996,0.1,0.9774791933,0.9134270349,0.0002157023706);
coh1.push_back(a);
a.set_init(0.6515494222,0.1,0.977462481,0.9183861224,0.0003442251617);
coh1.push_back(a);
a.set_init(0.6531377189,0.1,0.9774559972,0.9206472598,5.665502588e-005);
coh1.push_back(a);
```

```
a.set_init(0.660592541,0.1,0.9774226281,0.9312429381,0.0002010067121);
coh1.push_back(a);
a.set_init(0.6620681069,0.1,0.9774153752,0.9333369322,3.30772941e-005);
coh1.push_back(a);
a.set_init(0.7117169532,0.1,0.9771846638,1.003328904,7.952826643e-005);
coh1.push_back(a);
a.set_init(0.7149136504,0.1,0.9771697877,1.007810603,0.0003670901832);
coh1.push_back(a);
a.set_init(0.7179021425,0.1,0.9771560318,1.011998527,0.0001160507743);
coh1.push_back(a);
a.set_init(0.7201307294,0.1,0.9771480129,1.015120784,0.0002161904031);
coh1.push_back(a);
a.set_init(0.7256453225,0.1,0.9771211065,1.022841042,0.0001269435127);
coh1.push_back(a);
a.set_init(0.7587104691,0.1,0.9769735924,1.069025931,4.428829564e-005);
coh1.push_back(a);
a.set_init(0.760886685,0.1,0.9769642709,1.072060118,0.0002047190374);
coh1.push_back(a);
a.set_init(0.7629301732,0.1,0.9769563347,1.074909705,6.4803954e-005);
coh1.push_back(a);
a.set_init(0.7644591943,0.1,0.9769484618,1.077039751,0.000120839163);
coh1.push_back(a);
a.set_init(0.768265817,0.1,0.9769312298,1.082347296,7.112011323e-005);
coh1.push_back(a);
realtype S1 = 0.5948912593;
realtype S01 = RCONST(1);

clist coh2;
a.set_init(0.3044030533,0.1000000000,0.9769644702,1.0722295720,0.0003912733);
coh2.push_back(a);
a.set_init(0.3057868420,0.1000000000,0.9769497776,1.0770529890,0.0001506676);
coh2.push_back(a);
a.set_init(0.3073096129,0.1000000000,0.9769341592,1.0823580480,0.0000886753);
coh2.push_back(a);
a.set_init(0.4250646967,0.1000000000,0.9775279832,0.8984639844,0.0001855990);
coh2.push_back(a);
a.set_init(0.4286967247,0.1000000000,0.9775024795,0.9062557423,0.0008535492);
coh2.push_back(a);
a.set_init(0.4320479296,0.1000000000,0.9774794684,0.9134301612,0.0002689477);
coh2.push_back(a);
a.set_init(0.4343676864,0.1000000000,0.9774653751,0.9183886708,0.0004291981);
coh2.push_back(a);
a.set_init(0.4354256106,0.1000000000,0.9774553749,0.9206490472,0.0000706406);
coh2.push_back(a);
a.set_init(0.4405356983,0.1000000000,0.9774216191,0.9315421599,0.0002918679);
coh2.push_back(a);
a.set_init(0.4552296963,0.1000000000,0.9769739265,1.0690338970,0.0000552202);
coh2.push_back(a);
a.set_init(0.4565353591,0.1000000000,0.9769650936,1.0720687680,0.0002552542);
coh2.push_back(a);
a.set_init(0.4583600321,0.1000000000,0.9769519629,1.0763089710,0.0002314666);
coh2.push_back(a);
```

```
a.set_init(0.4609644193,0.1000000000,0.9769341592,1.0823580480,0.0000886753);
coh2.push_back(a);
a.set_init(0.4744785358,0.1000000000,0.9771858195,1.0033307170,0.0000991598);
coh2.push_back(a);
a.set_init(0.4766104445,0.1000000000,0.9771701668,1.0078141110,0.0004577083);
coh2.push_back(a);
a.set_init(0.4786034580,0.1000000000,0.9771563099,1.0120016080,0.0001446970);
coh2.push_back(a);
a.set_init(0.4800891069,0.1000000000,0.9771465793,1.0151235110,0.0002695576);
coh2.push_back(a);
a.set_init(0.4837652192,0.1000000000,0.9771210992,1.0228439440,0.0001582797);
coh2.push_back(a);
a.set_init(0.5058096674,0.1000000000,0.9769737419,1.0690317640,0.0000552204);
coh2.push_back(a);
a.set_init(0.5072599961,0.1000000000,0.9769643253,1.0720648980,0.0002552550);
coh2.push_back(a);
a.set_init(0.5086227564,0.1000000000,0.9769556954,1.0749151280,0.0000807999);
coh2.push_back(a);
a.set_init(0.5096425433,0.1000000000,0.9769490098,1.0770481810,0.0001506684);
coh2.push_back(a);
a.set_init(0.5121806825,0.1000000000,0.9769322473,1.0823547190,0.0000886759);
coh2.push_back(a);
a.set_init(0.6375970450,0.1000000000,0.9775279832,0.8984639844,0.0001855990);
coh2.push_back(a);
a.set_init(0.6428536252,0.1000000000,0.9775033468,0.9059821718,0.0007328338);
coh2.push_back(a);
a.set_init(0.6442074059,0.1000000000,0.9774972142,0.9079165225,0.0001207154);
coh2.push_back(a);
a.set_init(0.6480718943,0.1000000000,0.9774794684,0.9134301612,0.0002689477);
coh2.push_back(a);
a.set_init(0.6515515296,0.1000000000,0.9774653751,0.9183886708,0.0004291981);
coh2.push_back(a);
a.set_init(0.6531384159,0.1000000000,0.9774553749,0.9206490472,0.0000706406);
coh2.push_back(a);
a.set_init(0.6605950319,0.1000000000,0.9774227042,0.9312462209,0.0002506255);
coh2.push_back(a);
a.set_init(0.6620706729,0.1000000000,0.9774150256,0.9333405472,0.0000412424);
coh2.push_back(a);
a.set_init(0.7117178037,0.1000000000,0.9771858195,1.0033307170,0.0000991598);
coh2.push_back(a);
a.set_init(0.7149156668,0.1000000000,0.9771701668,1.0078141110,0.0004577083);
coh2.push_back(a);
a.set_init(0.7179051870,0.1000000000,0.9771563099,1.0120016080,0.0001446970);
coh2.push_back(a);
a.set_init(0.7201336603,0.1000000000,0.9771465793,1.0151235110,0.0002695576);
coh2.push_back(a);
a.set_init(0.7256478288,0.1000000000,0.9771210992,1.0228439440,0.0001582797);
coh2.push_back(a);
a.set_init(0.7587145011,0.1000000000,0.9769737419,1.0690317640,0.0000552204);
coh2.push_back(a);
a.set_init(0.7608899941,0.1000000000,0.9769643253,1.0720648980,0.0002552550);
coh2.push_back(a);
```

```
a.set_init(0.7629341346,0.1000000000,0.9769556954,1.0749151280,0.0000807999);
coh2.push_back(a);
a.set_init(0.7644638150,0.1000000000,0.9769490098,1.0770481810,0.0001506684);
coh2.push_back(a);
a.set_init(0.7682710238,0.1000000000,0.9769322473,1.0823547190,0.0000886759);
coh2.push_back(a);

realtype S2 = RCONST(0.5948917246);
realtype S02 = RCONST(1.1);
contfpS0_2fp(S1,S01,coh1,S2,S02,coh2,3,0.1,1.0e-005,1,300,1.0e-007,1.0e-007,1);
return 0;
```

The continuation for increasing S^0 to $S^0 = 3$, is started with the fixed points for $S^0 = 1$ and $S^0 = 1.1$. The starting step size is 0.1, the minimal step size is 10^{-5}, the maximal step size is 1, convergence parameters for both $\bar{S}$ and $\bar{b}_{tot}$ are 10^{-7} and maximally 300 map iterations are performed to check convergence. The same output files are printed as for the continuation with zero-order prediction.

6

The code for the adapted version of the pseudo-arclength continuation in §5.6.3 is the following.

```
clist coh;
cohort a;
a.set_init(0.3044004766,0.1,0.9769631555,1.072220671,0.0003138114937);
coh.push_back(a);
a.set_init(0.3057837264,0.1,0.9769497247,1.07704208,0.0001208391583);
coh.push_back(a);
a.set_init(0.3073064296,0.1,0.9769325896,1.08234719,7.112009176e-005);
coh.push_back(a);
a.set_init(0.4250644928,0.1,0.9775276242,0.8984629322,0.0001488541793);
coh.push_back(a);
a.set_init(0.4286958898,0.1,0.9775023404,0.9062543329,0.0006845618739);
coh.push_back(a);
a.set_init(0.4320463997,0.1,0.9774791933,0.9134270349,0.0002157023706);
coh.push_back(a);
a.set_init(0.4343662815,0.1,0.977462481,0.9183861224,0.0003442251617);
coh.push_back(a);
a.set_init(0.4354251459,0.1,0.9774559972,0.9206472598,5.665502588e-005);
coh.push_back(a);
a.set_init(0.4405340308,0.1,0.9774216033,0.9315388304,0.0002340840061);
coh.push_back(a);
a.set_init(0.4552265075,0.1,0.9769742554,1.069027251,4.42882791e-005);
coh.push_back(a);
a.set_init(0.4565316306,0.1,0.976963315,1.072060504,0.0002047192669);
coh.push_back(a);
a.set_init(0.4583553196,0.1,0.9769515892,1.0762975,0.000185643106);
coh.push_back(a);
```

```
a.set_init(0.4609596444,0.1,0.9769325896,1.08234719,7.112009176e-005);
coh.push_back(a);
a.set_init(0.4744779688,0.1,0.9771846638,1.003328904,7.952826643e-005);
coh.push_back(a);
a.set_init(0.4766091003,0.1,0.9771697877,1.007810603,0.0003670901832);
coh.push_back(a);
a.set_init(0.4786014284,0.1,0.9771560318,1.011998527,0.0001160507743);
coh.push_back(a);
a.set_init(0.4800871529,0.1,0.9771480129,1.015120784,0.0002161904031);
coh.push_back(a);
a.set_init(0.4837635483,0.1,0.9771211065,1.022841042,0.0001269435127);
coh.push_back(a);
a.set_init(0.5058069794,0.1,0.9769735924,1.069025931,4.428829564e-005);
coh.push_back(a);
a.set_init(0.50725779,0.1,0.9769642709,1.072060118,0.0002047190374);
coh.push_back(a);
a.set_init(0.5086201154,0.1,0.9769563347,1.074909705,6.4803954e-005);
coh.push_back(a);
a.set_init(0.5096394629,0.1,0.9769484618,1.077039751,0.000120839163);
coh.push_back(a);
a.set_init(0.5121772113,0.1,0.9769312298,1.082347296,7.112011323e-005);
coh.push_back(a);
a.set_init(0.6375967392,0.1,0.9775276242,0.8984629322,0.0001488541793);
coh.push_back(a);
a.set_init(0.6428520507,0.1,0.977503245,0.9059803063,0.000587746251);
coh.push_back(a);
a.set_init(0.6442081133,0.1,0.977496849,0.9079178877,9.681562286e-005);
coh.push_back(a);
a.set_init(0.6480695996,0.1,0.9774791933,0.9134270349,0.0002157023706);
coh.push_back(a);
a.set_init(0.6515494222,0.1,0.977462481,0.9183861224,0.0003442251617);
coh.push_back(a);
a.set_init(0.6531377189,0.1,0.9774559972,0.9206472598,5.665502588e-005);
coh.push_back(a);
a.set_init(0.660592541,0.1,0.9774226281,0.9312429381,0.0002010067121);
coh.push_back(a);
a.set_init(0.6620681069,0.1,0.9774153752,0.9333369322,3.30772941e-005);
coh.push_back(a);
a.set_init(0.7117169532,0.1,0.9771846638,1.003328904,7.952826643e-005);
coh.push_back(a);
a.set_init(0.7149136504,0.1,0.9771697877,1.007810603,0.0003670901832);
coh.push_back(a);
a.set_init(0.7179021425,0.1,0.9771560318,1.011998527,0.0001160507743);
coh.push_back(a);
a.set_init(0.7201307294,0.1,0.9771480129,1.015120784,0.0002161904031);
coh.push_back(a);
a.set_init(0.7256453225,0.1,0.9771211065,1.022841042,0.0001269435127);
coh.push_back(a);
a.set_init(0.7587104691,0.1,0.9769735924,1.069025931,4.428829564e-005);
coh.push_back(a);
a.set_init(0.760886685,0.1,0.9769642709,1.072060118,0.0002047190374);
coh.push_back(a);
```

```
a.set_init(0.7629301732,0.1,0.9769563347,1.074909705,6.4803954e-005);
coh.push_back(a);
a.set_init(0.7644591943,0.1,0.9769484618,1.077039751,0.000120839163);
coh.push_back(a);
a.set_init(0.768265817,0.1,0.9769312298,1.082347296,7.112011323e-005);
coh.push_back(a);
realtype Sa = 0.5948912593;
realtype S0a = 1.0;
contfpS0(Sa,S0a,coh,0.1,1.0e-5,1,10,1.0e-6,1.0e-6,1,500,0);
return 0;
```

500 fixed points are calculated for increasing S^0 starting from the fixed point for $S^0 = 1$. The starting step size is 0.1, the minimal step size is 10^{-5}, the maximal step size is 1, the maximum number of Newton steps N_{max} is 10, the convergence parameters for both $\bar{S}$ and $\bar{b}_{tot}$ are 10^{-6} and maximally 500 map iterations are performed to check convergence. Additional output files for this continuation method are cont_S0NSb.txt (containing a line for every calculated fixed point with S^0, N, $\bar{S}$, $\bar{b}_{tot}$), continuation.txt (containing S^0, N, $\bar{S}$, m_{01}, X_{01}, Y_{01}, A_{01}, $\bar{b}(x_{01}),\ldots,\bar{b}(x_{0N})$ for every calculated fixed point) and cont.txt (containing more extensive details about the continuation).

To use the map (5.5) as deterministic mapping from m_{birth} to X_{DIV}, set `cond_min` to 1, `cond_max` to 0, `cond_div` to 1 and `cond_div2` to 0. The following code can then be used for the calculation in §5.10.1.

```
clist coh;
cohort a;
a.set_init(0.3044004766,0.1,0.9769631555,1.072220671,0.0003138114937);
coh.push_back(a);
a.set_init(0.3057837264,0.1,0.9769497247,1.07704208,0.0001208391583);
coh.push_back(a);
a.set_init(0.3073064296,0.1,0.9769325896,1.08234719,7.112009176e-005);
coh.push_back(a);
a.set_init(0.4250644928,0.1,0.9775276242,0.8984629322,0.0001488541793);
coh.push_back(a);
a.set_init(0.4286958898,0.1,0.9775023404,0.9062543329,0.0006845618739);
coh.push_back(a);
a.set_init(0.4320463997,0.1,0.9774791933,0.9134270349,0.0002157023706);
coh.push_back(a);
a.set_init(0.4343662815,0.1,0.977462481,0.9183861224,0.0003442251617);
coh.push_back(a);
a.set_init(0.4354251459,0.1,0.9774559972,0.9206472598,5.665502588e-005);
coh.push_back(a);
a.set_init(0.4405340308,0.1,0.9774216033,0.9315388304,0.0002340840061);
coh.push_back(a);
```

```
a.set_init(0.4552265075,0.1,0.9769742554,1.069027251,4.42882791e-005);
coh.push_back(a);
a.set_init(0.4565316306,0.1,0.976963315,1.072060504,0.0002047192669);
coh.push_back(a);
a.set_init(0.4583553196,0.1,0.9769515892,1.0762975,0.000185643106);
coh.push_back(a);
a.set_init(0.4609596444,0.1,0.9769325896,1.08234719,7.112009176e-005);
coh.push_back(a);
a.set_init(0.4744779688,0.1,0.9771846638,1.003328904,7.952826643e-005);
coh.push_back(a);
a.set_init(0.4766091003,0.1,0.9771697877,1.007810603,0.0003670901832);
coh.push_back(a);
a.set_init(0.4786014284,0.1,0.9771560318,1.011998527,0.0001160507743);
coh.push_back(a);
a.set_init(0.4800871529,0.1,0.9771480129,1.015120784,0.0002161904031);
coh.push_back(a);
a.set_init(0.4837635483,0.1,0.9771211065,1.022841042,0.0001269435127);
coh.push_back(a);
a.set_init(0.5058069794,0.1,0.9769735924,1.069025931,4.428829564e-005);
coh.push_back(a);
a.set_init(0.50725779,0.1,0.9769642709,1.072060118,0.0002047190374);
coh.push_back(a);
a.set_init(0.5086201154,0.1,0.9769563347,1.074909705,6.4803954e-005);
coh.push_back(a);
a.set_init(0.5096394629,0.1,0.9769484618,1.077039751,0.000120839163);
coh.push_back(a);
a.set_init(0.5121772113,0.1,0.9769312298,1.082347296,7.112011323e-005);
coh.push_back(a);
a.set_init(0.6375967392,0.1,0.9775276242,0.8984629322,0.0001488541793);
coh.push_back(a);
a.set_init(0.6428520507,0.1,0.977503245,0.9059803063,0.000587746251);
coh.push_back(a);
a.set_init(0.6442081133,0.1,0.977496849,0.9079178877,9.681562286e-005);
coh.push_back(a);
a.set_init(0.6480695996,0.1,0.9774791933,0.9134270349,0.0002157023706);
coh.push_back(a);
a.set_init(0.6515494222,0.1,0.977462481,0.9183861224,0.0003442251617);
coh.push_back(a);
a.set_init(0.6531377189,0.1,0.9774559972,0.9206472598,5.665502588e-005);
coh.push_back(a);
a.set_init(0.660592541,0.1,0.9774226281,0.9312429381,0.0002010067121);
coh.push_back(a);
a.set_init(0.6620681069,0.1,0.9774153752,0.9333369322,3.30772941e-005);
coh.push_back(a);
a.set_init(0.7117169532,0.1,0.9771846638,1.003328904,7.952826643e-005);
coh.push_back(a);
a.set_init(0.7149136504,0.1,0.9771697877,1.007810603,0.0003670901832);
coh.push_back(a);
a.set_init(0.7179021425,0.1,0.9771560318,1.011998527,0.0001160507743);
coh.push_back(a);
a.set_init(0.7201307294,0.1,0.9771480129,1.015120784,0.0002161904031);
coh.push_back(a);
```

```
a.set_init(0.7256453225,0.1,0.9771211065,1.022841042,0.0001269435127);
coh.push_back(a);
a.set_init(0.7587104691,0.1,0.9769735924,1.069025931,4.428829564e-005);
coh.push_back(a);
a.set_init(0.760886685,0.1,0.9769642709,1.072060118,0.0002047190374);
coh.push_back(a);
a.set_init(0.7629301732,0.1,0.9769563347,1.074909705,6.4803954e-005);
coh.push_back(a);
a.set_init(0.7644591943,0.1,0.9769484618,1.077039751,0.000120839163);
coh.push_back(a);
a.set_init(0.768265817,0.1,0.9769312298,1.082347296,7.112011323e-005);
coh.push_back(a);
realtype Sp = 0.5948912593;
int k = 300;
loopMap_C(Sp,coh,k,1.0e-7,1.0e-7,1,0);
return 0;
```

To use the probability density function for X_{DIV} as in §5.10.2 with mean 0.1 and standard deviation 0.02, set `cond_min` to 1, `cond_max` and `cond_div` to 0, and `cond_div2` to 1. The same code as above can then be used to do the calculations. To use the probability density function with mean 0.1 and standard deviation 0.007, adjust the definition of `Xp` in `cohort::integrate_cohort_bis` to the one above the current definition.

CHAPTER 7

Future work

In this thesis we discussed structured population models for unicellular organisms with internal cell cycle. As cell cycle mechanism we incorporated the Toy model of Tyson and Novák, so the internal state of the cells is described by their mass and three chemical concentrations X, Y and A. We adjusted the equation for the mass so that the increase in mass depends on the nutrient concentration S with a Holling type II functional response. We assumed that the consumption rate is proportional to the rate of mass increase. In [71] the cell cycle is subdivided in a nutrient-dependent segment and a nutrient-independent segment (see Section 2.2.2). It might be interesting to incorporate such a distinction in our structured population model. We also incorporated the more extended cell cycle model for budding yeast of Tyson and Novák, but there are many more interesting models for the cell cycle that could be incorporated, such as the one of Csikász-Nagy in [14].

As cell division criteria, we initially use the ones that Tyson and Novák propose for their Toy model in [81]. A cell divides when $X = X_{DIV}$ (chosen as 0.1) and X is decreasing. We further considered a minimal mass criterion and two different ways to incorporate a maximal mass in the model (as an upper boundary for mass in the mass equation or as an explicit criterion for cell division). In Section 5.10 we considered other possibilities for X_{DIV}. We made the distinction between the case when the value of X_{DIV} is imprinted at birth and the case where it is determined

during the life cycle of the cell. For X_{DIV} imprinted at birth, we considered a discrete deterministic mapping from the mass at birth m_{birth} to the value of X_{DIV}. Other possibilities whose effect could be investigated are a continuous function for X_{DIV} dependent on m_{birth}, or the probabilistic counterpart of the discrete values for X_{DIV} or the continuous function for X_{DIV}. For the case that the value of X_{DIV} is decided during the ageing of the cell, we considered a probability density function for X_{DIV} in such a way that at certain ages it is checked if the value of X at that age (assuming that the side criteria for division are fulfilled) could be used as X_{DIV} using the cumulative distribution function for X_{DIV} and a random number generator. There is room for improvement in the implementation of this probability density function, since the use of the exponential distribution for the time between the evoking of the random number generator is arbitrary and might be replaced by a better motivated distribution. It would also be interesting if the probability density function for X_{DIV} would be dependent on the nutrient level. The decision for the value of X_{DIV} during the life cycle of the cell could also be made deterministic and/or with discrete values for X_{DIV}. It would also be interesting to consider other possibilities for the other cell division criteria, such as the minimal mass. For example, a probability density function for the division event that is dependent on all the division criteria could be used. Another nice extension of our model would be that not all cells in a cohort divide at the same age, but only a certain percentage using a rate of division. The code is implemented so that a rate of division can easily be included. The most tricky part would be to find a suitable function for the division rate. It could also be interesting to consider other options for the splitting parameter ϕ. We now assume that a dividing cell with mass m splits into two daughter cells with masses ϕm and $(1-\phi)m$. If we want to take a reproductive efficiency of less than 100% into account, we could use two parameters ϕ_1 and ϕ_2 with $\phi_1 + \phi_2 < 100\%$ and let a mother cell with mass m divide into two daughter cells with masses $\phi_1 m$ and $\phi_2 m$. Another extension for ϕ would be to consider a probability distribution instead of a fixed value.

In Sections 5.6 and 5.7 we discussed the continuation of the fixed point of the map corresponding with our structured population model. Three continuation methods were considered: a simple continuation with zero-order prediction, a continuation based on a chord prediction using the 2 previous fixed points and a more advanced continuation using an adapted version of the pseudo-arclength continuation. The

main difficulty for the continuation method is that because we use an adaptive mesh, the number of discretisation points and the location of the discretisation points can be different for every iteration of the map. This results in a very rough estimate of the Jacobian matrix when using finite differences and the mapping back of every new discretisation to the original one. For a free parameter S^0 the pseudo-arclength-like continuation works well (although it needs a lot more computational effort than the two other discussed methods), but for free D the region where this continuation method works is quite limited. Future work could include a thorough investigation of more suitable continuation methods.

We investigated the stability of the fixed points in terms of the map, but this does not tell us whether the corresponding equilibrium of the population model is stable in the dynamical sense of the evolution equations. The stability of the equilibria would be very interesting to study, the methods used in [17, 53, 54] could serve as a starting point.

The aim of the present work was to investigate mathematical and computational techniques for the study of population models. The practical validation for the studied case of a model with internal cell cycle remains to be done. One could check if changing the nutrient concentration in the feeding bottle or changing the dilution rate, results in the same changes to the distribution of the masses of the cells at equilibrium state. It would be interesting to be able to compare how well the experimental results match the computational results for different division criteria and for different underlying cell cycle models. This could then serve as a check for the cell cycle assumptions that are made and could lead to a better understanding of this extremely important biological mechanism.

Abstract

The main topic of this thesis is structured population models for unicellular organisms with an internal structure that describes the cell cycle. The individual organism is the basic unit in population models and for structured population models the distinction is made between different individuals on the basis of certain physiological characteristics which influence their life trajectory. This collection of physiological traits, is called the *i*-state and may include e.g. age, size or sex. The novelty in our models is that we use the chemical components of a mathematical model for the cell cycle as *i*-state. During the last fifteen years, Tyson and Novák and collaborators have presented several models for the cell cycle of different organisms based on the concentrations of chemicals such as cyclins. We incorporate two of these models to describe how the *i*-state of a cell changes during its life-time and, importantly, to describe when it divides. The state of the population is represented by a frequency distribution over all *i*-states and the population model reflects how this distribution changes during time given its current state and environmental conditions. We consider chemostat models, i.e. the cell population is inside a stirred bioreactor to which fresh nutrient is continuously added, while the culture liquid (containing both the cells and the nutrient) is continuously removed at the same rate to keep the culture volume constant. The only environmental factor in our models is the limiting nutrient concentration in the bioreactor. We incorporate a nutrient dependency in the equation for the mass increase of the cell cycle models. The equations for the population dynamics consist of a renewal equation coupled with a delay differential equation. We are particularly interested in the equilibria of the model. An equilibrium consists of a constant nutrient concentration and a time-invariant distribution of the births over the possible *i*-states. To be able to numerically solve the equilibrium

equations, we discretise the birth space resulting in a finite number of birth cohorts with corresponding equations. We use the funnel effect of the considered cell cycle models, to decrease the number of birth cohorts and use an adaptive mesh. The equilibrium of the population model can be calculated as the fixed point of a map. The calculation of the fixed point is implemented using `C++`. We consider different options for the cell division criteria, initially following Tyson and Novák who let a cell divide when the concentration of the cyclin-Cdk dimer is decreasing and equal to 0.1, but also consider e.g. the impact on the fixed point of a minimal mass criterion for division, of a discrete mapping of the mass at birth to the value of the dimers at division and of a density probability function for the value of the dimers at division.

In Chapter 3 we study the bifurcation structure of the budding yeast cell cycle model of Tyson and Novák using the Matlab numerical bifurcation software MatCont. The fundamental idea in these cell cycle models is that the cell cycle is an alternation between two stable steady states of a system of kinetic equations which respectively correspond to the G1 and S-G2-M phases of the cell cycle. We find that not only the S-G2-M phase but also the G1 phase contains both stable steady states and stable periodic orbits. We find and discuss a relation between the growth rate of the cell and the mass increase after DNA-replication. We relate this to a constant phase fraction of a periodic orbit traversed during S-G2-M phase and derive a relation between the growth rate and time spent in S-G2-M space. This relation is consistent with experimental results but so far was not found in other models. We further find that the boundary value problem of the cell cycle can be computed efficiently as the fixed point of a map. As another result, we find that the constitutive expression of the Starter kinase not only leads to a premature transition from G1 to S phase and smaller cells (as is experimentally known and confirmed by other models) but in this model can also lead to nonviable cells.

Next, in Chapter 4, we incorporate the cell cycle structure in a population model for unicellular organisms. In the major part of this research, an adjusted form (that incorporates nutrient dependency) of the Toy model of Tyson and Novák is used. We make the distinction between population models where cells can only divide when their mass satisfies a minimal mass criterion (Minal-Mass models MM1 and MM2) and a model without minimal mass criterion (No-Minimal-Mass model NMM). The only difference between the MM1 and MM2 model is the way the maximal mass

is incorporated in the models. We describe and motivate the adaptive mesh for the birth space and give the resulting equations for the population model.

In Chapter 5 we discuss the computational results for the structured population models introduced in Chapter 4. We briefly discuss how we implement the corresponding map (more details are given in Chapter 6) and give the first convergence results for the NMM, MM1 and MM2 models. In the NMM model, all cells divide immediately after birth, which is not very realistic. For the MM1 model, we find a non-trivial fixed point with 41 birth cohorts for the initial parameter values, which we discuss in more detail with e.g. a cohort-to-cohort representation that indicates graphically for every birth cohort to which birth cohorts the daughter cells of dividing cells that were born in this certain birth cohort, contribute. For the MM2 model, a similar non-trivial fixed point is found. We focus on the MM1 model for the calculations in the rest of the chapter. We discuss the numerical effects that have to be taken into account when calculating the fixed point by iterating the map. We investigate how the convergence behaviour changes under variation of the parameter S^0 (the nutrient concentration in the feeding bottle of the chemostat). For some values of S^0 non-trivial fixed points coexist with cycles of the map, both stable in terms of the map. This might be due to the combination of a subcritical period doubling bifurcation and a limit point bifurcation. We investigate how sensitive the fixed point is to perturbations for a parameter value for which there also exists a stable cycle. We consider a random shift of the mass of the cohorts, a fixed shift of the mass of the cohorts, doubling of the number of cohorts and a perturbation of the nutrient concentration and number of cells of the fixed point. The observed cyclic behaviour for several S^0 values is used to make an "educated" guess for the fixed point. This gives good results for some values, but it only works if the attraction region of the fixed point is big enough and the values of the points of the cycle are located quite symmetrical around the fixed point. We consider three different fixed point continuation methods for free S^0. The first is a very simple method which we call the zero-order prediction method and where the fixed point of the previous S^0 value is used as prediction. In the second method the prediction of the new fixed point is based on the 2 previously computed fixed points using linear extrapolation, which we call the chord prediction. Finally, a modified version of the pseudo-arclength continuation method is used. The resulting fixed point curves are given for every method. The fixed points of the non-trivial fixed point curve all have the same 41

cohorts, the same nutrient concentration, and the total number of cells born increases linearly with increasing S^0. We explain this result using the equilibrium equations. Next, we discuss the results of the same fixed point continuation methods applied to a free dilution rate D. D plays a more complex role in the system since it both influences the nutrient level and the death rate of the cells. This results in a more complex shape of the fixed point curve. The continuation method with chord prediction gives the best results for free D, meaning that it enables us to find the fixed points for the widest range of parameter values. We observe behaviour that is typical for a supercritical Neimark-Sacker bifurcation at $D = 0.0052$ min^{-1}. Further, we discuss which D value is optimal to maximize the yield of the chemostat and study the non-trivial fixed points with very few cohorts for small D values. In the last sections, we consider two adaptations as a generalisation of our population model. First, one of the cell division criteria proposed by Tyson and Novák is adapted and we study the effect on the resulting fixed point. We make the distinction between the case where the value of a critical chemical concentration for division is imprinted at birth and the case where the value is established during the progression through the cell cycle. For both cases, we study an example. Finally, we incorporate a more extended model for the cell cycle as internal structure for the cells, namely the budding yeast model of Tyson and Novák. We discuss the found non-trivial fixed point and compare the fixed points for several D values.

Nederlandstalige Samenvatting

Deze thesis behandelt gestructureerde populatiemodellen voor eencelligen waarbij de interne structuur de celcyclus beschrijft. De basiseenheid in populatiemodellen is het individu en bij gestructureerde populatiemodellen wordt een onderscheid gemaakt tussen verschillende individuen op basis van bepaalde fysiologische kenmerken die een invloed hebben op hun levensloop. Deze verzameling van fysiologische kenmerken noemt men de i-toestand en kan bijvoorbeeld de leeftijd, grootte of geslacht bevatten. De nieuwigheid in de door ons beschouwde modellen is dat we de chemische componenten van een wiskundig model voor de celcyclus gebruiken als i-toestand. Gedurende de laatste 15 jaren hebben Tyson en Novák en medewerkers verscheidene modellen voor de celcyclus voor verschillende organismen voorgesteld die gebaseerd zijn op concentraties van chemische stoffen zoals cyclines. We integreren twee dergelijke modellen om te beschrijven hoe de i-toestand van een cel verandert in de loop van haar leven en eveneens om te beschrijven wanneer een cel zal delen. De populatietoestand wordt voorgesteld door een frequentieverdeling over alle mogelijke i-toestanden en het populatiemodel geeft dan weer hoe deze verdeling verandert met de tijd, gegeven de huidige verdeling en omgevingsfactoren. We beschouwen chemostaatmodellen, hierbij bevindt de populatie cellen zich in een gemengde bioreactor waaraan verse nutriënt continu wordt toegevoegd en de bioreactorinhoud (dus zowel de cellen als de nutriënt) continu aan hetzelfde tempo wordt afgevoerd zodat het volume constant blijft. De enige omgevingsfactor die we beschouwen in onze modellen is de beperkende nutriëntconcentratie in de bioreactor. Deze nutriëntafhankelijkheid hebben we opgenomen in de vergelijking voor de massatoename. De populatievergelijkingen bestaan uit een vernieuwingsvergelijking gekoppeld aan een differentiaalvergelijking met vertragingsfactoren. We zijn voor-

namelijk geïnteresseerd in de evenwichtstoestanden van het model. Een evenwichtstoestand bestaat uit een constante nutriëntconcentratie en een tijdsinvariante verdeling van de geboortes over de mogelijke i-toestanden. Om de evenwichtsvergelijkingen numeriek te kunnen oplossen, moet de geboorteruimte gediscretiseerd worden, wat leidt tot een eindig aantal geboortecohorten met elk bijhorende vergelijkingen. We maken gebruik van het trechtereffect van de beschouwde celcyclusmodellen om het aantal geboortecohorten te beperken en we gebruiken een aanpasbaar rooster. De evenwichtstoestand van het populatiemodel kan berekend worden als het vast punt van een afbeelding. De berekening van het vast punt is geïmplementeerd met `C++`. We beschouwen verschillende celdelingscriteria. Initieel volgen we Tyson en Novák en laten een cel delen als de cycline-Cdk-concentratie dalend is en gelijk is aan 0.1. Verder beschouwen we echter ook de invloed op het vast punt van een delingscriterium gebaseerd op een minimale massa, van een discrete afbeelding van de geboortemassa naar de waarde van de cycline-Cdk-concentratie bij deling en van een kansdichtheidsfunctie voor de cycline-Cdk-concentratie bij deling.

In Hoofdstuk 3 bestuderen we de bifurcatiestructuur van het celcyclusmodel voor biergist van Tyson en Novák, gebruik makend van de Matlab numerieke bifurcatiesoftware MatCont. Het fundamentele idee van soortgelijke celcyclusmodellen is dat de celcyclus de afwisseling is tussen twee stabiele evenwichtstoestanden van een systeem van kinetische vergelijkingen, respectievelijk overeenkomend met de G1-fase en de S-G2-M-fase van de celcyclus. We ontdekken dat niet enkel de S-G2-M-fase, maar ook de G1-fase zowel stabiele evenwichtstoestanden als stabiele periodieke banen bevat. We ontdekken en bespreken een verband tussen het groeitempo van de cel en de massatoename na DNA-replicatie. We brengen dit in verband met een constant fasedeel van een periodieke baan dat doorlopen wordt tijdens de S-G2-M-fase en leiden een verband af tussen het groeitempo en de tijd doorgebracht in de S-G2-M-fase. Dit verband is consistent met experimentele resultaten maar was tot nog toe niet ontdekt in andere modellen. Verder vinden we dat het randwaardeprobleem van de celcyclus efficiënt berekend kan worden als het vast punt van een afbeelding. Tevens vinden we dat de constitutieve uitdrukking voor het Start-kinase niet enkel leidt tot een vroegtijdige overgang van G1- naar S-fase en kleinere cellen (zoals experimenteel geweten is en bevestigd werd door andere modellen) maar tevens kan leiden tot niet-levensvatbare cellen.

Vervolgens, in Hoofdstuk 4, integreren we de celcyclus-structuur in een populatiemodel voor eencelligen. In het grootste deel van dit onderzoek wordt hiervoor een aangepaste vorm (met nutriëntafhankelijkheid) van het Toy model van Tyson en Novák gebruikt. We maken een onderscheid tussen populatiemodellen waarbij cellen enkel kunnen delen wanneer hun massa groter is dan een minimale massa (Minimal-Mass-modellen MM1 en MM2) en een model zonder het criterium van minimale massa (No-Minimal-Mass-model NMM). Het verschil tussen het MM1- en het MM2-model is de manier waarop de maximale massa opgenomen is in de modellen. We beschrijven en motiveren het aanpasbaar rooster voor de geboorteruimte en geven de resulterende vergelijkingen voor het populatiemodel.

In Hoofdstuk 5 bespreken we de computationele resultaten voor de gestructureerde populatiemodellen met interne celcyclus-structuur die ingevoerd werden in Hoofdstuk 4. We bespreken beknopt hoe we de corresponderende afbeelding hebben geïmplementeerd (meer details zijn te vinden in Hoofdstuk 6) en geven de eerste convergentieresultaten voor het NMM-, MM1- en MM2-model. Bij het NMM-model delen alle cellen onmiddellijk na geboorte, wat niet realistisch is. Voor het MM1-model vinden we voor de initiële parameterwaarden een niet-triviaal vast punt met 41 geboortecohorten. We bespreken dit vast punt in detail met onder andere een cohorte-tot-cohorte-voorstelling die voor elk geboortecohorte aangeeft tot welke geboortecohorten de dochtercellen van delende cellen die geboren werden in dit bepaald cohorte bijdragen. Voor het MM2-model vinden we een soortgelijk niet-triviaal vast punt. Voor de verdere berekeningen beperken we ons tot het MM1-model.

We bespreken de numerieke effecten die in rekening gebracht moeten worden bij het berekenen van het vast punt door de map te itereren. We onderzoeken hoe het convergentiegedrag verandert bij variatie van de parameter S^0 (de nutriëntconcentratie in de voedingsfles van de chemostaat). Voor bepaalde S^0-waarden bestaan naast niet-triviale vaste punten tevens cykels van de afbeelding, beide stabiel in termen van de afbeelding. Dit is mogelijks veroorzaakt door de combinatie van een subkritische periodeverdubbelings-bifurcatie en een limietpunt-bifurcatie. We onderzoeken hoe gevoelig het vast punt is voor perturbaties voor een parameterwaarde waarvoor ook een stabiele cykel bestaat. We beschouwen een willekeurige verandering van de massa van de geboortecohorten, een vaste verandering van de massa van de geboortecohorten, het verdubbelen van het aantal geboortecohorten en een perturbatie van

de nutriëntconcentratie en het aantal cellen van het vast punt. Het geobserveerde cyclische gedrag is voor enkele S^0-waarden gebruikt om een "doordachte" gissing te maken voor het vast punt. Dit geeft voor sommige waarden goede resultaten, maar het werkt enkel als het aantrekkingsgebied van het vast punt groot genoeg is en de waarden van de punten van de cykel redelijk symmetrisch rond het vast punt liggen.

We beschouwen drie verschillende vast-punt-continuatiemethoden voor vrije S^0. De eerste methode, die we de zero-order-predictiemethode noemen, is heel eenvoudig en gebruikt het vast punt van een vorige S^0-waarde als predictie voor het nieuwe vast punt. Bij de tweede methode is de predictie van het nieuwe vast punt gebaseerd op de twee vorige vaste punten gebruik makend van lineaire extrapolatie, wat we de chord-predictie noemen. Tenslotte gebruiken we een aangepaste versie van de pseudo-arclength continuatie. De resulterende vast-punt-krommes worden gegeven voor elke methode. De vaste punten van de niet-triviale vast-punt-kromme hebben allemaal dezelfde 41 geboortecohorten, dezelfde nutriëntconcentratie en het totaal aantal geboren cellen stijgt lineair met stijgende S^0. We verklaren dit resultaat aan de hand van de evenwichtsvergelijkingen. Vervolgens bespreken we de resultaten van deze drie continuatiemethoden toegepast op een vrije parameter D. D stelt het verdunningstempo van de chemostaat voor en speelt een meer complexe rol in het populatiemodel aangezien D zowel de nutriëntconcentratie als het sterftetempo van de cellen beïnvloedt. Dit resulteert in een meer complexe vorm van de niet-triviale vast-punt-kromme. De continuatiemethode met chord-predictie geeft de beste resultaten voor vrije D, wat wil zeggen dat we met deze methode de vaste punten kunnen berekenen voor het grootste D-interval. We observeren typisch gedrag voor een Neimark-Sacker-bifurcatie voor $D = 0.0052$ min^{-1}. Verder bespreken we welke D-waarde optimaal is om de opbrengst van de chemostaat te maximaliseren en bestuderen we de niet-triviale vaste punten met heel weinig cohorten voor kleine D-waarden. In de laatste secties beschouwen we twee aanpassingen als veralgemeningen van het beschouwde populatiemodel. Eerst passen we één van de celdelingscriteria voorgesteld door Tyson en Novák aan en bestuderen het effect op het resulterende vast punt. We maken het onderscheid tussen het geval waarbij de waarde van de kritische chemische concentratie bij deling vastgelegd is bij de geboorte van de cel en het geval waarbij deze waarde pas tijdens de verdere levensloop van de cel wordt vastgelegd. Voor beide gevallen beschouwen we een voorbeeld. Tenslotte integreren we een uitgebreider model voor de celcyclus als

interne structuur voor de cellen, namelijk het celcyclusmodel voor biergist van Tyson en Novák. We bespreken de resulterende niet-triviale vaste punten en vergelijken de vaste punten onderling voor enkele D-waarden.

Scientific Output

Publications

Published

- Khoshsiar Ghaziani, R., Govaerts, W. and Sonck, C. [2011] "Codimension-two bifurcations of fixed points in a class of discrete prey-predator systems," *Discrete Dynamics in Nature and Society*.

- Khoshsiar Ghaziani, R., Govaerts, W. and Sonck, C. [2012] "Resonance and bifurcation in a discrete-time predator-prey system with Holling functional response," *Nonlinear Analysis - Real World Applications* **13(3)**, pp. 1451-1465.

- Govaerts, W. & Sonck, C. [2014] "Computational study of a budding yeast model of Tyson and Novák," *Mathematics and Computers in Simulation* **96**, pp. 207-223.

To be submitted

The main results of Chapters 4 and 5 will be submitted soon.

Presentations at Conferences

The results of my research were presented at several national and international conferences.

Contributed talks

- First International Workshop on Differential and Integral Equations with Applications in Biology and Medicine, September 7-10, 2010, Karlovassi - Samos, Greece.
  Talk entitled: **Bifurcations in slow-fast models for the budding yeast cell cycle**.

- 9th AIMS Conference on Dynamical Systems, Differential Equations and Applications, July 1 - 5, 2012, Orlando - Florida, USA.
  Talk entitled: **Numerical continuation of equilibria of cell population models with internal cell cycle**, session Modelling and Math Biology.

- European Conference on Complex Systems 2012, September 2-7, 2012, Brussels, Belgium.
  Talk entitled: **Numerical continuation of equilibria of cell population models with internal cell cycle**, session Population dynamics.

- The 14th International Conference on Systems Biology 2013, August 30 - September 3, 2013, Copenhagen, Denmark.
  Talk entitled: **Equilibria of structured cell population models with internal cell cycle**, session Complete cell modeling.

- BIOMATH 2015, June 14 - 19, 2015, Blagoevgrad, Bulgaria.
  Talk entitled: **Numerical computation of equilibria of cell population models with internal cell cycle**.

Invited talks

- BSL Mathematical Societies Conference, June 8, 2012, Luik, Belgium.
  Talk entitled: **Numerical continuation of equilibria of cell population models with internal cell cycle**, session Numerical Analysis.

- Spring Meeting Werkgemeenschap Scientific Computing, May 8, 2015, Antwerp, Belgium.
  Talk entitled: **Numerical computation of equilibria of cell population models with internal cell cycle**.

Poster presentations

- 11th International Conference on Systems Biology, October 10-16, 2010, Edinburgh, Scotland.
  Poster entitled: **Bifurcation study of a model for the cell cycle of budding yeast**.

- International Conference on Systems Biology 2011, August 28-September 1, 2011, Mannheim, Germany.
  Poster entitled: **MatcontM: a computational tool for the study of nonlinear discrete models**.

Informal talks

- TWIST-symposium, March 4, 2014, Ghent.
  Talk entitled: **Equilibria of structured cell population models with internal cell cycle**.

Prizes

- First place on the PhD presenters competition at the International Conference on Mathematical Methods and Models in Biosciences, June 14-19, 2015, with the talk entitled **Numerical computation of equilibria of cell population models with internal cell cycle**.

Bibliography

[1] E. Allgower and K. Georg. *Numerical Continuation Methods: An Introduction*. Springer Ser. Comput. Math. 13. Springer, New York, 1990.

[2] D. Battogtokh and J. J. Tyson. Bifurcation analysis of a model of the budding yeast cell cycle. *Chaos*, 14:653–661, 2004.

[3] A. Beuter, L. Glass, M. C. Mackey, and M. S. Titcombe. *Nonlinear Dynamics in Physiology and Medicine*. Springer-Verlag, New York, 2003. Vol. 25 of Interdisciplinary Applied Mathematics.

[4] M. T. Borisuk and J. J. Tyson. Bifurcation analysis of a model of mitotic control in frog eggs. *J. theor. Biol.*, 195:69–85, 1998.

[5] F. Brauer and C. Castillo-Chavez. *Mathematical Models in Population Biology and Epidemiology*. Springer-Verlag, New York, 2011.

[6] C. J. Briggs. Competition among parasitoid species on a stage-structured host and its effect on host suppression. *The American Naturalist*, 141(3):372–397, 1993.

[7] J. Briggs, K. Dabbs, M. Holm, J. Lubben, R. Rebarber, B. Tenhumberg, and D. Riser-Espinoza. Structured population dynamics: An introduction to integral modeling. *Mathematics Magazine*, 83(4):243–257, 2010.

[8] N. F. Britton. *Essential Mathematical Biology*. Springer-Verlag, London, 2003.

[9] H. Caswell. *Matrix Population Models: Construction, Analysis, and Interpretation*. Sinauer Associates, Sunderland, MA, 2nd edition, 2001.

[10] K. Chen, L. Calzone, A. Csikász-Nagy, F. R. Cross, B. Novák, and J. J. Tyson. Integrative analysis of cell cycle control in budding yeast. *Mol. Biol. Cell*, 15:3841–3862, 2004.

[11] K. Chen, A. Csikász-Nagy, B. Gyorffy, J. Val, B. Novák, and J. J. Tyson. Kinetic analysis of a molecular model of the budding yeast cell cycle. *Mol. Biol. Cell*, 11:369–391, 2000.

[12] F. R. Cross, V. Archambault, M. Miller, and M. Klovstad. Testing a mathematical model of the yeast cell cycle. *Mol. Biol. Cell*, 13:52–70, 2002.

[13] A. Csikász-Nagy. Computational systems biology of the cell cycle. *Briefings in Bioinformatics*, 10(4):424–434, 2009.

[14] A. Csikász-Nagy, D. Battogtokh, K. C. Chen, B. Novák, and J. J. Tyson. Analysis of a generic model of eukaryotic cell-cycle regulation. *Biophysical J.*, 90:4361–4379, 2006.

[15] N. Davydova. *Old and Young. Can they coexist?* Utrecht University, 2004. PhD thesis.

[16] A. M. de Roos. Numerical methods for structured population models: the escalator boxcar train. *Num. Meth. PDE*, 4:173–195, 1988.

[17] A. M. de Roos, O. Diekmann, P. Getto, and M. A. Kirkilionis. Numerical equilibrium analysis for structured consumer resource models. *Bulletin of Mathematical Biology*, 72:259–297, 2010.

[18] A. M. de Roos, O. Diekmann, and J. A. J. Metz. Studying the dynamics of structured population models: A versatile technique and its application to Daphnia. *Amer. Nat.*, 139:123–147, 1992.

[19] A. M. de Roos and L. Persson. *Population and Community Ecology of Ontogenetic Development*. Princeton University Press, New Jersey, 2013.

[20] A. Dhooge, W. Govaerts, and Yu. A. Kuznetsov. MatCont: A MATLAB package for numerical bifurcation analysis of ODEs. *ACM Trans. Math. Software 29*, pages 141–164, 2003. Software available via http://sourceforge.net/projects/matcont.

[21] O. Diekmann. Modeling and analysing physiologically structured populations. In V. Capasso, editor, *Mathematics Inspired by Biology*, volume 1714 of *Lecture Notes in Mathematics*, pages 1–37. Springer Berlin Heidelberg, 1999.

[22] O. Diekmann, M. Gyllenberg, H. Huang, M. Kirkilionis, J. Metz, and H. Thieme. On the formulation and analysis of general deterministic structured population models. II. nonlinear theory. *Journal of Mathematical Biology*, 43(2):157–189, 2001.

[23] O. Diekmann, M. Gyllenberg, and J. Metz. Steady-state analysis of structured population models. *Theoretical Population Biology*, 63:309–338, 2003.

[24] O. Diekmann, H. A. Lauwerier, T. Aldenberg, and J. A. J. Metz. Growth, fission and the stable size distribution. *J. Math. Biology*, 18:135–148, 1983.

[25] O. Diekmann and J. A. J. Metz. How to lift a model for individual behaviour to the population level? *Phil. Trans. R. Soc. B.*, 365:3523–3530, 2010.

[26] L. Dirick, T. Böhm, and K. Nasmyth. Roles and regulation of Cln-Cdc28 kinase at the start of the cell cycle of *saccharomyces cerevisiae*. *The EMBO Journal*, 14(19):4803–4813, 1995.

[27] E. Doedel, A. Champneys, T. Fairgrieve, Yu. A. Kuznetsov, B. Sandstede, and X. Wang. Auto97: Continuation and bifurcation software for ordinary differential equations (with homcont). 1997. http://indy.cs.concordia.ca/auto.

[28] E. J. Doedel. AUTO: A program for the automatic bifurcation analysis of autonomous systems. *Cong. Num.*, 30:265–284, 1981.

[29] E. J. Doedel. Lecture notes on numerical analysis of nonlinear equations. In B. Krauskopf, H. M. Osinga, and J. Galán-Vioque, editors, *Numerical Continuation Methods for Dynamical Systems*, chapter 1, pages 1–49. Springer-Verlag, 2007.

[30] E. J. Doedel, H. Keller, and Kernévez. Numerical analysis and control of bifurcation problems (I): Bifurcation in finite dimensions. *Internat. J. Bifur. Chaos Appl. Sci. Engrg.*, 1(3):493–520, 1991.

[31] E. J. Doedel, H. Keller, and Kernévez. Numerical analysis and control of bifurcation problems (II): Bifurcation in infinite dimensions. *Internat. J. Bifur. Chaos Appl. Sci. Engrg.*, 1(4):745–772, 1991.

[32] L. Edelstein-Keshet. *Mathematical Models in Biology*. SIAM, 2005.

[33] S. P. Ellner and J. Guckenheimer. *Dynamic Models in Biology*. Princeton Unversity Press, Princeton and Oxford, 2006.

[34] C. P. Fall, E. S. Marland, J. M. Wagner, and J. J. Tyson. *Computational Cell Biology*. Springer-Verlag, New York, 2002.

[35] D. Fisher, L. Krasinska, D. Coudreuse, and B. Novák. Phosphorylation network dynamics in the control of cell cycle transitions. *Journal of cell science*, 125(20):4703–4711, 2012.

[36] C. Gérard, J. J. Tyson, D. Coudreuse, and B. Novák. Cell cycle control by a minimal cdk network. *PLoS Comput Biol*, 11(2):e1004056, 2015.

[37] J. Goudriaan. Boxcartrain methods for modelling of ageing, development, delays and dispersion. In J. A. J. Metz and O. Diekmann, editors, *The Dynamics of Physiologically Structured Populations*, pages 453–473. Springer-Verlag, Berlin Heidelberg, 1986.

[38] W. Govaerts. *Numerical Methods for Bifurcations of Dynamical Equilibria*. SIAM, Philadelphia, 2000.

[39] W. Govaerts, V. De Witte, and L. Kheibarshekan. Using MatCont in a two-parameter bifurcation study of models for cell cycle controls. *Proc. of the ASME 2009 IDETC/CIE Conference*, 2009.

[40] W. Govaerts, R. Khoshsiar Ghaziani, Yu.. A. Kuznetsov, and H. G. E. Meijer. Numerical methods for two-parameter local bifurcation analysis of maps. *Siam. J. Sci. Comp.*, 29(6):2644–2667, 2007.

[41] W. Govaerts and C. Sonck. Computational study of a budding yeast model of Tyson and Novák. *Mathematics and Computers in Simulation*, pages 207–223, 2014.

[42] J.-P. Grivet. Nonlinear population dynamics in the chemostat. *Computing in Science and Engineering*, 3(1):48–55, 2001.

[43] J. Hale. *Functional Differential Equations*. Springer-Verlag, New York, 1977.

[44] L. H. Hartwell and M. W. Unger. Unequal division in *saccharomyces cerevisiae* and its implications for the control of cell division. *The Journal of Cell Biology*, 75:422–435, 1977.

[45] A. C. Hindmarsh, P. N. Brown, K. E. Grant, S. L. Lee, R. Serban, D. E. Shumaker, and C. S. Woodward. SUNDIALS: Suite of nonlinear and differential/algebraic equation solvers. *ACM Transactions on Mathematical Software*, 31(3):363–396, 2005.

[46] A. C. Hindmarsh and R. Serban. User documentation for CVODE v2.8.2 (SUNDIALS v2.6.2). 2015. Available via https://computation.llnl.gov/casc/sundials/main.html.

[47] H. Jannasch and R. Mateles. Experimental bacterial ecology studies in continuous culture. *Advances in Microbial Physiology*, 11:165–212, 1974.

[48] H. Keller. Numerical solution of bifurcation and nonlinear eigenvalue problems. In P. Rabinowitz, editor, *Applications of Bifurcation Theory*, pages 359–384. Academic Press, 1977.

[49] H. Keller. *Numerical Methods in Bifurcation Problems*. Springer-Verlag, Berlin, New York, 1987.

[50] A. Khibnik, Yu. A. Kuznetsov, V. Levitin, and E. Nikolaev. Continuation techniques and interactive software for bifurcation analysis of ODEs and iterated maps. *Phys. D*, 62:360–371, 1993.

[51] R. Khoshsiar Ghaziani, W. Govaerts, and C. Sonck. Codimension-two bifurcations of fixed points in a class of discrete prey-predator systems. *Discrete Dynamics in Nature and Society*, 2011.

[52] R. Khoshsiar Ghaziani, W. Govaerts, and C. Sonck. Resonance and bifurcation in a discrete-time predator-prey system with Holling functional response. *Nonlinear Analysis - Real World Applications*, 13(3):1451–1465, 2012.

[53] M. A. Kirkilionis, O. Diekmann, B. Lisser, M. Nool, A. de Roos, and B. Sommeijer. *Numerical continuation of equilibria of physiologically structured population models. I. Theory*. Technical Report R9714 (MAS), Amsterdam: Centre for Mathematics and Computer Science, 1997.

[54] M. A. Kirkilionis, O. Diekmann, B. Lisser, M. Nool, B. Sommeijer, and A. de Roos. Numerical continuation of equilibria of physiologically structured population models. I. theory. *Math. Models Methods Appl. Sci.*, 11(6):1101–1127, 2001.

[55] M. Kot. *Elements of Mathematical Ecology*. Cambridge University Press, Cambridge, UK, 2001.

[56] Yu. A. Kuznetsov. *Elements of Applied Bifurcation Theory*. Springer-Verlag, New York, 3rd edition, 2004. Vol. 112 of Applied Mathematical Sciences.

[57] P. H. Leslie. On the use of matrices in certain population mathematics. *Biometrika*, 33:183–212, 1945.

[58] P. G. Lord and A. E. Wheals. Asymmetrical division of *saccharomyces cerevisiae*. *J. of Bacteriology*, 142:808–818, 1980.

[59] C. M. Macal and M. J. North. Tutorial on agent-based modelling and simulation. *Journal of Simulation*, 4:151–162, 2010.

[60] T. R. Malthus. *An Essay on the Principle of Population*. Penguin Books, 1970. Originally published in 1798.

[61] A. G. McKendrick. Applications of mathematics to medical problems. *Proceedings of the Edinburgh Mathematical Society*, 44:98–130, 1926.

[62] J. A. J. Metz and O. Diekmann. *The Dynamics of Physiologically Structured Populations*. Springer-Verlag, Berlin Heidelberg, 1986. Available as eBook since 2014.

[63] J. Monod. La technique de culture continue: théorie et applications, (A technique for continuous culture: theory and applications). *Ann. Inst. Pasteur*, 79:390–410, 1950.

[64] J. D. Murray. *Mathematical Biology I: An Introduction*. Springer, New York, 2002.

[65] K. Nasmyth. At the heart of the budding yeast cell cycle. *Trends Genet.*, 12:405–412, 1996.

[66] B. Novák and Z. Pataki. Mathematical model of the cell division cycle of fission yeast. *Chaos*, 11:277–286, 2001.

[67] B. Novák, J. J. Tyson, B. Gyorffy, and A. Csikász-Nagy. Irreversible cell-cycle transitions are due to systems-level feedback. *Nature Cell Biol.*, 9:724–728, 2007.

[68] A. Novick and L. Szilard. Description of the chemostat. *Science*, 112:715–716, 1950.

[69] P. Nurse. Nobel lecture: Cyclin dependent kinases and cell cycle control, December 2001. Available via http://www.nobelprize.org.

[70] P. Nurse, P. Thuriaux, and K. Nasmyth. Genetic control of the cell division cycle in the fission yeast *schizosaccharomyces pombe*. *Molec. gen. Genet.*, 146:167–178, 1976.

[71] M. Pascual and H. Caswell. From the cell-cycle to population cycles in phytoplankton-nutrient interactions. *Ecology*, 78(3):897–912, 1997.

[72] W. Rheinboldt. Solution fields of nonlinear equations and continuation methods. *SIAM J. Numer. Anal.*, 17:221–237, 1980.

[73] W. Rheinboldt. *Numerical Analysis of Parametrized Nonlinear Equations*. J. Wiley, New York, 1986.

[74] R. Seydel. *From Equilibrium to Chaos. Practical Bifurcation and Stability Analysis*. Elsevier, New York, 1988.

[75] P. Taylor and P. J. LeB. Williams. Theoretical studies on the coexistence of competing species under continuous flow conditions. *Canadian J. Microbiology*, 21:90–98, 1975.

[76] H. R. Thieme. *Mathematics in Population Biology*. Princeton University Press, Princeton, 2003.

[77] F. J. Trueba. On the precision and accuracy achieved by *escherichia coli* cells at fission about their middle. *Arch. Microbiol.*, 131:55–59, 1982.

[78] S. Tuljapurkar and H. Caswell. *Structured population models in marine, terrestrial and freshwater systems*. Springer US, New York, 1997.

[79] J. J. Tyson, K. C. Chen, and B. Novák. Sniffers, buzzers, toggles and blinkers: dynamics of regulatory and signaling pathways in the cell. *Current Opinion in Cell Biology*, 15:221–231, 2003.

[80] J. J. Tyson and B. Novák. Regulation of the eukaryotic cell cycle: molecular antagonism, hysteresis, and irreversible transitions. *J. theor. Biol.*, 210:249–263, 2001.

[81] J. J. Tyson and B. Novák. Cell cycle controls. In C. P. Fall, E. S. Marland, J. M. Wagner, and J. J. Tyson, editors, *Computational Cell Biology*, chapter 10, pages 261–284. Springer-Verlag, New York, 2002.

[82] J. J. Tyson and B. Novák. Irreversible transitions, bistability and checkpoint controls in the eukaryotic cell cycle: a systems-level understanding. In M. A. J. Walhout, M. Vidal, and J. Dekker, editors, *Handbook of Systems Biology*, chapter 14, pages 265–285. Elsevier, San Diego CA, 2012.

[83] J. J. Tyson and B. Novák. Control of cell growth, division and death: information processing in living cells. *Interface focus*, 4(3):20130070, 2014.

[84] J. J. Tyson and B. Novák. Models in biology: lessons from modeling regulation of the eukaryotic cell cycle. *BMC biology*, 13(1):46, 2015.

[85] P.-F. Verhulst. Notice sur la loie que la population suit dans son accroissement. *Corr. Math. et Phys.*, 10:113–121, 1838.

[86] H. Von Foerster. Some remarks on changing populations. In F. J. Stohlman, editor, *The Kinetics of Cellular Proliferation*, pages 382–407. Grune and Stratton, New York, 1959.